Investigation des photocatalystes de Ruthénium à l'échelle Nano

Cleophas Wawire

UNIVERSITÉ DE GRENOBLE

THÈSE

Pour obtenir le grade de

DOCTEUR DE L'UNIVERSITÉ DE GRENOBLE

Spécialité : **Chimie Physique Moléculaire et Structurale**

Arrêté ministériel : 7 août 2006

Présentée par : **Cleophas Muhavini WAWIRE**

Thèse dirigée par : **Mark E. CASIDA**

Préparée au sein du Département de Chimie Moléculaire dans
l'École Doctorale Chimie et Sciences du Vivant

Theoretical Investigation of Ruthenium Photosensitizers

Thèse soutenue publiquement le **18 juin 2012**, devant le jury composé de:

Tomasz WESOLOWSKI, Président du Jury, Département de Chimie Physique, Professeur de l'Université de Genève

Max Latévi LAWSON DAKU, Rapporteur, Département de Chimie Physique, Chercheur associé, Université de Genève, Habilité en France

Chantal ANDRAUD, Rapporteur, Directeur de Recherche CNRS, Laboratoire de Chimie, École Normale Supérieur de Lyon

Fredérique LOISEAU, Membre du Jury, Département de Chimie Moléculaire, Professeure de l'Université Joseph Fourier (Grenoble 1)

Damien JOUVENOT, Membre du Jury, Département de Chimie Moléculaire, Maître de Conférence de l'Université Joseph Fourier (Grenoble 1)

Mark E. Casida, Directeur de thèse, Département de Chimie Moléculaire, Professeur de l'Université Joseph Fourier (Grenoble 1)

Université Joseph Fourier / Université Pierre Mendès France / Université Stendhal / Université de Savoie / Grenoble INP

ACKNOWLEDGEMENT

I would like to acknowledge a PhD scholarship from the French Government through its Embassy in Kenya. I would like to thank the very able team at the embassy for their timely communication and advice whenever it became necessary.

I am quite clear in my mind that were it not for the great desire on the part of my supervisor Prof. Mark E. Casida to make a difference to humanity, this thesis work would not have been realized. It required a high level of bravery to make such an unprecedented decision of accepting to do science despite the many challenges that we were sure were awaiting us. The desire to go an extra step made the whole difference in our working. Prof. Mark E. Casida kept on re-interpreting ideas and situations in such a way that there was really exposure and learning. Quantum chemistry calculations being a new phenomenon to me, it required a special kind of patience from my supervisor to ensure adjustment and which he demonstrated every time he guided me. I thank my supervisor specifically for the introduction to the linux operating system as well as Python and shell scripting languages.

I take this opportunity to thank all of you who agreed to review and examine my work. Thanks go to Prof. Max Latévi LAWSON DAKU, of the Département de Chimie Physique, Chercheur associé, Université de Genève, and to Dr. Chantal ANDRAUD, Rapporteur, Directeur de Recherche CNRS, Laboratoire de Chimie, École Normale Supérieur de Lyon. I am equally grateful to the other jury members. Prof. Tomasz WESOLOWSKI, of the Département de Chimie Physique, Professeur de l'Université de Genève. Prof. Fredérique LOISEAU, of the Département de Chimie Moléculaire, Professeure de l'Université Joseph Fourier (Grenoble 1) and Dr. Damien JOUVENOT, of the Département de Chimie Moléculaire, Maître de Conférence de l'Université Joseph Fourier (Grenoble 1)

I am indeed very happy to extend my gratitude to my family. My dear wife Kendi Lydia and two daughters namely Mariana Christa Kachitsa and Bertha Nyagoha. I specially thank you for understanding my situation during my studies. I really got the support that I needed to pursue this thesis work. I am sure on very many occasions, I "was not really there for you" but thank God you understood and stood by me.

I sincerely thank Prof. Anne MILET, Dr. Helène JAMET, Dr. Carlos PEREZ del VALLE of the Laboratoire de la Chimie Théorique (LCT) for their warm welcome and providing me with facilities and a conducive working environmnent. I also extend my thanks to Denis Charapoff, Régis Gras, Sébastien Morin, and Marie-Louise Dheu-Andries for the technical support at the (DCM) and for technical support in the context of the *Centre d'Expérimentation du Calcul Intensif en Chimie* (CECIC) computers used for the calculations reported in this work. I also acknowledge the fact that this work has been carried out in the

context of the French Rhône-Alpes *Réseau thématique de recherche avancée (RTRA): Nanosciences aux limites de la nanoélectronique* and the Rhône-Alpes Associated Node of the European Theoretical Spectroscopy Facility (ETSF). Special thanks to go to Dr. Helène JAMET for correcting our French during the abstract translation.

Special thanks go to Dr. Miquel Huix-Rotllant and Dr. Bhaarathi Natarajan with whom we shared a lot as students under Prof. Mark E. Casida. Thank you so much for your understanding. Special thanks also go to Pablo Baudin. Were it not for his Python scripting skills, perhaps we would not be writing this nice story today. Thanks a lot Pablo.

I also extend my thanks to the staff and personnel at the École Doctorale Chimie et Science du Vivant for their timely action whenever it came to administrative matters. I am also grateful to staff at the CROUS office for their assistance to do with my stay and stipend.

I am also grateful to my employer The Catholic University of Eastern Africa-CUEA. I sincerely thank the university for the time I was away on my doctoral studies. I thank specially my Dean of Faculty of Science Prof. Genevieve Mwayuli and Head of Department for understanding my difficult situation of studying and working at the same time. Mr. Bethwell O. Owuor (HOD) was very instrumental in more ways than one. We shared 'lonely weekends' in our offices pursuing our studies together. Many thanks also go to Mr. Emannuel Kiev of CUEA who actually showed me the connection and configurations necessary to ensure smooth use of sftp and ssh on the linux commandline from CUEA.

Special thanks go to Mr. Robert Momanyi and Mr. Benard Muronga Kadurenge. True friends indeed for sacrificing their time to take me to and from JKIA whenever it was necessary. I also extend my sincere thanks to Mr. Justus Tari who actually brought me the idea of this French Scholarship. Not forgetting Mr. Edward Mateche Ndombi and Mr. Paul E. Mutsoli for their sincere encouragement when things were terribly bad in my youth.

I also acknowledge encouragement from Prof. Jane Igoki Murungi and Dr. Nicholas Wanjala both members of staff of Kenyatta University. Thanks to Dr. Moses Keya Ochanji and Dr. Levi Molenje for their great desire to do more and more mathematics and sciences, desire that goes back to our undergraduate days in Kenyatta University.

Last but not least my thanks go to God the Almighty who gave me the strength to remain determined despite the many challenges.

DEDICATION

This Doctoral work is dedicated to my late maternal grand parents Onori Edokha and Mariana Kachitsa Mukamulamba and my late cousin Mary Nafuna Muyumbu. They genuinely perservered and sacrificed a lot to ensure that I acquired knowledge.

TABLE OF CONTENTS

LIST OF FIGURES

LIST OF TABLES

ABSTRACT

The American Nanotechnology Initiative (NNI) of the present millennium has helped to focus attention on objects sized 1-100 nm. Physicists and electrical engineers typically follow a "top-down approach" to synthesizing these objects by etching away the matter of larger objects while chemists often take a "bottom-up" approach of trying to synthesize nano scale objects from smaller molecular units. A particular flavor of the bottom-up approach is the chemical assembly of separate molecular units with different functions–such as chromophore antennas, spacer wires, and reactive centers—to make functional photochemical molecular devices (PMDs). One particularly popular type of chromophore unit consists of ruthenium complexes whose long-lived luminescent excited states may be used in charge transfer processes. Unfortunately tailoring such complexes to fit them into a larger PMD can result in destroying some of the very properties of the smaller unit which one would like to keep in the larger unit. In particular a well-chosen tridentate ligand for ruthenium may lead to a convenient chromophore with desirable charge transfer properties for use in a PMD while a badly chosen tridentate ligand may destroy the very photo-properties that one would like to exploit. This thesis presents a theoretical investigation of factors influencing luminescence lifetime in ruthenium complexes with tridentate ligands and was carried out in close collaboration with the experimental group of Frédérique Loiseau and Damien Jouvenot and their student Sébastien Liatard.

The work reported in this thesis was prompted by the observation that some ruthenium complexes failed to show luminescence at room temperature, but showed some luminescence at very low temperatures.

A common ligand-field theory (LFT) explanation of luminescence lifetimes in these clusters is in terms of the relative proximity of the energies of the $t_{2g} \rightarrow \pi^*$ metal-ligand charge transfer (MLCT) and the $t_{2g} \rightarrow e_g^*$ metal centered (MC) excitations. Close proximity of MC and MLCT states is expected to lead to rapid radiationless de-activation of the luminescent MLCT state. We put this theory to test by analyzing the predictions of more sophisticated density functional theory (DFT) and time-dependent DFT (TD-DFT) calculations and comparing with experimental luminescence lifetimes. DFT was judged to be adequate if it was able to reproduce experimental X-ray geometries and TD-DFT was able to provide quantitative absorption spectra. The simple LFT explanation could then be verified by extracting t_{2g}, π^*, and e_g^* energies using a partial density of states (PDOS) analysis.

The complexes that were studied in this project were: $[Ru(benzi)_2]^{2+}$, $[Ru(tpy)_2]^{2+}$, $[Ru(CNC)_2]^{2+}$, and $[Ru(CNC)(tpy)]^{2+}$ where bpy=2,2-bipyridine, tpy=2,2':6',2"-terpyridine, and CNC=2,6-{bis-N-(N-

methy limidazolylidene)methyl}-pyridine,benzi=2,6-bis-N-(N-benzimidazolylidene)methyl-pyridine). and the hypothetical complex $[Ru(oxa)_2]^{2+}$.

In all except the case of the hypothetical complex, geometries were optimized beginning from the X-ray geometry. Only small changes were observed, thus confirming the validity of DFT in this case. TD-DFT absorption spectra also agreed well with experiment. The extraction of LFT information from our DFT calculations was in reasonable qualitative agreement with the usual hypothesis, but agreement at this level is only qualitative. To some extent, this is to be expected because a more sophisticated description of the photophysical process should involve the coupling of potential energy surfaces of electronic states rather than orbitals. Nevertheless it is gratifying that the simpler and computationally less demanding orbital analysis is able to provide qualitative trends.

Heartened by these results we set out to predict what should happen for the as yet unsynthesized molecule $[Ru(oxa)_2]^{2+}$. Theoretical results are given and a prediction is made. The experiment has not yet been carried out. The thesis concludes with a discussion of more sophisticated approaches which could be used to gain still deeper insight into the problem of luminescence in ruthenium complexes.

Key Words: Nanotechnology, nanoscale, quantum chemistry, photochemistry, density-functional theory, time-dependent density functional theory, electronic excitation spectrum and excited states.

RESUMÉ

L'intiative américaine pour nanotechnologie (*NNI* pour l'anglais *National Nanotechnology Intiative*) du millenaire actuel a aidé à focaliser l'attention sur des objets de la taille de un à cent millimimètres. Les physiciens et les ingénieurs élèctriques suivent typiquement une approche *top-down* pour créer des objets à l'échelle nanométrique en enlevant progressivement de la matière des objets plus gros. Par contre, les chimistes prennent le plus souvent une approche *bottom-up* en faisant la synthèse d'objet à l'échelle nanométrique par l'assemblage de composants moléculaires ayant des fonctionnalités différentes—dont antennes chromophores, fils espaceurs et centres réactifs—pour créer des dispositifs photochimiques moléculaires (DPMs). Un composant de type chromophore particulièrement populaire est un complexe de ruthénium dont les états excités peuvent servir pour faire le transfert de charge. Malheureusement la confection de tels complexes pour les faire assembler en DPMs plus grands peuvent nuire justement aux propriétés des unités constituantes qu'on cherche à utiliser. En particulier un ligand de ruthénium bien choisi peut faire un bon chromophore avec la bonne propriété de transfert de charge pour servir dans un DPM, mais un autre ligand tridentate malchoisi peut justement détruire les propriétés qu'on cherche à exploiter. Il est présenté dans cette thèse une investigation théorique des facteurs influençant le temps de vie de luminescence dans les complexes de ruthénium à ligands tridentates. Ce projet a été mené en étroite collaboration avec le groupe d'expérimenteurs de Frédérique Loiseau, Damien Jouvenot et leur étudiant doctoral Sébastien Liatard. Spécifiquement le travail présenté a été grandement motivé par l'observation que certains complexes de ruthénium ne sont pas luminescent à température ambiante, mais uniquement aux températures très basses.

Une explication très répandue est basée sur la théorie de champs de ligands (TCL). Il s'agit d'une comparaison de la différence d'énergie entre l'état $t_{2g} \rightarrow \pi^*$ de type transfert de charge du métal aux ligands (*MLCT* pour l'anglais *metal-to-ligand charge transfer*) et l'état $t_{2g} \rightarrow e_g^*$ de type centré sur le métal (*MC* de l'angais *metal centered*). Il est anticipé qu'une petite différence d'énergie entre les états *MLCT* et *MC* serait associée avec une désactivation sans radiation plus rapide de l'état luminescent *MLCT*. Nous avons mis en place les outils pour tester cette théorie par l'analyse des prédictions des théories plus sophistiquées—en particulier la théorie de la fonctionnelle de la densité (*DFT* pour l'anglais *density-functional theory*) et DFT dépendante du temps (*TD-DFT* pour l'anglais *time-dependent DFT*)—en les comparant avec les temps de vie de luminescence mesurés. Les calculs *DFT* étaient jugés suffisant s'ils pouvaient reproduire les géométries cristallographiques et si les calculs *TD-DFT* associés étaient capable de simuler de manière quantitative les spectres d'absorption correspondants. Il a été alors possible de

valider l'explication simple de la TCL en retrouvant les énergies orbitalaires t_{2g}, π^* et e_g^* à partir d'une analyse de la densité partielle des états (*PDOS* pour l'anglais *partial density of states*).

Les complexes étudiés dans cette thèse sont $[Ru(bpy)_3]^{2+}$, $[Ru(benzi)_2]^{2+}$, $[Ru(tpy)_2]^{2+}$, $[Ru(CNC)_2]^{2+}$ et $[Ru(CNC)(tpy)]^{2+}$ où bpy=2,2-bipyridine, tpy=2,2':6',2"-terpyridine, CNC=2,6-{bis-N-(N-méthylimidazolylidene)méthyl}-pyridine et benzi=2,6-bis-N-(N-benzimidazolylidene)méthyl-pyridine). De plus un complexe hypothétique, $[Ru(oxa)_2]^{2+}$, a été étudié en attendant sa synthèse et la mesure de son degré de luminescence. Sauf pour le complexe non encore synthétisé, les géométries ont été optimisées en prenant la géométrie cristallographique comme la géométrie du départ. Les petites différences entre les géométrie rayon-x et les géométries optimisées valident la qualité du modèle *DFT*. Aussi les spectres d'absorption *TD-DFT* sont relativement en bon accord avec les spectres d'absorption mesurés en solution. L'extraction d'information semblable à celle de la TCL a été possible grâce à la technique *PDOS*. Ainsi nous avons pu confirmer un accord qualitatif avec l'explication usuelle de luminescence des complexes de ruthénium. Encouragé par ces résultats nous avons fait des calculs pour prédire les propriétés luminescentes du complexe pas encore synthétisé, $[Ru(oxa)_2]^{2+}$. La thèse conclut avec une discussion des approches plus sophistiquées qu'on peut penser utiliser pour obtenir une compréhension approfondie du problème de luminescence des complexes de ruthénium.

Mots Clés: Nanotechnologie, l'Echelle Nano, Chimie Quantique, Photochimie, Théorie de la Fonctionnelle de la Densité, Théorie de la Fonctionnelle de la Densité Dépendent du Temps, Spectre d'Excitation Électronique et État Excités.

ABBREVIATIONS & ACRONYMS

NNI	National Nanotechnology Initiative
PMD	Photochemical Molecular Devices
LFT	Ligand Field Theory
MLCT	Metal-Ligand Charge Transfer
MC	Metal Metal Centered
DOS	Density of States
PDOS	Partial Density of States
DFT	Density Functional Theory
TDDFT	Time Dependent Density Functional Theory
CIS	Configuration Interaction Singles
UV	Ultraviolet
HOMO	Highest Occupied Molecular Orbitals
LUMO	Lowest Unoccupied Molecular Orbitals
IC	Internal Conversion
ISC	Intersystem Crossing
PES	Potential Energy Surface
GHF	Generalized Hartree Fock
RHF	Restricted Hartree Fock
GTO	Gaussian-Type Orbital
DZ	Double Zeta
TZ	Triple Zeta
SCF	Self Consistent Field
LANL	Los Alamos National Laboratory
LDA	Local Density Approximation
UEG	Uniform Electron Gas
GGA	Generalized Gradient Approximation
AxcA	Adiabatic exchange Approximation
TEA	Triethylamino
AX	Avoided Crossing

CHAPTER 1

INTRODUCTION

This thesis reports work done on the application of computational chemistry to the determination of luminescent properties of ruthenium complexes. Luminescence generally is one of the most effective techniques to monitor the operation of molecular devices. In this context therefore this work is a contribution to the growth of the "bottom-up" approach to the construction of molecular-level devices which we shall describe here as photoactivated molecular devices (PMDs). In this approach, nanoscale molecular devices are built by assembling different types of molecular components, each of which has a well-defined purpose as a molecular 'antenna', 'wire', or even 'active site' where energy received is used to carry out specific chemical reactions.

These efforts are based on the understanding that the traditional "top-down" approach based on photolithography could soon reach its limits. Serious challenges are likely to emerge when components smaller than 100 nm are required for incorporation into nanoscale devices. This reasoning is based on the extrapolation of Moore's law on the limits of electronic circuit miniaturization with conventional technology roughly by 2012.

Therefore given the inevitability of nanoscale devices due to their efficiency in performance, convenience of storage, specifically more efficient utilization of energy, it is necessary to find new ways to make working microscopic devices. The need for devices that make efficient use of energy is also in realization that fossil fuels are both limited and polluting and that access to scarce resources is all too easily interrupted by political conflicts.

As might be expected, this thesis seeks not to solve all the problems implied by PMD fabrication. Rather I focus on the target problem of how to design a ruthenium complex 'antenna molecule' which will act as a chromophore to capture light and create a long-lived excitation which can be transfered via linking units ('wires') to other parts of a PMD. Specifically, we would like to gain insight via computational chemistry into how ligands designed for connecting into PMDs can enhance, preserve, or diminish luminescence in ruthenium complexes

The main goal of this thesis is to determine the molecular orbital picture in various ruthenium complexes and especially the π^* and e_g^* and their relative positions. The other key goal is to assess the relative separations between π^* and e_g^* and compare them with the length of their excited lifetimes at the room temperatures.

The specific objectives in this work are:

- optimize structures (x-ray ones or built ones),
- do a frequency calculation on each optimized structure to be sure that it is the global minimum,
- perform a UV-transitions calculation,
- perform calculation with appropriate GAUSSIAN options to generate information leading to calculation of partial density of states.

The rest of the thesis is organized as follows:

This is a complex project requiring a mastery of basics in a number of areas. These are described in 'Part I. Fundamentals.'
The various chapters in this part are as outlined below:

Chapter 2 introduces the ligand field theory which is important since it paves way for a clearer understanding of the various molecular orbitals in complexes. Their ordering, and closeness are critical in this study.

Chapter 3 deals with the basics of wave function-based electronic structure theory. This chapter captures only the parts of the wave function methods that bear a strong relationship with the real methods used in this thesis (DFT and TDDFT), i.e. HF, CIS, etc.

Chapter 4 extends our knowledge base to the Density Functional Theory, Time-dependent Density Functional Theory and response theory. This is pertinent in relating time-dependent perturbation to the resultant time-dependent response.

Chapter 5 looks at the basics of photochemistry and photophysics. These are necessary because the knowledge of potential energy surfaces, funnels and conical intersections are vital in explaining radiative and nonradiative deactivation of excited molecules. Phosphorescence and fluorescence are also easier to explain when linked to the above mentioned photochemical and photophysical properties. Phosphorescence and Stokes shifts are also discussed in this chapter.

Chapter 6 is on mulliken population analysis. This fits in nicely because the calculation of partial density of states requres knowledge in this field.

Chapter 7 reviews the literature related to the main work of this thesis. The ruthenium complexes and their applications are captured. Besides, similar work to the work in this thesis and the lessons learned are also taken into consideration.

" 'Part II. Original Work.' is the heart of this thesis"

Chapter 8 This chapter reports work on a number of ruthenium complexes. Calculations on ground state geometry optimization and property calculations, electronic transitions and spectra determination and comparison of the results with the experimental values. Besides, recovery of the ligand field theory formulation of the molecular orbitals was done by the partial density of states approach based on population analysis. Correlation of the excited lifetimes of these complexes and the separation between their π^* and e_g^* was done.

> "Finally ' chapters 9 and 10 in Part III. Perspectives and Conclusions' describes on-going work, summarizes what we have been able to accomplish during my PhD studies, and how I think my work could best be continued in the future."

There are three other parts in this thesis.
They form the appendices part which are; appendix A, which is the Spin-flip paper. This is an article in which a number of people made different contributions.

Appendix B is simply my curriculum vitae.

Appendix C is on the Computational Chemistry in Kenya. This brings out some of the pioneer efforts to start this important field in sub-Sahara Africa. The exact work of the computer connections between Nairobi and Grenoble.

Part I

Fundamentals

CHAPTER 2

LIGAND FIELD THEORY

In this chapter I discuss the origin of MOs in ligand field theory and how symmetry lowering due to ligand distortions leads to lifting of orbital degeneracy

2.1 Introduction

The metal-ligand bond in transition metal complexes is better represented by covalency considerations. Ligand field theory ([1, pp. 288] and [2, pp. 58]) is the appropriate bonding theory that deals with this covalency in such systems. A bond between the metal ion and the ligand is formed by the overlap between atomic orbitals [3, pp. 38] derived from the metal ion and those from the ligand donor atoms.

The best starting point in this area starts with the octahedral symmetry [4, pp. 243]. An octahedral complex is a high symmetry complex in which the resultant molecular orbitals have degeneracy which is usually broken by symmetry lowering ([5] and [6, pp. 106]) and this has a lot of implications in other fields such as spectroscopy of such complexes.

In a free metal ion the five d orbitals with different values of the magnetic quantum number (m) have the same energy.

During compound formation, the five d-orbitals interact [2, pp. 66] differently with the surrounding ligands and a ligand field splitting (Δ_o) is produced. As already mentioned above, a common coordination is octahedral (O_h point group) with six surrounding ligands.

In such complexes two of the d orbitals form the e_g set and are found at higher energy than the other three (d_{xy}, d_{xz} and d_{yz}, which are known as t_{2g}). Such a splitting occurs in all transition metals compounds with octahedral coordination [2, pp. 66]. This splitting is the basic consideration when attempting to understand electronic transitions in such chemical species. Figure 2.1 clearly shows the way the d-orbitals split and also the various molecular orbitals arranged according to their energies in a perfect octahedral geometry.

2.2 Molecular orbitals

Most ligands coordinate to the metal ion using nonbonding electrons. A ligand lone-pair orbital pointing directly towards the metal overlaps with the e_g orbitals but has the wrong symmetry [7, pp. 214] to interact

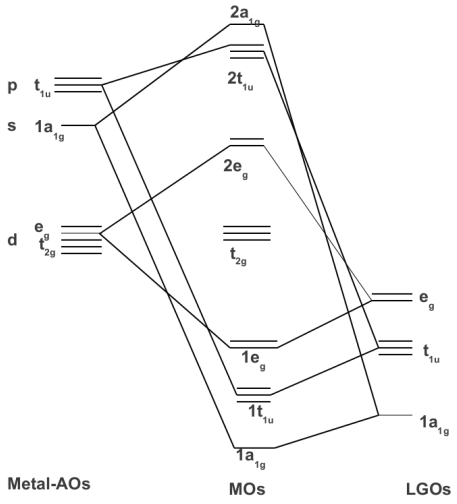

Figure 2.1: Arrangement of σ-molecular orbitals in a perfect octahedral complex. The metal-based atomic orbitals (Metal-AOs) are on the left of the diagram. At the center are found the molecular orbitals (MOs) and on the right are the ligand type of orbitals (LGOs). LGOs represent a linear combination of symmetry adapted atomic orbitals

with t_{2g}. The orientation of the t_{2g} orbitals makes them better suited for a different type of interaction altogether.

This kind of overlap gives rise to bonding (σ) and antibonding (σ^*) molecular orbitals. The bonding orbitals are occupied by the electrons from the ligand, while the σ antibonding levels among which the 'metal' e_g set belongs are centered mainly on the metal. Different ligands cause different splittings Δ_o between the t_{2g} and e_g sets.

Metal-ligand interaction can also lead to π bonding [3, pp. 99]. This arises when ligands having orbitals directed perpendicular [7, pp. 214] to the metal-ligand axis interact with the metal t_{2g} orbitals. These t_{2g} orbitals are described as having dπ symmetry because of this possibility to form π molecular orbitals (see figure 2.2). The nature of the ligand interacting with the metal ion finally determines what happens. Ligands such as halide ions have occupied pπ orbitals and act as π-donors. This interaction raises the energy of the metal t_{2g} orbitals, and decreases Δ_o.

On the other hand, π-acceptor ligands such as CO have empty antibonding π orbitals. Overlap with the metal in this case causes the t_{2g} orbitals to be lowered in energy so that Δ_o is increased.

2.3 Symmetry and Molecular Orbital Formation

Construction of the molecular orbitals of a complex, requires determining their shape, by which we mean the contributions of the metal and ligand orbitals to each one, as well as their relative energies.

Good knowledge of the symmetry [4, pp. 245] properties of these orbitals allows us to simplify the construction of these diagrams very considerably. If the two orbitals have the same symmetry properties, their overlap is non-zero and an interaction can occur.

Usually in its interaction the metal ion uses 9 atomic orbitals derived from $3d$, $4s$, and $4p$. The $3d$ contributes 5 atomic orbitals, $4s$ contributes 1 atomic orbital while the $4p$ contributes 3 yielding a total of nine atomic orbitals. These ones usually form the left side of the octahedral molecular orbital diagram.

According to group these atomic orbitals are labelled according to how they transform in the O_h point group. The orientation of the t_{2g} set is such that they transform as the t_{2g} irrep. The other set has an e_g symmetry. The $4s$ orbital transform as the a_1 irrep. while the $4p$ atomic orbitals transform as the t_{1u} irrep.

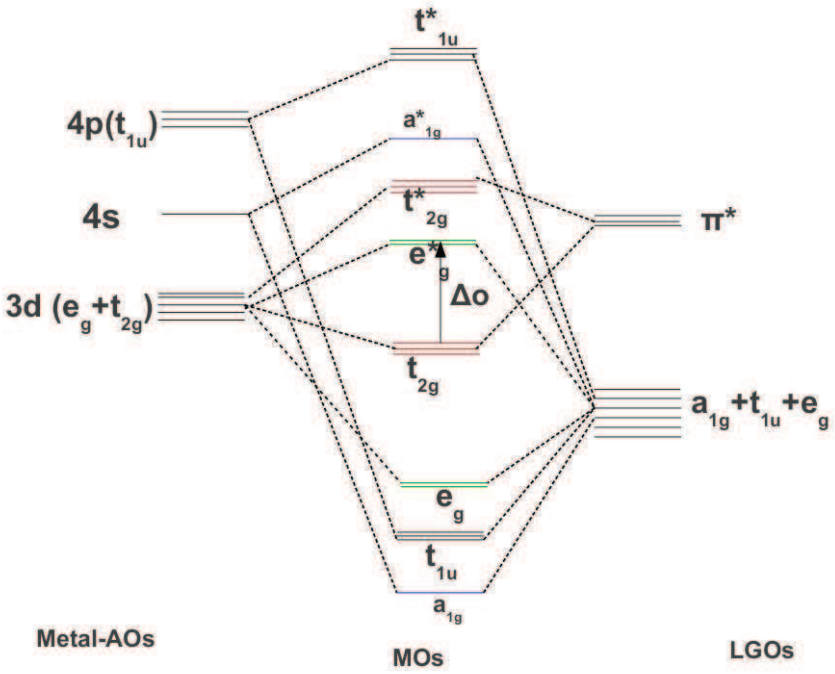

Figure 2.2: π and σ molecular orbitals in an octahedral complex

Group theory [1, pp. 114] knowledge helps in the formulation of the the so-called symmetry adapted linear combinations of the ligand σ orbitals. These ones as already mentioned, are six and on the molecular orbital diagrams are ordered according to their energies. An important outcome of this undertaking is that molecular orbitals are formed. These are labelled as a_{1g} and t_{1u} accordingly. These molecular orbitals form both bonding and their corresponding antibonding types.

In a general sense, there will result six bonding molecular orbitals, three degenerate nonbonding molecular orbitals, and six antibonding molecular orbitals in all octahedral complexes [3, pp. 45]. It is important to note that the lowest antibonding molecular orbitals (situated above the nonbonding t_{2g} orbitals) are always the two degenerate e_g orbitals. This is so because they involve the metal d orbitals, which are lower in energy than the s and p orbitals which contribute to the antibonding molecular orbitals a_{1g} and t_{1u}, respectively. However, the energetic ordering given in both the bonding and antibonding molecular orbitals can change depending on the nature of the metal and the ligands. For example, the bonding level e_g can be found between the bonding a_{1g} and t_{1u} levels, or the antibonding a_{1g} may be placed lower than the antibonding t_{1u} level.

The t_{2g} set usually remain unaffected and remain nonbonding molecular orbital unless they participate in π bonding in suitably oriented orbitals from the ligand, in a process referred to as backbonding.

In most of the synthesis, one usually ends up with complexes that are not exactly octahedral because they usually assume a distorted geometry. This distortion lowers symmetry [6, pp. 106] and this will have the result of lifting degeneracy of certain molecular orbitals when the O_h point group is maintained as the

reference. This is what results in D_3 complexes such as the famous $[Ru(bpy)_3]^{3+}$ and other even lower symmetry complexes that we have in our study.

In order to explain electronic transitions in complexes correctly, we must consider the fact that in pseudooctahedral complexes, there are many intervening π^* molecular orbitals between the t_{2g} and the e_g metal-based molecular orbitals. This argument then takes us to a more correct representation of molecular orbitals as seen in figure 2.3. Figure 9.2 shows a number of π^* molecular orbitals between the t_{2g} and e_g. Besides, there is alot of splitting of these two mainly metal-centered molecular orbitals.

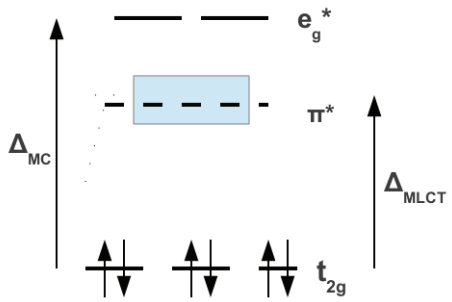

Figure 2.3: Ordering Molecular orbitals in an octahedral complex

With the observations made earlier about the mixing of both σ and π bond types and also that a number of intervening π^* exist between the t_{2g} and e_g^* it is easy to see that the correct electronic transitions in such complexes is best represented by figure 2.4.

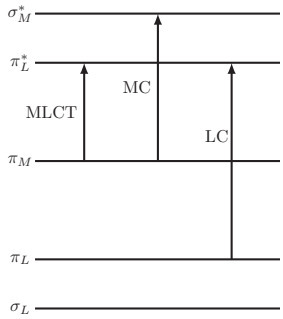

Figure 2.4: Possible electronic transitions between different MOs that lead to MLCT, LLCT and even d-d transition types

References

[1] F. A. Cotton, *Chemical Applications of Group Theory*. New York: John Wiley & Sons, 1990.

[2] G. A. Lawrance, *Introduction to Coordination Chemistry*. Callaghan, NSW, Australia: A John Wiley and Sons, Ltd., Publication, 2010.

[3] Y. Jean, *Molecular Orbitals of Transition Metal Complexes*. New College, Oxford, UK: Oxford University Press, 2004.

[4] D. M. Bishop, *Group Theory and Chemistry*. New York: Dover Publications, 1973.

[5] M. E. Eberhart, K. Johnson, D. Adler, R. O'Handley, and M. McHenry, "The Jahn-Teller Effect and Icosahedral Stability in Metallic Glasses," *J. Non-Cryst. Solids*, vol. 75, pp. 97–102, 1985.

[6] C. J. Jones, *d-and f-block Chemistry*. New York: Wiley Interscience, 2002.

[7] P. A. Cox, *Instant Notes: Inorganic Chemistry* 2^{nd}. LONDON AND NEW YORK: Garland Science/BIOS Scientific Publishers, 2004.

CHAPTER 3

WAVE FUNCTION-BASED ELECTRONIC STRUCTURE THEORY

Quantum mechanics is almost always formulated in terms of wavefunctions, so it makes sense to begin with this more familiar approach before discussing the density-based theory in the next few chapters. Quite a few concepts are presented in this chapter which go from the basic interpretation of quantum mechanics, to concepts arising from common and conceptually useful approximations, to numerical methods for solving the Schrödinger equation.

3.1 Quantum Mechanics and the Schrödinger Equation

Quantum mechanics grew from the realization that observations such as black-body radiation, the photoelectric effect and the ultraviolet catastrophe [1] could not be explained based upon the established physical theories of the end of the 19^{th} century. Following these observations, it was realized that light, which was considered to be a wave, also had a particle-like nature. These particles are known as photons and have the energy,

$$E_{photon} = h\nu\,, \tag{3.1}$$

where h is Planck's constant and ν is the frequency of the light. It was then noted that an electron which had been considered only as a particle could have wave-like nature as evidenced, for example, by the diffraction of electrons off surfaces. The wavelength of the wave is given by the de Broglie wavelength,

$$\lambda = \frac{p}{h}\,, \tag{3.2}$$

where,

$$\vec{p} = m\vec{c}\,, \tag{3.3}$$

is the particle momentum (whose magnitude is p). We thus see the birth of the particle-wave duality in quantum mechanics. It has taken many years to develop a clear understanding of this duality and some controversy over the exact interpretation of quantum mechanics remains. However, the most generally accepted interpretation is the Copenhagen one.

According to the Copenhagen interpretation of modern quantum mechanics, the state of the system *before making an observation* is described by a wave—that is, by a probability amplitude known as the wave function. For simplicity we will just consider a single particle and denote the wave function as $\psi(\vec{\mathbf{r}},t)$. However, *what is actually observed is a particle*. The probability density for finding the particle at position $\vec{r}$ is $|\psi(\vec{r},t)|^2$. Since there is a 100% probability of finding the particle somewhere, then the wave function is normalized so that,

$$\int |\psi(\vec{r},t)|^2 \, d\vec{r} = 1 \,. \tag{3.4}$$

The probability distribution for other physical observables is a bit more complicated to explain. To each classical expression of the observable, $A(\vec{r},\vec{p})$, there is a corresponding quantum mechanical operator, $\hat{A}$ made by replacing the cartessian position coordinates with the corresponding multiplication opertors,

$$\begin{aligned} x &\rightarrow \hat{x} = x\cdot \\ y &\rightarrow \hat{y} = y\cdot \\ z &\rightarrow \hat{z} = z\cdot \,, \end{aligned} \tag{3.5}$$

and by replacing the cartessian momentum coordinates with the corresponding differential operators,

$$\begin{aligned} p_x = mv_x &\rightarrow \hat{p}_x = -i\hbar\frac{\partial}{\partial x} \\ p_y = mv_y &\rightarrow \hat{p}_y = -i\hbar\frac{\partial}{\partial y} \\ p_z = mv_z &\rightarrow \hat{p}_z = -i\hbar\frac{\partial}{\partial z} \,, \end{aligned} \tag{3.6}$$

where,

$$\hbar = \frac{h}{2\pi} \,. \tag{3.7}$$

An example is the energy. Its classical expression is the sum of the kinetic and potential energies,

$$E = \frac{p^2}{2m} + V(\vec{r}) \,. \tag{3.8}$$

The corresponding quantum mechanical operator is the hamiltonian,

$$\hat{H} = -\frac{\hbar^2}{2m}\nabla^2 + V(\vec{r}) \,. \tag{3.9}$$

Now it is a principle of quantum mechanics that only the eigenvalues of the operator corresponding to an observable will actually be measured. Thus, for example, the only energies that can be observed[1] are those which satisfy the eigenvalue equation,

$$\hat{H}\psi_i(\vec{r}) = E_i\psi_i(\vec{r}) \,. \tag{3.10}$$

[1]Strictly speaking, only energy differences are observables. However, fixing the arbitrary energy zero at some physical value, such as the completely dissociated system, means that "absolute" energies on this energy scale are really given by energy differences with respect to the predefined energy zero.

That is, we can only actually measure one of the E_i. The probability $p_i(t)$ of observing E_i at time t is given by the square of the expansion coefficient,

$$p_i(t) = |c_i(t)|^2 , \tag{3.11}$$

where,

$$\psi(\vec{r},t) = \sum_i \psi_i(\vec{r}) c_i(t) . \tag{3.12}$$

Notice that this implicitly assumes that the eigenfunctions of every observable form a complete basis set which can be used to expand any observable. This, in fact, is just another postulate of quantum mechanics.

Let us do this over using a biased notation for a more general example. For an arbitrary operator $\hat{\Omega}$, its operation on its eigenfunction f_n, yields the eigenvalue ω_n,

$$\hat{\Omega} f_n = \omega_n f_n . \tag{3.13}$$

It can be shown that it is always possible to chose these eigenfunctions as orthonormal in the sense,

$$\langle f_m | f_n \rangle = \delta_{m,n} \equiv \begin{cases} 1 \; ; \; m = n \\ 0 \; ; \; m \neq n \end{cases} , \tag{3.14}$$

where the bra-ket notation is defined by,

$$\langle f | g \rangle = \int f^*(\vec{r}) g(\vec{r}) \, d\vec{r} . \tag{3.15}$$

We may then find the expansion coefficients in,

$$\psi(\vec{r},t) = \sum_n f_n(\vec{r}) c_n(t) \tag{3.16}$$

by left multiplying by $f_m^*(\vec{r})$ and integrating over $\vec{r}$ ("multigration"),

$$\langle f_m | \psi(t) \rangle = c_m(t) . \tag{3.17}$$

Notice how the $c_n(t)$ are then just another representation of $\psi(\vec{r},t)$. Dirac proposed to represent the state of the system by a generalized "ket" abstract vector $|\psi(t)\rangle$. The eigenfunctions of $\hat{\Omega}$ are also represented by ket vectors,

$$\hat{\Omega} | f_n \rangle = \omega_n | f_n \rangle . \tag{3.18}$$

We may expand our state vector,

$$|\psi(t)\rangle = \sum_n |f_n\rangle c_n(t) = \left(|f_1\rangle \; |f_2\rangle \; \cdots \; |f_n\rangle \right) \begin{pmatrix} c_1(t) \\ c_2(t) \\ \vdots \\ c_n(t) \end{pmatrix} , \tag{3.19}$$

and determine the coefficient as the projection of $|\psi(t)\rangle$ onto $|f_n\rangle$,

$$c_n(t) = \langle f_n | \psi(t) \rangle . \tag{3.20}$$

The dual abstract vector,

$$\langle\psi(t)| = \left(\, c_1^*(t)\; c_2^*(t)\; \cdots\; c_n^*(t)\,\right) \begin{pmatrix} \langle f_1| \\ \langle f_2| \\ \vdots \\ \langle f_n \end{pmatrix}, \tag{3.21}$$

is called the "bra."

Notice also that the quantum mechanical state of a system is actually an ensemble quantity since it describes the probability of observing different values of an observable ω_n associated with different systems (designated by the index n) in the ensemble. The expectation value is the mean value over the ensemble,

$$\langle\psi(t)|\hat{\Omega}|\psi(t)\rangle = \sum_n |c_n(t)|^2 \omega_n\,. \tag{3.22}$$

Also the classical limit of quantum mechanics is not just classical mechanics, but rather classical statistical mechanics. This is why the correspondance principle tells us that a quantum mechanical expectation value is something like a time-average value in the classical limit.

We have not yet explained from whence comes the wave function. In 1925, Erwin Schrödinger formulated his famous equation, whose most general form is the time-dependent one,

$$\left(-\frac{\hbar^2}{2m_e}\nabla^2 + V(\vec{r})\right)\psi(\vec{r},t) = i\hbar\frac{\partial}{\partial t}\psi(\vec{r},t)\,. \tag{3.23}$$

Once again, for the sake of simplicity, we consider only one particle. This general equation has stationary-state solutions,

$$\psi(\vec{r},t) = \psi(\vec{r})e^{-iEt/\hbar}\,, \tag{3.24}$$

which satisfy the time-independent Schrödinger equation,

$$\left(-\frac{\hbar^2}{2m_e}\nabla^2 + V(\vec{r})\right)\psi(\vec{r}) = E\,\psi(\vec{r})\,. \tag{3.25}$$

We see that the time-independent Schrödinger equation is a key step determining which energies are observable and with what probability they may be observed.

3.2 Many-Particle Problem and Born-Oppenheimer Separation

A molecule with N electrons and K nuclei is a complex many-body problem. The corresponding Schrödinger equation is,

$$\hat{H}(\mathbf{r},\mathbf{R})\Psi(\mathbf{x},\mathbf{R},t) = i\hbar\frac{\partial}{\partial}\Psi(\mathbf{x},\mathbf{R},t)\,. \tag{3.26}$$

Here, $\mathbf{r} = (\vec{r}_1,\vec{r}_2,\cdots,\vec{r}_N)$ is the matrix whose columns are the position vectors of the different electrons, $\mathbf{R} = (\vec{R}_1,\vec{R}_2,\cdots,\vec{R}_K)$ is the matrix whose columns are the position vectors of the different nuclei. Also $\mathbf{x} = (\vec{x}_1,\vec{x}_2,\cdots,\vec{x}_N)$ is the matrix made up of generalized spatial and spin coordinates, $\vec{x} = (\vec{r},\sigma)$. The nonrelativistic Hamiltonian operator is given by,

$$\hat{H}(\mathbf{r},\mathbf{R}) = \hat{T}_N(\mathbf{R}) + \hat{T}_e(\mathbf{r},\mathbf{R}) + \hat{V}_{N,el}(\mathbf{r},\mathbf{R}) + \hat{V}_{e,e}(\mathbf{r}) + \hat{V}_{N,N}(\mathbf{R})\,, \tag{3.27}$$

where the different terms correspond to the nuclear,

$$\hat{T}_N(\mathbf{R}) = -\sum_A \frac{\hbar^2}{2M_A}\left(\frac{\partial^2}{\partial x_A^2} + \frac{\partial^2}{\partial y_A^2} + \frac{\partial^2}{\partial z_A^2}\right) \tag{3.28}$$

$$= -\sum \frac{\hbar^2}{2M_A}\nabla_A^2\,, \tag{3.29}$$

where M_A is the mass of nucleus A, and electronic kinetic energy operators,

$$\hat{T}_e(\mathbf{r}) = -\frac{\hbar^2}{2m_e}\sum_i\left(\frac{\partial^2}{\partial x_i^2} + \frac{\partial^2}{\partial y_i^2} + \frac{\partial^2}{\partial z_i^2}\right) \tag{3.30}$$

$$= -\frac{\hbar^2}{2m}\sum_i \nabla_i^2\,, \tag{3.31}$$

the nuclear-nuclear repulsion,

$$\hat{V}_{N,N}(\mathbf{R}) = +\sum_{A,B}^{A<B} Z_A Z_B \frac{e^2}{R_{A,B}}\,, \tag{3.32}$$

where Z_A is the atomic number of nucleus A and $R_{A,B} = |\vec{R}_A - \vec{R}_B|$ is the distance between nuclei A and B, the electron-nuclear attraction,

$$\hat{V}_{N,e}(\mathbf{r},\mathbf{R}) = -\sum_A\sum_i Z_A \frac{e^2}{r_{A,i}}\,, \tag{3.33}$$

where $r_{A,i} = |\vec{r}_i - \vec{R}_A|$ is the distance between electron i and nucleus A, and the electron-electron repulsion,

$$\hat{V}_{e,e}(\mathbf{r}) = +\sum_{i,j}^{i<j} \frac{e^2}{r_{i,j}}\,, \tag{3.34}$$

where $r_{i,j} = |\vec{r}_i - \vec{r}_j|$ is the distance between electrons i and j.

Notice that we are using Gaussian electromagnetic units (otherwise there would be factors of $4\pi\varepsilon_0$). One reason for doing this is that it is habitual for theorists to write their equations in atomic units which are based upon Gaussian units rather than SI units. The idea is to use a principle of dimensional analysis that it takes only three quantities to define all the other units. In atomic units, these are $\hbar$, m_e, and e and all take on values of one in atomic mass units.

Notice also that this Hamiltonian is itself an approximation. Not included are, for example, (i) any relativistic correction to the kinetic energy, (ii) interaction of magnetic moments (orbit/orbit, spin/orbit, spin/spin) [2], and (iii) any interaction with external electric and magnetic fields. However, the Hamiltonian we are using suffices for many types of calculations and often extra terms can simply be added when needed.

As it stands we have both a gigantic computational and conceptual problem. Part of the problem is solved by making the Born-Oppenheimer approximation. This is based upon the idea of a separation of time scales: the electrons are much lighter than the nuclei and therefore move much faster. We will assume that they instantaneously adjust to each new position of the nuclei. Consequently we may define an electronic Schrödinger equation,

$$\hat{H}_e(\mathbf{r};\mathbf{R})\Psi_I^e(\mathbf{x};\mathbf{R}) = E_I^e(\mathbf{R})\Psi_I^e(\mathbf{x};\mathbf{R})\,, \tag{3.35}$$

where the electronic hamiltonian is just given by,

$$\hat{H}_e(\mathbf{r};\mathbf{R}) = \hat{T}_e(\mathbf{r}) + V_{N,e}(\mathbf{r};\mathbf{R}) + V_{e,e}(\mathbf{r})\,. \tag{3.36}$$

The semicolon (;) is used deliberately to show that $\mathbf{R}$ is a parameter. That is, the electronic problem is solved for a given set of fixed nuclear positions. Then, if desired, the nuclei are moved and the electronic problem is resolved for the new set of nuclear positions.

In the Born-Oppenheimer approximation, it is the mean field of the fast-moving electrons which bind the molecule together. The nuclei move in the potential,

$$V_I^N(\mathbf{R}) = V_{N,N}(\mathbf{R}) + E_I^e(\mathbf{R})\,, \tag{3.37}$$

according to the time-dependent Schrödinger equation,

$$\hat{H}_I^N(\mathbf{R})\chi_{n,I}(\mathbf{R},t) = -i\hbar\frac{\partial}{\partial t}\chi_{n,I}(\mathbf{R},t)\,, \tag{3.38}$$

where the nuclear Hamiltonian,

$$\hat{H}_I^N(\mathbf{R}) = \hat{T}_N(\mathbf{R}) + V_I^N(\mathbf{R})\,. \tag{3.39}$$

Notice that this is for Born-Oppenheimer dynamics (also called adiabatic dynamics) where the electronic state of the molecule remains fixed at the Ith state. The total wave function in the Born-Oppenheimer approximation is,

$$\Psi(\mathbf{r},\mathbf{R},t) = \chi_{n,I}(\mathbf{R},t)\Psi_I^e(\mathbf{r};\mathbf{R})\,. \tag{3.40}$$

3.3 More About the Nuclear Problem

The quantity $V_I^N(\mathbf{R})$ is very important. It is often referred to as the potential energy surface (PES) of the molecule. For a K-atom molecule there are $3K$ degrees of freedom of which 3 correspond to center of mass motion and another 3 correspond to rotations about the center of mass (only 2 if the molecule is linear). Thus the PES is really an energy-valued function of $3K-6$ ($3K-5$ for a linear molecule) internal degrees of freedom and so is really a hypersurface which requires $3K-5$ ($3K-4$ for a linear molecule) coordinates to plot (one extra for V_I^N itself). Nevertheless, the minima on the PES tell us the equilibrium geometries of stable species while saddle points give us information about transition states. In particular, geometry optimizations typically seek to find the global minimum for a given molecule. This must then be proven by showing that gradients (i.e., forces) are zero and that the curvature of the surface (corresponding to vibrational frequencies) are all real and positive. If not, then it is not a true minimum.

Note however that finding a minimum does not guarantee having found the global minimum since the minimum found may only be a local minimum on the global PES.

Changes in bond length and in the angles between chemical bonds provide the most significant and physically meaningful set of coordinates for the description of potential energy. These coordinates are called "internal coordinates" since they describe just the internal motions of the molecule—i.e., molecular vibrations. The types of internal coordinates which are generally used are the following:

- Bond stretching coordinate: variation of the length of a chemical bond
- In-plane bending coordinate: variation of the angle between two chemical bonds having one atom in common.

- Out-plane bending coordinate: variation of the angle between the plane defined by two bonds with one atom in common and a third bond connected to the common atom.

- Torsional coordinate: This is variation in the dihedral angle between the planes determined by three consecutive bonds connecting four atoms.

Since the variations in bond length and angles in a molecule can be written in terms of the variation in the cartesian displacement coordinates of the atoms, the problem we have to face is that one of writing the explicit form of the transformation from cartesian coordinates to the new set of internal coordinates.

Given s_k as a generic coordinate, the most general relation between s_k and the cartesian coordinates can be written in the form

$$s_k = \sum_i B_i^k x_i + \frac{1}{2}\sum_{ij} B_{ij}^k x_i x_j + \text{ higher terms} \tag{3.41}$$

where the coefficients $B_i^k x_i, B_{ij}^k$ etc, are determined by the molecular geometry. A drastic simplification can be achieved if we restrict our treatment to the case of infinitesimal amplitudes of vibration where we can drop all terms not linear in $\vec{x}$. If we call $\vec{s}$ and $\vec{x}$ the vectors whose components are the internal and the cartesian coordinates, then the linear equation in matrix notation is

$$\vec{s} = \mathbf{B}\vec{x}, \tag{3.42}$$

where $\mathbf{B}$ is the matrix whose elements are $B_{k,i} = B_i^k$. The matrix $\mathbf{B}$ is not in general a square matrix. The translations and rotations are not included in the set of internal coordinates which describe, by definition a molecular motion in which the relative positions of the atoms are not changed. Since $\mathbf{B}$ is not a square matrix, it can not be inverted. We can always include in the s-vector six additional coordinates to describe the three translations and the three rotations.

A special choice of internal coordinates [3, 4] often used as input to quantum chemical programs is the Z-matrix. The Z-matrix of a molecule is built from a list of the atoms. The coordinates of each new atom (A) are characterised by:

1. The distance to another, already defined atom B

2. The angle between the bond to atom B and the bond of atom B to an already defined atom C.

3. The dihedral angle between A,B,C and an already defined atom D.

The Z-matrix of a molecule is not unique. There are many different possibilities to order the atoms and to define distances, angles and dihedrals.

3.4 The Electronic Problem and Approximation Methods

To optimize the geometry of a molecule we need the PES and to get the PES we need to solve the electronic problem,

$$\hat{H}_e(\mathbf{r};\mathbf{R})\Psi_I^e(\mathbf{x};\mathbf{R}) = E_I^e(\mathbf{R})\Psi_I^e(\mathbf{x};\mathbf{R})\,. \tag{3.43}$$

Let us simplify the notation to write this same equation as just,

$$\hat{H}\Psi_I(\mathbf{x}) = E_I\Psi_I(\mathbf{x})\,. \tag{3.44}$$

This must be solved according to the Pauli principle which states that the total wave function must change sign when any two electrons are transposed,

$$\Psi(\vec{x}_1,\vec{x}_2,\cdots,\vec{x}_j,\cdots,\vec{x}_i,\cdots,\vec{x}_N) = -\Psi(\vec{x}_1,\vec{x}_2,\cdots,\vec{x}_i,\cdots,\vec{x}_j,\cdots,\vec{x}_N)\,, \tag{3.45}$$

since electrons are fermions. The most general such solution may be expressed as the linear combination of all possible Slater determinants [5],

$$|i_1 i_2 \cdots i_N| = \frac{1}{\sqrt{N!}} \begin{vmatrix} \psi_{i_1}(\vec{x}_1) & \psi_{i_2}(\vec{x}_1) & \cdots & \psi_{i_N}(\vec{x}_1) \\ \psi_{i_1}(\vec{x}_2) & \psi_{i_2}(\vec{x}_2) & \cdots & \psi_{i_N}(\vec{x}_2) \\ \vdots & \vdots & \ddots & \vdots \\ \psi_{i_1}(\vec{x}_N) & \psi_{i_2}(\vec{x}_N) & \cdots & \psi_{i_N}(\vec{x}_N) \end{vmatrix}, \tag{3.46}$$

of orthonormal spin-orbitals, $\psi_i(\vec{x})$. Typically these orthonormal spin-orbitals are taken as the solution to some one-electron problem. When both the set of spin-orbitals is complete (and hence infinite) and the set of Slater determinants is complete (and hence infinite), then one speaks of complete configuration interaction (complete CI) and the expansion is exact.

Even the time-independent Schrödinger equation can only be solved exactly for relatively few systems, such as the particle in a box, the hydrogen atom, the rigid rotor, and the harmonic and Morse oscillators. If we allow accurate numerical solutions, we can include pretty much any one-dimensional system (e.g., the vibrational wave function of a diatomic molecule, provided the potential is known) and the hydrogen molecule cation, H_2^+. More generally, crudely speaking, "exact solutions" are usually useless because either (i) they are simply unattainable or (ii) may require approximations in order to extract a physical or chemical interpretation. To go further, we need approximations and some way of judging which approximations should be better than others. For this reason we need approximations. There are two main classes of approximation methods in quantum mechanics, namely the variational principle and perturbation theory.

3.4.1 Variational Principle

The variational principle tells us how we can begin with some guessed form for the wave function and optimize it. The variational theorem says that any trial wave function, $\Psi(\mathbf{x})$, satisfying the physical boundary conditions of our problem is an upper bound on the exact ground state energy,

$$E_0 \leq \frac{\langle\Psi|\hat{H}|\Psi\rangle}{\langle\Psi|\Psi\rangle}\,. \tag{3.47}$$

Put another way,

$$E_0 = \min_{\Psi} \frac{\langle\Psi|\hat{H}|\Psi\rangle}{\langle\Psi|\Psi\rangle}\,, \tag{3.48}$$

but only if the variation is over all possible wave functions, Ψ, otherwise,

$$E_0 \leq E_\Psi = \min_{\Psi} \frac{\langle\Psi|\hat{H}|\Psi\rangle}{\langle\Psi|\Psi\rangle}\,, \tag{3.49}$$

An example application of the variational principle is truncated CI where we keep only a finite number, M, of terms of the (infinite) complete CI expansion,

$$\Psi = \sum_{I=1}^{M} \Phi_I C_I \,, \tag{3.50}$$

where the Φ_I are a set of orthonormal Slater determinants. The coefficients C_I are varied until the minimal value of the energy expectation value E_Ψ is found. In general Ψ is not normalized, so we must minimize,

$$E = \frac{A}{B} \,, \tag{3.51}$$

where,

$$A = \langle \Psi | \hat{H} | \Psi \rangle = \sum_K \sum_J C_K^* \langle \Phi_K | \hat{H} \Phi_j \rangle C_J \,, \tag{3.52}$$

and,

$$B = \langle \Psi | \Psi \rangle = \sum_K \sum_J C_K^* \langle \Phi_K | \Phi_J \rangle C_J \,. \tag{3.53}$$

Minimisation of E_ψ with respect to the variational parameters C_I,

$$\frac{\partial E_\psi}{\partial C_I} = 0 \,, \tag{3.54}$$

for $I = 1, 2, \ldots, M$, gives,

$$\frac{\partial E_\psi}{\partial C_I} = \frac{1}{B^2} (B \frac{\partial A}{\partial C_I} - A \frac{\partial B}{\partial C_I}) \tag{3.55}$$

$$= \frac{1}{B} (\frac{\partial A}{\partial C_I} - \frac{A}{B} \frac{\partial B}{\partial C_I}) \tag{3.56}$$

$$= 0 \,. \tag{3.57}$$

Because $B \neq 0$ (normalisation integral) and with $E_\psi = A/B$ we get

$$\frac{\partial A}{\partial C_I} - E_\psi \frac{\partial B}{\partial C_I} = 0 \,. \tag{3.58}$$

Which gives the generalised eigenvalue equation,

$$\sum_J (H_{I,J} - E_\Psi S_{I,J}) C_J = 0 \,, \tag{3.59}$$

for $i = 1, 2, \ldots, M$. Here we have introduced the Hamiltonian matrix whose matrix elements are defined by,

$$H_{K,J} = \langle \Phi_K | \hat{H} \Phi_J \rangle = H_{J,K}^* \,, \tag{3.60}$$

and the overlap matrix whose matrix elements are defined by,

$$S_{K,J} = \langle \Phi_K | \Phi_J \rangle \,. \tag{3.61}$$

Thus,

$$\sum_J H_{I,J} C_J = E_\Psi \sum_J S_{I,J} C_J \,, \tag{3.62}$$

may be written in matrix form as,

$$\mathbf{H}\vec{C} = E_\Psi \mathbf{S}\vec{C}\,. \tag{3.63}$$

In the CI problem, almost always $\mathbf{S} = \mathbf{1}$ because the determinants are constructed to be orthonormal. However the variational principle will also be applied to solving the Hartree-Fock equations (*vide infra*) where $\mathbf{S} \neq \mathbf{1}$.

The solution of this equation gives M energies E_K, where the lowest value is a variational upper bound to the true ground state energy. In fact, the lower the value of E_ψ, the closer we are to the true ground state energy. Hence we have a criterion for judging the relative quality of different approximate solutions. Very interestingly, in the case of linear variations, we have what mathematicians refer to as Cayley's and what physicists refer to as the Hylleraas-Undheim-MacDonald interleaving theorem which says that the K^{th} approximate energy is always an exact upper bound to the exact K^{th} energy [6].

We may also extract an approximate wave function. For each energy E_K, we get after inserting in the system of linear equations the coefficients $C_{J,K}$ and therefore the corresponding wavefunction Ψ_K.

3.4.2 Perturbation Theory

Perturbation theory [7] provides a second systematic way to find approximate solutions to some problem. The perturbations may either be real (e.g., an applied electric field) or fictive (e.g., electron repulsions). Later we will use time-dependent perturbation theory to find excited states from time-dependent density-functional theory. We content ourselves here with (time-independent) nondegenerate Rayleigh-Schrödinger perturbation theory.

It is assumed that we know the exact wave functions $\Psi_I^{(0)}$ and corresponding energies, $E_I(0)$, for some unperturbed (real or model) system with Hamiltonian $\hat{H}^{(0)}$,

$$\hat{H}^{(0)}\Psi_I^{(0)} = E_I^{(0)}\Psi_I^{(0)}\,. \tag{3.64}$$

We want to use this solution to solve a similar but different problem, namely,

$$\hat{H}\Psi_I = E_I\Psi_I\,, \tag{3.65}$$

where,

$$\hat{H} = \hat{H}^{(0)} + \lambda\hat{H}^{(1)}\,. \tag{3.66}$$

The quantity, $\hat{H}^{(1)}$, is the perturbation, and λ is its strength. When the perturbation is real—such as the case of an applied electric field—then λ may correspond to a real physical parameter which can be varied experimentally. In the case of a fictitious perturbation, typically λ is just a formal parameter which will be set to one at the end of the calculation. Both the energies,

$$E_I = E_I^{(0)} + \lambda E_I^{(1)} + \lambda^2 E_I^{(2)} + \lambda^3 E_I^{(3)} + \cdots\,, \tag{3.67}$$

and the wave function,

$$\Psi_I = \Psi_I^{(0)} + \lambda\Psi_I^{(1)} + \lambda^2\Psi_I^{(2)} + \lambda^3\Psi_I^{(3)} + \cdots\,, \tag{3.68}$$

are expanded in λ. These are then inserted into Eq. (3.66) which is then regrouped according to powers of λ to obtain a hierarchy of equations to be solved for the different orders of perturbation theory using the intermediate normalisation,

$$\langle\Psi_I|\Psi_I^{(0)}\rangle = 1\,, \tag{3.69}$$

For example,

$$E_I^{(p)} = \langle \Psi_I^{(0)} | \hat{H}^{(1)} | \Psi_I^{(p-1)} \rangle \,, \tag{3.70}$$

which gives us our first-order correction to the energy,

$$E_I^{(1)} = \langle \Psi_I^{(0)} | \hat{H}^{(1)} | \Psi_I^{(0)} \rangle \,, \tag{3.71}$$

The first-order correction to the wave function turns out to be,

$$\Psi_I^{(1)} = \sum_J^{J \neq I} \Psi_J^{(0)} \frac{\langle \Psi_J^{(0)} | \hat{H}^{(1)} | \Psi_I^{(0)} \rangle}{E_I^{(0)} - E_J^{(0)}} \,. \tag{3.72}$$

3.5 Hartree-Fock Approximation

One of the oldest useful approach for treating the many-electron problem is due to Hartree who used it for calculating ionization potentials [8]. The wave function in this approach is given by a simple product,

$$\Psi(\mathbf{x}) = \psi_1(\vec{x}_1)\psi_2(\vec{x}_2)\psi_3(\vec{x}_3)....\psi_n(\vec{x}_n) \,, \tag{3.73}$$

and is known as a Hartree product. Since such a wave function violates the Pauli principle, requiring that the wave function be antisymmetric with respect to any transposition of electrons, Fock replaced the Hartree product with a single determinant built from orthonormal spin orbitals, $\psi(\vec{x})$. The generalized Hartree-Fock (GHF) method consists of finding the energy and orbitals which minimize the variational integral.

More commonly an additional collinear spin approximation is made that the spin of each electron is either oriented up (spin α) so that,

$$\psi(\vec{x}) = \psi_\alpha(\vec{r})\alpha(\sigma) \,, \tag{3.74}$$

or oriented down (spin β) so that,

$$\psi(\vec{x}) = \psi_\beta(\vec{r})\beta(\sigma) \,, \tag{3.75}$$

We thus have different (spatial) orbitals for different spin (DODS). This defines the (spin) unrestricted Hartree-Fock (UHF) method.

If, in addition, we make the approximation of having the same (spatial) orbitals for different spin (SODS), then we may write,

$$\begin{aligned} \psi(\vec{x}) &= \psi(\vec{r})\alpha(\sigma) \\ \bar{\psi}(\vec{x}) &= \psi(\vec{r})\beta(\sigma) \,, \end{aligned} \tag{3.76}$$

where we have introduced the bar notation to distinguish between spin α and spin β spin-orbitals. This defines the (spin) restricted Hartree-Fock (RHF) method.

We are now in a position to understand the Pauli exclusion principle. This principle states that we may only put at most two electrons in a spatial orbital and then only if the two spins are different. This is automatically obeyed by the Hartree-Fock Slater determinant because as soon as two spin-orbitals have the spatial and spin part, then two columns of the Slater determinant will be identical and the wave function will be identically equal to zero (i.e., must be disallowed because it is no longer properly normalizable).

Another observation has to do with spin. Slater determinants are always eigenfunctions of $\hat{S}_z$. However, they are not necessarily eigenfunctions of $\hat{S}^2$ unless linear combinations of two or more Slater

determinants are taken. Such spin-adapted linear combination of determinants (configurations) are often needed to describe open-shell systems. An exception is found in closed-shell systems where the spins of all electrons are paired.

$$\Psi(\vec{x}_1,\vec{x}_2,\cdots,\vec{x}_N) = |\psi_1,\bar{\psi}_1,\psi_2,\bar{\psi}_2,\cdots,\psi_{N/2}\bar{\psi}_{N/2}|\,. \tag{3.77}$$

This RHF Slater determinant is an eigenfunction of $\hat{S}_z$ and $\hat{S}^2$ with $S = M_s$=0

We wish now to find the variationally best Slater determinant. We will work with spin-orbitals as in the GHF for simplicity of notation. The electronic energy,

$$\begin{aligned} E &= \sum_{i=1}^{N} h_{i,i} + \sum_{i,j=1,N}^{i<j} (J_{i,j} - K_{ij}) \\ &= \sum_{i=1}^{N} h_{i,i} + \frac{1}{2}\sum_{i,j=1,N} (J_{i,j} - K_{ij})\,, \end{aligned} \tag{3.78}$$

is the expectation value of the non-relativistic electronic Hamiltonian operator $\hat{H}$ with respect to the N-electron Slater determinant of orthonormal spin-orbitals. Here, the one-electron integrals over the core hamiltonian consisting of the electron kinetic energy plus the attraction to the nuclei have been denoted as,

$$h_{i,i} = \langle\psi_i|\hat{h}|\psi_i\rangle\,, \tag{3.79}$$

the Coulomb integrals are denoted by,

$$J_{i,j} = \int\int \psi_i^*(\vec{x}_1)\psi_i(\vec{x}_1)\frac{e^2}{r_{12}}\psi_j^*(\vec{x}_2)\psi_j(\vec{x}_2)\,d\vec{x}_1 d\vec{x}_2 = (ii||jj)\,, \tag{3.80}$$

and the exchange integrals are denoted by,

$$K_{i,j} = \int\int \psi_i^*(\vec{x}_1)\psi_j(\vec{x}_1)\frac{e^2}{r_{12}}\psi_i^*(\vec{x}_2)\psi_j(\vec{x}_2)\,d\vec{x}_1 d\vec{x}_2 = (ij||ji)\,. \tag{3.81}$$

Although all off these integrals have been expressed as integrals over spin-orbitals, the integration over spin reduces everything to integrals over spatial orbitals. Here we have introduced Mulliken (charge cloud) notation for electron repulsion integrals,

$$(ij||kl) = \int\int \psi_i^*(\vec{x}_1)\psi_j(\vec{x}_1)\frac{e^2}{r_{12}}\psi_k^*(\vec{x}_2)\psi_l(\vec{x}_2)\,d\vec{x}_1 d\vec{x}_2\,. \tag{3.82}$$

We must now minimize the HF energy expression [Eq. (3.78)] with respect to the constraint that the spin-orbials are orthonormal. This is most easily done using the method of Lagrange multipliers. Thus we must minimize the Lagrangian,

$$\mathscr{L} = E - \sum_{i,j}\varepsilon_{i,j}\left(\langle\psi_i|\psi_j\rangle - \delta_{i,j}\right)\,, \tag{3.83}$$

subject to spin-orbital orthonormality. The $\varepsilon_{i,j}$ are the Lagrange multipliers. Minimization gives,

$$\hat{f}\psi_i(\vec{x}) = \sum_{j=1}^{N} \varepsilon_{i,j}\psi_j(\vec{x}), \tag{3.84}$$

where $\hat{f}$ is the Fock operator, and given as

$$\hat{f} = -\frac{\hbar^2}{2m_e}\nabla^2 - \sum_{A=1}^{M}\frac{Z_A e^2}{r_{iA}} + \sum_{i=1}^{N}\left(\hat{J}_i - \hat{K}_i\right). \tag{3.85}$$

Here $\hat{J}_i$ is the Coulomb operator describig the Coulomb interaction due to an electron in a given spin-orbital and whose action on an arbitrary orbital is given by,

$$\hat{J}_i\psi(\vec{x}_1) = \left(\int \frac{e^2|\psi_i(\vec{x}_2)|^2}{r_{12}}\,d\vec{x}_2\right)\psi(\vec{x}_1). \tag{3.86}$$

The action of the exchange operator, $\hat{K}_i$, is given by,

$$\hat{K}_i\psi(\vec{x}_1) = \psi_i(\vec{x}_2)\int \frac{e^2\psi_i^*(\vec{x}_2)\psi(\vec{x}_1)}{r_{12}}\,d\vec{x}_2. \tag{3.87}$$

One of the purposes of the exchange operator is to remove a self-interaction error in the Coulomb energy because $K_{i,i} = J_{i,i}$.

It is important to notice that the operator $\hat{f}$ is hermitian and invariant to a unitary ransformation of the occupied orbitals. By choosing a unitary transformation Eq. (3.84) can be written in a diagonal form as,

$$\hat{f}\psi_i = \varepsilon_i\psi_i. \tag{3.88}$$

This is known as the canonical Hartree-Fock equation. The quantity ε_i is the energy of the spin-orbital ψ_i. The remaining task is to find those spin-orbitals which are eigenfunctions of the Fock operator.

Since the Fock operator, $\hat{f}$, depends upon the Hartree-Fock orbitals, the Hartree-Fock equations must be solved iteratively [9]. That is, one begins with an initial guess for the occupied orbitals, constructs the Fock operator, finds the new occupied orbitals from the eigenfunctions of $\hat{f}$, and so on and so forth, until convergence is reached. That is, the sequence above is stopped if the solutions in two consecutive iterations do not change (within a given tolerance). This is known as the self-consistent field (SCF) method.

We now want to discuss some of the properties of the canonical HF orbitals and orbital energies. The N spin-orbitals with the lowest orbital energies are just the spin-orbitals occupied in the determinant Φ. We will use the indices i,j,k,m,n,l for occupied orbital energies. The indices, $a,b,c,\cdots,g,h$, will be reserved for the remaining infinite number of unoccupied (or virtual) spin-orbitals with higher energies. The indices $r,s,\cdots,x,y,z$ represent orbitals which are free to be either occupiedd or unoccupied. The Fock matrix is diagonal in the basis of the canonical orbitals,

$$F_{i,j} = \langle\psi_i|\hat{f}|\psi_j\rangle = \varepsilon_i\langle\psi_i|\psi_j\rangle = \varepsilon_j\delta_{i,j}. \tag{3.89}$$

The orbital energies can be expressed as

$$\varepsilon_i = F_{i,i} \tag{3.90}$$
$$= \langle\psi_i|\hat{h}|\psi_i\rangle + \sum_k \langle\psi_i|(J_k - K_k)|\psi_i\rangle \tag{3.91}$$
$$= \langle\psi_i|\hat{h}|\psi_i\rangle + \sum_k \left(\langle\psi_i|\hat{J}_k|\psi_i\rangle - \sum_k \langle\psi_i|\hat{K}_k|\psi_i\rangle \right) \tag{3.92}$$
$$= \varepsilon_i^{(0)} + \sum_k ((ii||kk) - (ik||ki)) \,. \tag{3.93}$$

In particular we get for occupied orbitals,

$$\varepsilon_i = \varepsilon_i^{(0)} + \sum_j ((ii||jj) - (ij||ji)) \tag{3.94}$$
$$= \varepsilon_i^{(0)} + \sum_j^{j\neq i} ((ii||jj) - (ij||ji)) \,,, \tag{3.95}$$

and for virtual orbitals,

$$\varepsilon_a = \varepsilon_a^{(0)} + \sum_k ((aa||kk) - (ak||ka)) \,. \tag{3.96}$$

The occupied orbital energy ε_i represents the energy of an electron in the occupied spin-orbital ψ_i. This energy is the kinetic and the attraction to the nuclei $\varepsilon_i^{(0)}$ plus a Coulomb and exchange integration with each of the remaining $N-1$ electrons. The result for the unoccupied orbital energy, ε_a has a different character. It includes the kinetic energy and the nuclear attraction of an electron in $\varepsilon_a^{(0)}$, but includes Coulomb and exchange interactions with N electrons of the Hartree-Fock ground state. It is as if an electron has been added to the ground-state determinant, Φ, to produce an $(N+1)$-electron state. If we simply add up the orbital energies of the occupied states, we get

$$\sum_{i=1,N} \varepsilon_i = \sum_{i=1,N} \varepsilon_i^{(0)} + \sum_{j,k=1,N} ((jj||kk) - (ij||ji)) \,. \tag{3.97}$$

If we compare this with the total Hartree-Fock energy

$$E_{HF} = \sum_{i=1,N} \varepsilon_i^{(0)} + \frac{1}{2} \sum_{j,k=1,N} ((ii||jj) - (ij||ji)) \,. \tag{3.98}$$

We see that,

$$E_{HF} \neq \sum_{i=1,N} \varepsilon_i \,, \tag{3.99}$$

and that the total energy of the state Φ is not just the sum of the orbital energies. The reason is that the energy ε_i include Coulomb and exchange interactions between an electron in orbital ψ_i and electrons in all other occupied spin orbitals, in particular orbital ψ_j. But ε_j includes Coulomb and exchange interactions between an electron in ψ_j and electrons in all other occupied spin orbitals, in particular orbital ψ_i. Thus if we add ε_i and ε_j, then we include the electron-electron interactions between an electron in ψ_i and one in ψ_b twice. The sum of orbital energies counts the electron-electron interactions twice. This is the

reason for the factor $1/2$ in the correct energy expression for the total energy relative to the sum of orbital energies.

Koopmans' theorem states that, given an N-electron Hartree-Fock single determinant Φ with occupied and unoccupied (virtual) spin-orbital energies ε_i and ε_a, the ionization potential to produce an $(N-1)$-electron single determinant $\Phi_i = \hat{a}_i\Phi$ with identical spin-orbitals, obtained by removing an electron from spin-orbital ψ_i, and the electron affinity to produce an $(N+1)$-electron single determinant $\Phi^a = \hat{a}_a^\dagger\Phi$ with identical spin-orbitals, obtained by adding an electron to spinorbital ψ_a are just-ε_i and $-\varepsilon_a$, respectively. To see this, it suffices to calculate the ionization potential in the frozen orbital approximation,

$$\mathrm{IP} = {}^{N-1}E_i - {}^{N}E_0 = -\varepsilon_i\,, \tag{3.100}$$

where ${}^{N-1}E_i$ and ${}^{N}E_0$ are the expectation values of the energy of the two relevant single determinants. Occupied orbital energies are generally negative and ionisation potentials are positive. Similarly for the electron affinity,

$$\mathrm{EA} = {}^{N}E_0 - {}^{N+1}E^a = -\varepsilon_a\,. \tag{3.101}$$

This result is consistent with the earlier observation that ε_a included interactions with all N other electrons of the ground state and thus describes an $N+1$st electron.

Koopmans' ionisation potentials are reasonable first approximations to experimental ionisation potentials (missing are orbital relaxation and correlation effects which tend to cancel, at least for outer valence ionization). Koopmans' electron affinities are unfortunately often bad (because correlation and relaxation effects cancel less well). Many neutral molecules will add an electron to form a stable negative ion. Hartree-Fock calculations on neutral molecules, however, almost always give positive orbital energies for all the virtual orbitals.

Another occasionally useful observation is known as Brillouin's theorem which states that singly-excited determinants $\Phi_i^a = \hat{a}_a^\dagger\hat{i}\Phi$ constructed using canonical Hartree-Fock orbitals will not interact directly with the Hartree-Fock determinant Φ,

$$\langle\Phi|\hat{H}|\Phi_i^a\rangle = \langle i|\hat{h}|a\rangle + \sum_k\left((ia||kk) - (ik||ka)\right) = F_{i,a} = 0\,. \tag{3.102}$$

The matrix element that mixes singly-excited determinants with the ground-state determinant is thus equal to an off-diagonal element of the Fock matrix. Now, by definition, the canonical Hartree-Fock orbitals are the ones which make the matrix $\mathbf{F}$ diagonal, hence $F_{i,a} = 0$. One can say that solving the Hartree-Fock eigenvalue equation is equivalent to ensuring that the ground state determinant will not mix with any singly excited determinants.

3.6 Basis Sets and Pseudopotentials

Now that we have formulated the Hartree-Fock equations, we still have to solve them. This implies the choice of a numerical method. We will follow the usual route of quantum chemists and use a finite basis set of Gaussian-type orbitals (GTOs). However for the heavy ruthenium atom we must use a pseudopotential to include scalar relativistic effects of core electrons.

Roothaan [10] in 1951 made the Hartree-Fock approximation more practical for numerical solutions by introducing the concept of basis sets (linear combination of atomic orbitals or LCAO). The molecular orbitals are represented as a linear combination of carefully chosen three-dimensional one-electron

functions, χ_μ called "atomic orbitals" [2],

$$\phi_{i\sigma}(\vec{r}) = \sum_{\mu=1,K} \chi_\mu(\vec{r}) c^\sigma_{\mu,i}\,, \tag{3.103}$$

where K is an integer (the size of the basis set) larger than the number of electrons in the system. These occupied orbitals may be used to form Slater determinants which are then minimized with respect to the matrix of molecular orbital coefficients whose matrix elements are the coefficients $c^\sigma_{\mu,i}$. This results in a set of matrix equations. A sloppy derivation [3] of the equations is as follows: Using the basis set Eq. 3.103 yields

$$\hat{f}^\sigma \sum_{\mu=1}^{K} \chi_\mu(\vec{r}) c^\sigma_{\mu p} = \varepsilon_{p\sigma} \sum_{\mu=1}^{K} \chi_\mu(\vec{r}) c^\sigma_{\mu p}\,. \tag{3.104}$$

Multigration with χ_ν then results in,

$$\sum_{\mu=1}^{K} \langle \chi_\nu | \hat{f}^\sigma | \chi_\mu \rangle c^\sigma_{\mu p} = \varepsilon_{p\sigma} \sum_{\mu=1}^{K} \langle \chi_\nu | \chi_\mu \rangle c^\sigma_{\mu p} \tag{3.105}$$

where there are K such equations and $p = 1, 2, \cdots, K$. Writing these in a matrix equation yields the Roothaan equation,

$$\mathbf{F}^\sigma \mathbf{C}^\sigma = \mathbf{S}\mathbf{C}^\sigma \mathbf{E}^\sigma\,, \tag{3.106}$$

where,

$$\begin{aligned} F^\sigma_{\mu,\nu} &= \langle \chi_\mu | \hat{f}^\sigma | \chi_\nu \rangle \\ S_{\mu,\nu} &= \langle \chi_\mu | \chi_\nu \rangle \\ C^\sigma_{\mu,p} &= c^\sigma_{\mu p} \\ E^\sigma_{p,q} &= \varepsilon_p \delta_{p,q}\,. \end{aligned} \tag{3.107}$$

Since $\mathbf{F}^\sigma$ depends upon $\mathbf{C}^\sigma$ in Eq. (3.106), then the Roothaan equations must also be solved self-consistently. The final self-consistent energy is guaranteed to be an upper bound to the true (infinite basis set) Hartree-Fock energy.

Many different approximate methods [3] exist for solving the Schrödinger equation and which one to use for a specific problem is usually chosen by comparing its performance against known experimental data. Experimental data thus guides the selection of the computational model, rather than directly entering into the computational procedure. We have just described one level of approximation—that is, the restriction to a single determinantal wave function. If the determinants in a CI expansion of the exact solution of the many-electron wave function are viewed as N-electron basis functions, then the Hartree-Fock method is a drastic restriction to a single N-electron basis function. However, another of the the approximations inherent in essentially all *ab initio* methods is the introduction of a one-electron basis set. This is the one which proves to be the most important for the work reported in this thesis.

A basis set is a mathematical description of the orbitals within a system used to perform the theoretical calculation. Unknown functions such as molecular orbitals are normally expanded in a set of known functions (basis set). When the basis set is complete, the expansion is no longer an approximation. It is

[2] Note however that these "atomic orbitals" need not be—and usually are not—the exact solution of any atomic problem.

[3] A rigorous derivation uses the variational principle.

impossible to use a complete basis set for this would mean an infinite number of functions rendering the calculations impractical. When a finite basis set is used, only components of the molecular orbital along those coordinate axes corresponding to the selected basis functions can be represented. The smaller the basis set, the poorer the representation. The type of basis functions used also influences the accuracy. The better a single basis function is able to reproduce the unknown function, the fewer basis functions are necessary for achieving a given level of accuracy. Generally larger basis sets more accurately approximate the orbitals by imposing fewer restrictions on the locations of the electrons in space.

Much of our chemical intuition about how to chose a basis set comes from the hydrogen atom which is one of the few quantum mechanical problems with an analytic solution [11]. The potential energy has a simple $-\frac{1}{r}$ dependence, so separation of variables can be used for obtaining radial and angular components to the eigenstates of the wave function,

$$\Psi(r,\theta,\varphi) = R_n(r)Y_m^l(\theta,\varphi)\,. \tag{3.108}$$

The $Y_m^l(\theta,\varphi)$ are spherical harmonics, while the radial dependence $R_n(r)$has the form,

$$R_n(r) = L_n(r)e^{\frac{-r}{a_0}}\,, \tag{3.109}$$

where L_n is the n^{th} Laguerre polynomial. The eigenvalues of the spatial Hamiltonian are specified by the triple (n,l,m), known as quantum numbers. The number n fixes the total electron energy, the number l describes the orbital angular momentum, and m denotes the z component of the angular momentum. There is a fourth quantum number, m_s, which accounts for the spin the electron [2], either α (spin up) or β (spin down). The eigenfunctions that these quantum numbers specify are known as orbitals (or spin-orbitals if spin is included), and they form the foundation for understanding the way electrons behave in other atoms. And, more to the point, this analytic solution has had a large influence upon how we construct basis sets.

The one-electron basis sets which most closely resembles the hydrogen atom solution are Slater-type orbitals (STOs). These have the form $Y_{l,m}(\theta,\varphi)r^n e^{-\zeta r}$ or $x^n y^m z^l e^{-\zeta r}$. The exponential dependence on the distance between the nucleus and electrons mirrors the behavior of the exact orbitals for the hydrogen atom. However, the STOs do not have any radial nodes. That is not such a great problem for a variational calculation is easily shown to make linear combinations of STOs having the proper nodal structure. Nowadays STOs are primarily used for atomic and diatomic systems where high accuracy is required, and in semi-empirical methods where all three- and four-centre integrals are neglected. They can also be used with density functional methods that do not include exact exchange and where the Coulomb energy is calculated by fitting the density into a set of auxiliary functions, such as in the ADF (Amsterdam Density-Functional) program. The main difficulty with STO basis sets is the difficulty of calculating three and four center electron repulsion integrals.

The usual response is to use Gaussian-type orbitals (GTOs) which have the form $x^n y^m z^l e^{-\alpha r^2}$. GTOs are not as efficient as STOs in terms of the number of basis functions which must be used, but all necessary integrals have analytic formulae in a GTO basis set which is not the case for STOs. Thus the r^2 dependence in the exponential makes the GTO inferior to the STOs in two respects. At the nucleus a GTO has a zero slope, in contrast to a STO which has a 'cusp' (a discontinous derivative), and GTOs have a problem representing the proper behavior near the nucleus. The other problem is that the GTO falls off too rapidly far from the nucleus compared with an STO, and the "tail" of the wavefunction is consequently represented poorly. Both STOs and GTOs can be chosen to form a complete basis, but the above considerations indicate that more GTOs are necessary for achieving a certain accuracy compared with

STOs. The increase in the number of GTO basis functions, however, is more than compensated for by the ease with which the required integrals are calculated. In terms of computational efficiency, GTOs are therefore preferred and are used almost universally as basis functions in electronic structure calculations.

Having decided on the type of function and the location (nuclei), the most important factor is the number of functions to be used. There is now a well-established hierarchy of approximations built up over many decades for how to more or less systematically improve the basis set used in a calculation in order to converge to good numbers. The smallest number of functions possible is for a minimum basis set. In this basis set, only enough functions are employed to contain all the electrons of the neutral atom(s) and any empty valence orbitals.

The next improvement of the basis sets is a doubling of all basis functions producing a double zeta (DZ) type basis. Doubling the number of basis functions allows for a much better description of the fact that the electron distribution is different in different directions. A variation of the DZ basis is the split valence basis sets where the doubling of basis functions is only done for valence orbitals.

The next step up basis set size is a triple zeta (TZ). Such a basis contains three times as many functions as the minimum basis. Some of the core orbitals mayagain be saved by only splitting the valence, producing a triple split valence basis.The term TZ is used to cover both cases. The terms auadruple zeta (QZ) and quintuple or pentuple zeta (PZ or 5Z,but not QZ) for the next levels of basis sets are also used, but large basis sets are given explicitly in terms of the number of basis functions of each type.

Standard basis sets for electronic structure calculations use linear combinations of gaussian functions to form athe orbitals. GAUSSIAN offers a wide range of pre-defined basis sets, which may be classified by the number and types of basis functions that they contain. Basis sets assign a group of basis functions to each atom within a molecule to approximate its orbitals. These basis functions themselves are composed of a linear combination of gaussian functions and such basis functions are referred to as contracted functions, and the component gaussian l functions are referred to as primitives. A basis function consisting of a single gaussian function is termed uncontracted.

Since the choice of basis set is very important, let us take a moment to take stock of some of the important choices and vocabulary needed when working with basis sets and the GAUSSIAN program:

Split valence basis set

This is away to make a basis set larger and it is done by increasing the number of basis functions per atom. Split valence basis sets, such as 3-21G and 6-31G*,have two or more sizes of basis functions for each valence orbital. The double zeta basis sets, form molecular orbitals from linear combination of two sizes of functions for each atomic orbital. Similarly,triple split valence basis sets,like 6-311G, use three sizes of contracted functions for each orbital-type.

Polarized valence basis set

Split valence basis sets allow orbitals to change size, but not to change shape. Polarized basis sets remove this limitation by adding orbitals with angular momentum beyond what is required for the ground state to the description of each atom. For example, polarized basis sets add d functions to carbon atoms and f functions to transition metals, and some of them add p functions to hydrogen atoms. An example of a polarized basis set is 6-31G(d). What it means is that it is a 6-31G basis set with d functions added to heavy atoms. It is also known as 6-31G*. Another popular polarized basis set 6-31G(d,p), also known as 6-31G**, which adds p functions to hydrogen atoms in addition to d functions on heavy atoms.

Diffuse functions

Diffuse functions are large-size versions of s-and p-type functions (as opposed to the standard valence-size functions). They allow orbitals to occupy a larger region of space. Basis sets with diffuse functions are important for systems where electrons are relatively far from the nucleus: molecules with lone pairs, anions and other systems with significant negative charge,systems in their excited states, systems with

low ionization potentials, descriptions of absolute acidities, and so on. The 6-31+G(d) basis set is the 6-31G(d) basis set with diffuse functions added to heavy atoms. the double plus version, 6-31++G(d), adds diffuse functions to the hydrogen atoms as well.

High angular momentum basis set

Much larger basis sets are now practical for many systems. Such basis sets add multiple polarization functions per atom to the triple zeta basis set. The 6-31G(2d) basis set adds two d functions per heavy atom instead of just one, while the 6-311++G(3df, 3pd) basis set contains three sets of valence region functions, diffuse functions on both heavy atoms and hydrogens, and multiple polarization functions: 3 d functions and 1 f function on heavy atoms and 3 p functions and 1 d function on hydrogen atoms. Such basis sets are useul for describing the interactions between electrons in electron correlation methods; they are not generally needed for Hartree-Fock calculations. Some large sets specify different sets of polarization functions for heavy atoms depending upon the row of the periodic table in which they are located. For example the 6-311+(3df,2df,p) basis set places 3 d functions and 1 f function on heavy atoms in the second and higher rows of the periodic table, and it places 2 d functions and 1 f function on first row heavy atoms and 1 p function on hydrogen atoms.

Basis set for Post-Third-Row Atoms

Basis sets for atoms beyond the third row of the periodic table are handled somewhat differently. For these very heavy nuclei, electrons near the nucleus are treated in an approximate way, via core potentials(ECPs). This treatment includes some relativistic effects, which are important in these atoms. The LANL2DZ basis set is the best known of these.

In density function theory the same kind of basis sets can be used as in Hartree-Fock calculations. In principal the parameters would have to be newly optimised (e.g. for a 6-31G* type basis). However, it turned out that such optimised parameters only have a minor effect on results and the expense needed for the optimisation is not justifiable. It is therefore common to use the same basis sets in density functional theory that are also used in wavefunction calculations. In Kohn-Sham density functional theory only simple orbitals have to be described. Therefore, the demand on the basis is comparable to other independent particle models like the Hartree-Fock model. Basis sets of double quality with one set of polarisation functions are often sufficient to get good results. Triple-type of basis sets with two sets of polarisation functions are formost cases close to converged results.

A final consideration, important for this thesis, is the concept of pseudopotential. Generally, a trade-off between speed and accuracy is necessary, as there is an N^4 dependence on the basis set size. In a system of the size of a ruthenium polypyridyl complex (on the order of 100 atoms), a reasonable compromise is to use the LanL2DZ basis set and electron-core potential of Dunning, Hay and Wadt. For the atoms C, H and N, LanL2DZ uses the Dunning/Huzinaga10 valence double-ζ basis set. Following the usual notation for basis sets, H, C and N are described by (10s5p/4s)[3s2p/2s].

The treatment of heavy atoms (third row and lower) by LanL2DZ involves the use of a pseudopotential or effective core potential (ECP) for the core electrons. The ECP is an analytical function which is used to account for the effect of the combined nuclear-electronic core on the remaining electrons. This approach is justified by the fact that the inner electrons of a heavy atom are unimportant, in a chemical sense, their spatial distribution and energies are largely unchanged when they form a chemical bond. In addition, relativistic effects, which are important for atoms as heavy as ruthenium, can be "folded in" to the ECP. These effects would otherwise be neglected. The LanL2DZ ECP accounts for the innermost 28 electrons of Ru ([Ar]3d^{10})and the innermost 60 electrons of Os ([Kr]4d^{10}4f^{14}). In both cases the remaining 16 electrons ($4s^2 4p^6 4d^7 5s^1$ for Ru,i and $5s^2 5p^6 5d^7 6s^1$ for Os) are treated using a double-ζ basis set. The name LanL2DZ comes from the fact that it uses the Los Alamos National Laboratory (LANL) ECPs along with a doubleζ (DZ) basis set.

3.7 Beyond Hartree-Fock

Although the Hartree Fock theory lays the foundation for understanding what goes on in quantum chemistry, it is known not to give accurate answers. This energy difference between the Hartree Fock energy and the exact energy is called the correlation energy. Other so-called correlated or post Hartree Fock methods [3, 4]. To recover this correlation energy, the correlated methods use more and more determinants. Such methods include the following:

- Complete Active Space SCF (CASSCF),
- Multi-Configurational SCF (MCSCF),
- Configuration Interaction (CI),
- Coupled Cluster Method (CC), etc.

The problem with the additional determinants is that they make the calculations more expensive. This limitation is what necessitated the search for and use of a method that yields good results but is not computationally so costly. This method is the Density Functional Theory (DFT) and its time dependent version the so-called Time Dependent Density Functional Theory (TDDFT). This method will be dealt with in the next chapter.

References

[1] M. V. D. Planck, "On an Improvement of Wien's Equation for the Spectrum," *Phys. Ges.*, vol. 2, p. 202, 1900.

[2] K. Balasubramian, *Relativistic Effects in Chemistry Part A*. New York: John Wiley and Sons, 1997.

[3] F. Jensen, *An Introduction to Computational Chemistry*. New York: John Wiley and Sons, 1998.

[4] C. J. Cramer, *Essentials of Computational Chemistry: Theories and Models*. New York: Wiley, 2002.

[5] J. C. Slater, "A simplification of the Hartree-Fock method," *Phys. Rev.*, vol. 81, pp. 385–390, 1951.

[6] L. Piela, *Ideas of Quantum Chemistry*. Amsterdam: Elsevier, 2007.

[7] D. J. Tannor, *Introduction to quantum mechanics: A time dependent perspective*. Weizmann Institute of Science: Univesity Science books, 2007.

[8] D. R. Hartree, "The wave mechanics of an atom with non-coulombic central field: parts I, II, III,," *Proc. Cambridge Phil. Soc.*, vol. 24, pp. 89,111,426, 1928.

[9] C. F. Fischer, *The Hartree-Fock Method for Atoms: A Numerical Approach*. New York: John Wiley and Sons, 1977.

[10] C. C. J. Roothaan, "New Developments in Molecular Orbital Theory," *Rev. Mod. Phys.*, vol. 23, pp. 69–89, 1951.

[11] C. Cohen-Tannoudji, B. Diu, and F. Laloë, *Quantum Mechanics*. Paris: Wiley-Interscience, 1977.

CHAPTER 4

DENSITY-FUNCTIONAL THEORY AND TIME-DEPENDENT DENSITY-FUNCTIONAL THEORY

This chapter provides a brief description of density-functional theory (DFT) and of time-dependent DFT (TD-DFT).

4.1 Density-Functional Theory

Density-functional theory (DFT) [1, 2] is built around the idea of an electron density $\rho(\vec{r})$, which basically represents the number of electrons per unit volume at some position $\vec{r}$ in a molecule or in an atom. DFT leads to a paradigm shift from the wave-function approach. The electron density $\rho(\vec{r})$, is used as the main variable instead of the many-body wave function. In essence, the purpose of DFT is to replace the (perhaps) unnecessarily complicated N-electron wave function $\Psi(\vec{x}_1,\vec{x}_2,\vec{x}_3,\cdots,\vec{x}_N)$ and the computationally-expensive part of solving the many-electron problem by a functional of the electronic density. By the term "functional" is simply meant a function whose argument is itself a function. This is unlike the familiar function which maps one number onto another number. A functional is normally denoted by the use of a square bracket for its argument (i.e., $F[f]$) to distinguish it from an ordinary function (e.g., $f(\vec{r})$). Some quantities, such as the exchange-correlation potential $v_{xc}[\rho](\vec{r})$ are simultaneously functionals and functions.

This realization that the electron density could be exploited in the study of ground state properties of an atom or a molecule led to a lot of efforts towards understanding it. Some of the work in this direction is captured below.

4.1.1 The Thomas-Fermi Model

In 1927, Thomas and Fermi [3] came up with the first ever approach to use the electron density as the key variable in atomic calculations. They realized that statistical mechanics instead of quantum mechanics could be used to approximate the distributions of the electrons in the atomic systems. In their formulation, they used the same electron kinetic energy as that of a uniform electron gas,

$$E_{TF}[\rho] = C_F \int \rho^{\frac{5}{3}}(\vec{r})d\vec{r} - Z\int \frac{\rho(\vec{r})}{\vec{r}}d\vec{r} + \frac{1}{2}\int\int \frac{\rho(\vec{r}_1)\rho(\vec{r}_2)}{|\vec{r}_1-\vec{r}_2|}d\vec{r}_1 d\vec{r}_2\,, \tag{4.1}$$

where $C_F = \frac{3}{10}(3\pi^2)^{\frac{2}{3}}$. The above equation [Eq. (4.1)], ignores the terms of exchange and correlation and only considers the traditional electrostatic energies of attraction (electron-nuclei) and repulsion (electron-electron). It is thus, the functional for the energy in the Thomas-Fermi model for atoms. This model does not give very accurate results. It is a model that did not work well when applied to molecules. This was considered one of those oversimplified models that did not have any importance in quantitative predictions in atomic and solid-state physics.

According to this model atoms can not bind and when nuclei are moved infinitely far apart this lowers the energy [4, 5]

4.1.2 Hohenberg-Kohn

Hohenberg and Kohn (HK) [6] established the two theorems which constitute the theoretical foundation of DFT:

> *First HK Theorem (The Existence Theorem).*
> For a nondegenerate system of interacting electrons in an external potential $v_{ext}(\vec{r})$, there is a one-to-one (apart from an irrelevant additive constant) correspondence between $v_{ext}(\vec{r})$ and the ground-state particle density, $\rho_0(\vec{r})$. Given that $v_{ext}(\vec{r})$ in turn fixes $\hat{H}$ [up to an arbitrary additive constant (energy zero)] it is seen that the full many-particle ground state is a unique functional of $\rho_0(\vec{r})$.

For an N-electron system, the existence theorem legitimizes the use of the $\rho_0(\vec{r})$ instead of N and v_{ext}(r). Thus it is possible from $\rho_0(\vec{r})$ to determine not only N and $v_{ext}(\vec{r})$, but all the other properties of the ground state such as the kinetic energy, the potential energy as well as the total energy. More to the point, there is no longer any need for the complicated many-electron wave function, $\Psi(\vec{x}_1,\vec{x}_2,\vec{x}_3,\cdots,\vec{x}_N)$. The proof of this first theorem is done by considering the fact that if there are two systems with N electrons and both are of equal electron density, then showing that the variational principle then requires that the two systems must have the same external potential $v_{ext}(\vec{r})$. The proof is by contradiction. Assume that two systems with different external potentials, $v_{ext}^{(1)}$ and $v_{ext}^{(2)}$, and hence different wave functions, Ψ_1 and Ψ_2, have the same ground-state charge density. Then, according to the variational principle,

$$\begin{aligned} E_1 &< \langle\Psi_2|\hat{H}_1|\Psi_2\rangle \\ &= \langle\Psi_2|\hat{H}_2 + v_{ext}^{(1)} - v_{ext}^{(2)}|\Psi_2\rangle \\ &= \langle\Psi_2|\hat{H}_2|\Psi_2\rangle + \langle\Psi_2|v_{ext}^{(1)} - v_{ext}^{(2)}|\Psi_2\rangle \\ &= E_2 + \int \left(v_{ext}^{(1)}(\vec{r}) - v_{ext}^{(2)}(\vec{r})\right)\rho(\vec{r})\,d\vec{r}. \end{aligned} \tag{4.2}$$

Similarly,

$$E_2 < E_2 + \int \left(v_{ext}^{(2)}(\vec{r}) - v_{ext}^{(1)}(\vec{r})\right)\rho(\vec{r})\,d\vec{r}. \tag{4.3}$$

Taking sum of Eqs. (4.2) and (4.3) gives the contradiction,

$$E_1 + E_2 < E_1 + E_2\,. \tag{4.4}$$

We are thus forced to conclude that our intial assumption that two systems with different external potentials may have the same ground state density must be false. Or, put a different way, we are forced to conclude that the density of a system with a nondegenerate ground state determines the external potential up to an additive constant.

The greatest achievement of this first HK theorem was the confirmation that there exists a direct connection between the $v_{ext}(\vec{r})$ and $\rho_0(\vec{r})$. As a mere existence theorem, it failed to clarify the form of the density functional. It is thus not possible on the basis of this first theorem to calculate E_0 from the external potential $v_{ext}(\vec{r})$. This weakness is what the second HK theorem seeks to address.

> *Second HK Theorem (The Variational Theorem).*
> The ground-state charge density minimizes a variational expression for the ground state energy,
>
> $$E_{v_{ext}}[\rho] = T[\rho] + V_{ne}[\rho] + V_{ee}[\rho] = \int \rho(\vec{r}) v_{ext}(\vec{r})\, d\vec{r} + F_{HK}[\rho]\,. \tag{4.5}$$
>
> Here, $E_{v_{ext}}$ simply stresses the dependence of the total electronic energy on the external potential, $v_{ext}(\vec{r})$ and $\rho(\vec{r})$ in the equation only becomes equal to the ground-state density, ρ_0(r), for the exact variational minimum. Any remaining unaccounted parts of the energy are included in $F_{HK}[\rho]$ which is a universal functional in the sense that it is independent of the system under consideration (i.e., does not depend upon $v_{ext}(\vec{r})$). Furthermore, $F_{HK}[\rho]$ is minimal at the exact ground-state density $\rho_0(\vec{r})$, and its minimum gives the exact ground-state energy, E_0, of the system.

Mathematically, an approximate density $\tilde{\rho}$ of an N-electrons system, yields an approximate energy $\tilde{E}_{v_{ext}}$ which is an upper bound to the exact ground state energy,

$$E_0 \leq \tilde{E}_{v_{ext}}\,. \tag{4.6}$$

By applying the variational principle of the second HK theorem to the HK energy functional we obtain the Euler equation,

$$\mu = \frac{\delta E_{v_{ext}}[\rho]}{\delta \rho(\vec{r})} = v_{ext}(\vec{r}) + \frac{\delta F_{HK}[\rho]}{\delta \rho(\vec{r})}\,, \tag{4.7}$$

where μ is the chemical potential. This equation [Eq. (4.7)] forms the main working equation in orbital-free DFT. In fact, we have here the formally exact generalization of Thomas-Fermi theory. It is also an empty theory unless we can find useful approximations for the universal functional $F_{KS}[\rho]$. This means that we tend to fall back on Thomas-Fermi-like approximations which are not usually sufficiently accurate for chemistry.

4.1.3 Kohn-Sham Formalism

Kohn and Sham recognized that the main difficulty is the problem of finding a density functional for the kinetic energy. In the Kohn-Sham approach [7] N orthonormal auxiliary functions (the Kohn-Sham orbitals) are introduced to create a formal theory with a density-functional which turned out to be much easier to approximate. The result is a system of N noninteracting electrons moving in a local potential $\hat{v}_s$ (the s stands for "single particle") whose ground-state density is assumed to be exactly the same as the ground-state density of the real interacting system of N electrons. The kinetic energy of the noninteracting system is (in atomic units, $\hbar = m_e = e = 1$),

$$T_s = -\frac{1}{2}\sum_{i=1}^{N} n_i \langle \psi_i | \nabla^2 | \psi_i \rangle\,, \tag{4.8}$$

where the ψ_i and n_i are the Kohn-Sham (spin-)orbitals and their occupation numbers respectively. This noninteracting kinetic energy is in general not the same as the kinetic energy of the interacting system.

Normally these occupation numbers are assumed to have values of either zero or one in which case the assumption that the ground state densities be the same for the interacting and noninteracting systems is called noninteracting v-representability. However there is an ensemble generalization which allows the occupation numberes to be fractional.

The Kohn-Sham reference system has a one-electron Hamiltonian,

$$\hat{h}_s = -\frac{1}{2}\sum_i^N \nabla_i^2 + \sum_i^N v_s(\vec{r}_i)\,, \tag{4.9}$$

in which there are no electron-electron repulsion terms, and which yields an exact ground state electron density ρ. For this system there is a corresponding exact determinantal ground state wave function.

$$\Phi_s = |\psi_1, \psi_2, \psi_3, \cdots, \psi_N|\,. \tag{4.10}$$

If we apply the first Hohenberg-Kohn theorem to noninteracting systems, then we find that the noninteracting kinetic energy of Eq. (4.8) must also be a functional of the density, $T_s[\rho]$. However now instead of having to make a Thomas-Fermi-like approximation for this part of the kinetic energy, we have a new implicit expression involving Kohn-Sham orbitals which themselves must be functionals of the ground-state charge density.

Let us now turn to the second Hohenberg-Kohn theorem where we see that we can now write that,

$$F[\rho] = T_s[\rho] + J[\rho] + E_{xc}[\rho]\,, \tag{4.11}$$

where the exchange-correlation (xc) energy is at first sight a sort of "rubbish bin" for putting all the terms that we cannot or do not want to calculate,

$$E_{xc}[\rho] = T[\rho] - T_s[\rho] + V_{ee}[\rho] - J[\rho]\,. \tag{4.12}$$

Note that the terms $V_{ee}[\rho] - J[\rho]$ correspond fairly well to what is normally called exchange and correlation, but that the xc-energy of DFT also includes the kinetic energy difference between the true interacting and fictitious noninteracting system.

We want to minimize this with respect to the constraint that the orbitals be orthonormal. Once again using the method of Lagrange multipliers (but this time using functional derivatives), we carry out,

$$0 = \frac{\delta \mathscr{L}}{\delta \psi_i^*(\vec{r})} = \left(\hat{h}_s - \varepsilon_i\right)\psi_i(\vec{r})\,, \tag{4.13}$$

where,

$$\mathscr{L} = -\frac{1}{2}\sum_{i=1}^N n_i \langle\psi_i|\nabla^2|\psi_i\rangle + \int v_{ext}(\vec{r}) + V_{ee}[\rho] + E_{xc}[\rho] - \sum_{i=1}^N \varepsilon_i\left(\langle\psi_i|\psi_i\rangle - 1\right)\,. \tag{4.14}$$

Of course, Eq. (4.13) is just the Kohn-Sham orbital equation,

$$\hat{h}_s\psi_i(\vec{r}) = \varepsilon_i\psi_i(\vec{r})\,, \tag{4.15}$$

except that we may now write out the noninteracting potential more explicitly as,

$$v_s(\vec{r}) = v_{ext}(\vec{r}) + v_H[\rho](\vec{r}) + v_{xc}[\rho](\vec{r})\,, \tag{4.16}$$

where the Hartree (or Coulomb) potential is,

$$v_H[\rho](\vec{r}_1) = \int \frac{\rho(\vec{r}_2)}{r_{12}}\, d\vec{r}_2\,, \tag{4.17}$$

and the xc-potential is,

$$v_{xc}[\rho](\vec{r}) = \frac{\delta E_{xc}[\rho]}{\delta \rho(\vec{r})}\,. \tag{4.18}$$

Thus far everything is exact and it would seem that, instead of paying the high computational price for multiple determinants in the wave-function-based methods discussed earlier, the better way forward is to seek for ways of improving the exchange-correlation functionals.

To make this a useful theory, we need to find approximations for $E_{xc}[\rho]$. The search for efficient exchange-correlation functionals is an active area of study in DFT and below (in the next subsection) are more details about some of the approximations and some representative functionals. Let us assume for the moment that we already have a reasonable approximate $E_{xc}[\rho]$ and can form its derivative $v_{xc}[\rho](\vec{r})$. Then the similarity of the Kohn-Sham equations to the Hartree-Fock equations makes it relatively easy to implement Kohn-Sham DFT in program that already does Hartree-Fock calculations. Like Hartree-Fock calculations, Kohn-Sham calculations are done *self-consistently*. One obtains $\rho(\vec{r})$ for a given v_s which satisfies the Euler equation by solving the one-electron equation,

$$\left[-\frac{1}{2}\nabla^2 + v_s(\vec{r})\right]\psi_i = \varepsilon_i \psi_i\,. \tag{4.19}$$

For completeness, let us also derive the form of v_{xc} a somewhat different way. We begin with the Hohenberg-Kohn F functional which we rewrite as,

$$F[\rho] = T[\rho] + J[\rho] + E_{xc}[\rho]\,, \tag{4.20}$$

where,

$$E_{xc}[\rho] = T[\rho] - T_s[\rho] + V_{ee}[\rho] - J[\rho]\,. \tag{4.21}$$

The quantity E_{xc} is the same xc-energy as before. The Euler equation becomes,

$$\mu = v_s(\vec{r}) + \frac{\delta T_s[\rho]}{\delta \rho(\vec{r})}\,, \tag{4.22}$$

where the KS effective potential is defined by,

$$v_s(\vec{r}) = v_{ext}(\vec{r}) + \frac{\delta J[\rho]}{\delta \rho(\vec{r})} + \frac{\delta E_{xc}[\rho]}{\delta \rho(\vec{r})} = \int \frac{\rho(\vec{r}')}{|\vec{r}-\vec{r}'|} d\vec{r}' + v_{xc}(\vec{r})\,, \tag{4.23}$$

where,

$$v_{ext}(\vec{r}) = -\sum_A^M \frac{Z_A}{r_{1A}}\,, \tag{4.24}$$

with the exchange-correlation potential,

$$v_{xc}(\vec{r}) = \frac{\delta E_{xc}[\rho]}{\delta \rho(\vec{r})}\,. \tag{4.25}$$

The total electronic energy may be calculated from the Kohn-Sham orbitals in a variety of ways. One which makes use of the Kohn-Sham orbital energies is,

$$E = \sum_{i=1}^{N} \varepsilon_i - \frac{1}{2} J[\rho] + E_{xc}[\rho] - \int v_{xc}[\rho](\vec{r})\rho(\vec{r})\, d\vec{r}. \tag{4.26}$$

4.1.4 Exchange-Correlation Approximations

In some ways the Kohn-Sham formalism resembles the Hartree-Fock approximation. However Hartree-Fock is an approximation, while Kohn-Sham promises to be exact when the exact xc-functional is used. Unfortunately no exact practical form is known for the xc-functional. However the forms that are known perform so well that Hartree-Fock calculations are now rarely performed unless the intension is to follow up with explicitly correlated *ab initio* calculations. This is in large part due to the successes in developing new and better xc-functionals in DFT. For the purposes of the presentation here, the development of xc-functionals may divided into three generations.

4.1.4.1 First Generation: Local Density Approximation

Much of the success of DFT is due to that fact that $E_{xc}[\rho]$ can be reasonably approximated by a local or nearly local functional of the density. The first and most widespread approximation to $E_{xc}[\rho]$ is the local density approximation (LDA), which assumes that the xc-energy of a real system behaves locally as that of a uniform electron gas (UEG). Thus the LDA assumes that the exchange-correlation (xc) energy density, $E_{xc}[\rho]$, depends only upon the density at $\vec{r}$. Thus,

$$E_{xc}^{LDA} = \int \varepsilon_{xc}^{UEG}(\rho(\vec{r})\rho(\vec{r}\, d\vec{r}, \tag{4.27}$$

where $\varepsilon_{xc}^{UEG}(\rho(\vec{r}))$ is the energy density of the UEG evaluated at $\vec{r}$ for the density $\rho(\vec{r})$ at that point in the system. Clearly, the LDA is eact in the limit of slowly varying densities.

The exchange-correlation energy for the homogeneous electron gas can be written as,

$$E_{xc}^{LDA} = E_x^{LDA} + E_c^{LDA}. \tag{4.28}$$

The first part of the term is the Dirac exchange energy and has a relatively simple analytic form,

$$E_x^{LDA} = -\frac{2}{3}\left(\frac{3}{4\pi}\right)^{\frac{1}{3}} \int \left[\rho(\vec{r})\right]^{\frac{4}{3}} d\vec{r}. \tag{4.29}$$

The correlation term however, does not have a known analytic form. However, the correlation part has been obtained by parameterizing [8, 9] the results of Monte Carlo simulations [10].

Remarkably the LDA works even for molecules where the electron density is far from uniform. Typically the LDA yields a good accuracy in reproducing experimental structural and vibrational properties of strongly bound systems. It usually overestimates bonding energies and underestimates bond lengths.

The next step beyond the LDA is the local spin density approximation where up and down spins are treated differently. Nowadays the term LDA almost always implies the local spin density approximation.

4.1.4.2 Second Generation: Generalized Gradient Approximation

The first try at a second generation of xc-functionals was the gradient expansion approximation (GEA). In this approach, the exchange correlation energy is treated as a Taylor expansion about the density at

every point,

$$E_{xc}^{GEA}[\rho] = \int \varepsilon_{xc}^{UEG}(\rho)\rho(\vec{r})\,d\vec{r} + \int C_{xc}(\rho(\vec{r})x(\vec{r})\,d\vec{r}. \tag{4.30}$$

Unfortunately this approach never worked very well.

Equation 4.30, is assymptotically valid for densities that vary slowly over space. For instance for finite systems, the terms in the expansion of the exchange energy of order equal to or greater than four diverge. The exchange potential performs even more poorly for it diverges at the second order [11].

A more successful approach has been generalized gradient approximations (GGA) of the form ,

$$E_{xc}^{GGA} = \int \varepsilon_{xc}(\rho(\vec{r}), x(\vec{r}))\rho(\vec{r})\,d\vec{r}, \tag{4.31}$$

where the reduced gradient,

$$x(\vec{r}) = \frac{|\vec{\nabla}\rho(\vec{r})|}{\rho^{4/3}(\vec{r})}. \tag{4.32}$$

The three most popular parametrizations are that of Becke (B88), Perdew and Wang (PW91), and Perdew, Burke, and Enzerhof (PBE) [12]. The GGA greatly improves upon the LDA in the prediction of the binding energies of real substances.

4.1.4.3 Third Generation: Hybrid Functionals

Axel Becke introduced hybrid functionals [13] as the third generation of density functionals in the 1990s. These functionals have a contribution of Hartree-Fock exchange. For example,

$$E_{xc} = E_{xc}^{GGA} + C_x\left(E_x^{HF} - E_x^{GGA}\right). \tag{4.33}$$

The work reported in this thesis was carried out using a particular hybrid functional called B3LYP whose formulation is,

$$E_{xc}^{B3LYP} = (1-a)E_x^{LDA} + aE_{xc}^{LDA} + bE_x^{B88} + cE_c^{LYP} + (1-c)E_c^{LSD} \tag{4.34}$$

4.1.4.4 New Generation of functionals

In recent times a new generation of functionals has emerged and it comprises among others the following:

- Meta-Generalized Gradient Approximation-meta-GGA
- Range-separated functionals
- Double hybrid functionals

A “meta-GGA functional [14]” is basically an extension of the GGA in which the non-interacting Laplacian (second derivative) of the density or kinetic energy density is used as input to the functional as well as the electron density and its gradient. The concept of “range separation” was introduced in order to combine DFT and wavefunction theory. More details on this can be found in reference [15].

The double-hybrid (DH) [16] density-functional approximations mix HF exchange with a semilocal exchange density functional and second-order Møller-Plesset (MP2) correlation with a semilocal correlation density functional.

4.2 Time-Dependent Density Functional Theory

It should be clear by now that ordinary DFT is restricted to time-independent ground-state problems. However there are many problems in chemistry where we are interested in the dynamic response of the charge density or in electronic excited states. Fortunately there is a time-dependent variant on DFT.

4.2.1 Runge and Gross Formulations

Runge and Gross [17] formalized time-dependent DFT (TD-DFT) and extended the Hohenberg-Kohn theorems into the time domain, by proving that two spatially different external potentials cannot induce the same time-dependent densities. The formulation that follows is done in such a wy as to bring out the similarity with the conceptual structure of ground-state DFT

> *Existence Theorem*.
> For any system of interacting electrons in an external time-dependent potential $v_{ext}(\vec{r},t)$, which can be expanded in Taylor series with respect to time, and given an initial state $\Psi(t_0)$ =Ψ_0, there is a one-to-one correspondence between $v_{ext}(\vec{r},t)$ and the time-dependent electron density $\rho(\vec{r},t)$ up to an additive function of time.

According to this theorem—which is the analogue of the first Hohenberg-Kohn theorem—we can consider the time-dependent electronic density [18] as the fundamental variable that determines all the properties of the system. It is important to notice that, different from DFT, this case requires setting an initial condition, since we are following an evolution in time.

Now what about an analogue of the second Hohenberg-Kohn theorem? There is no energy variational principle for the time-dependent case. Instead what is often used is the

> *Frenkel-Dirac Variational Principle*.
> Making the action,
> $$A = \int_{t_0}^{t_1} \langle \Psi(t) | i\frac{\partial}{\partial t} - \hat{H}(t) | \Psi(t) \rangle \, , \tag{4.35}$$
> stationary, with respect to all possible variations of $\Psi(t)$ subject to the fixed point conditions $\delta\Psi(t_0) = \delta\Psi(t_1)$ gives the time-dependent Schrödinger equation,
> $$\hat{H}(t)\Psi(t) = -i\frac{\partial}{\partial t}\Psi(t) \, . \tag{4.36}$$

It is important to realize that the exact solution is only obtained if there are no constraints on the variations. Otherwise, the Frenkel Dirac variational principle provides a way to derive an appropriate approximate time-dependent equation from a given trial function (e.g., one of single-determinantal form). This extra degree of freedom is an advantage in most applications.

In the Runge-Gross paper, they propose an

> *Action Theorem*.
> The Frenkel-Dirac action is a functional of the time-dependent density, $A[\rho]$.

This has actually been shown to be incorrect and is known as the "causality problem." The problem is that we are asking something more than what is usually required from the Frenkel-Dirac action—an exact equation, rather than an appropriate approximate equation. Vignale has shown that the problem stems

from the fact that time propagation means that $\Psi(t_0)$ actually determines $\Psi(t_1)$ (even in the wave function case). He shows that an extra term must be added to restore causality [19]. Fortunately many correct results may be (and have been) obtained without taking this extra term needed in rigorous derivations into consideration.

Runge and Gross then go on to derive a time-dependent Kohn-Sham equation. First they partition the action as,

$$A[\rho] = S[\rho] - \int_{t_0}^{t_1} \int \rho(\vec{r},t) v_{ext}(\vec{r},t) dt d\vec{r}, \tag{4.37}$$

in which $S[\rho]$ is a universal functional of the time-dependent density and $A[\rho]$ is stationary for variations around the exact density of the system. Let $S_0[\rho]$ denote the S functional for noninteracting electrons. Then,

$$A[\rho] = S_0[\rho] + S_H[\rho] + S_{XC}[\rho] - \int_{t_0}^{t_1} \int \rho(\vec{r},t) v_{ext}(\vec{r},t) dt d\vec{r}, \tag{4.38}$$

where

$$S_H[\rho] = -\frac{1}{2} \int_{t_0}^{t_1} \int \int \frac{\rho(\vec{r},t)\rho(\vec{r}',t)}{|\tilde{\mathbf{r}} - \tilde{\mathbf{r}}'|} dt d\vec{r} d\vec{r}', \tag{4.39}$$

and the xc-action S_{xc}, similar to ground-state DFT, contains all the missing contributions to the functional $A[\rho]$. The stationary action principle then leads to the equation

$$\frac{\delta S_0[\rho]}{\delta(\vec{r},t)} - v_s(\vec{r},t) = 0, \tag{4.40}$$

where,

$$\begin{aligned} v_s(\mathbf{r},t) &= v_H((\mathbf{r},t) + v_{xc}((\vec{r},t) + v_{ext}((\vec{r},t) \\ &= \int \frac{n(\vec{r}',t)}{|\vec{r} - \vec{r}'|} d\vec{r}' - \frac{\delta A_{xc}[\rho]}{\delta \rho(\vec{r},t)} + v_{ext}(\vec{r},t). \end{aligned} \tag{4.41}$$

Equation (4.40) is the Euler equation of a system of independent electrons moving in a time-dependent potential equal to $v_s(\vec{r},t)$. Therefore, the exact density of the many-body system can be obtained from the one-particle time-dependent Schrödinger equation,

$$i\frac{\partial}{\partial_t} \psi_i(\mathbf{r},t) = \left[-\frac{1}{2}\nabla^2 + v_s(\vec{r},t) \right] \psi_i(\vec{r},t), \tag{4.42}$$

called the time-dependent Kohn-Sham (TD-KS) equation. The density is to be built from the orbitals $\psi(\vec{r},t)$ through the relation,

$$\rho(\vec{r},t) = \sum_{N_v}^{i} |\psi_i(\mathbf{vec},t)|^2, \tag{4.43}$$

where the sum is over the occupied states.

4.2.2 Adiabatic approximation

Thus far the theory is pretty much exact and so useless unless we can find suitable approximations for the time-dependent xc-functional. The exact v_{xc} depends nonlocally on the density both in the *spatial* and in the *time* variables (memory dependence). Fortunately, by disregarding the memory dependence,

we obtain an approximation which is not too bad and that has been successfully applied in many cases. This approach, called the adiabatic exchange [20] -correlation approximation (AxcA). It may be written formally as,

$$v_{xc}^{adia}[\rho](\mathbf{r},t) = \frac{\delta E_{xc}[\rho(t)]}{\delta\rho(\vec{r};t)}\,. \tag{4.44}$$

It is important to understand this equation. On the left-hand side, we have the functional derivative of a functional of a function of four variables (x,y,z,t) (and spin),

$$v_{xc}[\rho](\vec{r},t) = \frac{\delta S_{xc}[\rho]}{\delta\rho(\vec{r},t)}\,, \tag{4.45}$$

but on the right-hand side, we only have the functional derivative of a functional of a function of three variables (x,y,z) (and spin) because time is treated as a fixed parameter (hence the semicolon) which does not enter into the functional differentiation,

$$\frac{\delta E_{xc}[\rho(t)]}{\delta\rho(\vec{r};t)} = v_{xc}[\rho(t)](\vec{r};t)\,. \tag{4.46}$$

This allows us to replace the xc-functional S_{xc} about which relatively little is known with the somewhat betterer known xc-functional E_{xc}. In the limit of an external potential that varies slowly in time, the AxcA becomes exact if the true xc ground-state functional is known. In practice the results are also affected by the faults of the ground-state approximations, such as the lack of spatial nonlocality of the LDA or the GGA. Nevertheless, despite its crudeness, the AxcA, often yields calculated optical spectra that are comparable with those of more demanding many-body methods.

4.3 Linear Response Theory

Many of the applications of TD-DFT concern the calculation of absorption spectra in the linear regime using the dipole approximation. With a weak external perturbing field, the results of such calculations can be compared to the findings of standard spectroscopic experiments by using linear response theory.

Linear response theory [21] is a straightforward consequence of the time-dependent Schrödinger equation in a perturbative treatment. For convenience, the equations will be considered in the frequency (energy) representation, obtained by Fourier transformation of time-dependent quantities.

Basically, the purpose of linear response theory is to study the variation of a given physical observable due to the application of a weak external perturbation. As it is usual in quantum mechanics, both the observable and the perturbation are represented by Hermitian operators.

4.3.1 Susceptibility

The fundamental quantity in time-dependent linear response theory is the generalized susceptibility which in the frequency domain can be written as,

$$\begin{aligned}\chi(\vec{r},\vec{r}',\omega) = \sum_n \Bigg[& \frac{\langle\Psi_0|\hat{\psi}^\dagger(\vec{r})\hat{\psi}(\vec{r})|\Psi_n\rangle\langle\Psi_n|\hat{\psi}^\dagger(\vec{r}')\hat{\psi}(\vec{r}')|\Psi_0\rangle}{\omega-(E_n-E_0)+i\eta} \\ & - \frac{\langle\Psi_0|\hat{\psi}^\dagger(\vec{r}')\hat{\psi}(\vec{r}')|\Psi_n\rangle\langle\Psi_n|\hat{\psi}^\dagger(\vec{r})\hat{\psi}(\vec{r})|\Psi_0\rangle}{\omega+(E_n-E_0)+i\eta}\Bigg]\,,\end{aligned} \tag{4.47}$$

where η is an infinitesimal positive number, Ψ_0 and Ψ_n are respectively the groundstate and excited-state wave functions that correspond to the energies E_0 and E_n, and $\hat{\psi}^\dagger(\vec{r})$ and $\hat{\psi}(\vec{r})$ are second-quantization field operators. The operator $\hat{\psi}^\dagger(\vec{r})\hat{\psi}(\vec{r})$ is the second-quantized version of the density operator,

$$\hat{\rho}(\vec{r}) = \sum_i^N \delta(\vec{r} - \vec{r}_i)\,, \tag{4.48}$$

where N is the number of electrons. The poles in Eq. (4.47) correspond to the excitation energies of the system. Using Eq. (4.47), the Fourier transform of the response of the expectation value of a local operator, $\hat{A}$ to a local time-dependent perturbation $v'_{ext}(\vec{r}',t)$ becomes,

$$A'(\omega) = \int A(\vec{r})\chi(\vec{r},\vec{r}')v'_{ext}(\vec{r}',\omega)d\vec{r}d\vec{r}'\,. \tag{4.49}$$

For an independent-particle system Ψ_0 and Ψ_n become Slater determinants of single-particle orbitals, $\psi_r(\mathbf{r})$, which correspond to the energies ε_r and Eq. (4.47) can then be written as,

$$\chi(\vec{r},\vec{r}',\omega) = \sum_{rs}(n_s - n_r)\frac{\phi_s^*(\vec{r})\phi_r(\vec{r})\phi_r^*(\vec{r}')\phi_s'(\vec{r})}{\varepsilon_s - \varepsilon_r + \omega + i\eta}\,, \tag{4.50}$$

where n_s and n_r are the occupation numbers. This equation is particularly important in TD-DFT since it is used to calculate the susceptibility of the Kohn-Sham system of noninteracting particles.

4.3.2 Polarizability

Polarizability is particularly important since it is strictly related to the absorption of electromagnetic radiation in the dipole approximation. In linear response theory, the dynamic polarizability is given by,

$$\alpha_{ij}(\omega) = \int r_i\chi(\vec{r},\vec{r}',\omega)r'_j d\vec{r}d\vec{r}'\,, \tag{4.51}$$

where r_i and r'_j are the components of the position operators $\vec{r}$ and $\vec{r}'$ in the first-quantized form. If we indicate with $\vec{d}'(\omega)$ the linear response of the dipole to the external perturbation $v'_{ext}(\vec{r}',\omega) = \vec{\mathscr{E}}(\omega)\cdot\vec{r}$ (where $\vec{\mathscr{E}}(\omega)$ is a weak electric field), we can write polarizability as,

$$\alpha_{ij}(\omega) = \frac{d'_i(\omega)}{\mathscr{E}_j(\omega)}\,, \tag{4.52}$$

which is also referred to as the *response tensor* of the dipole to an external electric field. In the case of unpolarized radiation, the mean polarizability is usually written in the form

$$\bar{\alpha}(\omega) = \frac{1}{3}Tr\alpha(\omega) = \sum_n \frac{f_n}{(E_n - E_0)^2 - \omega^2}\,, \tag{4.53}$$

where the spectroscopic oscillator strengths,

$$f_n = \frac{2}{3}(E_n - E_0)(|\langle\psi_0|x|\psi_n\rangle|^2 + |\langle\psi_0|y|\psi_n\rangle|^2 + |\langle\psi_0|z|\psi_n\rangle|^2)\,, \tag{4.54}$$

and x, y and z are the components of the position operator. Eq. (4.53) is a straightforward consequence of Eq. (4.47) and of Eq. (4.51).

For a molecular system we can write the absorption coefficient as,

$$I(\omega) \propto \omega \Im m(\bar{\alpha}(\omega + i\eta)). \tag{4.55}$$

Normally, the absorption coefficient I is defined by the relation,

$$F(z) = F_0 e^{Iz}, \tag{4.56}$$

where F indicates the intensity of an electromagnetic beam propagating along the z direction. We also note that the density of the energy of radiation is given by,

$$\rho = \frac{\mathscr{E}^2}{8\pi}, \tag{4.57}$$

where $\mathscr{E}$ is the norm of the electric field associated with the wave. The intensity F is provided by the product $c\rho$ where c is the speed of light. Using these relations, the energy per unit of time which is provided to the system under investigation by the light beam is written as,

$$\frac{dU}{dt} = c\frac{dU}{dz} = \frac{Vc}{8\pi}\frac{d\mathscr{E}^2}{dz} = -\frac{Vc}{8\pi} I\mathscr{E}^2, \tag{4.58}$$

where V indicates the volume. Inversion of this equation gives the I-equation as

$$I = -\frac{8\pi}{Vc\mathscr{E}^2}\frac{dU}{dt}. \tag{4.59}$$

In order to establish a connection with microscopic theory we rewrite Eq. (eq:energy-unit) as,

$$\frac{dU}{dt} = \sum_{if} \omega_{fi} W_{if} \tag{4.60}$$

where i and f denote occupied and empty energy levels, ω_{fi} is their difference in energy, and W_{if} is the transition probability per unit of time between levels i and f. To go further we have now to evaluate W_{if} using quantum mechanics. Reference here is made to the simple case of a single electron subject to an external potential $v_{ext}(\mathbf{r})$ and to electromagnetic radiation. The Hamiltonian for this system can be expressed as,

$$\hat{H} = \frac{1}{2}(-i\vec{\nabla} - \frac{\vec{A}}{c})^2 + v_{eff}(\vec{r}), \tag{4.61}$$

where $\mathbf{A}$ is the vector potential associated with the electromagnetic wave. Using the Coulomb gauge $\vec{\nabla} \cdot \mathbf{A}$ = 0 and ignoring the quadratic term in the vector potential, Eq. (4.61) can be simplified as,

$$\hat{H} = -\frac{1}{2}\nabla^2 + v_{eff}(\vec{r}) + \frac{i}{c}\vec{A} \cdot \vec{\nabla}, \tag{4.62}$$

where the last term of the Hamiltonian can be treated perturbatively. For an electromagnetic wave propagating along z, the vector potential can be chosen to be,

$$\vec{A}(z,t) = \vec{A}_0 e^{i(kz-\omega t)}\,, \tag{4.63}$$

where k is the wave number and ω is the frequency. In general, if the wavelength of the radiation is large in comparison with the dimension of the system under investigation, the vector potential can be expanded in powers of $kz = \frac{2\pi}{\lambda} z$,

$$\vec{A}(z,t) = \vec{A}_0 e^{-i\omega t}\left[1 + ikz - \frac{1}{2}(kz)^2 + ...\right] \tag{4.64}$$

The dipole approximation is then obtained by limiting the expansion to the first term, namely by discarding the dependence on the position. Using Fermi's golden rule, the transition probability per unit of time between two levels i (occupied) and f (unoccupied) is given by,

$$W_{if} = \frac{2\pi}{c^2}\left[\vec{A}_0 \cdot \langle \psi_f | \vec{\nabla} | \psi_i \rangle\right]^2 \delta(\omega_{fi} - \omega)\,. \tag{4.65}$$

Through the identity $\left[\vec{r}, \hat{H}\right] = \vec{\nabla}$ the term $\langle \Psi_f | \vec{\nabla} | \Psi_i \rangle$ can be expressed as,

$$\langle \psi_f | \vec{\nabla} | \psi_i \rangle = -\omega_{fi} \langle \psi_f | \vec{r} | \psi_i \rangle\,, \tag{4.66}$$

and Eq. (4.65) can finally be written as,

$$W_{if} = 2\pi\left[\vec{\mathscr{E}}_0 \cdot \langle \psi | \vec{r} | \psi \rangle\right]^2 \delta(\omega_{fi} - \omega)\,, \tag{4.67}$$

where we used the relation $\vec{\mathscr{E}}_0 = \frac{i\omega_{fi}}{c}\vec{A}_0$. Now W_{if} is ready to be inserted in Eq. (4.60) to obtain the absorption coefficient through Eq. (4.59). It is now straightforward to note the equivalence of Eq. (4.55) and Eq. (4.59).

4.3.3 Linear-Response TDDFT and Dyson-Like Equation

For an interacting system, the perturbation v'_{ext} [see Eq. (4.49)] introduces a first-order change in the electronic density that can be expressed as,

$$\rho'(\vec{r},\omega) = \int \chi(\vec{r},\vec{r}',\omega) V'_{ext}(\vec{r}',\omega) d\vec{r}'\,, \tag{4.68}$$

where χ is the generalized susceptibility as per Eq. (4.47). Since the the noninteracting Kohn-Sham equation [Eq. (4.42)] has the same time-dependent density as the many-body problem, the response of the density $\rho'(\vec{r},\omega)$ is also the same. In this case in which the equations are a bit more complicated due to the dependence of the effective potential on the internal variables, the resultant response of the density can be written as,

$$\rho'(\vec{r},\omega) = \int \chi_s(\vec{r},\vec{r}',\omega) v'_s(\vec{r},\omega) d\vec{r}'\,, \tag{4.69}$$

where ,

$$v'_s(\vec{r},\omega) = v'_{ext}(\vec{r},\omega) + v'_H(\vec{r},\omega) + v'_{xc}(\vec{r},\omega)\,, \tag{4.70}$$

and χ_s is the KS susceptibility,

$$\chi_s(\vec{r},\vec{r}',\omega) = \sum_{ij}(n_j - n_i)\frac{\phi_j^*(\vec{r})\psi_i(\vec{r})\psi_i^*(\vec{r}')\psi_j(\vec{r}')}{\varepsilon_j - \varepsilon_i + \omega + i\eta}\,, \tag{4.71}$$

where ψ_i and ψ_j indicate the ground-state KS orbitals corresponding to the eigenvalues ε_i and ε_j. It is important to note that, if i and j are both occupied or empty levels, the corresponding contribution to χ vanishes. Equation (4.70) also introduces the first-order response of the Hartree+xc correlation potential induced by the application of v'_{ext},

$$v'_{Hxc}(\vec{r},\omega) = v'_H(\vec{r},\omega + v'_{xc}(\vec{r},\omega) = \int \kappa(\vec{r},\vec{r}',\omega)n'(\vec{r}',\omega)d\vec{r}'\,. \tag{4.72}$$

The kernel κ is defined by,

$$\kappa(\vec{r},\vec{r}',\omega) = \frac{1}{|\vec{r}-\vec{r}'|} + \frac{\delta v_{xc}(\vec{r},\omega)}{\delta_n(\mathbf{r}')}\bigg|_{n=n_0}\delta(t-t')\,, \tag{4.73}$$

where the second term is a functional of the ground-state density only. In the AxcA the dependence of Eq. (4.73) on the frequency is not explicit because the xc contribution to the kernel is local in time,

$$f_{xc}^{adia} = \chi_s(\vec{r},\vec{r}',t'_t) = \frac{\delta v_{xc}(\vec{r})}{\delta_n(\vec{r}')}\bigg|_{n=n_0}\delta(t-t')\,. \tag{4.74}$$

By equating the density response in Eq. (4.68) and Eq. (4.69) and by using Eq. (4.72), one obtains the Dyson-like equation of TDDFT linear response,

$$\chi(\vec{r},\vec{r}',\omega) = \chi_s(\vec{r},\vec{r}',\omega) + \int\int \chi_s(\vec{r},\vec{r}',\omega)\kappa(\vec{r}_1,\vec{r}_2,\omega)\chi(\vec{r}_2,\vec{r}',\omega)\,d\vec{r}_1 d\vec{r}_2\,. \tag{4.75}$$

As already noted earlier, the poles of the response function χ are excitation energies of the interacting system and the residues are the corresponding oscillator strength. The kernel κ is responsible for the corrections to the non interacting KS susceptibility Eq. (4.71). Setting $\kappa = 0$ gives exactly $\chi = \chi_s$. It is important to notice that the optical spectra can be obtained from the Dyson-like equation through Eq. (4.51).

The practical solution of Eq. (4.75) is quite an expensive operation from both computational and memory-requirement points of view. Practically, because of its unfavorable scaling, this approach is feasible only for systems consisting of a small number of atoms. As a result of these limitations, more efficient ways to cope with the problem of optical properties have been devised.

4.3.4 Casida's equations

The absorption spectrum is given in stick form by the poles of the dynamic polarizabiity (excitation energies ω_I) and by its residues (oscillator strengths, f_I). The problem is how to calculate these quantities efficiently. Casida's equations [22] entail a reformulation of the calculation of the poles (which are the transition energies) of the response function χ into a generalized Hermitian eigenvalue problem. This applies to frequency-independent kernels. The Casida approach is the most widespread among quantum chemists and this has seen it implemented in many *ab initio* codes. It is especially appropriate for the calculation of optical properties. Its limitation is in terms of its inability to access broad energy ranges.

The derivation of Casida's equations starts with Eq. (4.69) where V'_{Hxc} in turn depends linearly upon the response of the density through Eq. (4.72). By explicitly substituting the KS susceptibility [Eq. (4.71)] in

Eq. (4.69), one notices that the factorization allows for a direct integration of the product of the response function and of the first order change in the potential. The induced density change can then be written as,

$$\rho'(\vec{r},\omega) = \sum_{ij} P'_{ij}\phi_j^*(\vec{r})\phi_i(\vec{r})\,, \tag{4.76}$$

in which the expansion coefficients are given by,

$$Pij'(\omega) = \frac{n_j - n_i}{\varepsilon_j - \varepsilon_i + \omega + i\eta} \int \phi_i^*(\mathbf{r}) v'_s(\vec{r},\omega)\phi_j(\vec{r})d\vec{r}. \tag{4.77}$$

These coefficients are nonzero only if they connect virtual states with occupied states and vice versa. Explicit insertion of ρ' in the form of Eq. (4.76) in Eq. (4.73) and by use of this last equation to evaluate Eq. (4.77), one obtains the linear system,

$$\sum_{kl}\left[\frac{\omega - (\varepsilon_k - \varepsilon_l)}{n_j - n_i}\delta_{ik}\delta_{jl} - k_{ij,kl}\right]P'_{kl}(\omega) = \int \phi_i^*(\vec{r})v'_{ext}(\vec{r},\omega)\phi_j(\vec{r})d\vec{r}\,, \tag{4.78}$$

where,

$$k_{ij,kl}(\omega) = \int\int \phi_i^*(\vec{r})\phi_j(\vec{r})\kappa(\vec{r},\vec{r}',\omega)\phi_k^*(\vec{r}')\phi_l(\vec{r}')\,, \tag{4.79}$$

is the coupling matrix and $\kappa(\vec{r},\vec{r}',\omega)$ is the xc-kernel kernel given by Eq. (4.73). With some more algebraic manipulations and by setting $v'_{ext} = 0$, Eq. (4.78) can be written in the final form of Casida's equations,

$$\Omega\vec{F}_I = \omega_I\vec{F}_I\,. \tag{4.80}$$

where

$$\Omega_{ij,kl} = (\varepsilon_l - \varepsilon_k)^2\delta_{ik}\delta_{jl} + 2\sqrt{(n_i - n_j)(\varepsilon_j - \varepsilon_i)}k_{ij,kl}\sqrt{(n_k - n_l)(\varepsilon_l - \varepsilon_k)}\,, \tag{4.81}$$

is a Hermitian matrix. The eigenvalues of Eq. (4.80) provide the excitation energies of the system; the eigenvectors, instead, can be used to obtain the spectroscopic oscillator strengths and to assign the symmetry of each transition. The solution to Casida's equations requires that one diagonalizes the ground-state Hamiltonian in order to obtain all (or at least many of) the empty KS states.

This process has an unfavorable scaling, which makes this approach not particularly suitable for large basis sets, such as plane-waves. The most straightforward (and naïve) approach is to calculate the $N_v N_c$ dimensional matrix $\Omega_{ij,kl}$ explicitly and to store it. The most computational demanding task is to calculate the coupling matrix in Eq. (4.79). Indeed, if we suppose to calculate it in real space, the computational cost amounts to $N_{grid}^2 N_v^2 N_c^2$, but it usually decreases for the xc part since this term is local (at least in ALDA). This rough estimation shows a really unfavorable scaling as the 6^{th} power of the system dimension. Once the matrix is constructed it is diagonalized and this requires a cost that scales as $N_v^3 N_c^3$. In practice this is never done. It is possible to take advantage of iterative techniques that do not require the explicit calculation and storage of the full matrix. The coupling matrix can be evaluated using techniques, which are already well established for ground-state calculations. These techniques include the auxiliary function expansion method for localized basis sets and fast Fourier transforms in plane-wave implementations. In this scheme the computational cost is significantly reduced. The real shortcoming of this approach is that iterative techniques allow for the calculation of only a limited number of the lowest eigenvalues. The approach is prone to serious problems when particularly large systems have to be treated. Normally an increase in the size of the system leads to an increase in the density of transitions in a given energy range.

References

[1] W. Koch and M. C. Holthausen, *A Chemists' Guide to Density Functional Theory*. Weinheim: Wiley-VCH, 2001.

[2] R. G. Parr and W. Yang, *Density-Functional Theory of Atoms and Molecules*. New York: Oxford University Press, 1989.

[3] L. H. Thomas, "The calculation of atomic fields," *Proc. Cambridge Phil. Roy. Soc.*, vol. 23, pp. 542–548, 1927.

[4] R. J. Baxter, "Inequalities for potentials of particle systems," *III.J.Math.*, vol. 24, pp. 645–652, 1980.

[5] E. H. Lieb, "Thomas-Fermi and related theories of atoms and molecules," *Rev.Mod.Phys.*, vol. 53, pp. 603–641, 1981.

[6] P. Hohenberg and W. Kohn, "Inhomogeneous electron gas," *Phys. Rev.*, vol. 136, pp. B864–871, 1964.

[7] W. Kohn and L. J. Sham, "Self-consistent equations including exchange and correlation effects," *Phys. Rev.*, vol. 140, pp. A1133–1138, 1965.

[8] J. P. Perdew and A. Zunger, "Self-interaction correction to density-functional approximations for many-electron systems," *Phys. Rev.*, vol. B 23, p. 5048, 1981.

[9] L. W. S. Vosko and M. Nusair, "Accurate spin-dependent electron liquid correlation energies for local spin density calculations: a critical analysis," *Can. J. Phys.*, vol. 58, p. 1200, 1980.

[10] D. M. Ceperley and B. J. Alder, "Ground state of the electron gas by a stochastic method," *Phys. Rev. Lett.*, vol. 45, pp. 566–569, 1980.

[11] C. Filippi, X. Gonze, and C. Umrigar, "Generalized gradient approximations to density functional theory: comparison with exact results." Recent Develoments of Density Functional Theory, 1996.

[12] K. B. J. P. Perdew and M. Ernzerhof, "Generalized gradient approximation made simple," *Phys. Rev. Lett.*, vol. 77, pp. 3865–3868, 1996.

[13] G. C. Evans, *Functionals and Their Applications*. New York: Dover, 1964.

[14] J. Tao, J. P. Perdew, V. N. Staroverov, and G. E. Scuseria, "TPSS: Climbing the Density Functional Ladder: Nonempirical Meta-Generalized Gradient Approximation Designed for Molecules and Solids," *Phys. Rev. Lett.*, vol. 91, p. 146401, 2003.

[15] A. V. Krukau, G. E. Scuseria, J. P. Perdew, and A. Savin, "Hybrid functionals with local range separation," *J. Chem. Phys.*, vol. 129, p. 124103, 2008.

[16] K. Sharkas, J. Toulouse, and A. Savin, "Double-hybrid density-functional theory made rigorous," *J. Chem. Phys.*, vol. 134, p. 064113, 2011.

[17] E. K. U. Gross and E. Runge, "Density-functional theory for time-dependent systems," *Phys. Rev. Lett.*, vol. 52, pp. 997–1000, 1984.

[18] A. L. Fetter and J. D. Walecka, *Quantum Theory of many-particle systems*. New York: McGraw, 1971.

[19] G. Vignale, "Real-time resolution of the causality paradox of time-dependent density-functional theory," *Phys. Rev. A*, vol. 77, p. 062511, 2008. "Real-Time Resolution of the Causality Paradox of Time-Dependent Density-Functional.

[20] X. Gonze, "Adiabatic density-functional perturbation theory," *Phys. Rev.*, vol. A 52, pp. 1096–1114, 1995.

[21] E. K. U. Gross and W. kohn, "Local Density-functional Theory of Frequency-Dependent Linear Response," *Phys. Rev. Lett.*, vol. 55, pp. 2850–2852, 1985.

[22] M. E. Casida, *In Recent Advances in Density Functional Methods, Part I Chong, P., editor*. Singapore: World Scientific, 1995.

CHAPTER 5

BASICS OF PHOTOCHEMISTRY AND PHOTOPHYSICS

5.1 Introduction

Photochemistry is the study of chemical reactions that are light-induced or light producing [1]. Excitation by light of a chemical species is common to many fields including photophysics, photocatalysis, electrochemistry, chemical and electrochemical luminescence and photoelectrochemistry .

Some uses of photochemistry include: targetting specific sites during reactions due to absorptions of specific energies, use of chlorophyll as a photocatalyst, photography, vision, cycloaddition reactions, photochemical synthesis (green chemistry), ultrashort pulses, electron dynamics versus efficiency of photovoltaic cells, solar cells (conversion of solar to electric energy), optical devices for data processing, pharmacology, cancer treatment, Human Immuno-deficiency Virus (HIV) treatment, photo-induced asymmetric synthesis and organic sunscreens,

Most of the interesting absorptions in the excitation-related processes above occur in the ultraviolet (UV) (UV 200-400 nm) or visible (400-800 nm) region of the electromagnetic spectrum [2].

An excited electronic state will have a completely different electron distribution from that of the ground state, a different geometry, and will most likely undergo different chemical reactions from those of the ground state.

5.2 Absorption and Emission

A system may be excited by absorbing radiation, through a chemical reaction or by an energy transfer process [3].

Photochemistry has been viewed as affording an alternative route to thermal-based synthesis. In a photochemically-driven process, the chemical reaction passes through an excited electronic state.

The energy of a photon ($E = \frac{hc}{\lambda}$) required to produce a particular excited state is the difference in energy between that state and the ground state.

5.2.1 Vertical Excitations

Electronic transitions are usually vertical [4, 5]. The reason for this is that the electron is so light compared to the nuclei such that the electron transition time is too short for the nuclei to adjust correspondingly. All

electronic transitions end up in higher vibrational states of the excited state. Electron transition changes the electron density in the molecular system [6]. The consequence of this is usually the increase in bond lengths. This development then leads to complete adjustment in which the molecule now starts to vibrate around the new lengths. For every electronic transition, one obtains a series of normal vibrations associated with it. The many vibrational levels have their corresponding excited rotational sublevels in the gas phase. The situation is more complicated in the liquid phase because, among other things the frequent collisions caused by the surrounding solvent molecules. These contribute to peak broadening.

Another important outcome of absorption, related to the vertical transition idea, is that due to rapid vibrational relaxation from the highest vibrational levels, it does not matter the variation in excitation energies, the photon emission (fluorescence and phosphorescence) is usually independent of that variation for it always starts after the initial relaxation to the lowest vibrational level [2, 7].

5.2.2 Spin Multiplicity and Electronic States

The vertical nature of the electronic transition discussed in the preceding subsection is governed by the spin multiplicity ($2S+1$, where S is the total spin of all electron spins) requirement. Given a singlet ground state, it can only be excited into an excited state with the same spin multiplicity. This is in accordance with the spin preservation requirement. Quantum mechanics forbids spin flip during electronic transitions in the sense that it violates the $\Delta S = 0$ rule. This requirement then imposes serious constraints to what formally can happen and what can not. For closed shell systems a singlet is one with paired electrons. For an open system the possible spin-down and spin-up electronic configurations are linearly combined. The sum of such combinations yields a singlet state while the difference yields a triplet state. Figure 5.1 illustrates the nature of these configurations.

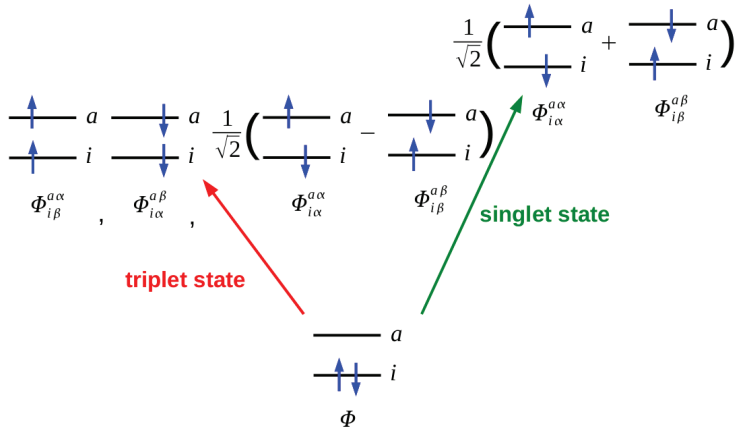

Figure 5.1: Diagram illustrating how to determine singlet states from closed and open shell molecules

5.2.3 Energies of Electronic States

As already seen above, electronic states of closed shell molecules are usually classified into two main categories, singlet states and triplet states based on their spin multiplicities.

A point to note here is that the two different excited electronic state types differ significantly in their properties as well as in their energies. A triplet state will always lie lower in energy than its corresponding singlet state.

Another factor in energy determination is the type of transitions taking place. The metal-to-ligand transitions are the least energetic while those involving only the ligand molecular orbitals can turn out to be so energetic as seen on the figure 5.2.

The difference in the energies of different electronic states is as a result of *spin correlation effect*. Besides the coulomb interaction, the Fermi correlation keeps the electron pairs with parallel spins spatially separated thereby reducing the electron repulsion energy. In a triplet excited state, the two single electrons found on the HOMO and the LUMO, respectively, tend to adopt a configuration that maximizes their spatial separation and, thus, the transition dipole moment. This results in a lower energy level for T_1 compared to S_1 state. This spin correlation effect is more noticeable for spatially overlapping HOMO and LUMO orbitals, such as in (π, π^*) state, and is less important for (n, π^*) state, for instance.

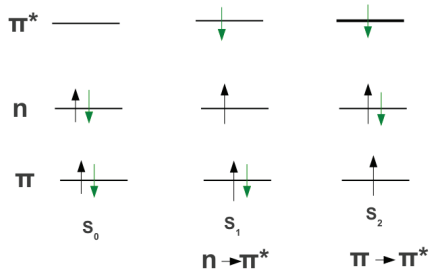

Figure 5.2: Arrangement of molecular orbitals showing the origin between the different energies of MLCT and LLCT states

5.2.4 Spin-Orbit Coupling

This kind of coupling has tremendous effects on the photophysical and photochemical phenomena involving the triplet excited state. For heavy atoms there is coupling between the orbital magnetic moment and the spin magnetic moment [8–10]. The consequence of this is to yield vibrational levels that are iso-energetic though belonging to both the two (impure singlet and impure triplet) excited states. In the presence of spin-orbit term, S is no longer a nice quantum number for it allows the singlet and the triplet to mix. In this sense, we see a contamination of a singlet state by some triplet contributions as well as that of the triplet state by the singlet state. For this reason we talk about impure (contaminated) states.

Apparently it is the generation of a considerable orbital magnetic moment that actually matters in this whole exercise. It can be due to a heavy metal ion that is part of the molecule such as a transition metal ion or what is emerging is that besides that requirement, even heavy atoms [10] just around the system can generate orbital magnetic moment that help in mixing the singlet and triplet vibrational levels even more and this has the effect of increasing the ISC efficiency.

5.3 Luminescence

Luminescence is the emission of light by cold substances [2]. It differs from incandescence which is black body radiation. Luminescence as an emissive process has many causes, differentiated by the specific type of initial excitation that finally leads to that emission. Some of them include the following; chemiluminescence, sonoluminescence, bioluminescence, electroluminescence and photoluminescence In the following we mean photoluminescence whenever we refer to luminescence emission that is is triggered by photoexcitation. This way, luminescence may be divided into fluorescence and phosphorescence.

It is photoluminescence, that the concept of luminescence will refer to in this work. This is emission that is is triggered by photoexcitation. It generally refers to fluorescence and phosphorescence.

5.3.1 Stokes Shift

The Stokes shift is the difference (in energy units) between positions of the band maxima of the absorption and emission spectra of the same electronic transition [11]. A small Stokes shift is indicative of a rigid molecule, with little change in the equilibrium nuclear configuration in the ground- and excited states.

5.3.2 The Jablonski Diagram

This diagram (figure 5.3) describes many of the photochemical and photophysical phenomena. On any Jablonski diagram [2], one observes a vertical arrangement of electronic states (with increasing energy) while the states with different spin multiplicities are arranged horizontally. For every electronic state there are a number of vibrational states (see section 5.2.1). The vibrational state with the lowest energy in every electronic state is denoted by a thick line. The other vibrational states shown by use of thin lines.

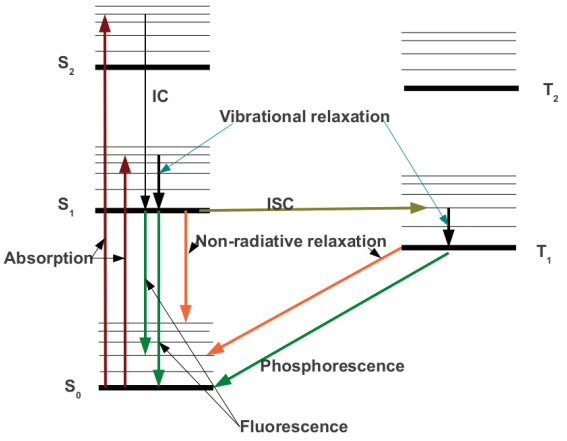

Figure 5.3: Jablonski diagram. It shows the key absorptive and emissive processes that usually characterize a photophysical and photochemical process

The critical point to observe from the figure the Jablonski diagram is that there is a range of wavelengths that can lead to a transition between any two electronic states, which account for the fact that electronic spectra generally occur as broad bands and not as single lines. This is based on the fact that we can have transitions originating from ground state but ending up into different vibrational states of a given excited state. One rarely sees any arrow (transition) from the ground state to the triplet state. This is due to the forbiddenness of such transitions which makes them highly unlikely (improbable) (see section 5.2.2).

5.4 Potential Energy Surfaces

With the consideration of Born-Oppenheimer approximation,it is possible to determine the adiabatic energy E_I^e which is the energy of the electrons calculated at fixed nuclear positions plus the nuclear repulsion energy.

$$\hat{H}^e(\mathbf{r},\mathbf{R})\Psi_I^e(\mathbf{x},\mathbf{R}) = E_I^e(\mathbf{R})\Psi_I^e(\mathbf{x},\mathbf{R}) \tag{5.1}$$

A plot of this energy against different nuclear positions yields what is called the potential energy surface (PES). This energy is only valid in situations where the nuclei move much more slowly than the electrons and is only observed in ground state processes. In photoexcitation, the reactants in the

minimum basin of the ground state PES absorb energy to get to the excited state where they start moving along its PES. A pathway to decay back to the ground state happens when the system reaches the *conical intersection* (CX) region on figure 5.4 . This is a point where the ground state and the excited state are degenerate. At this point, the the nuclei and the electrons are equally fast and as a result, the Born-Oppenheimer separation is invalidated. The description of the processes at the conical intersection done diabatically since the electronic and nuclear motions can not be separated.

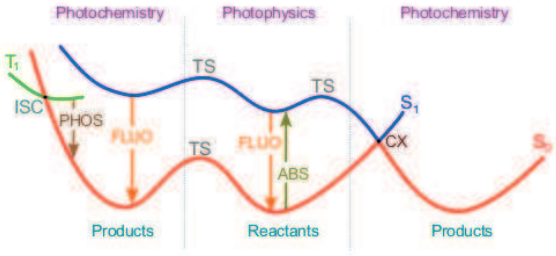

Figure 5.4: Potential Energy Surfaces (PES). An interesting point on this PES is the conical intersection (CX). A point where the system either reverts to the ground state or the absorbed energy transforms it into a new species, the product. Figure from Ref [12]

5.5 Excited state lifetime and Quantum Yield

The excited-state lifetime (τ) is a measure of the time a given excited state survives before relaxing by radiative or nonradiative mechanisms to the ground state. The luminescence lifetime is the time a luminescent species stays in its excited state before it emits a photon [2].

Quantum yield Φ in the sense of luminescence is given as

$$\Phi = \frac{photons\ \ emitted}{photons\ \ absorbed} \tag{5.2}$$

According to this equation, the calculated value of Φ above is an indication of the emission efficiency of a luminescent species.

It is important to distinguish between quantum yield and quantum efficiency (QE). Which is the incident photon to converted electron ratio of a photosensitive device. In this sense it is seen as a measure of the device's electrical sensitivity to light. Taking an example of a solar cell, its external quantum efficiency $E\Phi E$ is given by,

$$E\Phi E = \frac{electrons/sec}{photons/sec} \tag{5.3}$$

A low value of $E\Phi E$ clearly shows that the solar cell is performing very badly for its active part is not able to make good use of the incident photons.

Applying a very short pulse of light to a dilute solution of fluorescent molecules leads to their excitation from the ground state S_0 to the excited state S_1. Taking the concentration of the excited molecules as $[^1B^*]_0$, their rate of return to ground state is given as

$$-\frac{d[^1B^*]}{dt} = (k_r^s + k_{nr}^s)[^1B^*] \tag{5.4}$$

where k_r^s is the sum of the radiative rate constants while k_{nr}^s is the sum of the nonradiative rate constants. On integration of equation 5.4 one gets equation 5.5,

$$[^1B^*] = [^1B^*]_0 exp(\frac{t}{\tau_s}) \tag{5.5}$$

where $[^1B^*]_0$ is the concentration of excited molecules at time 0 resulting from pulse light excitation and τ_s the lifetime of excited state S_1, is given by

$$\tau_s = \frac{1}{k_r^s + k_{nr}^s} \tag{5.6}$$

The fluorescence intensity i_F(t) at time t after excitation and which is defined as the amount of photons (in moles) emitted per unit time (s) and per unit volume of solution (liter: L) is proportional, at any time, to the instantaneous concentration of molecules still excited. The proportionality factor is the rate constant for the radiative de-excitation k_r^s

$$i_F(t) = k_r^s[^1B^*] = k_r^s[^1B^*]_0 exp(\frac{t}{\tau_s}) \tag{5.7}$$

5.6 De-activation mechanisms

Once in an excited state, a system seeks to relax to the lowest attainable stationary state. Usually the relaxation process entails loss of excess energy through either radiative or non-radiative mechanisms. According to Kasha-Vavilov's rule [7], a molecule in an electronic excited state, quickly relaxes to the lowest vibrational level and from there they can decay to the lowest electronic state via radiative (photon emission) or non-radiative processes.

5.6.1 Non-radiative pathways

The mechanisms comprise internal conversion (IC) intersystem crossing(ISC). Internal conversion [2] refers to the transfer that takes place between states of the same spin multiplicity. Internal conversion implies the transformation of electronic excitation into vibrational energy. This process takes place through **nuclear tunneling** from the excited state potential surface to that of the ground state. Strong overlap of vibrational wave functions is necessary. Since back-tunneling can also readily occur, fast vibrational relaxation (VR) is an important condition for the efficiency of this deactivation pathway.

Intersystem crossing [2, 13] takes place between an electronic excited state and another excited state characterized by a different spin multiplicity such as in $S_1 \rightarrow T_1$. This process involves a simultaneous change in spin. Vibrational relaxation is also necessary to avoid crossing back to the initial system.

It is worth noting that the smaller is the energy gap between the states, the higher is the probability for transfer. It therefore follows that the most favorable topology for the transfer is the **conical intersection point** [12, 14] where the crossing occurs between states of the same *spatial* and *spin* symmetry. The next section (5.4) deals with these special features.

5.7 Fluorescence and Phosphorescence

These are the two forms of luminescence that have a direct bearing to the discussions in this thesis. This section gives a more detailed treatment of this kind of luminescence. The luminescence in section is described as a form of radiative deactivation (photoemission). They involve electronic transitions and condition which makes them be submitted to the same selection rules as the ones for light absorption . The mechanisms consist of Fluorescence and Phosphorescence.

5.7.1 Fluorescence

Fluorescence [2] is the radiative deactivation (occurring over a time interval ranging between 10^{-9} s and 10^{-5} s) pathway that occurs between two states of identical spin multiplicity. This transition is spin allowed. This is so because the absorption process occurs over a short time interval (10^{-15}s) and does not change the direction of the electron spin. Because vibrational relaxation occurs about 1000 times faster than de-excitation, most molecules return to a low-vibrational state before the de-excitation takes place. Vibrational relaxation [15] (emission of IR while lowering vibrational state) occurs in 10^{-12} s It should be noted that even though a quantum of radiation is emitted in fluorescence this quantum will be lower in energy on the average than the quantum absorbed by the molecule, due to vibrational relaxation (both after absorption and after emission). The change in photon energy causes a shift of the fluorescence spectrum to longer wavelength, relative to the absorption spectrum, this is referred to as the Stokes Shift (see section 5.3.1).

5.7.2 Phosphorescence

Although population of triplet states by direct absorption from the ground state is insignificant, the process of intersystem crossing provides a more efficient method to populate triplet states from the lowest excited singlet state in many molecules. This is basically a spin-dependent internal conversion process.

The mechanism for intersystem crossing (see section 5.2.4) involves vibrational coupling between an excited singlet state and a triplet state. This is the reason why the less probable singlet-triplet processes occurs within the lifetime of an excited singlet state (10^{-8} sec).

Given that singlet-triplet processes are less probable than singlet-singlet processes by a factor of 10^{-5} to 10^{-6}, and that radiationless vibrational processes (such as internal conversion) occur in approximately 10^{-13} sec, the time required for a spin-forbidden vibrational process would be approximately 10^{-8} to 10^{-7} sec, which is the same order of magnitude as the lifetime of an excited singlet state. Therefore intersystem crossing can compete with fluorescence emission from the zeroth vibrational level of an excited singlet state but cannot compete with vibrational deactivation from higher vibrational level of a singlet state.

Once intersystem crossing has occurred the molecule undergoes the usual internal conversion process (10^{-13} to 10^{-11} sec) and falls to the zeroth vibrational level of the triplet state. Since the difference in energy between the zeroth vibrational level of the triplet state and the zeroth vibrational level of the lowest exited singlet state is large compared to thermal energy, repopulation of a singlet state from a triplet state is highly improbable.

There are two factors which tend to enhance a radiationless transition between the lowest triplet state and the ground state. First, the energy difference between the triplet state and the ground state is smaller than the difference between the lowest singlet state and the ground state. This tends to enhance *vibrational coupling* between these two states, and therefore to enhance internal conversion. Secondly, and more important, the *life time* of a triplet state is much longer than that of an excited singlet state (about 10^{-4} to 10 sec) and therefore loss of excitation energy by collisional transfer is generally enhanced. Indeed, this second process is so important that in solution at room temperature it is often the dominant mechanism for the loss of triplet state excitation energy.

5.8 Luminescence (Fluorescence) Quenching

Quenching [2, 16] is an idea which means the reduction in the fluorescence intensity of a given fluorophore. Quite a number of processes lead to quenching of excitations. Some of these processes include complex-formation, excited state reactions, collisions and energy transfer. Factors such as temperature

and pressure that affect those processes directly become critical parameters when dealing with he quenching process.

What is tricky here is the factor that at a glance, quenching may seem as a problem. Indeed it depends largely on what aspect the observer is stressing. Quenching is finding use in a number of interesting applications. A typical example is the use the quenching effect of oxygen on certain ruthenium complexes. O_2 is a triplet quencher which is good for trapping radicals. The process helps in the determination of the extent of oxygen saturation in solution.

Molecular oxygen [13] used in the quenching process above belongs to a class of what are referred to as chemical quenchers. Other chemical substances capable of causing similar quenching are I^-, Cl^-, Br^- and C_3H_5NO. The quenching ability seems to be dependent on the nature of the anion. Among the halide ions, the ion with the strongest quenching ability is I^- and the one with the weakest quenching capability is Cl^-. This observation implies that the mechanism of quenching involves a charge transfer reaction. So the easier it is for an ion to release an electron, the higher is its quenching ability.

Generally heavy atoms are good quenchers [17]. This is based on the spin-orbit coupling effect discussed earlier. The mixing of singlet and triplet vibrational levels facilitates energy transfer.

Collision between the excited states and the ground state molecules is also a nice quenching route. Chemical reactions such as dimerizations can occur between excites molecules, certain photoisomerization processes an also occur. All these processes lead to increased quenching.

5.9 Solvation dynamics

In addition to internal nuclear coordinates, consideration of the solvation coordinate has also to be done whenever a molecule is dissolved in a polar solvent [2] absorbs light. On photoexcitation, the dipole moment of a solvated fluorophore is usually modified. The change in the molecular dipole moment is as a result of the energy differences between the ground state and the excited states.

Solvent dipoles have then to rearrange around the excited molecule as shown on Figure 5.5. This process entails the rotation of solvent molecules and depends on the viscosity. It is also referred to as solvent relaxation . It is fast enough to take place just before the fluorescence process.

Given the fact that absorption is a much faster process than solvent relaxation, it follows that absorption is not dependent on solvent polarity. Normally excitation of a fluorophore leads to higher vibrational levels of the first excited singlet state S_1. For this fluorophore to come back to the lowest vibrational level, it must rapidly lose energy to the surrounding solvent molecules. The solvent relaxation process has an even more critical contribution. The relaxation process lowers the energy of the excited state. This has the consequence of decreasing the energy separation between the excited state and the ground state. This leads to red shift in the fluorescence emission. Increasing solvent polarity means correpondingly increasing

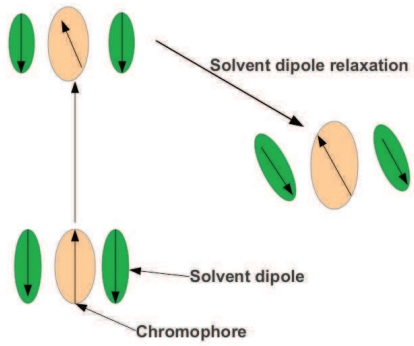

Figure 5.5: Solvation dynamics on photoexcitation. The solvent relaxation process contibutes to the lowering of the energy of the excited state. This ultimately leads to the red shift in the emission spectra

the reduction in the energy level of the excited state. This greatly reduces its separation from the ground state, with the result of increased wavelength of the fluorescence emission. It is worthy noting that decreasing solvent polarity reduces its effect on the energy of the excited state. Naturally one then asks the most logical question of whether or not the fluorophore polarity does have any effect. Fluorophore polarity determines the sensitivity of the excited state to solvent effects. Polar fluorophores are more affected than the non-polar ones.

References

[1] A. Kutateladze(Ed.), *Computational Methods in Photochemistry*. Denver, Colorado: Taylor & Francis, 2005.

[2] B. Valeur, *Molecular Fluorescence: Principles and Applications*. Paris: Wiley-VCH Verlag GmbH, 2001.

[3] C. T. Sanderson, J. A. Quinlan, R. C. Conover, M. K. Johnson, M. Murphy, R. A. Dluhy, and C. Kutal, "Characterization of the Low-Energy Electronic Excited States of Benzoyl-Substituted Ruthenocenes," *Inorg. Chem.*, vol. 44, pp. 3283–3289, 2005.

[4] E. Condon, "A theory of intensity distribution in band systems," *Phys. Rev. 28(6)*, pp. 1182–1201, 1926.

[5] J. Franck and E. G. Dymond, "Elementary processes of photochemical reactions," *Trans. Faraday Soc.*, vol. 21, pp. 536–542, 1926.

[6] F. P. Schäfer, *Principles of Dye Laser Operation. Dye Lasers*. Berlin: Springer-Verlag, 1990.

[7] M. Kasha, "Characterization of electronic transitions in complex molecules," *Discuss. Faraday Soc.*, vol. 9, pp. 14–19, 1950.

[8] M. Kasha, "Collisional perturbation of spin-orbital coupling and the mechanism of fluorescence quenching. a visual demonstration of the perturbation," *J. Chem. Phys.*, vol. 20(1), pp. 71–74, 1952.

[9] S. P. McGlynn, T. Azumi, and M. Kinoshita, *Molecular spectroscopy of the triplet state*. Englewood Cliffs: Prentice-Hall, 1969.

[10] G. A. Ketsle, L. V. Levshin, and V. V. Bryukhanov, "Mechanism of the external heavy atom effect on intersystem crossing in rhodamine dye solutions," *J. Appl. Spectrosc.*, vol. 24(5), pp. 573–577, 1976.

[11] G. G. Stokes, "On the change of refrangibility of light," *Phil. Trans. R. Soc. Lond.*, pp. 463–562, 1852.

[12] B. Natarajan, M. E. Casida, and T. Deutsch, *Non-Born-Oppenheimer dynamics and conical intersections. In E. K. U. Gross, M. A. L. Marques, F. Nogueira, and A. Rubio, editors, Fundamentals of Time-Dependent Density-Functional Theory, Lecture Notes in Physics.* Springer, 2012.

[13] F. Stracke, M. Heupel, and E. Thiel, "Singlet molecular oxygen photosensitized by Rhodamine dyes: correlation with photophysical properties of the sensitizers," *J. Photochem. Photobiol., A*, vol. 126(1-3), pp. 51–58, 1999.

[14] G. A. Worth and L. S. Cederbaum, "Beyond Born-Oppenheimer: Molecular dynamics through a conical intersection," *Annu. Rev. Phys. Chem.*, vol. 55, pp. 127–158, 2004.

[15] M. Mueller, *Fundamentals of Quantum Chemistry: Molecular Spectroscopy and Modern Electronic Structure Computations*. New York: Kluwer Academic/Plenum Publishers, 2002.

[16] J. R. Lakowicz, *Principles of fluorescence spectroscopy*. New York: Springer, 2006.

[17] M. Rae, A. Fedorov, and M. N. Berberan-Santos, "Fluorescence quenching with exponential distance dependence: Application to the external heavy-atom effect," *J. Chem. Phys.*, vol. 119(4), pp. 2223–2231, 2003.

CHAPTER 6

MULLIKEN POPULATION ANALYSIS-MPA

*This chapter serves as a precursor to bring an understanding to the section on Partial Density of States. PDOS (***see APPENDIX A: PARTIAL DENSITY OF STATES ANALYSIS-chapter 8***, of the attached manuscript). PDOS calculations require mulliken charges and the details of this are captured in the following section.*

It is usually desirable to describe molecular orbitals in terms of fragment orbitals [1, 2]. By fragments are meant basis functions (AOs), atoms [3, 4] or ligands. It is more meaningful to be able to determine how the various fragments contribute to a given molecular orbital. Population analysis [1] approaches partition all the electrons of a molecule among the various fragments according to some rules. This charge density analysis has been done by many methods. Among the many alternatives the oldest and most commonly used is Mulliken's. Results with this method tend to be only qualitative and have a strong basis set dependence, but Mulliken's method is widely implemented, fast, and simple. In order to understand Mulliken's method [5–11], let us write a molecular orbital (MO) as a linear combination of atomic orbitals (AOs) [12–14] on different atomic centers.

$$\psi_i(\mathbf{r}) = \sum_A \sum_{\mu \in A} \chi_{\mu A}(\mathbf{r}) c_{\mu A,i} \,. \tag{6.1}$$

The corresponding charge density [15–18] is,

$$\rho_i(\mathbf{r}) = \sum_A \sum_B \sum_{\mu \in A} \sum_{\nu \in B} \chi_{\mu A}(\mathbf{r}) \chi_{\nu B}(\mathbf{r}) c_{\mu A,i} c_{\nu B,i} \,, \tag{6.2}$$

which integrates to,

$$1 = \sum_A \sum_B \sum_{\mu \in A} \sum_{\mu \in B} S_{\mu A,\nu B} P^{(i)}_{\mu A,\nu B} \,, \tag{6.3}$$

where,

$$S_{\mu A,\nu B} = \langle \mu A | \nu B \rangle \,, \tag{6.4}$$

defines the overlap matrix [19, 20] and,

$$P^{(i)}_{\mu A,\nu B} = c_{\mu A,i} c_{\nu B,i}\,, \tag{6.5}$$

defines the density matrix for MO i. Mulliken chose to rewrite Eq. (6.3) as,

$$1 = \sum_A \sum_{\mu \in A} q^{(i)}_{\mu A}\,, \tag{6.6}$$

where the charge due to orbital μ on atom A is given by,

$$q^{(i)}_{\mu A} = \sum_B \sum_{\nu B} S_{\mu A,\nu B} P^{(i)}_{\mu A,\nu B}\,. \tag{6.7}$$

The all-electron generalization is obtained by using the total density matrix,

$$P_{\mu A,\nu B} = \sum_i^{\text{occ}} n_i P^{(i)}_{\mu A,\nu B}\,. \tag{6.8}$$

where n_i is the MO occupation number [17, 21, 22]. The partial charge on atom A due to MO i is just given by,

$$q^{(i)}_A = \sum_{\mu \in A} q^{(i)}_{\mu A}\,. \tag{6.9}$$

If this atom is just the central ruthenium atom in our complex, then the intensity of the Ru PDOS (before Gaussian convolution) is just given by,

$$q^{(i)}_{\text{Ru}} = \sum_{\mu \in \text{Ru}} q^{(i)}_{\mu \text{Ru}}\,. \tag{6.10}$$

The rest of the MO charge is on the ligands,

$$q^{(i)}_L = 1 - q^{(i)}_{\text{Ru}}\,. \tag{6.11}$$

If we are only interested in the d-orbitals on the ruthenium atom, then the intensity of the Ru d-orbital PDOS is given by,

$$q^{(i)}_{\text{Ru}d} = \sum_{\mu \in \text{Ru}d} q^{(i)}_{\mu \text{Ru}}\,. \tag{6.12}$$

Quantum chemistry programs print out enough information to calculate these quantities by hand or automatically by some programs.

Our own in-house Python program PDOS.PY used the printed information to calculate the PDOS and DOS and further plot them on the same set of axes. From the plotted PDOS and DOS peaks it is possible to determine the electron density distribution on each atom or fragment of interest.

References

[1] A. E. Reed, R. B. Weinstock, and F. Weinhold, "Natural Population Analysis," *J. Chem. Phys.*, vol. 83, pp. 735–746, 1985.

[2] S. Dapprich and G. Frenking, "Investigation of Donor-Acceptor Interactions: A Charge Decomposition Analysis Using Fragment Molecular Orbitals," . *Phys. Chem.*, vol. 99, pp. 9352–9362, 1995.

[3] F. Bader, "Atoms in Molecules," *Acc. Chem. Res.*, vol. 18, pp. 9–15, 1985.

[4] R. F. W. Bader, *Atoms in Molecules- A Quantum Theory, Volume 22 of International Series of Monographs on Chemistry*. Oxford: Oxford Science Publications, 1990.

[5] D. C. .Young, *Computational Chemistry: A Practical Guide for Applying Techniques to Real-World Problems*. New York: John Wiley & Sons, Inc., 2001.

[6] P. R. Schleyer, *Encyclopedia of Computational Chemistry*. New York: John Wiley & Sons, Inc., 1998.

[7] R. S. J. Mulliken, "Electronic Population Analysis on LCAO-MO Molecular Wave Functions.I.," *Chem. Phys.*, vol. I, pp. 1833–1840, 1955.

[8] R. S. J. Mulliken, "Electronic Population Analysis on LCAO-MO Molecular Wave Functions.II.," *Chem. Phys.*, vol. II, pp. 1841–1846, 1955.

[9] R. S. J. Mulliken, "Electronic Population Analysis on LCAO-MO Molecular Wave Functions.III.," *Chem. Phys.*, vol. III, pp. 2338–2342, 1955.

[10] R. S. J. Mulliken, "Electronic Population Analysis on LCAO-MO Molecular Wave Functions.IV," *Chem. Phys.*, vol. IV, pp. 2343–2346., 1955.

[11] J. P. Lowe and K. A. Peterson, *Quantum Chemistry 3^{rd} Edition*. Oxford: Elsevier Academic Press, 2006.

[12] E. R. Davidson, "Electronic Population Analysis of Molecular Wavefunctions," *J. Chem. Phys.*, vol. 46, pp. 3320–3324, 1967.

[13] J. D. Roberts, *Notes on Molecular Orbital calculations*. Massachusetts, 01 867, U.S.A.: THE BENJAMINICUMMIMGS PUBLISHING COMPANY, INC, 1961.

[14] S. R. Mulliken, "Criteria for the Construction of Good Self Consistent Field Molecular Orbital Wave Functions, and the Significance of LCAO-MO Population Analysis," *J. Chem. Phys.*, vol. 36, p. 3428, 1962.

[15] F. B.-K. J. Hinze and A. G. Lowe, "Molecular Charge Density Analysis," *Can. J. Chem.*, vol. 74, pp. 1049–1053, 1996.

[16] K. I. Ramachandran and G. D. K. Namboori, *Computational Chemistry and Molecular Modeling Principles and Applications*. Berlin Heidelberg: Springer-Verlag, 2008.

[17] K. R. Roby, "Quantum Theory of Chemical Valence Concepts. I. Definition of the Charge on an Atom in a Molecule and of Occupation Numbers for Electron Density Shared between Atoms," *Mol. Phys.*, vol. 27, pp. 81–104, 1974.

[18] S. M. Bachrach, *Population Analysis and Electron Densities from Quantum Mechanics Volume 5 of Rev. Comp. Chem., Chapter 3, S. 171-227*. New York: VCH Publishers, 1994.

[19] L. Pauling, *The Nature of the Chemical Bond and the Structure of Molecules and Crystals*. Ithaca: Cornell University Press, 1948.

[20] T. Hughbanks and R. Hoffmann, "Chains of trans-edge-sharing molybdenum octahedra: Metal-metal bonding in extended systems," *J. Am. Chem. Soc.*, vol. 105, pp. 3528–3537, 1983.

[21] L. Szasz, *The Electronic Structure of Atoms*. New York: John Wiley & Sons, 1992.

[22] C. Ehrhardt and R. Ahlrichs, "Population Analysis Based on Occupation Numbers II. Relationship between Shared Electron Numbers and Bond Energies and Characterization of Hypervalent Contributions," *Theor. Chim. Acta*, vol. 68, pp. 231–245, 1985.

CHAPTER 7

LITERATURE REVIEW OF LUMINESCENCE IN RUTHENIUM COMPLEXES

This chapter examines the general "bottom-up" approach to the construction of photochemical molecular devices (PMDs). It looks at the thinking that underlies the synthesis of suitable components and the difficulties encountered in this field. It then goes on to look at the possible use of computational tools to reduce some of these difficulties. Finally it concludes with a consideration of theoretical calculations similar to those done by us in this project and with particular focus on the nature of methods currently in use.

7.1 Introduction

The motivation behind the work carried out in this thesis was the desire to assemble larger systems from smaller units. This approach is what is commonly referred to as the "bottom-up" approach [1, 2].

Such assemblies are also referred to as supramolecules. They are capable of performing very complex functions. Supramolecules may be natural man-made (artificial). The functioning of functional supramolecules is often based on efficient charge separation [3, 4]. A pertinent biological example is photosystem II (PSII), an assembly of many parts working in harmony to ensure successful photosynthesis process occurs. Light activates the system and the energized electrons are transferred through a series of many intervening coenzymes and cofactors to sites where they cause reductions. The hole left by the transferred electrons then oxidizes water to give oxygen molecules and hydrogen ions. In this natural system, it is therefore seen that it is the electrons obtained from water that drive the photosynthesis [5] process.

Man-made light-activated assemblies intended to perform complex functions similar to those carried out by natural systems are collectively called photochemical (photoactivated) molecular devices (PMDs). They normally consist of many distinct components connected mainly by intermolecular forces [6–8].

Inspired especially by the natural systems that perform complex functions, we embarked on a process to design and build photochemical molecular devices. Since this process is component-based, our work was to start with the most critical component, the photosensitizer. Since there are all sorts of photosensitizers, we chose to focus mainly on the ones that are Ru(II)-based. Important experimental properties of

the parent complex $[Ru(bpy)_3]^{2+}$ are discussed in the section below for this is the complex that forms the basis of Ru(II) complexes that are our preferred photosensitizers.

7.2 Experimental Properties of the Archetype Compound $[Ru(bpy)_3]^{2+}$

The study of polypyridyl Ru(II) complexes usually starts with the prototype $[Ru(bpy)_3]^{2+}$ [9–12]. The other useful complexes are derived by application of various modification strategies to this particular species. Following the full characterization [13] of $[Ru(bpy)_3]^{2+}$, it is now known that its suitability is in part, based on its thermodynamic stability and kinetic inertness.

The characterization of $[Ru(bpy)_3]^{2+}$ is normally done by use of absorption spectroscopy and molecular fluorescence spectroscopy.

The determination of the extinction coefficient at a given absorption wavelength is done by plotting the absorbance against the concentration and then calculating the gradient of the resultant line which gives the extinction coefficient at that wavelength.

Spectroscopically, $[Ru(bpy)_3]^{2+}$ shows mainly three peaks in its absorption spectrum at 243 nm, 286 nm and at 450 nm. Besides, its lowest excited state ^{3}MLCT is long-lived in deaerated acetonitrile at 298 K. It also shows intense emission at about 610 nm in deaerated acetonitrile at 298 K.

The absorptions at 243 nm and 286 nm are assigned to $\pi \rightarrow \pi^*$ while the one at 450 nm is assigned to the metal-to-ligand charge transfer (MLCT). The ^{3}MLCT state has an excited lifetime (τ) of about 1 μs in organic solvents and 600 ns in water and a quantum yield (Φ) of about 6%.

Electrochemically, $[Ru(bpy)_3]^{2+}$ shows localized oxidation that is metal-centered (MC) and also corresponding localized reduction that is ligand-centered (LC). An even more interesting feature is that $[Ru(bpy)_3]^{2+}$ in its ^{3}MLCT excited state is both a reductant as well as an oxidant. The electron transferred leaves a hole on Ru and this makes the complex act as an oxidizing agent. On the other hand, the gain of an electron by the excited ligand π^* MO makes the complex a reducing agent because it can donate it. Stated differently, the redox potentials of excited states are different from those of the ground states.

The two key observations— that excited $[Ru(bpy)_3]^{2+}$ is reactive, and also that $[Ru(bpy)_3]^{2+}$ had been observed to induce photosplitting of water by acting as a photosensitizer as well as a photocatalyst —served to motivate and sustain interest in the study of these complexes.

Inspired, in part by $[Ru(bpy)_3]^{2+}$, several thousands of Ru(II) polypyridyl complexes have been synthesized and characterized. Control of the photophysical and electrochemical properties of these polypyridyl complexes can be accomplished by either changing the ligand or modifying its substituents.

7.3 Design Considerations for Experimental PMDs

The sustained intense and rigorous study of Ru(II) polypyridyl complexes has led to their use as major components in building of PMDs. The main factor in all these incorporations is the combination of good photochemical and electrochemical properties that make them appropriate photoactive centers in these molecular devices and machines [14, 15].

At this level we look at what is usually considered during the various stages. The whole exercise normally starts with design of appropriate ligands that are then reacted with a suitable transition metal ion [in our case it is the Ru(II) ion] to form a complex that performs the work of a photosensitizer. The main consideration in this treatment is that we need a strong field ligand which then gives good separation between the t_{2g} MO (d-orbitals) and the e_g^* MO. This separation ultimately has a direct link to the energy

separations between the various electronic states and especially the ^{3}MLCT and ^{3}MC that are of great relevance to our work.

Many ligand-related factors are potentially important, including (among others) the design of a ligand that on forming a complex gives an octahedral geometry or one that is very close. Octahedral geometry usually gives the greatest separation between the t_{2g} and e_g^* MOs and by extension also this is the geometry that keeps the ^{3}MLCT and ^{3}MC farthest apart. Thus a feature to consider during ligand design, if possible, is to create ligands that will increase the size of the metallocycle that finally forms. Reduced constraints around the metal reduce the distorsion and hence destabilizes the ^{3}MC state even more.

A ligand with π-acceptor groups is a good one for this will possibly lead to the widening of the crystal splitting field and which is part of the strong field requirement as noted above. The ligand should also be rigid. This is an important consideration because later on during the assembly of the triad, the key factor is to keep the donor and the acceptor as far apart as possible. This is supposed to ensure no possibility of unwanted charge recombination during the process of photoinduced charge separation. It is also useful to consider the aromaticity of the ligand. Given that the desire is to have a highly stabilized ^{3}MLCT state, then the π conjugation in the ligand helps to lower the energy of this state. The metal more easily transfers an electron towards such a ligand thus lowering the energy of the ^{3}MLCT state.

As already stated earlier, Ru(II) complexes have just the right photochemical, photophysical and electrochemical properties that make them suitable in most of the supramolecular assemblies. $[Ru(bpy)_3]^{2+}$ and many other bpy-type ligands manifest the best of those cited qualities. Unfortunately, at the point of synthesis and incorporation of such bidentate ligands [3], one encounters serious problems to do with the control of stereoisomerism at its six coordinated centers. This problem becomes even worse when one ends up with a mixture of triads during the supramolecular or PMDs construction. This leads to a serious and costly problem of isolation.

Research has shifted to tridentate ligands which are less troublesome. Tridentate ligands form achiral complexes on reaction with the Ru(II) ion. Such species are better suited for the intended tasks in the sense that in it, one observes the possibility of a more efficient photoinduced charge separation process. Besides, the formed triad (the D,P,A components on figure 7.1) comprising the donor (D), photosensitizer (P) and acceptor (A) allow for room to add other important groups between D and P and P and A.

Spacers (S) [16] play an extremely important role in PMD designs. Spacers connect different parts of the whole arrangement but besides, they control the electronic communication between various components and especially in situations with through-bond electron and energy transfers. This then means that its nature is critical in the whole matrix. A good spacer should be rigid. This is mainly afforded by aromatic rings. There are many other such rigid molecules but the motivation for the preference of aromatic rings is the additional efficiency in its electronic communication. Such added groups which could be aromatic rings for example lead to increase in the separations between those components. This increase in the separation reduces the chances of charge recombination before full charge purification.

Figure 7.1: An arrangement of a triad with spacers (S) separating the major components D,P,A

For the arrangement D-S-P-S-A to work efficiently, there has to be conscious consideration of certain constraints. The oxidation of the donor and reduction of the acceptor should lead to intense absorption changes to enable detection of electron transfer by a suitable spectroscopic approach.

Ultimately, when all important considerations and precautions are taken care of, the next most logical thing now is the putting together of all the ideas and skills to produce functional devices. Two very excellent sources for detailed information on the various devices are references [17] and [18].

Now I look at some photoactivated molecular devices. The first one is the dye-sensitized solar cell (DSSC). This is a device whose design is such that a dye (photosensitizer) is adsorbed onto a transparent semiconductor such as (TiO_2). Photoexcitation of the adsorbed dye with visible light excites an electron from its highest occupied molecular orbital (HOMO) to its lowest unoccupied molecular orbital (LUMO). Following this, charge transfer from the dye to the semiconductor may take place if the LUMO overlaps energetically with the conduction band of the semiconductor. At the level of designing and building this device, care is normally taken to improve on the overall solar-to-electrical energy conversion efficiency. This is normally done by modifying the structure of the sensitizer and varying the other parts of the device. A common modification at the dye level is that of increasing the π-conjugation extension in order to increase the molar extinction coefficient of the dye. One could also further optimize the DSSC itself by using an appropriate electrolyte and a suitable texture of the nanocrystaline TiO_2 electrode.

Another nice example is the production of hydrogen fuel through an assembly consisting of mixed-metal supramolecular complexes that have been designed to photochemically absorb solar light, undergo photo-initiated electron collection which then reduces water to produce hydrogen fuel. This process interestingly uses low energy visible light.

An important observation to bring out in all these devices is that the photosensitizer a critical component in their functioning. Knowledge of its structure, stability and excited lifetime is vital. These are the factors that influence the properties of such systems. There have been cases like our own where, even with the precautions cited above having been taken, the synthesized complexes have very short excited state lifetimes or zero excited state lifetime at room temperature. This character in such complexes is a bad sign in the sense that such complexes can not perform the intended role of a photosensitizer. Lack of luminescence especially is an indication that the complex undergoes rapid nonradiative deactivation. This poses a problem because it means that there is no time for electron transfer from the excited state. Efforts to understand what could be happening here require understanding of the electronic structure of the complex in question. Faced with this problem, an affordable way to try and understand it had to be sought. The final method chosen by us was density-functional theory (DFT/TD-DFT). The next section reviews some of DFT calculations from the literature.

7.4 Theoretical Modeling of $[Ru(bpy)_3]^{2+}$

In 2002 Baranovskii *et al.* carried out a study on estimation of the changes in the geometrical structural parameters of $[Ru(bpy)_3]^{2+}$ and $[Ag(bpy)]^{+}$ complexes during charge-transfer electron excitations. They combined several methods including the experimental Raman resonance data, the wave packet dynamics and quantum-chemical calculations of the geometry and vibrational spectra of relatively small fragments of the complex ion. For theoretical calculations they used the GAMESS software in a restricted Hartree-Fock (RHF) approximation in the DZV+P, 3-21G, 6-31G, 6-31G* bases. They also used the GAUSSIAN 94 program with the B3LYP functional with the 6-31+G* basis. For the ground state, they used 6-31G for the C,N,H and SBK for Ru. As part of their results they reproduced the dependence of bond length on the bond position in the ring. Calculated angles differed from the experimental ones by about 1-3%. In consideration of the discrepancies between the experimental data and the fact that the experimental values differ between the rings of the same ligand, this agreement was taken to be good enough [19].

In 2007 Lundqvist [20] *et al* reported the calculated optoelectronic properties of $[Ru(bpy)_3]^{2+}$ dyes containing the oligophenyleneethylene rigid rod linkers in different chemical environments. In this study

they used DFT/TD-DFT method as implemented in the GAUSSIAN 03 package. They used the B3LYP functional together with the LanL2DZ effective core potentials. More interestingly they carried out a more detailed theorretical comparison between a selected complex and the archetype $[Ru(bpy)_3]^{2+}$. In this particular comparison, they used different combinations of DFT functionals such as B3LYP, BLYP, HCTH, PBE1PBE and effective core potential (ECP)/basis combinations such as LANL2DZ,CEP-31,CEP-121 and SDD. These calculations were performed on the B3LYP/LANL2DZ gas-phase optimized geometry of their selected complex to test the robustness of the calculated electronic properties.

In 2009 Heully *et al.* carried out a detailed study of the photophysics of $[Ru(bpy)_3]^{2+}$. They used a number of programs for different purposes [21]. The NEWCHEM package was used for the calculation of energy. The circular dichroism values were determined using the ORCA program. The minimum crossing point between the ^{3}MC and the ground state arising from spin-orbit coupling was obtained by the use of the GAMESS program. They used the B3LYP functional for the DFT/ TD-DFT calculations. A key feature of their findings is a detailed model for the mechanism of nonradiative decay of the ^{3}MC (*dd*) state. It is a short-lived structure that is the route through which the ^{3}MLCT state deactivates nonradiatively. Usually at this point one notes the possibility of competition between the luminescence of ^{3}MLCT state and the nonradiative decay back to the ground state through populating the ^{3}MC state which easily deactivates to the ground state through a deactivation funnel. The factor that now counts is the extent of the barrier to the population of the ^{3}MC state.

Waskasi *et al.* in 2010 reported the findings of their work in an International Electronic Conference on Synthetic Chemistry. Their work was on the Computational studies of water splitting by use of Ruthenium organometalic compounds [22]. They did theoretical work on the determination of molecular geometries, electronic structures and optical absorption of $[Ru(bpy)_3]^{2+}$. They did the calculation the HF/3-21G and at the DFT/TDDFT B3LYP/3-21G levels for the heteroleptic ruthenium dye (heteroleptic because of the functionalization done using phosphonate and malonate ligands in the 4-positions of the 2,2'-bipyridyl ligands in order to adsorb strongly to TiO_2. For Ru, they used the LanL2DZ basis set. They used the CPCM solvation model since they were doing this work in a solvent. The findings indicated that HOMO molecular orbitals are the Ru 4d-orbitals. Their conclusion was that Ru-based complexes might be effective for the next generation dye-sensitized photoelectrochemical cell.

Tavernelli *et al.* did a nonadiabatic molecular dynamics study with solvent effects on $[Ru(bpy)_3]^{2+}$ in 2011. They used a linear response time-dependent density-functional theory (LR-TD-DFT) and quantum mechanics/molecular mechanics (QM/MM).The DFT/TD-DFT claculations were done using Becke-Perdew (BP) GGA xc-functional. The plane waves with cutoff of 75 Ryd. were used to expand the valence electrons in a cubic box of side length of 18Å. For scalar relativistic effects, the core electrons were replaced by norm-conserving pseudo potentials of the Martins-Troullier type. The quality of LR-TDDFT/BP results was assessed by means of additional calculations using the M06 functional on different molecular geometries extracted from the excited states dynamics. The M06 and BP calculations were done using the GAUSSIAN 09 package. The LANL2DZ basis set was used for the ruthenium atom while the 6-311G* basis set was used for all other atoms. Spin orbit couplings (SOCs) were calculated using the perturbation approach of Ziegler and co-workers. They used the approach as is implemented in the ADF2009.01. A TZP basis set was used for all atoms and relativistic effects were introduced using ZORA. Water was described by a continuum model using COSMO. All molecular representations were produced by use VMD (version 1.8.7). Nonadiabatic dynamics was performed using the fewest-switches trajectory surface hopping algorithm of Tully as implemented in the plane wave code CPMD. Some of the results from this study indicate that in order to get non-vanishing SOC matrix elements between MLCT states, the singlet and triplet excited states need to: (i) have the excited π^* orbitals localized on the same ligand, and (ii) involve metal d-orbitals of different symmetries. It was also shown that for the kind of

system dealt with in this work, the GGA functionals have been shown to give good agreement with the experiment [23].

7.5 Theoretical Modeling of Other Ru(II) Polypyridine Compounds

While elaborate computational-resource intensive calculations can be justified for the parent compound $[Ru(bpy)_3]^{2+}$, such calculations are rarely performed for other Ru(II) polypyridyl compounds. In this latter case the goals are typically less ambitious. Nevertheless, as a complementary approach to experimental work on Ru(II) polypyridyl complexes, a number of theoretical calculations have been done. A diversity of electronic, structural and other features have been determined. The following examples picked from the literature represent a few of such efforts. This survey was critical in helping us select the right computational parameters such as functionals, basis sets etc, for our calculations.

Gorelsky and Lever in 2001 carried out DFT calculations on the series $[Ru(bqdi)_n(bpy)_{3-n}]^{2+}$ (bpy=2,2'-bipyridine, bqdi=o-benzoquinonediimine) to explore the degree of coupling between 4*d* and π and π^* orbitals [24]. The DFT calculations here were done using the B3LYP functional and an effective core potential basis set LanL2DZ. Time-dependent density functional response theory (TD-DFT) was used to predict the complex spectra which were compared with the experimental data. Comparison of the calculated results with those of INDO/S method (where INDO stands for Intermediate Neglect of Differential Overlap) was done. The results showed good agreement in terms of orbital energies, orbital mixing and electronic spectra. These results confirmed that for complexes of the type studied here, the INDO/S approach is a good model and reproduces the results of the computationally more demanding but more reliable TD-DFT calculations.

In 2007 Li *et al.* studied the structures, trends in DNA-binding and the spectral properties of molecular light " light switch" complexes using DFT/TDDFT [25]. They used the B3LYP functional, LANL2DZ basis set (with its ECP) for Ru and D95 basis set for all the other atoms. Structurally, the results indicated that there was a trend in their deoxyribonucleic acid (DNA)-binding constants. This revealed trend related very well to the luminescence properties of the complexes in DNA. The explanation behind this observation is that simply increasing the planar area of the intercalating ligand may not be effective in improving the DNA-binding of the resulting complex because of the increase in the LUMO energy, but introduction of more electronegative heteroatoms into the ring skeleton of the ligand should be effective. This effectiveness is due to the decrease in the LUMO (and LUMO+y) energy to some extent.

In 2002 Zheng *et al.* did study the effect of the ligands on the electronic structure and related properties [26] of $[Ru(L)_3]^{2+}$ (L=bpy,bpmbpz). They used DFT with the B3LYP functional and the LANL2DZ basis set. From a general point of view, they clearly established that variation of ligand structure and composition affects the molecular orbital energies and especially the frontier molecular orbitals. The incorporation of a heteroatom such as N into a ligand had a significant impact on the position of negative charge. Most negative charges are populated on the negative atom.

In 2009 Le Bahers *et al.* investigated the ground- and excited-state properties in indoline dyes used for dye-sensitized solar cells [27]. They used DFT and TDDFT with the hybrid functional PBE0. For heavier atoms they used the 6-31G(d) basis set for the calculation of ground state properties. For the vertical excitations they carried out TD-DFT at he same theory level but added a diffuse function on all the non-hydrogen atoms (6-31+G(d) basis set). Their results for both ground and excited states allow for quantitative description of absorption and emission properties of the studied dyes in solution. In addition, their results also led to a qualitative rationalization of the different efficiencies of these dyes DSSCs. The most important part of this result is that it paved a way for possible *in-silico* designed new dyes.

Schramm *et al* in 2009 studied a mononuclear Ru(II) polypyridyl complex with an enlarged coordination cage [28]. In this complex, the enlargement of the coordination sphere done by introducing two additional carbon bridges between the aromatic pyridine groups of the terdentate ligand. Several techniques were used to study different features of interest. Theoretical calculations using DFT/TD-DFT were carried out on the ground state, the singlet excited states and triplet states. The results show a triplet metal-to-ligand charge transfer with an unprecedented substantial quantum yield of 13% and a lifetime of 1.36μs at room temperature and in the presence of oxygen. Generally, the exceptional properties of this expanded cage compound opened the possibility of exploiting the terpyridyl-like Ru(II) complexes in photochemical device under room conditions.

The density-functionals, basis sets and ECPs used in these studies are summarized in Table 7.1. These may be compared with the B3LYP functional and 631G (for C,N,O,H atoms) and LANL2DZ (for Ru) basis sets and associated Ru ECP in the calculations reported in chapters 8 and 9.

Table 7.1: Summary of some important theoretical calculations

Author	Study	Year	Functional, Basis set, ECP
Torres [29] *et al*	A quantum dynamics study on hydrogen elimination	2003	B3LYP, LAN2LDZ + its ECP (Ru) 6-31G (other atoms)
Aiga and Tada [30]	Molecular and electronic structures of black dye	2003	PBE0, 3-21G+polarization functions
Barolo [31] *et al*	Synthesis, Characterization and DFT-TDDFT study of a Ru(II)-functionalized tetradentate-ligand complex	2006	B3LYP, 3-21G* (all atoms) LANL2DZ + its ECP (Ru), 6-31G* SDD + (MWB quasi-ecp)-Ru, 6-31G*
Persson [32] *et al*	Sensitizers for Rod-Like Molecular Arrays	2008	B3LYP, LANL2DZ (Ru) 6-31G, 6-31+G(d,p)
Yin [33] *et al*	Impact of ancillary ligands on the photophysical properties of Ru(II)-conjugated diimine ligand complexes	2009	B3LYP, LANL2DZ (Ru), 6-31G* SDD ecp for Ru
Bryan [34] *et al*	Systematic Manipulation of the Light-Harvesting Properties for Tridentate Cyclometalated Ruthenium(II) Complexes	2009	B3LYP LANL2DZ
Anbarasan [35] *et al*	DFT and TD-DFT Calculations of Some Metal Free Phthalonitrile Derivatives for Enhancement of the Dye Sensitized Solar Cells	2011	B3LYP 6-311++G(d,p)
Chandrasekharam [36] *et al*	A molecularly engineered fluorene-substituted Ru-complex for efficient mesoscopic dye-sensitized solar cells	2011	B3LYP, 6-31G(d) LANL2DZ (Ru)
Albert [37] *et al*	The Frenkel exciton Hamiltonian for functionalized Ru(II)-bpy complexes	2011	B3LYP 6-31G* (ligand atoms) LANL2DZ (Ru)

From the modeling reviews done in this section and the preceding one (section 7.4), it is observed that one can afford to do very elaborate calculations for a single compound such as $[Ru(bpy)_3]^{2+}$ but not when screening a large number of compounds.

7.6 Summary

As a summary of this chapter, one notes that the there was need to synthesize photosensitizers that could be used for the production of photochemical molecular devices. Precautionary measures were taken to ensure the correct design and synthesis strategies were adapted. For example though Ruthenium complexes

are known to have good photochemical and photophysical properties necessary for good functioning in a PMD, those based on the bidentate ligands such as bipyridine are a problem to handle due to their stereoisomerism. A better approach is to use terdentate ligands. This strategy was put in place and terdentate ligands and complexes synthesized in readiness for incorporation as photosensitizers. Unfortunately, a number of these complexes did not show luminescence at at all at room temperature or those that did, had very short excited lifetimes. This basically meant that they are not good candidates as photosensitizers. This implied that there are nonradiative ways through which the complex goes back to the ground state. To understand the likely reasons as to why a particular compound would behave like this, it requires understanding its structure, stability and excited lifetime. It is at this point that computational techniques were sought. The search for a suitable theoretical method entailed consideration of the fact that the final method ought to be computationally affordable and this is why DFT/TDDFT was chosen. An intensive literature review of the methods in use revealed that for screening purposes we were not going to use very elaborate calculations but rather simpler, accurate and fast approaches. This is how we ended up with the functional and basis sets that were used in the calculations reported in this thesis.

References

[1] V. Balzani, A. Credi, and M. Venturi, "The Bottom-Up Approach to Molecular-Level Devices and Machines," *Chem. Eur. J.*, vol. 8, pp. 5524–5532, 2002.

[2] M. Ruben, J.-M. Lehn, and P. Muller, "Addressing metal centres in supramolecular assemblies," *Chem. Soc. Rev.*, vol. 35, pp. 1–13, 2006.

[3] J. P. Sauvage, J. P. Collin, J. C. Chambron, S. Guillerez, C. Coudret, V. Balzani, F. Barigelletti, L. D. Cola, and L. Flamigni *Chem. Rev.*, vol. 94, p. 993, 1994.

[4] M. M. Toyama, M. Franco, L. Catalani, K. Araki, and H. Toma, "Spectroelectrochemical and photophysical properties of a (3,4-pyridyl) porphyrazine supermolecule containing four $[Ru(bipy)_2Cl]^+$ groups," *J. Photochem. Photobiol., A*, vol. 118, pp. 11–17, 1998.

[5] J. Koepke, X. Hu, C. Muenke, K. Schulten, and H. Michel, "The crystal structure of the light-harvesting complex II (b800-850) from rhodospirillum molischianum," *Struct.*, vol. 4, p. No. 5, 1996.

[6] V. Berl, M. Schmutz, M. J. Krische, R. G. Khoury, and J. Lehn, "Supramolecular Polymers Generated from Heterocomplementary Monomers Linked through Multiple Hydrogen-Bonding Arrays-Formation, Characterization, and Properties," *Chem. Eur. J.*, vol. 8, pp. 1227–1244, 2002.

[7] H. Toma and K. Araki, "Supramolecular assemblies of ruthenium complexes and porphyrins," *Coord. Chem. Rev.*, vol. 196, pp. 307–329, 2000.

[8] J.-M. Lehn, "Supramolecular chemistry-scope and perspectives: Molecules-supermolecules-molecular devices." Nobel lecture, December 1987.

[9] G. A. Crosby, W. G. Perkins, and D. M. Klassen, "Luminescence from transition-metal complexes: Tris(2,2′-bipyridine) and tris(1,10-phenanthroline)ruthenium(II)," *J. Chem. Phys.*, vol. 43, pp. 1498–6, 1965.

[10] H. D. Gafney and A. W. Adamson, "Excited state $[Ru(bipyr)_3]^{2+}$ as an electron-transfer reductant," *J. Am. Chem. Soc.*, vol. 94 (23), pp. 8238–8239, 1972.

[11] P. Natarajan and J. F. Endicott, "Photoredox behavior of transition metal-ethylenediaminetetraacetate complexes. Comparison of some group viii metals," *J. Phys. Chem.*, vol. 77 (17), pp. 2049–2054, 1973.

[12] V. Balzani, L. Moggi, M. Manfrin, F. Bolletta, and M. Gleria, "Solar energy conversion by water photodissociation," *Sci.*, vol. 189, p. 852, 1975.

[13] A. Juris, V. Balzani, F. Barigelletti, S. Campagna, P. Belser, and A. von Zelewsky, "Ru(II) polypyridine complexes: Photophysics, photochemistry, electrochemistry, and chemiluminescence," *Coord. Chem. Rev.*, vol. 84, p. 85, 1988.

[14] V. Balzani, P. Ceroni, and B. Ferrer, "Molecular devices," *Pure Appl. Chem.*, vol. 76, pp. 1887–1901, 2004.

[15] J. L. Atwood, G. W. Orr, R. K. Juneja, S. G. Bott, and F. Hamada, "Supramolecular assemblies based on calixarenes," *Pure App. Chem.*, vol. 65, pp. 1471–1476, 1993.

[16] V. Balzani, A. Juris, and M. Venturi, "Luminescent and Redox-Active Polynuclear Transition Metal Complexes," *Chem.Rev.*, vol. 96, pp. 759–833, 1996.

[17] J.-P. Sauvage(Ed.), *Molecular Machines and Motors*. Springer, 2001.

[18] V. Balzani and C. Campagna, *Photochemistry and Photophysics of Coordination Compounds I-(Vol-280)*. Springer, 2007.

[19] V. Baranovskii, O. Lyubimova, A. Makarov, and O. Sizova, "Geometry of Transition Metal Complexes with Bipyridine in the Excited State," *J. Struct. Chem.*, vol. 43, pp. 373–382, 2002.

[20] M. J. Lundqvist, E. Galoppini, G. J. Meyer, and P. Persson, "Calculated Optoelectronic Properties of Ruthenium Tris-bipyridine Dyes Containing Oligophenyleneethynylene Rigid Rod Linkers in Different Chemical Environments," *J. Phys. Chem. A*, vol. 111, pp. 1487–1497, 2007.

[21] J.-L.Heully, A. Fabienne, and M. Boggio-Pasqua, "Spin-orbit effects on the photophysical properties of $[Ru(bpy)_3]^{2+}$," *J. Chem. Phys.*, vol. 131, p. 184308, 2009.

[22] M.M.Waskasi, S. M. Hashemianzadeh, O. M. Srahangi, and B. Sohrabi, "Computational studies of the water splitting by using ruthenium organometalic compounds." 14^{th} International Electronic Conference on Synthetic Organic Chemistry (ECSOC-14), 130, November 2010.

[23] I. Tavernelli, B. Curchod, and U. Rothlisberger, "Nonadiabatic molecular dynamics with solvent effects: A LR-TDDFT QM/MM study of ruthenium (II) tris (bipyridine) in water," *Chem. Phys.*, vol. 391, pp. 101–109, 2011.

[24] S. Gorelsky and A. Lever, "Electronic structure and spectra of ruthenium diimine complexes by density functional theory and INDO/S: Comparison of the two methods," *J. Organomet. Chem.*, vol. 635, pp. 187–196, 2001.

[25] J. Li, J.-C. Chen, L.-C. Xu, K.-C. Zheng, and L.-N. Ji, "A DFT/TDDFT study on the structures, trend in DNA-binding and spectral properties of molecular -light switch complexes $[Ru(phen)_2(L)]^{2+}$ (L=dppz, taptp, phehat)," *J. Organomet. Chem.*, vol. 692, pp. 831–838, 2007.

[26] K. Zheng, J. Wang, W. Peng, X. Liu, and F. Yun, "Theoretical studies on the electronic structures and related properties of $[Ru(L)_3]^{2+}$ (l=bpy,bpm,bpz) with dft method," *J. Mol. Struct.*, vol. 582, pp. 1–9, 2002.

[27] T. Bahers, T. Pauporté, G. Scalmani, C. Adamo, and I. Ciofini, "A TD-DFT investigation of ground and excited state properties in indoline dyes used for dye-sensitized solar cells," *Phys. Chem. Chem. Phys.*, vol. 11, pp. 11276–11284, 2009.

[28] F. Schramm, V. Meded, H. Fliegl, K. Fink, O. Fuhr, Z. Qu, W. Klopper, S. Finns, T. E. Keyes, , and M. Ruben, "Expanding the coordination cage: A Ruthenium(II)-Polypyridine Complex Exhibiting High Quantum Yields under Ambient Conditions," *Inorg.Chem.*, vol. 48, pp. 5677–5684, 2009.

[29] L. Torres, R. Gelabert, M. Moreno, and J. M. Lluch, "Fast hydrogen elimination from the $[Ru(PH_3)_3(CO)(H)_2]$ complex in the first singlet excited states: A quantum dynamics study," *Chem. Phys.*, vol. 286, pp. 149–163, 2003.

[30] F. Aiga and T. Tada, "Molecular and electronic structures of black dye; an efficient sensitizing dye for nanocrystalline TiO_2 solar cells," *J. Mol. Struct.*, vol. 658, pp. 25–32, 2003.

[31] C. Barolo, M. K. Nazeeruddin, S. Fantacci, D. D. Censo, P. Comte, P. Liska, G. Viscardi, P. Quagliotto, F. D. Angelis, S. Ito, and M. Gratzel, "Synthesis, Characterization, and DFT-TDDFT Computational Study of a Ruthenium Complex Containing a Functionalized Tetradentate Ligand ," *Inorg. chem.*, vol. 45, pp. 4642–4653, 2006.

[32] P. Persson, H.-C. Becker, O. Johansson, and L. Hammarstrom, "Bistridentate Ruthenium(II)polypyridyl-Type Complexes with Microsecond ^{3}MLCT State Lifetimes: Sensitizers for Rod-Like Molecular Array," *J. Am. Chem. Soc.*, vol. 130, pp. 15533–15542, 2008.

[33] J.-F. Yin, D. Bhattacharya, P. Thanasekaran, C.-P. Hsu, T.-W. Tseng, and K.-L. Lu, "Effect of ancillary ligands on the photophysical properties of Ru(II) complexes bearing a highly conjugated diimine ligand: A density functional theory study," *Inorg. Chim. Acta*, vol. 362, pp. 5064–5072, 2009.

[34] K. Bryan, R. Kiyoshi, , and C. P. Berlinguette, "Systematic Manipulation of the Light-Harvesting Properties for Tridentate Cyclometalated Ruthenium(II) Complexes ," *Inorg. Chem.*, vol. 48, pp. 9644–9652, 2009.

[35] P. Anbarasan, P. S. Kumar, K. Vasudevan, S. M. Babu, and V. Aroulmoji, "DFT and TD-DFT Calculations of Some Metal Free Phthalonitrile Derivatives for Enhancement of the Dye Sensitized Solar Cells ," *Acta Phys. Pol., A*, vol. 119, 2011.

[36] M. Chandrasekharam, G. Rajkumar, C. S. Rao, T. Suresh, P. Y. Reddy, J. Yum, M. K. Nazeeruddin, and M. Graetzel, "A molecularly engineered fluorene-substituted Ru-complex for efficient mesoscopic dye-sensitized solar cells," *Adv. Nat. Sci.: Nanosci. Nanotechnol.*, vol. 2, p. 035016 (15pp), 2011.

[37] V. V. Albert, E. Badaeva, S. Kilina, M. Sykora, and S. Tretiak, "The Frenkel exciton Hamiltonian for functionalized Ru(II)-bpy complexes," *J. Lumin.*, vol. 131, pp. 1739–1746, 2011.

Part II

Original Work

CHAPTER 8

ABSORPTION SPECTRUM AND PARTIAL DENSITY OF STATES (PDOS) CALCULATIONS ON LUMINESCENT RUTHENIUM COMPLEXES

Introduction

This chapter is the gist of my thesis work. There were two parts in this project. There was the synthesis and determination of all the experimental details as captured in the attached manuscript. The team that did the experimental is also well represented here. The other part was the team that did the theoretical work reported in this thesis. We did specifically the optimizations, visualization of molecular orbitals, frequency calculations, calculation of UV transitions and partial density of states. The modeling work on optimizations, visualization of molecular orbitals, frequency calculations, calculation of UV transitions went on quite well with the expected difficulties usually encountered in every new field.

Through networking and asking candid questions where we were not sure, we made quite some considerable progress.

A problem arose when it became very clear that visualization alone was not sufficient to enable one describe a given MO as belonging exclusively to either a metal or a ligand. This is due to the mixing of metal d orbitals and ligand π orbitals. The way to overcome this was through the application of the Partial density of states (PDOS) approach. In this method, one determines MOs based on their energies and the contributing fragments from (d or π orbitals). Manual calculation of density of states (DOS) and (PDOS) curves was very difficult. Even with the gaussian output files carrying all the necessary details such as MO energies, Atomic orbital coefficients and overlap integrals, it was a nightmare to work out the contributions of various orbitals. This was compounded especially by the size of the $n \times n$ matrices (sometimes n of over 600 and where n= number of Atomic orbitals = number of MOS) involved in our kind of calculations. It is at this point that Pablo Baudin a third year undergraduate Chemistry student working under my supervisor (Prof. Mark E. Casida) on a *Numerical Analysis* project proved extremely useful. He wrote functional python programs that that were able to go far beyond where I had managed to reach by use of GAUSSSUM program. These programs which had functions customized and tailored towards our unique needs were able to perform the following:

- Extract the wavelength and corresponding oscillator strength from a tddft-calculation (UV-transitions) output and prepare an input file for theoretical spectra calculation.
- Interconvert energy units from eV to λ and wavenumbers and also convert oscillator strengths to absorption coefficients and plot the the necessary curves (oscillator versus wavelength).
- Prepare input file from experimental absorption data to be plotted alongside the theoretical curve for comparison purposes.
- Extract enough details from a PDOS calculation to be able to prepare an input file consisting of required metal d-orbitals and ligand p-orbitals.
- Calculation of the contributions of the metal d-orbitals and ligand p-orbitals into a given MO. This information helps the convolution calculation of Dos and Pdos that eventually enables the accurate determination of MOs, their energies and the contributions from selected orbitals of interest.

Density-Functional Study of Lumininescence in Polypyridine Ruthenium Complexes

C. Muhavini Wawire[1,2,†] Damien Jouvenot[2], Frédérique Loiseau[2], Pablo Baudin[2], Sébastien Liatard[2], Lydia Njenga[3], Geoffrey N. Kamau[3], and Mark E. Casida[2‡]

[1] *The Catholic University of Eastern Africa, P. O. Box 62157, 00200, Nairobi, Kenya*
[2] *Département de Chimie Moléculaire (DCM, UMR CNRS/UJF 5250), Institut de Chimie Moléculaire de Grenoble (ICMG, FR2607), Université Joseph Fourier (Grenoble 1), 301 rue de la Chimie, BP 53, F-38041 Grenoble Cedex 9, France*
[3] *Department of Chemistry, University of Nairobi, P.O. Box 30197, Nairobi, Kenya*

A density-functional theory (DFT) study of five ruthenium complexes has been carried out with the goal of gaining deeper insight into factors governing luminescence lifetimes. The five compounds are $[Ru(bpy)_3]^{2+}$ (**1**), $[Ru(L1)_2]^{2+}$ (**2**), $[Ru(tpy)_2]^{2+}$ (**3**), $[Ru(L1)(tpy)]^{2+}$ (**4**), and $[Ru(L2)_2]^{2+}$ (**5**), where bpy=2,2'-bipyridine, tpy=2,2':6',2"-terpyridine, L1=1,1'-[2,6-pyridinediylbis(methylene)]bis[3-methylimidazolium] and L2=1,1'-[2,6-pyridinediylbis(methylene)]bis[3-methylbenziimidazolium]. Experimental work, including the synthesis and photophysical properties of **5** is also reported in the context of this study. Gas phase geometries optimized using x-ray crystallography geometries as start geometries were found to be close to the start geometries. Gas phase absorption spectra calculated using time-dependent DFT were found to be in good agreement with spectra measured in solution. A partial density of states (PDOS) analysis of the molecular orbitals shows that it is possible to recover the ligand field theory (LFT) like picture. On the basis of this PDOS-derived LFT-like procedure we propose two orbital-based luminescence indices, both motivated my the idea that luminescence quenching results from a low ^{3}MLCT $\rightarrow$ ^{3}MC barrier. The first luminescence index is ΔE, the difference between the e_g^* and lowest energy π^* PDOS bands. The second luminescence index is $d \times \pi$, the product of the amount of π character in the t_{2g} band with the amount of ruthenium d character in the $1\pi^*$ band. These luminescence measures are intended as qualitative rather than quantitative predictors. Low values of ΔE and high values of $d \times \pi$ are shown to correlate with lack of luminescence for the five compounds studied in this paper, while high values of ΔE and low values of $d \times \pi$ correlate well with luminescence.

Keywords: polypyridine ruthenium complexes, luminescence, DFT, TD-DFT.

I. INTRODUCTION

Polypyridine ruthenium complexes have special photophysical properties which make them ideal for use as components in photochemical molecular devices (PMDs) [1], including but by no means limited to dye-sensitized solar cells [2–4]. In an ideal bottom-up molecular electronics approach, ever more elaborate photomolecular devices would be tailor-made to have specific properties designed for specific uses. Of course, it is not that simple since both quantum mechanics and synthesis place their own restrictions on what is currently possible to "engineer." This paper concerns a particular problem, namely the design of ligands which would allow the interconnection of ruthenium complexes while still maintaining a long luminescence lifetime. PMD components based upon linking charge-conducting ("molecular wires") or isolating ("spacers") chains to bidentate ligands is plagued by the problem of multiple isomers. This is why recent work [5–11] focuses on the synthesis of ruthenium complexes using tridentate ligands, while still attempting to maintain good photophysical properties. Such work [12] could benefit from computational support for testing some of the working hypotheses currently used in ligand design. The computational model should be able (i) to quantitatively reproduce the known x-ray structures and absorption spectra and yet (ii) be interpretable in the ligand field theory (LFT) [13] terminology commonly used by experimentalists working on the problem of PMD ligand design. In this article, we show by explicit calculations on the five compounds shown in **Fig. 1** the extent to which density-functional theory (DFT) calculations can meet both of these requirements and hence constitute a valuable part of the PMD ligand designer's toolbox.

Much of our understanding of luminescence in ruthenium complexes is based upon a long history of studies (see, e.g., Refs. [1, 11, 14–28]) of the prototypi-

[†] muhavini@cuea.edu,muhavini.wawire@ujf-grenoble.fr
[‡] Mark.Casida@UJF-Grenoble.Fr

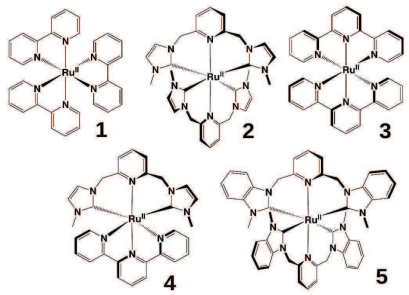

FIG. 1: The five molecules considered in this study: $[Ru(bpy)_3]^{2+}$ (**1**), $[Ru(L1)_2]^{2+}$ (**2**), $[Ru(tpy)_2]^{2+}$ (**3**), $[Ru(tpy)(L1)]^{2+}$ (**4**), $[Ru(L2)_2]^{2+}$ (**5**), where bpy=2,2'-bipyridine, tpy=2,2':6',2"-terpyridine, L1=1,1'-[2,6-pyridinediylbis(methylene)]bis[3-methylimidazolium] and L2=1,1'-[2,6-pyridinediylbis(methylene)]bis[3-methylbenziimidazolium].

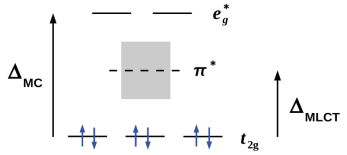

FIG. 2: Generic ligand field theory diagram for octahedral ruthenium(II) polypyridyl complexes. MC refers to metal-centered while MLCT refers to metal-to-ligand charge transfer transitions.

cal tris(2,2'-bipyridine)ruthenium(II) cation (compound **1** in Fig. 1), which we shall simply refer to using the common abbreviation $[Ru(bpy)_3]^{2+}$. The LFT picture which emerges is one of a pseudooctahedral complex with ruthenium-centered filled bonding t_{2g} orbitals and empty antibonding e_g^* orbitals separated by a typically unspecified number of unoccupied ligand π^* orbitals (**Fig. 2**). This picture has been used and continues to be used as a convenient and servicable working model for analysing photophysical properties and designing ligands. However DFT has proven its value for first-principles quantitative predictions of molecular structure and time-dependent DFT (TD- DFT, Ref. [29–31] provide recent reviews) has been able to do an excellent job in the quantitative prediction of absorption spectra of ruthenium complexes. As will be seen later in this article, DFT molecular orbitals (MOs) correspond well with the LFT picture of Fig. 2. Assigning the experimental absorption spectrum [32] which shows two broad peaks, one at about 22 500 cm^{-1} and the other at about 35 000 cm^{-1}, is much less straightforward as this apparently simple spectral structure hides a number of nearly degenerate ligand-centered (LC) $\pi \rightarrow \pi^*$ and metal-to-ligand charge transfer (MLCT) $d \rightarrow \pi^*$ transitions. Nevertheless (TD-)DFT calculations, including spin-orbit coupling, have been performed [14] and analyzed producing the picture shown schematically in **Fig. 3**. Initial absorption of a photon, possibly followed by radiationless relaxation, leads to a singlet MLCT state (^{1}MLCT) which rapidly converts through an intersystem-crossing mechanism to the correspondingly energetically slightly lower triplet (^{3}MLCT). Note that spin-orbit coupling due to the presence of ruthenium favors intersystem crossings. The luminescence phenomenon is presumed to be phosphorescence from the ^{3}MLCT minimum to the singlet ground state (^{1}GS) since the lifetime is long.

A mechanism for luminescence quenching is provided by nearby electronic states [1]. Thus the ^{3}MLCT undergoes an avoided crossing (shown by the dashed lines in Fig. 3) with the triplet MC (^{3}MC) $t_{2g} \rightarrow e_g^*$ state whose minimum is at a larger metal-ligand distance than for the ^{3}MLCT state, leading to the possibility of a reaction barrier for the interconversion,

$$^3\text{MLCT} \rightleftharpoons {}^3\text{MC}\,, \tag{I.1}$$

between the two states. Radiationless relaxation may occur from either the ^{3}MLCT or ^{3}MC state, but probably occurs most efficiently from the ^{3}MC state,

$$^3\text{MC} \rightarrow {}^1\text{GS}\,, \tag{I.2}$$

by passing through an intersystem crossing conical intersection to the ground state at still larger metal-ligand distances corresponding to partial ligand dissociation or displacement by the solvent [14]. Simulation of triplet excited state dynamics has been described recently [15] and (very recently) mixed TD-DFT/surface hopping photodynamics simulations of this reaction has also been reported [16].

In contrast to the situation for $[Ru(bpy)_3]^{2+}$, even a cursory study of the relevant literature shows that working hypotheses for designing new ligands for PMDs rely heavily on the LFT model. This is in part because, while the above-mentionned state-of-the-art calculations are indeed impressive and illuminating, they are too long and costly in computing resources to be useful for PMD ligand design. This is especially true when going to larger ligands with less symmetry. Not only would the calculations be still longer and more costly to perform, especially for routine screening purposes, but there is another problem. This is an interpretational problem due to the fact that the antibonding ruthenium e_g^* orbital is now mixing with an increasingly dense manifold of ligand orbitals, potentially losing all contact with the traditional LFT language. We are thus left with the somewhat unfortunate situation that the working hypotheses are rarely validated by actual MO calculations.

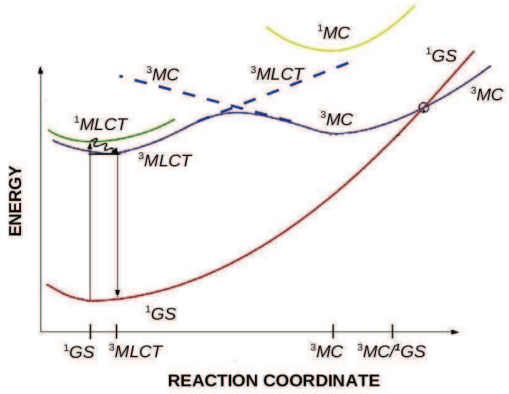

FIG. 3: The diagram shows the principle potential energy curves in our model. The abscissa corresponds roughly to the simultaneous stretching of the Ru-N bonds (breathing mode) while the ordinate represents the state energy. Abbreviations: GS, ground state; MLCT, metal-ligand charge transfer state; MC, metal-centered state. The dashed lines indicate diabatic states whose avoided crossing leads to the energetic barrier on the adiabatic surface between the ^{3}MLCT and ^{3}MC minima.

The results indicated in this paper show that appropriate use of (TD-)DFT may indeed be used to validate working hypotheses and hence have potential value in PMD ligand design. In the next section we first (Sec. II A) show that (TD-)DFT is a quantitative tool for first principles determination of geometries and absorption spectra for the five molecules shown in Fig. 1. The well-studied molecule $[Ru(bpy)_3]^{2+}$ serves as a convenient well-studied reference. Bis(terpyridine)ruthenium(II), molecule **3** in Fig. 1 and denoted in this paper by $[Ru(tpy)_2]$, is also well-characterized experimentally [35–37]. Molecules **2** and **4** in Fig. 1, denoted in this paper respectively as $[Ru(L1)_2]^{2+}$ and $[Ru(tpy)(L1)]^{2+}$, have been recently studied experimentally in a work co-authored by some of us [10]. The experimental results for molecule **5** are reported here for the first time. The section then continues (Sec. II B) with an analysis of the MOs. We show that the problem of fractionation of e_g^* density over numerous MOs can be resolved using the technique of partial density of states (PDOS) analysis (Appendix A). This information is used to discuss the calculated TD-DFT spectra and the observed luminescence lifetimes shown in **Table I**. Finally, Sec. III concludes.

TABLE I: Experimental luminescence lifetimes and PDOS-derived indicators.

Compound	Lifetime	ΔE (eV)[a]	$d \times \pi$[b]
$[Ru(bpy)_3]^{2+}$	0.855 μs [c]	2.49	170
$[Ru(tpy)_2]^{2+}$	0.25 ns[d]	1.93	256
$[Ru(tpy)(L1)]^{2+}$	5 ns[e]	2.34	299
$[Ru(L1)_2]^{2+}$	NL[fe]	1.87	410
$[Ru(L2)_2]^{2+}$	NL[fg]	2.00	672

[a] $\Delta E = \Delta_{MC} - \Delta_{MLCT}$.
[b] Column 4 of Table VI.
[c] Room temperature in CH_3CN [33]. The same reference gives 0.630 μs for the lifetime in aqueous solution.
[d] Room temperature in H_2O [34].
[e] From Ref. [10].
[f] Not luminescent at room temperature in CH_3CN.
[g] Present work.

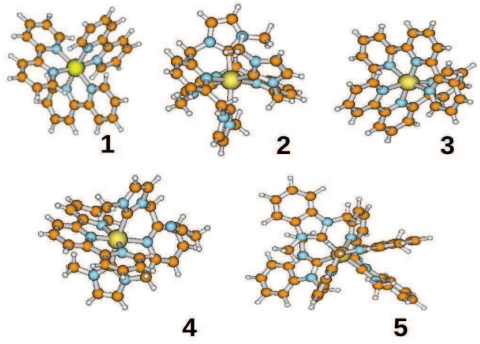

FIG. 4: Ball and stick representations of DFT-optimized geometries of the molecules shown in Fig. 1: Ru, yellow; C, orange; N, blue; H, white.

II. DFT CALCULATIONS

A Structure and Spectra

In this subsection we give a brief idea of the quality of the results of our DFT calculations (see Appendix C for computational details) by direct comparison with experimental results (see Appendix B for the experimental section). Two types of comparisons may be made, namely (i) comparison of DFT-optimized gas phase geometries with crystallographic data and (ii) comparison of TD-DFT absorption spectra with experimental absorption spectra.

1 Geometries

Figure 4 provides ball and stick representations of the five molecules studied in this paper. Start geome-

TABLE II: Comparison of theory and experiment for selected geometric parameters (distances in Ångströms, angles in degrees) of the five complexes. Note that each ligand is described by a single set of geometric parameters. Within each ligand the bite atoms are numbered starting from one end of the ligand going to the other end.

		$[Ru(bpy)_3]^{2+}$		
bpy	$R(RuN_1)$	$\angle(N_1RuN_2)$		
Expt.	2.056	78.7		
Theory	2.11	77.9		
		$[Ru(tpy)_2]^{2+}$		
tpy	$R(RuN_1)$	$R(RuN_2)$	$\angle(N_1RuN_2)$	$\angle(N_1RuN_2N_3)$
Expt.	2.07	2.00	79.4	102.8
Theory	2.13	2.04	78.4	101.6
		$[Ru(tpy)(L1)]^{2+}$		
tpy	$R(RuN_1)$	$R(RuN_2)$	$\angle(N_1RuN_2)$	$\angle(N_1RuN_2N_3)$
Expt.	2.09	1.95	79.1	179.8
Theory	2.14	1.99	78.7	179.9
L1	$R(RuC_1)$	$R(RuN_2)$	$\angle(C_1RuN_2)$	$\angle(C_1RuN_2C_3)$
Expt.	2.08	2.18	87.1	178.1
Theory	2.16	2.28	85.6	179.1
		$[Ru(L1)_2]^{2+}$		
L1	$R(RuC_1)$	$R(RuN_2)$	$\angle(C_1RuN_2)$	$\angle(C_1RuN_2C_3)$
Expt.	2.07	2.12	86.7	175.9
Theory	2.13	2.21	85.9	180.0
		$[Ru(L2)_2]^{2+}$		
L2	$R(RuC_1)$	$R(RuN_2)$	$\angle(C_1RuN_2)$	$\angle(C_1RuN_2C_3)$
Expt.	2.07	2.12	86.6	179.6
Theory	2.13	2.21	85.9	180.0

tries for these DFT-optimized gas phase geometries were taken from crystallographic data. The degree of agreement between the start crystal geometries and the final optimized gas phase geometries is illustrated in **Table II** by selected geometric parameters for the inner sphere of ligand atoms of the five complexes. With one exception, the calculated angles differ from the experimental angles by no more than 1.5°. The exception is the dihedral angle $\angle(C_1RuN_2C_3)$ for $[Ru(L1)_2]^{2+}$ where theory indicates that the ligands are essentially planar but the x-ray crystal structure indicates a 4.1° bending. Calculated bond lengths are longer than measured ones. This bond-length difference is too large to be attributed to errors in the approximate functional used in the calculations, but rather must be attributed to compression due to "chemical pressure" in the condensed phase. Multiplication of the theoretical results by an emprical factor of 0.97 brings the theoretical bond lengths into much better agreement with experiment (**Fig. 5**).

2 Spectra

Figures 6, **8**, **9**, **10**, and **11** compare our calculated TD-DFT absorption spectra for the gas phase molecules with the experimentally-measured solution absorption spectra. In all cases we used the DFT-optimized ground state geometries, but in the case of $[Ru(tpy)_2]^{2+}$, $[Ru(L1)_2]^{2+}$, and $[Ru(L1)(tpy)]^{2+}$ TD-DFT results are also shown at the x-ray crystal geometries. It is to be emphasized that these are *absolute* comparisons of theoretical and experimental molar extinction coefficients in which the only empirical parameter is the full-width-at-half-height used in the gaussian-convolution to account for measurement-related, vibrational, and/or solvent related broadening of peaks. It should also be emphasized that each theoretical peak is built of many different electronic transitions (**Fig. 7** shows the underlying stick spectrum for Fig. 6). For this reason, we have had to calculate on the order of 100 singlet excited states to obtain reasonable agreement with the first two peaks of the experimental spectra. Nevertheless, inclusion of still more singlet excited states in the theoretical calculations may lead to increasing the height of the higher-energy peaks in the theoretical spectra.

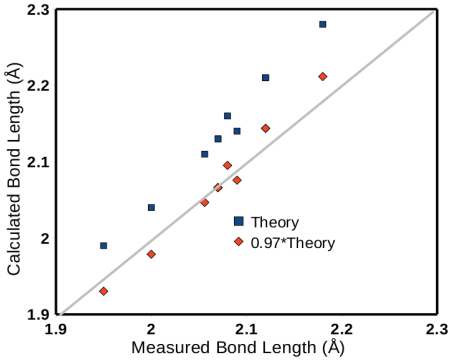

FIG. 5: Correlation graph between DFT-calculated gas phase bond lengths and measured x-ray crystallographic bond lengths.

After gaussian broadening, Figs. 6, 8, 9, 10, and 11 agree with experiment in showing only a few main absorption peaks. **Table III** gathers together rough values for the corresponding main calculated and measured peak positions. **Figure 12** shows that there is quite a reasonable correlation between the calculated gas phase absorption peak positions and the measured solution absorption peak positions—particularly after the theoretical values are multiplied by an empirical factor of 0.92. One reason that the theory is blue shifted compared to experiment may be solvent effects. Figure 6 shows that a dielectric cavity simulation of CH_3CN solvation effects results in a blue shift with respect to the gas-phase spectrum.

All things considered, the level of agreement between theory and experiment is excellent for geometries and at least semiquantitative, if not quantitatative, for absorp-

FIG. 6: Comparison of calculated and experimental $[Ru(bpy)_3]^{2+}$ molar extinction coefficients: experimental curve, measured at room temperature in H_2O [32]; calculated curve in CH_3CN, TD-DFT calculation, 100 singlet states [18]; calculated curve, TD-DFT calculation, 100 singlet states (present work).

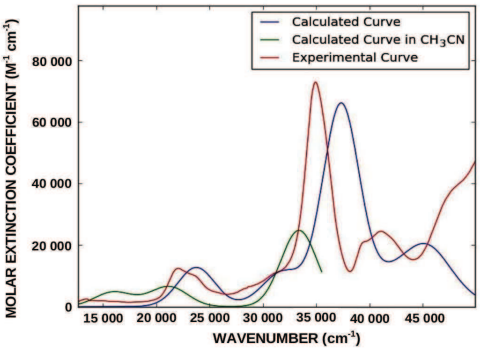

tion spectra. This gives us confidence in the DFT model and encourages us to take a closer look at the underlying DFT orbitals which we do in the next subsection.

B Recovery of a Ligand Field-Like Theory

In the previous section we have established the existance of a quantitative relationship between TD-DFT gas-phase and experimental solution absorption spectra. The next logical step would seem to be to assign the peaks in the spectra in terms of orbital transitions. While this is a sensible common practice for small molecules, the literature abounds with less than satisfactory attempts to do just this for the absorption spectra of ruthenium

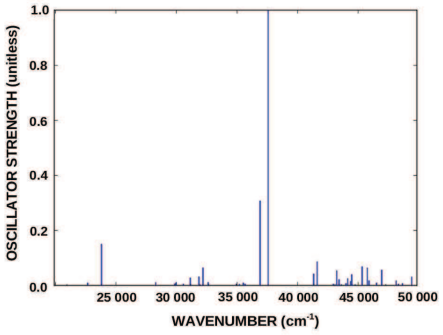

FIG. 7: Stick spectrum for $[Ru(bpy)_3]^{2+}$.

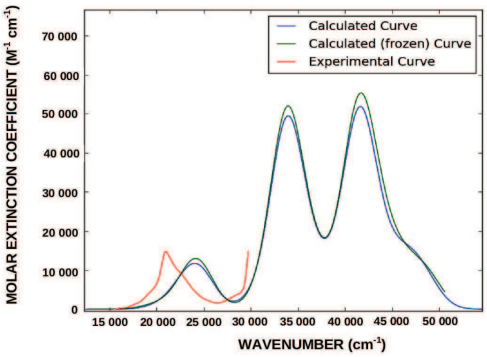

FIG. 8: Comparison of calculated and experimental $[Ru(tpy)_2]^{2+}$ molar extinction coefficients: experimental curve, measured at room temperature in acetonitrile (from Fig. 6 of Ref. [1]); calculated curve, TD-DFT calculation, 100 singlet states; calculated (frozen) curve, TD-DFT calculation using the experimental x-ray structure.

complexes. There is already a problem at the molecular orbital (MO) level. Explicit visualization of ruthenium complex orbitals often permits the identification of high-lying occupied orbitals dominated by ruthenium d orbitals which can be clearly identified with t_{2g} orbitals from ligand field theory (LFT). Unfortunately attempts to identify ruthenium complex MOs with the e_g^* antibonding orbitals of LFT is much more difficult and also less convincing because of the (expected and observed) strong mixing of ruthenium d orbitals with ligand orbitals. Furthermore, even supposing that we have succeeded in making a plausible classification of ruthenium complex MOs into metal-centered, ligand-centered, and metal-to-ligand charge transfer types, we soon discover that each broad peak in the calculated TD-DFT absorption spectra is the convolution of stick spectra belonging to a formidable mixture of different types of transitions. Thus "the classification of the orbitals is not unambiguous, as both d and π contributions are present in all molecular orbitals, and explicit calculation of the total energy of the states is motivated" [38], which at first sight appears to be tantamount to abandonning the simple LFT picture as being useless. If true, this would be very bad news for experimentalists who need a simple picture, such as that provided by LFT, to provide guidance in their everyday work. Fortunately, as we show in this subsection, it is possible to recover an LFT-like picture.

1 *Partial density of states*

If the problem described above is already quite bad for ruthenium complexes, then it becomes even worse in

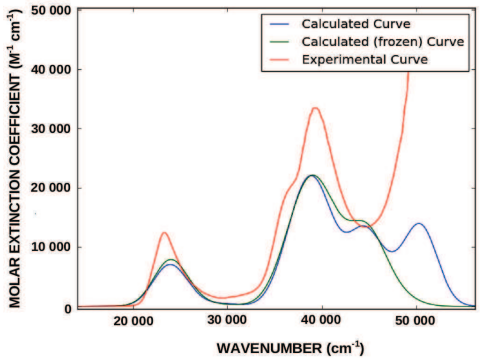

FIG. 9: Comparison of calculated and experimental $[Ru(L1)_2]^{2+}$ molar extinction coefficients: experimental curve, measured at room temperature in acetonitrile (measured in the context of Ref. [10] but reported here in full for the first time); calculated curve, TD-DFT calculation, 100 singlet states; calculated (frozen) curve, TD-DFT calculation using the experimental x-ray structure.

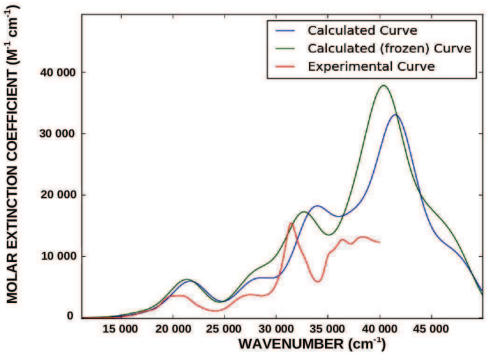

FIG. 10: Comparison of calculated and experimental $[Ru(L1)(tpy)]^{2+}$ molar extinction coefficients: experimental curve, measured at room temperature in acetonitrile [10]; calculated curve, TD-DFT calculation, 100 singlet states; calculated (frozen) curve, TD-DFT calculation using the experimental x-ray structure.

the case of solids where the dense manifold of MOs turn into bands. This is why condensed-matter physicists and physical chemists working on problems such as catalysis which also involve solids have learned to replace molecular orbitals with the concept of density of states (DOS) and to analyze the different atomic and molecular contributions to the DOS in terms of the concept of partial density of states (PDOS). Roald Hoffmann does a good job of explaining these concepts to chemists [39]. We will use these to recover an LFT-like picture (Fig. 2) for the ruthenium complexes described in this paper. For completeness, and because there are several variants of PDOS analysis in the literature, we also give a more technical explanation of what we actually do in Appendix A and illustrate how this idea works by applying it to the familiar textbook example of the diatomic MO diagram of nitrogen.

Now let us look at the less trivial, but still relatively simple example of $[Ru(bpy)_3]^{2+}$ whose PDOS analysis is shown in **Figure 13**. The stick spectrum on the bottom of the figure shows the occupied MOs (blue sticks) and the unoccupied MOs (red sticks). The three MOs whose explicit visualization permit them to be identified as t_{2g} LFT-like orbitals like around -11 eV and have been split into two sets through the symmetry-lowering presence of the ligands. Two e_g^* orbitals may be identified at about -5 eV in the sense that these MOs have a significantly larger ruthenium d contribution than do the other unoccupied MOs. Elsewhere in the diagram are many MOs of primarily ligand nature so that the stick spectrum is relatively dense. Introducing an artificial 1 eV broadening of the stick spectrum produces the DOS shown in the upper-half of the figure. Higher peaks correspond to a greater bunching of MO levels. By analogy with solid-state language, we will refer to these peaks as "bands," even though there is no notion of periodicity in our calculations.

We now separate our atomic orbital (AO) basis into d orbitals on ruthenium, p orbitals on carbon and nitrogen, and other AOs. Then Mulliken population analysis (Appendix A) allows us to separate the ruthenium d-orbital contribution (d-PDOS) to the DOS from the ligand carbon and nitrogen p-orbital contributions (π^*-PDOS). The purple curve allows us to see quite clearly that the MOs around -11 eV are of clear ruthenium d character and hence may be identified with t_{2g} nonbonding orbitals. The purple curve also shows us that the band around -5 eV is the first set of unoccupied orbitals of significant ruthenium d character. Hence this must be the energetic region of the antibonding e_g^* orbitals, though comparison with the DOS and π^*-PDOS shows that these MOs are also heavily mixed with ligand π^* orbitals. A little reflection indicates that this is normal in so far as both bonding and antibonding (as opposed to nonbonding) LFT orbitals should mix with ligand orbitals. Thus this should have been expected. Notice that there is some ruthenium d character in other bands, but that it is relatively small. The lowest π^* band has been labeled as $1\pi^*$ in Fig. 13. The next higher band could have been labeled as $2\pi^*$. In this way we recover a LFT-like picture in close agreement with Fig. 2.

Notice our use of the term "LFT-like." That is because this is not the classic LFT of, say, Ref. [13], though it looks very similar. In fact, we might expect the PDOS $e_g - t_{2g}$ energy difference, $\Delta_{MC} \approx 48000\,\mathrm{cm}^{-1}$ to be about the same as the LFT splitting. However the classic LFT splitting is a different spectroscopically-derived quantity

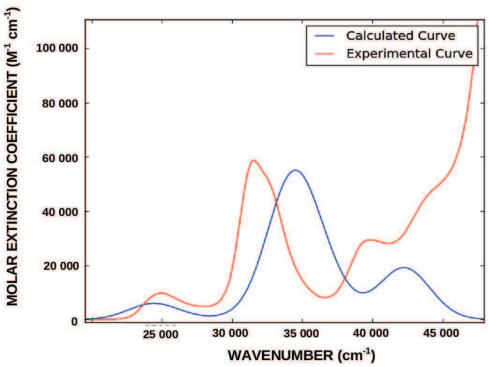

FIG. 11: Comparison of calculated and experimental $[Ru(L2)_2]^{2+}$ molar extinction coefficients: experimental curve, measured at room temperature in acetonitrile; calculated curve, TD-DFT calculation, 80 singlet states; calculated (frozen) curve.

which may be estimated for $[Ru(bpy)_3]^{2+}$ using the well-known formula (see, e.g., pg. 218 of Ref. [13]),

$$\Delta_{\rm LFT} = fg\,, \tag{II.1}$$

where $f = 20000\ {\rm cm}^{-1}$ (Ref. [40] p. 367) is the LFT splitting for the hexaaqua complex and $g = 1.43$ (Ref. [13] p. 219) for three bipyridine ligands. Since $\Delta_{\rm LFT} = 28600\ {\rm cm}^{-1}$ is considerably smaller than $\Delta_{\rm MC}$, then the PDOS is providing us with a LFT-like picture but not with conventional LFT.

Figure 14, **15**, **16**, and **Fig. 17** show the (P)DOS for $[Ru(tpy)_2]^{2+}$, $[Ru(L1)_2]^{2+}$, $[Ru(tpy)(L1)]^{2+}$, and $[Ru(L2)_2]^{2+}$ respectively. **Table V** shows the respective values of $\Delta_{\rm MC}$. Notice how symmetry-lowering ligands lead to splitting of both the t_{2g} band (all complexes except $[Ru(bpy)_2]^{2+}$ and $[Ru(tpy)_2]^{2+}$) $[Ru(L2)_2]^{2+}$) and of the e_g^* band (all complexes except $[Ru(bpy)_2]^{2+}$). In assigning, $\Delta_{\rm MC}$, we are more or less following Kasha's rule [41] which states that the most important photoprocesses are expected to be those from the lowest relevant excited state—hence between the lowest e_g^* band and the highest t_{2g} band. Table V then leads to the spectrochemical series,

$$\Delta_{\rm MC}:\ {\rm bpy}\ >\ {\rm L2}\ >\ {\rm tpy}\ >\ {\rm L1}\ . \tag{II.2}$$

Part, but not all, of what we are seeing here is due to band splitting due to ligand-induced symmetry lowering. It is interesting that the two complexes with the L1 ligand—namely, $[Ru(tpy)(L1)]^{2+}$ and $[Ru(L1)_2]^{2+}$—have essentially the same value of $\Delta_{\rm MC}$, though this may be only coincidental.

TABLE III: Comparison of the position of calculated and measured spectral peaks (cm^{-1}) from Figs. 6, 8, 9, 10, and 11

Compound	Expt.	Theory	Theory-Expt.
$[Ru(bpy)_3]^{2+}$	21 875	23 750	1 875
		31 563	
	35 000	37 500	2 500
	40 938	45 62	4 687
$[Ru(tpy)_2]^{2+}$	21 428	23 929	2 501
		33 928	
		41 429	
$[Ru(L1)_2]^{2+}$	23 546	24 255	709
	36 383		
	39 574	38 865	-709
		44 255	
		50 709	
$[Ru(tpy)(L1)]^{2+}$	20 649	21 948	1 299
	27 597	28 247	650
	31 623	33 896	2 273
	37 273[a]	41 948	4 675
$[Ru(L2)_2]^{2+}$	24 205	24 673	468
	31 168	34 439	3 271
	39 206	42 196	2 990

[a]Average of the values for the two neighboring peaks at 36 298 cm^{-1} and 38 247 cm^{-1}.

2 *Spectra*

Having shown that our LFT-like theory is not the classic LFT theory, we now wish to show that our LFT-like theory is useful for understanding spectra. At the simple LFT level, the features we see in the spectra of Figs. 6, 8, 9, 10, and 11 should correspond to MLCT transitions. This is because $d \rightarrow d$ transitions are expected to be symmetry forbidden or at least weak in complexes. The π^* PDOS gives us an easy way to calculate approximate values for $\Delta_{\rm MLCT}$ (**Table V**). This, in turn, provides a quick estimate of the ^{1}MLCT peaks calculated from TD-DFT since basic theoretical reasons (see, e.g., Ref. [31]) indicate that the positions of the ^{1}MLCT absorption peaks should be given roughly by the values of $\Delta_{\rm MLCT}$. This is confirmed in **Fig. 18**. That this works is all the more remarkable because the absorption spectra peaks are themselves convolutions of stick spectra of varying degrees of ^{1}MC and ^{1}MLCT (and even ligand-to-ligand character) which are being analyzed using PDOS bands which involve various mixed degrees of MC and MLCT character. Yet this underlying complexity is not preventing us from recovering and using a simple LFT-like picture, albeit in the form of "fuzzy bands," does seem to work reasonably well.

FIG. 12: Correlation graph between DFT-calculated gas phase absorption peaks and measured absorption peaks in solution.

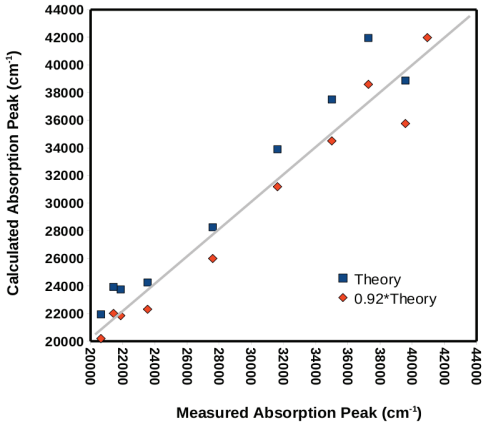

3 *Luminescence*

We now turn to the question of whether our simple LFT-like model can say something about the luminescence data shown in Table I. To this end we investigate two "luminescence indices," shown in the last two columns of the table. Neither one is strictly quantitative but each is intended to be a logical consequence of the model presented in the introduction and, taken together, may provide useful orbital-based indications of whether a compound might or might not be luminescent before it is synthesized. The data indicates that there are three classes of luminescent compounds: (i) $[Ru(bpy)_3]^{2+}$ and $[Ru(tpy)(L1)]^{2+}$ are luminescent, (ii) $[Ru(tpy)_2]^{2+}$ is less luminescent, and (iii) neither $[Ru(L1)_2]^{2+}$ nor $[Ru(L2)_2]^{2+}$ were found to luminesce.

Our job is thus to extract a luminescence indices from the model shown in Fig. 3. The model suggests that the luminescence lifetime should increase with increasing difficulty of crossing the potential energy barrier between the luminescent ^{3}MLCT minimum and the nonluminescent ^{3}MC minimum. Kasha's rule indicates that only the lowest π^* state is of concern when describing luminescence. The simplest theory then suggests that luminescence will be quenched when the lowest e_g^* state is closest to the lowest π^* state (Fig. 2)—i.e., that the height of the ^{3}MLCT and ^{3}MC avoided crossing is directly related to a relatively simple orbital energy difference. This energy difference (ΔE)—or more exactly PDOS band energy difference—is our first luminescence index and is given in column 3 of Table I. Indeed the higher values of ΔE do correspond qualitatively to the two most luminescent species, $[Ru(bpy)_3]^{2+}$ and $[Ru(tpy)(L1)]^{2+}$.

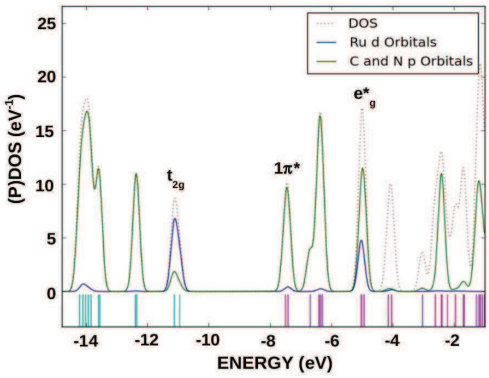

FIG. 13: Total and partial density of states of $[Ru(bpy)_3]^{2+}$ partitioned over ruthenium d orbitals and ligand C and N p orbitals.

Note that no simple quantitative relation is proposed between ΔE and the luminescence lifetime as we expect many competing factors to enter into a quantitative model. Thus it is not unreasonable that the less luminescent species $[Ru(tpy)_2]^{2+}$ and the nonluminescent species $[Ru(L2)_2]^{2+}$ have similar "small" values of ΔE.

The second proposition of a luminescence index is motivated by the avoided crossing in Fig. 3. We might expect that the lower the barrier, then the stronger the configuration mixing should be. This in turn suggests that we look for a possible departure from $t_{2g} \rightarrow \pi^*$ character. This is done in **Table VI** where we make a rough estimate of the of the amount of d character in the first

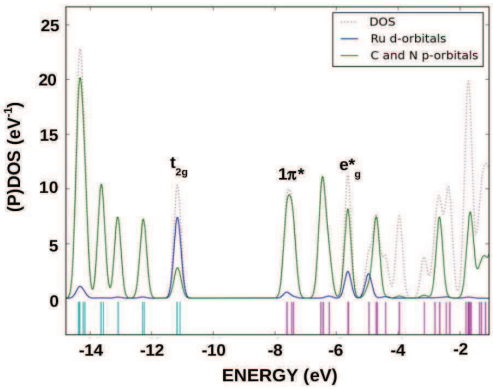

FIG. 14: Total and partial density of states of $[Ru(tpy)_2]^{2+}$ partitioned over ruthenium d orbitals and ligand C and N p orbitals.

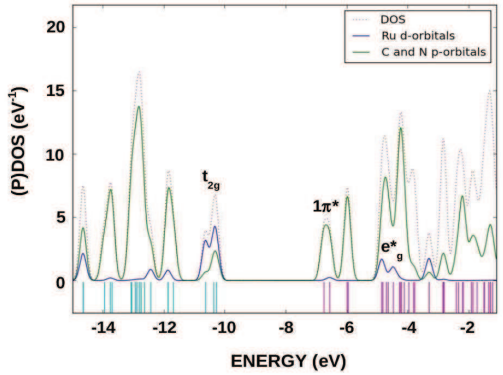

FIG. 15: Total and partial density of states of $[Ru(L1)_2]^{2+}$ partitioned over ruthenium d orbitals and ligand C and N p orbitals.

π^* ("$1\pi^*$") peak (obtained simply from a rough ratio of the ruthenium d PDOS height to the height of the corresponding DOS peak) and the amount of π character in the primary t_{2g} peak (obtained in a similar manner). Column 4 of Table I indicates that the product of these two numbers also gives a reasonable luminescence index in that the three luminescent compounds have the lowest value of the product $d \times \pi$ given by multiplying columns 2 and 3 in Table VI and that the nonluminescent species have markedly higher values.

Taken together the two luminescence indices, ΔE and $d \times \pi$, provide a "quick" indication of ruthenium complex luminescence. This is particularly noteworthy be-

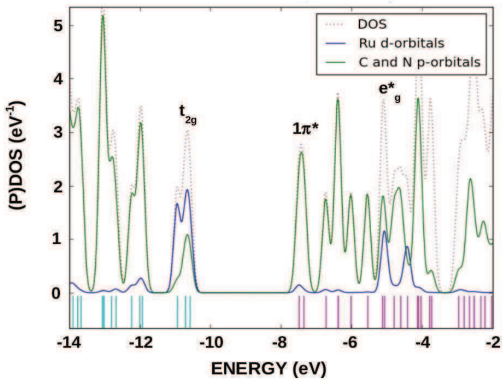

FIG. 16: Total and partial density of states of $[Ru(tpy)(L1)]^{2+}$ partitioned over ruthenium d orbitals and ligand C and N p orbitals.

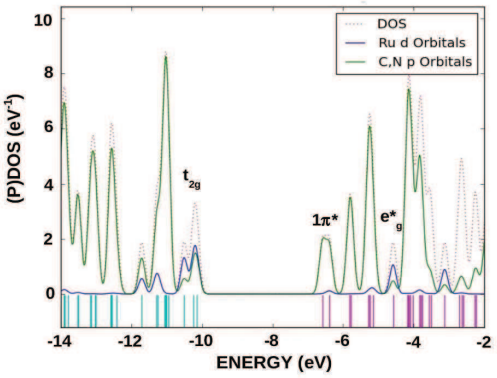

FIG. 17: Total and partial density of states of $[Ru(L2)_2]^{2+}$ partitioned over ruthenium d orbitals and ligand C and N p orbitals.

TABLE IV: Location of ruthenium t_{2g} and e_g^* orbitals obtained from the PDOS analysis. Notice the splitting of the O_h orbitals due to symmetry lowering. The quantity Δ_{MC} reported here is the smallest $t_{2g} - e_g^*$ energy difference.

Compound	t_{2g} (eV)	e_g^* (eV)	Δ_{MC} (cm^{-1})
$[Ru(bpy)_3]^{2+}$	-11.13	-5.02	49 283
$[Ru(tpy)_2]^{2+}$	-11.20	-5.65	44 766
		-5.00	
$[Ru(tpy)(L1)]^{2+}$	-11.00		
	-10.79	-5.09	43 159
		-4.39	
$[Ru(L1)_2]^{2+}$	-10.70		
	-10.35	-5.00	43 153
		-4.60	
$[Ru(L2)_2]^{2+}$	-10.50		
	-10.20	-4.60	45 169
		-3.10	

TABLE V: Comparison of LFT orbital energy differences and positions of calculated absorption peaks.

Compound	t_{2g} (eV)	π^* (eV)	Δ_{MLCT} (cm^{-1})	^{1}MLCT (cm^{-1})
$[Ru(bpy)_3]^{2+}$	-11.0	-7.5	28 200	24 000
		-6.2	38 700	37 000
$[Ru(tpy)_2]^{2+}$	-11.5	-7.5	32 200	24 000
		-6.5	40 300	34 000
$[Ru(tpy)(L1)]^{2+}$	-10.75	-7.5	26 200	22 000
		-6.5	34 300	28 000
$[Ru(L1)_2]^{2+}$	-10.5	-6.5	32 300	24 000
		-6.0	36 300	39 000
$[Ru(L2)_2]^{2+}$	-10.25	-6.5	30 200	25 000
		-5.8	35 900	35 000

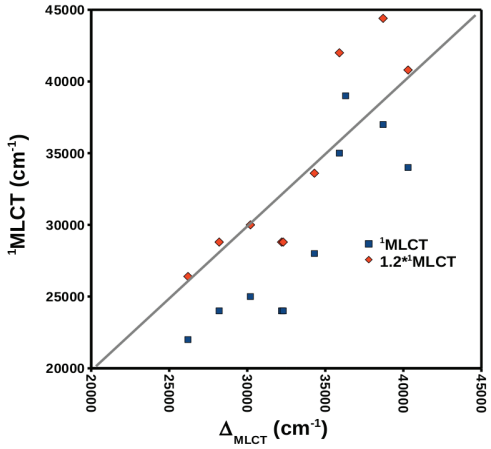

FIG. 18: Correlation graph between estimated values of Δ_{MLCT} and calculated values of ^{1}MLCT peaks.

TABLE VI: PDOS criteria which may have an influence on luminescence lifetimes.

Compound	% d in "$1\pi^*$"	% π in "t_{2g}"	$d \times \pi$ [a]
$[Ru(bpy)_3]^{2+}$	7.4	23	170
$[Ru(tpy)_2]^{2+}$	9.5	27	256
$[Ru(tpy)(L1)]^{2+}$	8.6	34.8	299
$[Ru(L1)_2]^{2+}$	13	31.5	410
$[Ru(L2)_2]^{2+}$	12.5	53.8	672

[a] Product of columns 2 and 3.

cause the determination of these indices is considerably less computationally demanding than calculating potential energy curves for N-electron states.

III. CONCLUSION

The initially stated goal of this paper was to investigate the extent to which (TD-)DFT could provide computation support for experimentalists seeking to design ligands for photochemical molecular devices. We emphasized that the computational model should be able (i) to quantitatively reproduce the known x-ray structures and absorption spectra and yet (ii) be interpretable in the ligand field theory (LFT) terminology commonly used by experimentalists working on the problem of PMD ligand design. We have largely accomplished what we set out to do. Thus our gas-phase optimized structures differ little from the x-ray crystallographic start geometries that we used, except for a small (3%) contraction expected from chemical pressure in the condensed phase. Our calculated gas-phase spectra are also in good agreement with, though slightly blue shifted (by about 7%) compared to, spectra measured in solution. The main peaks in the spectra can also be explained in terms of LFT-like orbital energy differences extracted using the technique of partial density of states (PDOS) analysis in so far as trends in Δ_{MLCT} provide a good prediction of the principle ^{1}MLCT absorption peaks. This is good news as DFT geometry optimizations and PDOS analysis are much less computationally intensive than TD-DFT calculations. Finally we showed how our (P)DOS plots may provide rough indicators of when a compound is likely to luminesce without carrying out a much longer and more computational resource intensive calculation of excited states and their surfaces and/or dynamics.

ACKNOWLEDGMENTS

C. M. W. would like to acknowledge a scholarship from the French Embassy in Kenya. Those of us at the *Université Joseph Fourier* would like to thank Denis Charapoff, Régis Gras, Sébastien Morin, and Marie-Louise Dheu-Andries for technical support at the (DCM) and for technical support in the context of the *Centre d'Expérimentation du Calcul Intensif en Chimie* (CECIC) computers used for the calculations reported here. We would also like to thank Ilaria Ciofini for help with GAUSSIAN input files. The work reported here constitutes part of the doctoral work of C. M. W. P. B. aided C. M. W. in the context of a series of undergraduate projects. The experimental work reported here is part of the doctoral work of S. L. and appears in part in his Ph. D. thesis [12] as does a preliminary account of the theoretical work presented here (Sec. 1.5 of the thesis.) This work has been carried out in the context of the French Rhône-Alpes *Réseau thématique de recherche avancée (RTRA): Nanosciences aux limites de la nanoélectronique* and the Rhône-Alpes Associated Node of the European Theoretical Spectroscopy Facility (ETSF).

APPENDIX A: PARTIAL DENSITY OF STATES ANALYSIS

Partial density of states (PDOS) analysis is a well-established procedure in condensed matter theory, though there are several variants of the PDOS procedure to be found in the literature. The variant we use is essentially the same as the one proposed by Roald Hoffmann and sketched on pp. 32-36 of Ref. [39]. For concreteness, we give here a brief description of our PDOS analysis.

The density of states (DOS) function is given by,

$$\mathrm{DOS}(\epsilon) = \sum_i g(\epsilon - \epsilon_i)\,, \tag{A1}$$

where g is a normalized gaussian,

$$\int g(\epsilon)\, d\epsilon = 1\,, \tag{A2}$$

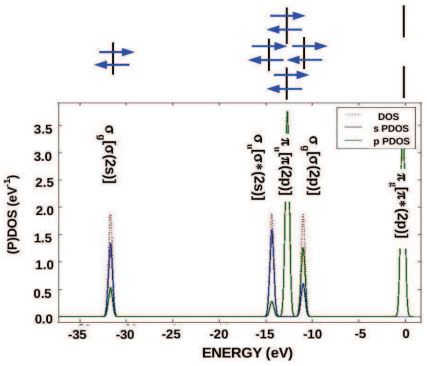

FIG. 19: N_2 PDOS analysis. The familiar MO diagram of N_2 has been turned sidewise with respect to its familiar position and placed above the (P)DOS. Orbital labels indicate both the MO symmetry and the expected chemical nature of the MOs which is largely confirmed by the MO analysis.

with fixed full-width-at-half-maximum (FWHM, chosen to be 1 eV in the present study) and ϵ_i is the energy of the ith molecular orbital (MO). The formula for the PDOS for the μth atomic orbital (AO) is,

$$\mathrm{PDOS}_\mu(\epsilon) = \sum_i q_{\mu,i} g(\epsilon - \epsilon_i)\,, \tag{A3}$$

where $q_{\mu,i}$ is the Mulliken charge of the μth AO in the ith MO. It is calculated as,

$$q_{\mu,i} = \sum_\nu S_{\mu,\nu} P^{(i)}_{\mu,\nu}\,. \tag{A4}$$

where,

$$S_{\mu,\nu} = \langle \mu | \nu \rangle\,, \tag{A5}$$

is the AO overlap matrix and,

$$P^{(i)}_{\mu,\nu} = C_{\nu,i} C_{\mu,i}\,, \tag{A6}$$

is the ith MO density matrix calculated from the MO coefficient matrix, **C**. Normally we are interested in the PDOS for a group of orbitals (such as al the d orbitals on the ruthenium atom). In that case, the appropriate PDOS is obtained as a sum over the PDOS of all relevant orbitals,

$$\mathrm{PDOS}(\epsilon) = \sum_\mu \mathrm{PDOS}_\mu(\epsilon)\,. \tag{A7}$$

These equations were implemented in our own in-house Python program PDOS.py. **Figure 19** shows an application of the method to the familiar homonuclear diatomic MO diagram of N_2. As expected, the lowest σ bonding and antibonding orbitals have mixed atomic s and p character, but are dominately of s-type. On the other hand, the higher energy σ orbital shown in the figure is of mixed s and p character, but is of dominately p-type. As expected from simple symmetry arguments, the π bonding and antibonding orbital have only p character and no atomic s character whatsoever.

Another program with the same functionality is the Python program GaussSum (`http://gausssum.sourcegourge.net/`) and PDOS.py has been checked against GaussSum. An advantage of PDOS.py is that multiple PDOS as well as the total DOS may be plotted on the same graph. We needed this for the present article

TABLE VII: X-ray coordinates (Cartessian in Å) of the $[Ru(L2)_2]^{2+}$ complex.

	Atom	x	y	z		Atom	x	y	z
1	Ru	-2.2881	3.3610	23.1656	51	C	-1.9361	-0.8580	22.9876
2	N	-1.3473	3.8790	24.9896	52	C	-2.4081	-2.1370	22.7076
3	N	0.2071	3.2600	21.2147	53	C	-1.5861	-3.1730	23.1016
4	N	0.2729	4.8360	22.6806	54	C	-0.3792	-2.9540	23.7386
5	N	5.3172	3.2100	24.1546	55	C	0.0878	-1.6730	23.9886
6	N	-3.8883	2.4310	25.5466	56	C	-0.7172	-0.6410	23.5946
7	N	-3.2110	2.8810	21.3127	57	C	0.6038	1.3560	24.2846
8	N	-3.6682	6.1660	23.7166	58	H	-0.6558	2.3640	19.6677
9	N	-3.1810	5.7950	21.6447	59	H	0.6222	1.6320	20.1567
10	N	-2.4951	0.4060	22.8006	60	H	-0.6979	1.5110	20.9617
11	N	-0.5892	0.7370	23.7246	61	H	2.3442	3.1150	19.3687
12	C	-0.5020	3.8010	22.2457	62	H	4.0993	4.6790	19.4067
13	C	-3.9812	2.9630	24.3036	63	H	4.1431	6.3881	20.9347
14	C	-3.0561	5.2610	22.9006	64	H	2.4600	6.6420	22.5416
15	C	-1.6941	1.3890	23.2656	65	H	0.5708	6.2911	23.9856
16	C	-0.1640	2.0910	20.4317	66	H	-0.9102	6.1681	23.5396
17	C	1.3691	3.9710	20.9777	67	H	0.8156	5.9650	26.2106
18	C	2.3682	3.8160	20.0077	68	H	0.2504	4.9110	28.2066
19	C	3.3932	4.7490	20.0397	69	H	-1.3086	3.1740	28.1606
20	C	3.4221	5.7710	20.9587	70	H	-2.2254	1.3780	25.6616
21	C	2.4390	5.9280	21.9167	71	H	-2.7615	1.8270	27.0456
22	C	1.4130	4.9790	21.9137	72	H	-4.8846	1.4520	28.0186
23	C	-0.1342	5.6840	23.7956	73	H	-7.1796	1.5450	28.5246
24	C	-0.4433	4.8940	25.0436	74	H	-8.6895	2.4480	27.0566
25	C	0.1696	5.2690	26.2156	75	H	-8.0193	3.2800	24.9626
26	C	-0.1515	4.6430	27.3906	76	H	-5.4171	3.6420	22.2207
27	C	-1.0655	3.6210	27.3586	77	H	-6.8011	3.3180	22.8436
28	C	-1.6324	3.2460	26.1536	78	H	-6.1311	4.6910	23.1156
29	C	-2.6094	2.0980	26.1476	79	H	-3.1743	5.4450	25.4866
30	C	-5.1214	2.3250	26.1776	80	H	-3.6133	6.9321	25.5356
31	C	-5.5115	1.8200	27.4066	81	H	-4.6763	5.8130	25.3756
32	C	-6.8686	1.8810	27.6926	82	H	-5.0452	8.5781	24.2906
33	C	-7.7725	2.4150	26.8116	83	H	-5.7461	10.0031	22.5636
34	C	-7.3914	2.9120	25.5716	84	H	-5.2819	9.5681	20.3667
35	C	-6.0413	2.8330	25.2776	85	H	-4.1028	7.6641	19.7217
36	C	-5.9731	3.7630	22.9826	86	H	-1.7309	5.0490	20.5317
37	C	-3.7933	6.0830	25.1496	87	H	-2.8878	5.6600	19.6977
38	C	-4.1821	7.2451	22.9856	88	H	-3.8567	4.1210	18.3647
39	C	-4.8642	8.3841	23.3766	89	H	-4.6587	1.9530	17.9757
40	C	-5.2601	9.2161	22.3487	90	H	-4.5938	0.4210	19.7247
41	C	-4.9829	8.9551	21.0267	91	H	-4.3811	1.0080	22.8656
42	C	-4.2909	7.8451	20.6357	92	H	-4.1470	-0.1450	21.8537
43	C	-3.8810	6.9951	21.6577	93	H	-3.2410	-2.2870	22.2757
44	C	-2.6749	5.1310	20.4557	94	H	-1.8591	-4.0670	22.9276
45	C	-3.2589	3.7780	20.2767	95	H	0.1428	-3.7000	24.0106
46	C	-3.8138	3.4640	19.0497	96	H	0.9228	-1.5220	24.4126
47	C	-4.3027	2.1970	18.8247	97	H	1.3768	0.9550	23.9046
48	C	-4.2608	1.3020	19.8547	98	H	0.6127	1.2330	25.2256
49	C	-3.7430	1.6610	21.0757	99	H	0.6008	2.2860	24.0866
50	C	-3.8000	0.6720	22.1937					

and it does not seem to be very easy to do with GaussSum. Our Figs. 13, 14, 15, 16, and 17 are all made using PDOS.py.

Users of GaussSum should note that GaussSum and PDOS.py differ in their definitions of the gaussian convolution. In GaussSum, the gaussians always have unit *height*. In PDOS.py, the gaussians always have unit *area*. This latter choice seems more logical to us. This means that the ratio of peak heights calculated with GaussSum to that of PDOS.py is ,

$$\frac{\text{GaussSum}}{\text{PDOS.py}} = \sqrt{\frac{\pi}{\log 2}}\frac{\mathrm{FWHM}}{2}\,. \tag{A8}$$

APPENDIX B: EXPERIMENTAL

The crystal structure of $[Ru(bpy)_3]^{2+}$ is from Ref. [27].

The synthesis and crystal structure of $\mathbf{[Ru(tpy)_2]^{2+}}$ were reported in Ref. [35].

The synthesis and characterization of $\mathbf{[Ru(L1)_2]^{2+}}$ and $\mathbf{[Ru(tpy)(L1)]^{2+}}$ were reported in Ref. [10]. We have taken the

crystal structures for the bromides of these compounds crystalized from acetonitrile from that study. The absorption spectra have been taken from that same study, but are only reported in full in the present work. The measurements were for acetonitrile solutions at room temperature. Luminescence lifetime measurements were measured under the same conditions at room temperature.

The synthesis and photophysical data for $\mathbf{[Ru(L2)_2]^{2+}}$ are reported for the first time in this article. The synthesis of $[Ru(L2)_2]^{2+}$ was carried out following the same method as that used to synthesize $[Ru(L1)_2]^{2+}$ in Ref. [10]. Specifically, $\mathbf{[Ru(L2)_2](PF_6)_2}$ was prepared in the following manner: A suspension of anhydrous $RuCl_3$ (121 mg, 0.58 mmol), L2 (500 mg, 1.17 mmol) and potassium carbonate (650 mg, 4,68 mmol) in 15 mL ethylene glycol was stirred at 150°C for 5 hours. After cooling to room temperature, addition of a saturated aqueous solution of KPF_6 caused the precipitation of a yellowish compound. After filtration, the resulting solid was purified by column chromatography ($CHCl_3$:CH_3CN 2:1) affording 161 mg (15% yield). ^{1}H NMR (CD_3CN, 300 MHz): δ (ppm) 8.01 (t, 2H), 7.84 (d, 4H), 7.73 (d, 4H), 7.37 (m, 4H), 7.30 (d, 8H), 5.69 (d, 4H), 4.49 (d, 4H), 2.20 (s, 12H). ESI-MS: m/z = 989.1 ($[M\text{-}PF_6]^+$, calculated for $C_{46}H_{50}F_6N_{10}PRu$ = 989.29.

Absorption spectra were recorded a Varian Cary 300 Scan UV-Visible spectrophotometer. Emission spectra were recorded on a Varian Cary Eclipse spectrofluorimeter. Samples in acetonitrile solutions were placed in 1 cm path length quartz cuvettes for room temperature measurements. $[Ru(L2)_2]PF_6$ was crystalized by slow evaporation from acetonitrile. The x-ray crystal structure is given in **Tables VII**. It has been deposited on the Cambridge database under the reference CCDC-800433.

APPENDIX C: COMPUTATIONAL DETAILS

DFT and TD-DFT calculations were carried out using the GAUSSIAN 03 program [42]. The 6-31G basis set was used for carbon, nitrogen, and hydrogen. The LANL2DZ effective core potential and accompanying basis set was used for ruthenium.

Since no practical exact exchange-correlation functional is known (TD-)DFT, approximate functionals must be used in practice. We chose to use the B3LYP functional used in previous TD-DFT studies of the absorption spectrum of $[Ru(bpy)_3]^{2+}$ [18, 19]. This is is a hybrid functional, meaning that it incorporates a fixed amount of "exact" (Hartree-Fock) exchange into a generalized gradient approximation (GGA). The parameters used in the B3LYP functional are taken without reoptimization from Becke's B3PW functional [43] even though the original Perdew-Wang (PW) correlation functional [44] is replaced by the Lee-Yang-Parr (LYP) correlation functional [45]. Becke's exchange GGA (B) is the same in the B3PW and B3LYP functionals.

Gas-phase ground-state geometries were optimized beginning from the x-ray crystallography start geometries. D_3 symmetry was imposed along with a multiplicity of 1 and a charge of 2+. Potential energy minima were checked by calculating vibrational frequencies without the symmetry constraint. SCF convergence was set to tight andd the grid was set to fine. Visualization of molecular orbitals was done using MOLDEN [46].

Gas-phase absorption spectra were calculated by TD-DFT using the adiabatic approximation and same B3LYP functional as for the ground state calculations (i.e., TD-B3LYP calculations). As a large number of excited states is needed to compare with experiment, special use was made of the keyword `add`. By using `add=20`, we were able to add 20 states at a time to our spectra until we had on the order of 100 excited states. It as also necessary to set the keyword `maxdavidson=500` to widen the Krylov subspace dimensions in order to facilitate convergence in the block Davidson algorithm. This gives us the spectral function,

$$S(\omega) = \sum_I f_I \delta(\omega - \omega_I)\,, \tag{C1}$$

where f_I is the oscillator strength corresponding to the electronic excitation energy $\omega_I = E_I - E_0$.

The spectral function must be converted to the molar extinction coefficient before it may be compared against experiment. To do so, we wrote an in-house PYTHON program, SPECTRUM.PY, which uses the well-known formula [47–49] (see also, e.g., Ref. [13] p. 180),

$$\epsilon(\omega) = \frac{\pi N_A e^2}{2\epsilon_0 m_e c \ln(10)} S(\omega)\,, \tag{C2}$$

expressed here in SI units. Actual calculations were gaussian broadened with a FWHM of 4 000 cm^{-1} to account for spectral broadening due to vibrational structure, solvent effects, and finite experimental resolution. Note that the FWHM is the only empirical parameter involved in the comparison of theoretical and measured spectra in this paper.

APPENDIX D: LIST OF ABBREVIATIONS

Due to its somewhat multidisciplinary nature, this article contains a large numbere of abbreviations. Some of these have been collected in this appendix as a convenience to the reader.

6-31G A double ζ quality split valence gaussian-type orbital basis set.

AO Atomic orbital.

B3LYP A hybrid density functionl using Becke's exchange functional and the Lee-Yang-Parr correlation functional as well as 3 semi-empirical parameters taken from the B3PW functional.

B3PW The original hybrid functional consisting of Becke's exchange functional and the Perdew-Wang correlation functional, assembled with Hartree-Fock exchange using 3 empirical parameters.

bpy The ligand bipyridine.

e_g^* Metal-centered ligand field theory antibonding d orbitals.

DFT Density-functional theory.

DOS Density of states.

ESI-MS Electron spray ionization mass spectroscopy.

FWHM Full width at half maximum.

GGA Generalized-gradient approximation.

GS Ground state. ^{1}GS emphasizes that the ground state is a singlet.

L1 The ligand 1,1'-[2,6-pyridinediylbis(methylene)]bis[3-methylimidazolium].

L2 The ligand 1,1'-[2,6-pyridinediylbis(methylene)]bis[3-methylbenziimidazolium].

LANL2DZ The effective core potential used for ruthenium in this paper.

LFT Ligand field theory.

MC Metal centered. ^{1}MC and ^{3}MC indicate, respectively, the singlet and triplet metal-centered excited states.

MLCT Metal-to-ligand charge transfer transition. ^{1}MLCT and ^{3}MLCT indicate, respectively, the singlet and triplet metal-to-ligand charge transfer excited states.

MO Molecuar orbital.

π^* Ligand-centered antibonding orbitals.

PDOS Partial density of states.

PMD Photochemical molecular devices.

SI *Système international*.

t_{2g} Metal-centered ligand field theory nonbonding d orbitals.

TD-B3LYP TD-DFT using the B3LYP functional.

TD-DFT Time-dependent density-functional theory.

tpy The ligand terpyridine.

UV Ultraviolet.

REFERENCES

[1] J.-P. Sauvage, J.-P. Collin, J.-C. Chambron, S. Guillerez, C. Coudret, V. Balzani, F. Barigelletti, L. D. Cola, and L. Flamigni, Chem. Rev. **94**, 993 (1994), Ruthenium(II) and osmium(II) bis(terpyridine) complexes in covalently-linked multicomponent systems: Synthesis, electrochemical behavior, absorption spectra, and photochemical and photophysical properties.

[2] B. O'Regan and M. Grätzel, Nature **353**, 737 (1991), A low-cost, high-efficiency solar cell based on dye-sensitized colloidal TiO_2 films.

[3] M. Grätzel, Prog. Photovoltaics **8**, 171 (2000), Perspectives for Dye-sensitized Nanocrystalline Solar Cells.

[4] M. Grätzel, Nature **414**, 338 (2001), Photoelectrochemical cells.

[5] E. A. Medlycott and G. S. Hanan, Chem. Soc. Rev. **34**, 133 (2005), Designing tridentate ligands for ruthenium(II) complexes with prolonged room temperature luminescence lifetimes.

[6] M. Abrahamsson, M. Jäger, T. Österman, L. Eriksson, P. Persson, H.-C. Becker, O. Johansson, and L. Hammarström, J. Am. Chem. Soc. Commun. **128**, 12616 (2006), A 3.0 μs room temperature excited state lifetime of a bistridentate Ru^{II}-polypyridine complex for rod-like molecular arrays.

[7] A. Vlček Jr. and S. Záliš, Coord. Chem. Rev. **251**, 258 (2007), Modeling of charge-transfer transitions and excited states in d^6 transition metal complexes by DFT techniques.

[8] L. Fodor, G. Lendvay, and A. Horváth, J. Phys. Chem. A **111**, 12891 (2007), Solvent Dependence of Absorption and Emission of $Ru(bpy)_2(CN)_2$: Experiment and Explanation Based on Electronic Structure Theory.

[9] V. Balzani, G. Bergamini, S. Campagna, and F. Puntoriero, Top. Curr. Chem. **280**, 1 (2007), Photochemistry and photophysics of coordination compounds: Overview and general concepts.

[10] J. Dinda, S. Liatard, J. Chauvin, D. Jouvenot, and F. Loiseau, Dalton Trans. **40**, 3683 (2011), Electronic and geometrical manipulation of the excited state of bis-terdentate homo- and heteroleptic ruthenium complexes.

[11] A. Juris, V. Balzani, F. Barigelletti, S. Campagna, P. Belser, and A. V. Zelewsky, Coord. Chem. Rev. **84**, 85 (1988), Ru(II) polypyridine complexes: Photophysics, photochemistry, electrochemistry, and chemiluminescence.

[12] S. Liatard, Ph.D. thesis, Université de Grenoble, Grenoble, France (2012), Complexes de Ruthénium Bisterdentates pour la Réalisation d'Assemblages Photoactivables.

[13] B. N. Figgis and M. A. Hitchman, *Ligand Field Theory and Its Applications* (Wiley-VCH, New York, 2000).

[14] J.-L. Heully, F. Alary, and M. Boggio-Pasqua, J. Chem. Phys. **131**, 184308 (2009), Spin-orbit effects on the photophysical properties of $[Ru(bpy)_3]^{2+}$.

[15] M.-E. Moret, I. Tavernelli, M. Chergui, and U. Rothlisberger, Chem. Eur. J. **16**, 5889 (2010), Electron Localization Dynamics in the Triplet Excited State of $[Ru(bpy)_3]^{2+}$ in Aqueous Solution.

[16] I. Tavernelli, B. F. E. Curchod, and U. Rothlisberger, Chem. Phys. **391**, 101 (2011), Nonadiabatic molecular dynamics with solvent effects: A LR-TDDFT QM/MM study of ruthenium (II) tris (bipyridine) in water.

[17] J. E. B. Freitas, D. Lomonaco, G. Mele, and S. E. Mazzetto, J. Luminescence **129**, 1260 (2009), Luminescence quenching of $[Ru(bpy)_3]^{2+}$ by ruthenium(II) tetraphosphite complexes with different phosphite ligands.

[18] M. J. Lundqvist, E. Galoppini, G. J. Meyer, and P. Persson, J. Phys. Chem. A **111**, 1487 (2007), Calculated Optoelectronic Properties of Ruthenium Tris-bipyridine Dyes Containing Oligophenyleneethynylene Rigid Rod Linkers in Different Chemical Environments.

[19] S. I. Gorelsky and A. B. P. Lever, J. Organomet. Chem. **635**, 187 (2001), Electronic structure and spectra of ruthenium diimine complexes by density functional theory and INDO/S. Comparison of the two methods.

[20] C. Daul, E. J. Baerends, and P. Vernooijs, Inorg. Chem. **33**, 3538 (1994), A density functional study of the MLCT states of $[Rh(bpy)_3]^{3+}$ in D_3 symmetry.

[21] G. Calzaferri and R. Rytz, J. Phys. Chem. **99**, 12141 (1995), Electronic transition oscillator strength by the extended Hückel molecular orbital method.

[22] M. Buchs and C. Daul, Chimia **52**, 163 (1998), Geometry optimization and excited states of tris(2,2'-bipyridine)ruthenium(II) using density functional theory.

[23] D. Wang, R. Mendelsohn, E. Galoppini, P. G. Hoertz, R. A. Carlisle, and G. J. Meyer, J. Phys. Chem. B **108**, 16642 (2004), Excited state electron transfer from Ru(II) polypyridyl complexes anchored to nanocrystalline TiO_2 through rigid-rod linkers.

[24] R. W. Harrigan and G. A. Crosby, J. Chem. Phys. **59**, 3468 (1973), Symmetry assignments of the lowest CT excited states of ruthenium (II) complexes via a proposed electronic coupling model.

[25] D. C. Baker and G. A. Crosby, Chem. Phys. **4**, 428 (1974), Spectroscopic and magnetic evidence for multiple-state emission from tris(2,2'-bipyridine) ruthenium (II) sulfate.

[26] F. Felix, J. Ferguson, H. U. Gudel, and A. Ludi, Chem. Phys. Lett. **62**, 153 (1979), Electronic spectra of $M(bipy)_2^{+3}$ complexions (M = Fe, Ru and Os).

[27] D. P. Rillema, D. S. Jones, and H. A. Levy, J. Chem. Soc. Chem. Commun. **1979**, 849 (1979), Structure of tris(2,2-bipyridyl)ruthenium(II) hexafluorophosphate, $[Ru(bipy)_3][PF_6]_2$; X-ray crystallographic determination.

[28] J. Ferguson and F. Herren, Chem. Phys. **76**, 45 (1983), A model for the interpretation of the electronic spectra of the complex ions $M(bpy)_3^{2+}$ (M = Fe, Ru, Os) in D_3 and C_2 sites.

[29] M. E. Casida, J. Molec. Struct. (Theochem) **914**, 3 (2009), Review: Time-dependent density-functional theory for molecules and molecular solids.

[30] M. E. Casida, B. Natarajan, and T. Deutsch, in *Fundamentals of Time-Dependent Density-Functional Theory*, edited by M. A. L. Marques, N. Maitra, F. Noguiera, E. K. U. Gross, and A. Rubio (Springer Verlag, 2011), vol. 837 of *Lecture Notes in Physics*, p. 279, http://arxiv.org/abs/1102.1849, Non-Born-Oppenheimer dynamics and conical intersections.

[31] M. E. Casida and M. Huix-Rotllant, Annu. Rev. Phys. Chem. **63**, 287 (2012), Progress in Time-Dependent Density-Functional Theory.

[32] H. Yersin, W. Humbs, and J. Strasser, Coord. Chem. Rev. **159**, 325 (1997), Low-lying electronic states of $[Rh(bpy)_3]^{3+}$, $[Pt(bpy)_2]^{2+}$, and $[Ru(bpy)_3]^{2+}$. A comparative study based on highly resolved and time-resolved spectra.

[33] J. V. Caspar and T. J. Meyer, J. Am. Chem. Soc. **105**, 5583 (1983), Photochemistry of tris(2,2'-bipyridine)ruthenium(2+) ion $[Ru(bpy)_3]^{2+}$. Solvent effects.

[34] J. R. Winkler, T. L. Netzel, C. Creutz, and N. J. Sutin, J. Am. Chem. Soc. **109**, 2381 (1987), Direct observation of metal-to-ligand charge-transfer (MLCT) excited states of pentaammineruthenium(II) complexes.

[35] S.Pyo, E. Pérez-Cordero, S. Bott, and L. Echegoyen, Inorg. Chem. **38**, 3337 (1999), Crystal Structure of $[Ru(terpy)_2]^0$: A New Crystalline Material from the Reductive Electrocrystallization of $[Ru(terpy)_2]^{2+}$.

[36] A. Amini, A. Harriman, and A. Mayeux, Phys. Chem. Chem. Phys. **6**, 1157 (2004), The triplet excited state of ruthenium(II) bis(2,2':6',2''-terpyridinen): Comparison between theory and experiment.

[37] E. Jakubikova, R. L. Martin, and E. R. Batista, Inorg. Chem. **49**, 2975 (2010), Systematic study of modifications to ruthenium(II) polypyridine dyads for electron injection enhancement.

[38] O. A. Borg, S. S. M. C. Godinho, M. J. Lundqvist, S. Lunell, and P. Persson, J. Phys. Chem. A **112**, 4470 (2008), Computational Study of the Lowest Triplet State of Ruthenium Polypyridyl Complexes Used in Artificial Photosynthesis.

[39] R. Hoffmann, *Solids and Surfaces: A Chemist's Vview of Bonding in Extended Structures* (VCH Publishers, New York, 1988).

[40] G. Wulfsberg, *Inorganic Chemistry* (University Science Books, 55D Gate Five Road, Sausalito, California 94965, 2000).

[41] K. Kasha, Discuss. Faraday Soc. **9**, 14 (1950), Characterization of Electronic Transitions in Complex Molecules.

[42] M. J. Frisch, G. W. Trucks, H. B. Schlegel, G. E. Scuseria, M. A. Robb, J. R. Cheeseman, J. A. Montgomery Jr., T. Vreven, K. N. Kudin, J. C. Burant, J. M. Millam, S. S. Iyengar, J. Tomasi, V. Barone, B. Mennucci, M. Cossi, G. Scalmani, N. Rega, G. A. Petersson, H. Nakatsuji, M. Hada, M. Ehara K. Toyota, R. Fukuda, J. Hasegawa, M. Ishida, T. Nakajima, Y. Honda, O. Kitao, H. Nakai, M. Klene, X. Li, J. E. Knox and H. P. Hratchian, J. B. Cross, C. Adamo, J. Jaramillo, R. Gomperts, R. E. Stratmann, O. Yazyev, A. J. Austin, R. Cammi, C. Pomelli, J. W. Ochterski, P. Y. Ayala, K. Morokuma, G. A. Voth, P. Salvador, J. J. Dannenberg, V. G. Zakrzewski, S. Dapprich, A. D. Daniels, M. C. Strain, O. Farkas, D. K. Malick, A. D. Rabuck, K. Raghavachari, J. B. Foresman, J. V. Ortiz, Q. Cui, A. G. Baboul, S. Clifford, J. Cioslowski, B. B. Stefanov, G. Liu, A. Liashenko, P. Piskorz, I. Komaromi, R. L. Martin, D. J. Fox, T. Keith, M. A. Al-Laham, C. Y. Peng, A. Nanayakkara, M. Challacombe, P. M. W. Gill, B. Johnson, W. Chen, M. W. Wong, C. Gonzalez, and J. A. Pople, GAUSSIAN 03, Revision B.05, Gaussian, Inc., Pittsburgh PA, 2003.

[43] A. D. Becke, J. Chem. Phys. **98**, 5648 (1993), Density-functional thermochemistry. III. The role of exact exchange.

[44] J. P. Perdew, J. A. Chevary, S. H. Vosko, K. A. Jackson, M. R. Pederson, D. J. Singh, and C. Fiolhais, Phys. Rev. **B 46**, 6671 (1993), Atoms, molecules, solids, and surfaces: Applications of the generalized gradient approximation for exchange and correlation.

[45] C. Lee, W. Yang, and R. Parr, Phys. Rev. B **37**, 785 (1988), Development of the Colle-Salvetti correlation energy formula into a functional of the electron density.

[46] G. Schaftenaar and J. H. Noordik, J. Comput.-Aided Mol. Design **14**, 123 (2000), MOLDEN: a pre- and post-processing program for molecular and electronic structures.

[47] R. C. Hilborn, Einstein coefficients, cross sections, f values, dipole moments, and all that, an updated version of *Am. J. Phys.* **50**, 982 (1982), http://arxiv.org/abs/physics/020202.

[48] R. C. Hilborn, Am. J. Phys. **50**, 982 (1982), Einstein coefficients, cross sections, f values, dipole moments and all that.

[49] R. C. Hilborn, Am. J. Phys. **51**, 471 (1983), Erratum:

"Einstein coefficients, cross sections, f values, dipole moments and all that" [*Am. J. Phys.* **50**, 982 (1982)].

Part III

Perspectives and Conclusions

This part comprises two parts which are; the chapter on the hypothetical complex. This is an ongoing work which is an extension of the thesis work that is reported here. The next chapter is on Conclusion, and here I look at the specific achievements. The formulated tools to be used in other situations as well. The chapter looks at what next and what lessons have we learned if any.

CHAPTER 9

THE HYPOTHETICAL COMPLEX

9.1 Introduction

$[Ru(oxa)_2]^{2+}$ This section deals with a hypothetical complex that we intend to synthesize in future. The oxa ligand is yet to be named accordingly. It has been included here as a way of extending the work that has been carried out in this thesis. A number of techniques [1] that were applied on the five complexes studied in this work were applied and results documented and presented here. With an imagined structure, optimization (using DFT) was done, partial density of states and TDDFT (UV transitions) were done. The calculations were based on the B3LYP functional, and the 6-31G basis set for the C,N,O,H atoms and with Lanl2dz basis set with its associated ECP for Ru atom. The following parts are a report of the findings.

9.2 Geometry calculations

The structure below represents the hypothetical complex before optimization. Each ligand is tridentate and uses nitrogen as its donor atom.

From the optimization process we end up with table 9.1 below which gives an insight on the nature of the frontier molecular orbitals in this complex. The determination of the character of these MOs was done using MOLDEN and it shows localized MOs as well as delocalized MOs. Molecular orbitals are usually either metal-centred (MC), ligand-centred (LC) or centred on both the metal and the ligand (MLC). This table is fundamental when it comes to to assigning electronic transitions. This kind of work will be dealt with later in this section.

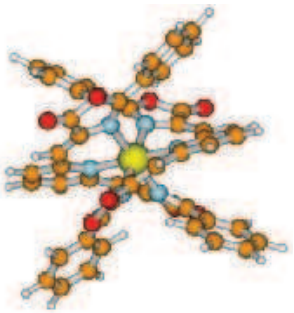

Figure 9.1: The optimized structure of the hypothetical complex

Table 9.2 indicates that ligands are slightly bent. The bond lengths and angles are similar to those of the complexes dealt with in this work.

Table 9.1: Some frontier molecular orbitals and their energies

Number	MO	Energy (eV)	Character
236	LUMO+10	-5.99	MC
235	LUMO+10	-6.04	LC
234	LUMO+8	-6.09	LC
233	LUMO+7	-6.53	MLC
232	LUMO+6	-6.90	LC
231	LUMO+5	-7.01	LC
230	LUMO+4	-7.15	MLC
229	LUMO+3	-8.11	LC
228	LUMO+2	-8.58	LC
227	LUMO+1	-8.60	LC
226	LUMO	-8.80	MLC
225	HOMO	-11.08	MC
224	HOMO-1	-11.20	MC
223	HOMO-2	-11.65	MC
222	HOMO-3	-11.93	LC
221	HOMO-4	-12.08	MC
220	HOMO-5	-12.18	LC
219	HOMO-6	-12.18	LC
218	HOMO-7	-12.19	LC
217	HOMO-8	-12.24	MLC
216	HOMO-9	-12.37	MLC
215	HOMO-10	-12.37	MLC
214	HOMO-11	-12.60	LC
213	HOMO-12	-12.83	LC
212	HOMO-13	-13.07	LC
211	HOMO-14	-13.17	LC
210	HOMO-15	-13.32	LC
209	HOMO-16	-13.38	LC
208	HOMO-17	-13.41	LC
207	HOMO-18	-13.42	LC
206	HOMO-19	-14.16	LC
205	HOMO-20	-14.23	LC

The bending leads to distortions that finally leads
to the lowering of the symmetry.

Table 9.2: Comparison of theoretical geometric parameters (distances in Ångströms, angles in degrees) of the "two ligand moities". Note that the two ligands are actually not different. They are described as being two because of the differences in their geometric parameters. Within each ligand the bite atoms are numbered starting from one end of the ligand going to the other end.

oxa_1	$R(RuN_1)$	$R(RuN_2)$	$R(RuN_3)$	$\angle(N_1RuN_2)$	$\angle(N_1RuN_2N_3)$
Theory	2.17	2.11	2.16	91.1	179.5
oxa_2	$R(RuN_1)$	$R(RuN_2)$	$R(RuN_3)$	$\angle(C_1RuN_2)$	$\angle(N_1RuN_2N_3)$
Theory	2.11	2.17	2.12	91.1	179.8

As seen in the discussions done earlier in this thesis, it is very difficult to uniquely identify and describe MOs as belonging to the metal or ligand exclusively. This as already known and also illustrated by visualization using MOLDEN is due to the mixing of d orbitals with the ligand π orbitals. This difficult prompted the invocation of the Partial density of states approach discussed in section 9.3 below.

9.3 Partial density of states-PDOS

The Partial density of states method enables one to determine the various MOs based on their energies. Using this approach and which is already discussed in detail in this thesis we can now identify the t_{2g}, π^* and e_g as shown on the figure 9.2.

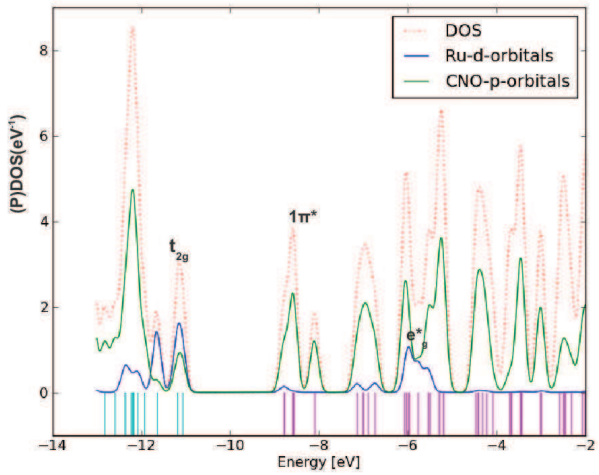

Figure 9.2: Total and partial density of states of $[Ru(oxa)_2]^{2+}$ partitioned over ruthenium d orbitals and ligand C, N and O p orbitals.

Table 9.3 consists of extracted energies for the important MOs, it also gives Δ_{MC}, Δ_{MLCT}. The table also captures the calculated ^{1}MLCT energy which is extracted from figure 9.4 in section 9.4. The inclusion

of ^{1}MLCT in this table is meant to facilitate its comparison with the pdos-determined Δ_{MLCT} which is supposed to be the same thing in situations where the partial density of states approach performs excellently well. These two values agree very well and this means that the pdos approach affords us a quick way to estimate ^{1}MLCT.

Table 9.3: Energy levels of t_{2g}, π^* and e_g^* obtained by PDOS analysis of $[Ru(oxa)_2]^{2+}$ and the resultant Δ_{MC} Δ_{MLCT} and comparison with calculated ^{1}MLCT energies

t_{2g} (eV)	π^* (eV)	e_g^* (eV)	Δ_{MC} (cm^{-1})	Δ_{MLCT} (cm^{-1})	Absorption peaks (^{1}MLCT)
-11.3	-8.5	-6.0	41118.4	22574.7	23000

Besides the Δ_{MLCT}, we also have the Δ_{MC} in the table, a quantity that helps alot in determining the separation between the t_{2g} and e_g^* levels. In our particular case the pdos method enables us to calculate this value as 41118.4 cm_1. This value which is calculated from the difference between -11.3 eV of t_{2g} and -6.0 eV of e_g^* and eventual conversion to wavenumbers forms a basis of positioning it in our spectrochemical series in our manuscript paper of chapter 8. The new spectrochemical series then becomes:

$$\Delta_{MC} : bpy > L2 > tpy > L1 > oxa \tag{9.1}$$

where oxa is the ligand on our hypothetical complex.

Thus, the pdos picture has enabled us to recover the ligand field-like theory in especially two ways. First, the pdos diagram in figure 9.2 clearly shows an arrangement of MOs similar to the familiar generic ligand field theory diagram. On this diagram one sees a number of π MOs between t_{2g} and e_g^*. Secondly, the Δ_o is estimated in terms of Δ_{MC}, which is easy to extract from such diagrams.

Table 9.4: The d$\times\pi$ product criteria for luminescence determination

% d in 1 π^*	% π in t_{2g}	$d \times \pi$
5	30	150

9.4 Excitation and luminescence

This section deals with the absorption process and the processes that follow thereafter. As already noted the pdos method through the Δ_{MLCT} approximation can be used to estimate ^{1}MLCT energy.

What follows is proof that usually spectral peaks comprise many mixed transitions. This is clearly seen in table 9.5. In this table, the major peaks observed on figure 9.4 are analyzed and the % contribution of each transition noted. In addition, the character of each transition is also determined.

As part of the overall objectives, we assess the luminescence status of this hypothetical complex. Based on the two indices developed in this work, the ΔE and the product $d \times \pi$ one can proceed as follows to attempt important predictions. Given that ΔE=Δ_{MC}-Δ_{MLCT}, our calculations here yield a ΔE value of 2.29 eV calculated from a Δ_{MC} = 41118.4 cm^{-1} and Δ_{MLCT} = 22574.4 cm^{-1} and its conversion to electron volts using the relationship 1eV= 8062.4 cm^{-1}. This ΔE and the $d \times \pi$ value of 150 (see table 9.6),

are and indication of a luminescent complex. The ΔE value is a quantification of the energy barrier between the luminescent ^{3}MLCT and the nonluminescent ^{3}MC state. It is so hard to populate the ^{3}MC

Table 9.5: Spectral Analysis of the transitions in the peaks of the spectra of $[Ru(oxa)_2]^{2+}$

Excited State	Wavelength (nm)	Intensity (oscillator strength)	Contributions (%)	Character
Number 1	813.13	0.0106		
HOMO-4	→	LUMO	3%	MC → MLC
HOMO	→	LUMO	97%	MC → MLC
Number 3	680.90	0.0501		
HOMO	→	LUMO	100%	MC → MLC
Number 12	476.44	0.1656		
HOMO-3	→	LUMO	90%	LC → MLC
HOMO-1	→	LUMO+3	10%	MC → LC
Number 12	331.61	0.3799		
HOMO-17	→	LUMO+2	3%	LC → LC
HOMO-16	→	LUMO	5%	LC → MLC
HOMO-14	→	LUMO	47%	LC → MLC
HOMO-13	→	LUMO+1	2%	LC → LC
HOMO-11	→	LUMO+2	6%	LC → LC
HOMO-10	→	LUMO	3%	M(L)C → MLC
HOMO-9	→	LUMO+1	6%	M(L)C → LC
HOMO-8	→	LUMO+3	4%	MLC → LC
HOMO-4	→	LUMO+3	3%	MC → LC
HOMO-3	→	LUMO+2	3%	LC → LC
HOMO-1	→	LUMO+6	18%	MC → LC

Table 9.6: The d$\times\pi$ product criteria for luminescence determination

% d in $1\pi^*$	% π in t_{2g}	$d \times \pi$
5	30	150

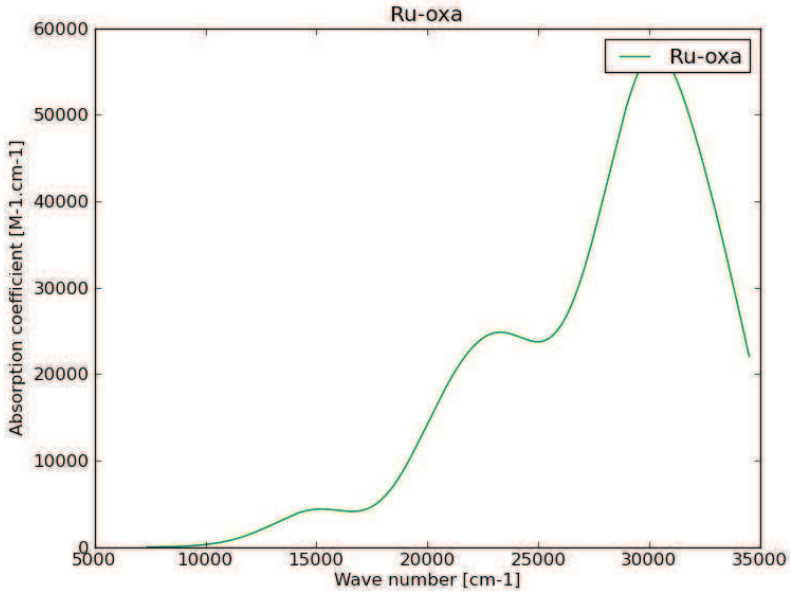

Figure 9.3: Calculated absorption spectra of $[Ru(oxa)_2]^{2+}$

state hence the excited state prefers the ^{3}MLCT minimum from which luminescence can occur. Thus the low $d \times \pi$ value of 150 and large value of ΔE (2.29 eV) favor luminescence just like the luminescent complexes which have this combination.

9.5 Conclusion

In conclusion, it is hoped that finally this hypothetical complex will be synthesized and measurements corresponding to the calculated ones determined. The outcome of such measurements will help to check on the predictive capability of the methods developed in this work. The results will help in refining our methods if they prove good and lead to radical modifications. With our methods working, as hoped, we shall have devised an affordable tool to be used for the prediction of chemical properties prior to synthesis of any complex of interest. This then is likely to drastically reduce dangerous and costly ventures in our laboratories.

References

[1] C. M. Wawire, D. Jouvenot, F. Loiseau, P. Baudin, S. Liatard, L. Njenga, G. N. Kamau, and M. E. Casida, "Density-Functional Study of Lumininescence in Polypyridine Ruthenium Complexes," *Submitted*.

CHAPTER 10

CONCLUSION

The objectives of this work were to determine the molecular orbital picture in various ruthenium complexes, and especially the relative positions of the π^* and e_g^*. This objective was largely achieved. We succeeded to determine what we described in this thesis as the ligand field-like picture.

The optimizations, the frequency calculations, the UV transitions, and partial density of states were carried out as earlier planned.

The thesis work led to the formulation of a method based on partial density of states which has proved very useful. The partial density of states peaks enabled determination of Δ_{MC} and Δ_{MLCT} which enabled the determination ΔE. ΔE and the $d \times \pi$ are the two important indices determined in this work which have proved that the use of DFT and TDDFT in conjunction with the partial density of states can provide a cheaper way to assess the luminescence properties of complexes in a cheaper way.

The future of this kind of research lies in exploring cheap ways to attain credible results. This was nicely demonstrated in this project. The need to work in a multi-disciplinary manner also came out quite clearly. The partial density of states technique borrowed from solid state physics enabled the progress that was made in this project.

There is also need to formulate ways of determining the properties of molecules before their synthesis This is exactly what the previous chapter is dealing with. In this chapter we decided to come up with a hypothetical complex and perform all the necessary calculations before the real synthesis. Depending on what results the synthesis will reveal at an appropriate time, it will have paved a way to apply the formulated tool for predictive purposes. The experimental results will be used as a way to calibrate of our pdos method.

Part IV

Appendices

APPENDIX A

TDA-TDDFT FOR THE PHOTOCHEMICAL RING-OPENING OF OXIRANE

Overview

This article lies outside the main objectives of this thesis and so has been relegated to an appendix. Nevertheless, for myself and the two other doctoral students (Miquel Huix-rotllant and Bhaarathi Natarajan) the work reported here represents a first and hence an important introduction to photochemical modeling using TD-DFT. Previous work (refs 7 and 21 of the published paper) indicates that TD-DFT can be attractive in describing the photochemistry of oxirane ring opening. However, conventional TD-DFT failed to describe avoided crossings and conical intersections which are conventionally thought to explicit require inclusion of 2-electron excited states. We thought that spin-flip TD-DFT could resolve some of the problems. The article describes our implementation of spin-flip TD-DFT and testing of its performance. My contribution to this paper consisted of calculations along the asymmetric ring opening pathway.

Assessment of noncollinear spin-flip Tamm–Dancoff approximation time-dependent density-functional theory for the photochemical ring-opening of oxirane

Miquel Huix-Rotllant,[a] Bhaarathi Natarajan,[ab] Andrei Ipatov,[a] C. Muhavini Wawire,[ac] Thierry Deutsch[b] and Mark E. Casida*[a]

Received 19th April 2010, Accepted 6th July 2010
DOI: 10.1039/c0cp00273a

Under the usual assumption of noninteracting *v*-representability, density-functional theory (DFT) together with time-dependent DFT (TDDFT) provide a formally exact single-reference method suitable for the theoretical description of the electronic excited-states of large molecules, and hence for the description of excited-state potential energy surfaces important for photochemistry. The quality of this single-reference description is limited in practice by the need to use approximate exchange–correlation functionals. In particular it is far from clear how well approximations used in contemporary practical TDDFT calculations can describe funnel regions such as avoided crossings and conical intersections. These regions typically involve biradical-like structures associated with bond breaking and conventional wisdom would seem to suggest the need to introduce explicit double excitation character to describe these structures. Although this is lacking in ordinary spin-preserving (SP) TDDFT, it is present to some extent in spin-flip (SF) TDDFT. We report our tests of Wang–Ziegler noncollinear SF-TDDFT within the Tamm–Dancoff approximation for describing the avoided crossing in the C_{2v} CC ring-opening reaction of oxirane and for describing the conical intersection relevant for the more physical asymmetric CO ring-opening reaction of oxirane. Comparisons are made with complete active space self-consistent field and quantum Monte Carlo benchmark results from two previous papers on the subject [*J. Chem. Phys.*, 2007, **127**, 164111; *ibid* **129**, 2008, 124108]. While the avoided crossing in the C_{2v} pathway is found to be reasonably well described, the method was found to be only partially successful for the conical intersection (CX) associated with the physically more important asymmetric pathway. The origin of the difficulties preventing the noncollinear SF-TDDFT method from giving a completely satisfactory description of the CX was traced back to the inability of SF-TDDFT based upon a single triplet reference state to correlate all potentially relevant configurations involving not just two but three nearly degenerate orbitals (n, σ_{CO}, and σ^*_{CO}). This article is also the first report of our implementation of SF-TDDFT within the DEMON2K program.

I. Introduction

Due to its rigorous formal foundations and computational efficiency, time-dependent density-functional theory (TDDFT) is currently a method of choice for treating electronic excited states. It is thus one of several tools to be found in today's photochemical modeling kit (see *e.g.*, ref. 1–4). Nevertheless applications of TDDFT are limited by a number of problems due to the inevitable use of approximate functionals in practical applications. Overcoming these limitations is important for extending the domain of applicability of TDDFT. Here we investigate the ability of spin-flip TDDFT (SF-TDDFT) to overcome problems encountered by ordinary TDDFT near funnel regions, namely avoided crossings and conical intersections (CXs). This is especially important in light of the recent development of Tully-type[5,6] mixed TDDFT/classical trajectory surface-hopping dynamics.[7–12] Surface-hopping dynamics may also have inspired very recent work by Minezawa and Gordon[13] focusing on characterizing the CXs of ethylene using one formulation of SF-TDDFT[14,15] and the BHHLYP functional (50% Hartree–Fock plus 50% Becke exchange[16] plus Lee–Yang–Parr correlation[17]). In the present study, we have chosen the photochemical ring opening of oxirane [(I) in Fig. 1] as a test case for evaluating the ability of a different formulation of SF-TDDFT[18,19] in describing funnel regions because oxiranes are an important class of compounds in photochemistry (see ref. 20 and the brief review in Appendix B of ref. 21 as well as ref. 22 where the photochemical ring-opening of diphenyloxirane has been studied, not by TDDFT, but by a different DFT approach) and

[a] *Laboratoire de Chimie Théorique, Département de Chimie Moléculaire (DCM, UMR CNRS/UJF 5250), Institut de Chimie Moléculaire de Grenoble (ICMG, FR2607), Université Joseph Fourier (Grenoble I), 301 rue de la Chimie, BP 53, F-38041 Grenoble Cedex 9, France. E-mail: Mark.Casida@UJF-Grenoble.Fr*
[b] *CEA, INAC, SP2M, L_Sim, 38054 Grenoble Cedex 9, France*
[c] *The Catholic University of Eastern Africa, P. O. Box 62157, 00200, Nairobi, Kenya*

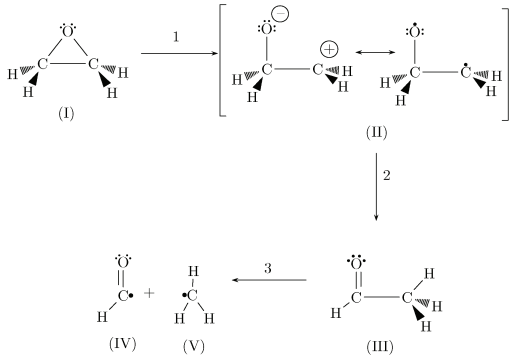

Fig. 1 Gomer–Noyes mechanism for the ring-opening of oxirane (I).[77]

because of the availability of high-quality comparison results.[7,21]

Let us review the fundamental problems encountered by density-functional theory (DFT) for such applications. Hohenberg, Kohn, and Sham showed that the static ground state properties of a real system of interacting electrons could in principle be treated exactly by replacing it with a fictitious system of noninteracting electrons.[23,24] In the absence of degeneracies, the wave function of the noninteracting system is single determinantal in nature. The orbitals obey the well-known Kohn–Sham equation,

$$(\hat{h}_{\mathrm{C}}^{\sigma} + v_{\mathrm{H}} + v_{\mathrm{xc}}^{\sigma})\psi_{\mathrm{p}}^{\sigma} = \varepsilon_{\mathrm{p}\sigma}\psi_{\mathrm{p}}^{\sigma}, \tag{I.1}$$

where $\hat{h}_{\mathrm{C}}^{\sigma}$ is the usual core (*i.e.*, kinetic energy plus external potential, $v_{\mathrm{ext}}^{\sigma}$), v_{H} is the Hartree (*i.e.*, Coulomb) potential, and (assuming a pure spin-density functional) the exchange–correlation (xc) potential,

$$v_{\mathrm{xc}}^{\sigma}[\rho_{\alpha},\rho_{\beta}](\mathbf{r}) = \frac{\delta E_{\mathrm{xc}}[\rho_{\alpha},\rho_{\beta}]}{\delta\rho_{\sigma}(\mathbf{r})}, \tag{I.2}$$

is the functional derivative of the xc-energy, E_{xc}. (Hartree atomic units are used throughout this paper: $\hbar = m_e = e = 1$.) While the Hohenberg–Kohn–Sham DFT is formally exact in principle, it is limited in practice by the use of approximate xc-functionals. The result is that DFT, whose equations resemble those of Hartree–Fock (HF) theory, "inherits" some of the problems of HF theory, notably molecular orbital symmetry breaking when describing the rupture of covalent bonds. Indeed simple arguments show that no symmetry breaking should occur for a closed-shell molecule when the xc-functional is exact.[21] In practice, the broken symmetry solution becomes lower in energy than the unbroken symmetry solution beyond some critical bond distance (the Coulson–Fischer point) because of the use of approximate functionals. The above arguments rest on the supposition of noninteracting *v*-representability (NVR), which means that the energy is minimized with the *Aufbau* filling of the Kohn–Sham orbitals. Interestingly there is some indication that NVR fails for biradicals,[7] indicating the need for an ensemble formalism which, however, is beyond the scope of the present paper.

Modern TDDFT is based upon the formalism of Runge and Gross who presented Hohenberg–Kohn-like theorems for the time-dependent case and a time-dependent Kohn–Sham equation,[25]

$$(\hat{h}_{\mathrm{C}}^{\sigma} + v_{\mathrm{H}} + v_{\mathrm{xc}}^{\sigma})\psi_{\mathrm{p}}^{\sigma} = i\frac{\partial}{\partial t}\psi_{\mathrm{p}}^{\sigma}, \tag{I.3}$$

in which the xc-potential is, in principle, a functional of the time-dependent density, $\rho_{\sigma}(\mathbf{r}, t)$, and the wave functions of the interacting and noninteracting systems at some initial time. However the first Hohenberg–Kohn theorem tells us that these wave functions are also functionals of the initial density, meaning that the xc-potential depends only on the density for the case of a system initially in its ground stationary state perturbed by a time-dependent applied potential.[23] Linear response (LR) theory may then be used to extract information about excited states. This leads, in Casida's formulation,[26] to the LR-TDDFT equation,

$$\begin{bmatrix} \mathbf{A}(\omega) & \mathbf{B}(\omega) \\ \mathbf{B}^{*}(\omega) & \mathbf{A}^{*}(\omega) \end{bmatrix}\begin{pmatrix} \mathbf{X} \\ \mathbf{Y} \end{pmatrix} = \omega\begin{bmatrix} \mathbf{1} & \mathbf{0} \\ \mathbf{0} & -\mathbf{1} \end{bmatrix}\begin{pmatrix} \mathbf{X} \\ \mathbf{Y} \end{pmatrix}, \tag{I.4}$$

which has paired excitation and de-excitation solutions,

$$\begin{pmatrix} \mathbf{X}_I \\ \mathbf{Y}_I \end{pmatrix} \leftrightarrow \omega_I = E_I - E_0 = -\omega_I \leftrightarrow \begin{pmatrix} \mathbf{Y}_I \\ \mathbf{X}_I \end{pmatrix} \tag{I.5}$$

Here

$$\begin{aligned} A_{ia,jb}^{\sigma,\tau}(\omega) &= \delta_{a,b}\delta_{i,j}\delta_{\sigma,\tau}(\varepsilon_{a\sigma} - \varepsilon_{i\sigma}) + K_{ia,jb}^{\sigma,\tau}(\omega) \\ B_{ia,jb}^{\sigma,\tau}(\omega) &= K_{ia,bj}^{\sigma,\tau}(\omega), \end{aligned} \tag{I.6}$$

and the coupling matrix,

$$K_{ia,jb}^{\sigma,\tau}(\omega) = (ia|\delta_{\sigma,\tau}f_H + \mathrm{f}_{\mathrm{xc}}^{\sigma,\tau}(\omega)|bj), \tag{I.7}$$

where,

$$f_H(\mathbf{r}_1,\mathbf{r}_2) = \frac{1}{r_{12}}, \tag{I.8}$$

is the Hartree kernel and,

$$f_{\mathrm{xc}}^{\sigma,\tau}(\mathbf{r}_1,\mathbf{r}_2;\omega) = \int_{-\infty}^{+\infty} e^{i\omega(t_1-t_2)}\frac{\delta v_{\mathrm{xc}}^{\sigma}(\mathbf{r}_1,t_1)}{\delta\rho_{\tau}(\mathbf{r}_2,t_2)}\mathrm{d}(t_1-t_2), \tag{I.9}$$

is the xc-kernel. Integrals are written in Mulliken charge-cloud notation,

$$(pq|f|rs) = \iint \psi_p^{*}(\mathbf{r}_1)\psi_q(\mathbf{r}_1)f(\mathbf{r}_1,\mathbf{r}_2)\psi_r^{*}(\mathbf{r}_2)\psi_s(\mathbf{r}_2)\mathrm{d}\mathbf{r}_1\mathrm{d}\mathbf{r}_2. \tag{I.10}$$

Since LR-TDDFT is the primary application of TDDFT and the only one treated in the present article, we will normally just refer to LR-TDDFT as TDDFT. Like conventional DFT, the underlying formalism of TDDFT has been the subject of much healthy criticism (*e.g.*, ref. 27–29). Nevertheless is our expectation that, like the static ground-state formalism, formal TDDFT—either as is or suitably modified—will stand the test of time, for at least some time to come. The reader interested in further information about TDDFT is referred to a recent book[30] and two special journal issues[31,32] devoted to TDDFT.

Problems arise in practice because of the use of approximate functionals. These have been extensively reviewed in the

literature (*e.g.*, ref. 33 and 34). Suffice it to say that the normal domain of validity of TDDFT with existent approximate xc-functionals is low-lying 1-electron excitations which are not too delocalized in space and do not involve too much charge transfer.

The present paper is primarily concerned with the limitation to 1-electron excitations. This limitation arises from the basic adiabatic approximation (AA) which is almost universally used in practice. This approximation assumes that the xc-potential reacts instantaneously and without memory to any temporal change of the charge density. Mathematically, the AA means that the xc-potential,

$$v_{\mathrm{xc}}^{\sigma}(\mathbf{r},t)=\frac{\delta E_{\mathrm{xc}}[\rho_{\alpha}^{t},\rho_{\beta}^{t}]}{\delta\rho_{\sigma}^{t}(\mathbf{r})}, \qquad \text{(I.11)}$$

may be evaluated in terms of the xc-functional of static ground-state DFT. Here $\rho_{\sigma}^{t}(\mathbf{r})$ means $\rho_{\sigma}(\mathbf{r},t)$ regarded as a function of the spatial coordinate $\mathbf{r}$ at fixed time t. It is easily seen that the AA limits TDDFT to 1-electron excitations (albeit "dressed" to include some electron correlation effects). In particular, the AA implies that the coupling matrix is frequency-independent and hence that the number of excitation solutions obtained from the LR-TDDFT equation is exactly equal to the number of 1-electron excitations. This is a problem for some applications, such as excitations in polyenes and open-shell molecules, and an active area of research is aimed at going beyond the AA by explicit inclusion of 2- and higher-electron excitations through the frequency-dependence of the xc-kernel.[35–40] The limitation to 1-electron excitations is *a priori* also a problem for photochemical reactions passing through biradicals since the conventional description of biradical formation involves the mixing of the ground state configuration with a doubly-excited state. Thus for the breaking of the σ bond in H_2,

$$H_A\text{–}H_B \rightarrow [H_A\uparrow + H_B\downarrow \leftrightarrow H_A\downarrow + H_B\uparrow], \qquad \text{(I.12)}$$

the final state corresponds to the wave function,

$$\frac{1}{\sqrt{2}}(|s_A,\bar{s}_B|+|s_B,\bar{s}_A|)=\frac{1}{\sqrt{2}}(|\sigma,\bar{\sigma}|-|\sigma^*,\bar{\sigma}^*|). \qquad \text{(I.13)}$$

The 2-electron excited state, $|\sigma^*,\bar{\sigma}^*|$, is excluded by the AA. A subtler, but important point, is that mixing of the ground and excited configurations is also forbidden by the AA but is rigorously necessary to have a CX.[7,21,41]

The present and previous work applying TDDFT to oxirane photochemistry[7,21] also makes use of the Tamm–Dancoff approximation (TDA).[42] [The work of Friedrichs and Frank on the photochemical dynamics of diphenyloxirane uses a different (non-TDDFT) DFT approach.[22]] The TDA consists of neglecting the $\boldsymbol{B}$ matrix to obtain just,

$$\mathbf{AX} = \omega\mathbf{X}. \qquad \text{(I.14)}$$

While the TDA is simpler than full LR-TDDFT and so is both a bit easier to interpret as well as being computationally a bit simpler, the main advantage of the TDA is that it bypasses the triplet instability problem—that is, symmetry breaking in the ground state occurs if and only if an imaginary triplet excitation energy is found in TDDFT.[21,33,43,44] The reason, of course, is that TDDFT excitation energies obtained by LR theory are intrinsically limited by the quality of the DFT description of the ground state which in the NVR case should not show any symmetry breaking. Underestimates of corresponding singlet excitation energies are also often associated with triplet instabilities. However when the TDA is applied to LR time-dependent HF, then the fully variational configuration interaction singles (CIS) is obtained, indicating that the excited-state problem has been decoupled from the ground-state problem in a way that avoids the problem of variational collapse. The situation in TDDFT is similar and TDDFT TDA calculations give much improved excited-state potential energy surfaces (PESs) compared to full TDDFT calculations.[21,43,44]

(It may be worth noting that use of the TDA comes with a cost. TDDFT absorption spectra are derived using linear response theory from the poles of the dynamic polarizability.[26] This implies that the spectral intensities should be reasonably correct. For example, it is known that the Thomas–Reiche–Kuhn "*f*-sum" rule holds in a sufficiently extended basis set.[45] However the *f*-sum rule is lost and the reliability of calculated spectral intensities is diminished when making the TDA with potentially important effects on spectra. Consequently the TDA should be used with extreme caution when calculating oscillator strength distributions.[46] Here however we are interested in potential energy surfaces not oscillator strengths.)

Though it yields improved PESs, the TDA does not solve the problem that mixing of the ground and excited configurations is forbidden by the AA but is rigorously necessary to have a CX, nor does the TDA provide the 2-electron excited states needed for describing biradialoïd intermediates. At first thought such an absence of CX might seem fatal for photodynamics applications. Though the situation is not actually as dark as might at first seem,[7] it would be nice to find a way to recover a true CX.

Levine *et al.* suggest that SF-TDDFT might be good for this purpose.[41] The main idea of SF-TDDFT is shown in Fig. 2. We must first make the common pragmatic assumption that DFT applies not only to the ground state but also to the lowest energy state of a given spin-symmetry. This assumption is

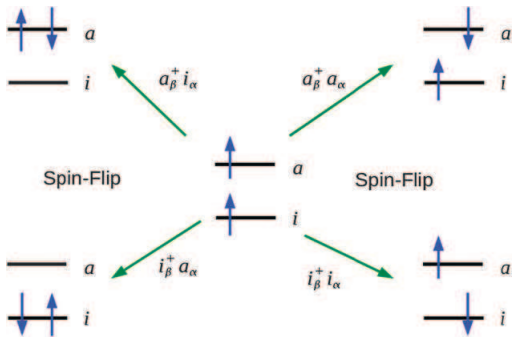

Fig. 2 Two-orbital model of TDDFT excitations with a triplet reference configuration.

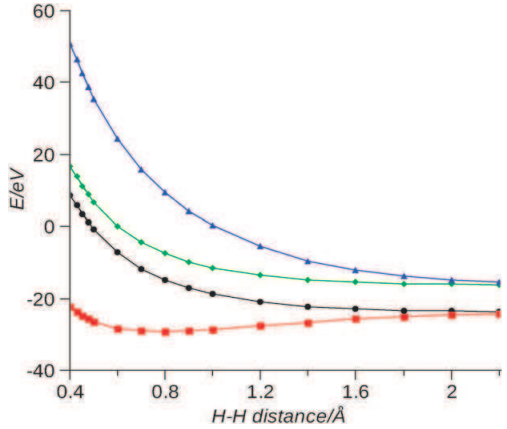

Fig. 3 Dissociation of H_2 obtained with the present implementation of SF-TDDFT. The black $1^3\Sigma_u$ curve (circles) is the triplet SCF reference state from which excitations are taken. It is nearly degenerate with the $M_S = 0$ triplet state (not shown) generated by SF-TDDFT. The red $1^1\Sigma_g$ ground state curve (squares) is a mixture of $|\sigma,\bar{\sigma}|$ and $|\sigma^*,\bar{\sigma}^*|$ configurations, with the $|\sigma,\bar{\sigma}|$ dominating at the equilibrium geometry. The $1^1\Sigma_g$ and $1^3\Sigma_u$ states dissociate to the same neutral "diradical" limit, namely $[H\uparrow + H\downarrow \leftrightarrow H\downarrow + H\uparrow]$. The blue $2^1\Sigma_g$ state curve (triangles) is also a mixture of $|\sigma,\bar{\sigma}|$ and $|\sigma^*,\bar{\sigma}^*|$ configurations, but the "doubly-excited" $|\sigma^*,\bar{\sigma}^*|$ configuration dominates at the ground state equilibrium geometry. The green curve (diamonds) is the $1^1\Sigma_u(\sigma \rightarrow \sigma^*)$ singly-excited state. The $2^1\Sigma_g$ and $1^1\Sigma_u(\sigma \rightarrow \sigma^*)$ states dissociate to the same ionic limit, namely $[H^+ + H^- \leftrightarrow H^- + H^+]$.

especially plausible if a single-determinant provides a reasonable first approximation to the state in question. Excited states normally excluded from TDDFT are included in SF-TDDFT by beginning from the lowest triplet state and flipping spins while exciting electrons from one orbital to another. In this manner we arrive at exactly the ground configuration and the doubly-excited configuration needed to describe bond breaking. Ideally then H_2 will dissociate correctly without recourse to symmetry breaking and this is indeed the case[18] (Fig. 3). Moreover the problem of an effective failure of NVR is very much reduced leading to much improved convergence. Historically designing an appropriate functional for SF-TDDFT has proven to be not entirely straightforward. This problem is reviewed in some detail the next section.

Computational details and a brief description of our own implementation of SF-TDDFT are given in Sec. III. In Sec. IV, we report results pertinent to oxirane photochemistry. Section V summarizes our main conclusions about the effectiveness of SF-TDDFT for describing photochemical funnels.

II. Spin-flip TDDFT

No new solution to the SF-TDDFT problem is proposed in the present paper, but this section reviews existent solutions to the problem of developing appropriate functionals for SF-TDDFT. We do this partly to keep this paper self-contained, but also to point out that some aspects of present SF solutions might also be improved if the goal is complete compatibility between SF-TDDFT and conventional TDDFT.

The most basic requirement of the SF method is the generalization of the one-component collinear approach in which each orbital is associated with either spin α or spin β aligned along an arbitrary z-axis, to a two-component noncollinear approach in which each orbital is a linear combination of spin α and spin β components. Lifting of the collinear requirement is needed to allow spins to rotate in response to an external spin-dependent perturbation and hence to be able to flip. Orbitals become two-component spinors,

$$\boldsymbol{\psi}_p(\mathbf{r}) = \begin{pmatrix} \psi_p^{\alpha}(\mathbf{r}) \\ \psi_p^{\beta}(\mathbf{r}) \end{pmatrix}, \tag{II.1}$$

which are obtained by solving the 2×2 matrix equation in spin,

$$\begin{bmatrix} \hat{h}_C^{\alpha,\alpha} + v_{Hxc}^{\alpha,\alpha} & \hat{h}_C^{\alpha,\beta} + v_{xc}^{\alpha,\beta} \\ \hat{h}_C^{\beta,\alpha} + v_{xc}^{\beta,\alpha} & \hat{h}_C^{\beta,\beta} + v_{Hxc}^{\beta,\beta} \end{bmatrix} \begin{pmatrix} \psi_p^{\alpha}(\mathbf{r}) \\ \psi_p^{\beta}(\mathbf{r}) \end{pmatrix} = \varepsilon_p \begin{pmatrix} \psi_p^{\alpha}(\mathbf{r}) \\ \psi_p^{\beta}(\mathbf{r}) \end{pmatrix}. \tag{II.2}$$

Note that the core Hamiltonian may now have a spin-dependence due to a spin-dependent external potential. The density is also a 2×2 matrix in spin,

$$\boldsymbol{\rho}(\mathbf{r}) = \begin{bmatrix} \rho_{\alpha,\alpha}(\mathbf{r}) & \rho_{\alpha,\beta}(\mathbf{r}) \\ \rho_{\beta,\alpha}(\mathbf{r}) & \rho_{\beta,\beta}(\mathbf{r}) \end{bmatrix}. \tag{II.3}$$

Consequently the xc-kernel has four spin indices,

$$f_{xc}^{\sigma,\sigma';\tau,\tau'}(\mathbf{r}_1,\mathbf{r}_2;\omega) = \int_{-\infty}^{\infty} e^{i\omega(t_1-t_2)} \frac{\delta v_{xc}^{\sigma,\sigma'}(\mathbf{r}_1,t_1)}{\delta \rho_{\tau,\tau'}(\mathbf{r}_2,t_2)} \mathrm{d}(t_1-t_2), \tag{II.4}$$

or, in the AA,

$$f_{xc}^{\sigma,\sigma';\tau,\tau'}(\mathbf{r}_1,\mathbf{r}_2) = \frac{\delta^2 E_{xc}[\boldsymbol{\rho}]}{\delta \rho_{\sigma,\sigma'}(\mathbf{r}_1)\delta \rho_{\tau,\tau'}(\mathbf{r}_2)}. \tag{II.5}$$

Naturally the TDDFT coupling matrix also has four spin indices.

Normal practice is to apply SF-TDDFT using orbitals and orbital energies obtained from an ordinary one-component collinear calculation, rather than as a post two-component noncollinear calculation. Thus the assumption is that the one-component noncollinear calculation is an adequate approximation at the SCF level to a full two-component noncollinear SCF calculation. In the end, the noncollinear model only serves in deriving the SF-TDDFT formalism, not in actually carrying it out.

Applying the SF-TDDFT formalism to the usual collinear pure xc-functionals leads to nothing new because,

$$f_{xc}^{\sigma,\sigma';\tau,\tau'} = \delta_{\sigma,\sigma'}\delta_{\tau,\tau'} f_{xc}^{\sigma,\tau}. \tag{II.6}$$

This however is not true in HF because the kernel of the exchange operator, $\hat{\Sigma}_x^{\sigma,\tau}$, is given by,

$$\Sigma_x^{\sigma,\tau}(\mathbf{r}_1,\mathbf{r}_2) = -\frac{\gamma_{\sigma,\tau}(\mathbf{r}_1,\mathbf{r}_2)}{r_{12}}, \tag{II.7}$$

where $\gamma_{\sigma,\tau}(\mathbf{r}_1,\mathbf{r}_2)$ is the one-electron reduced density matrix. Consequently,

$$f_x^{\sigma,\tau;\sigma',\tau'}(\mathbf{r}_1,\mathbf{r}_2;\mathbf{r}'_1,\mathbf{r}'_2) = \frac{\delta\Sigma_x^{\sigma,\tau}(\mathbf{r}_1,\mathbf{r}_2)}{\delta\gamma_{\sigma',\tau'}(\mathbf{r}'_1,\mathbf{r}'_2)} = -\delta_{\sigma,\sigma'}\delta_{\tau,\tau'}\frac{\delta(\mathbf{r}_1-\mathbf{r}'_1)\delta(\mathbf{r}_2-\mathbf{r}'_2)}{r_{12}}, \quad \text{(II.8)}$$

and the exchange-part of the HF coupling matrix is,

$$K_{pq,rs}^{\sigma,\tau;\sigma',\tau'} = -\delta_{\sigma,\sigma'}\delta_{\tau,\tau'}(ps|f_H|rq). \quad \text{(II.9)}$$

This means that hybrid functionals allow SF because they include a portion of HF exchange. This in fact was the first form of SF-TDDFT. It was proposed by Anna Krylov and coworkers who used their approach to study the ground and excited states of diradicals.[14,15] In order to get good agreement with experiment, they found it necessary to use a significantly higher amount of HF exchange (50%) than is typically used for ground state properties ($\sim$25%). Even higher percentages of HF exchange ($>$50%) have been reported to be necessary for calculating second hyperpolarizabilities of diradical systems by this spin-flip method.[47] Although the use of a different functional for ground and excited states is disturbing, the basic idea is admirable and this method continues to be used.[47–49] In particular, this is the SF-TDDFT approach mentioned in the introduction in the context of its recent use by Minezawa and Gordon who found the method to give a relatively good description of CXs in ethylene.[13]

The next and most recent major advance in SF-TDDFT came with an article by Wang and Ziegler.[18] (See also ref. 19.) It is intimately related to work by Wenjian Liu and coworkers on relativistic four-component TDDFT.[50] Basing their approach on ideas from relativistic two-component DFT,[51,52] Wang and Ziegler proposed that any pure spin-density xc-functional, $E_{xc}[\rho_\alpha,\rho_\beta]$, could be used to make a noncollinear xc-functional suitable for SF calculations by making the substitution,

$$\rho_\alpha \to \rho_+ = \tfrac{1}{2}(\rho + s)$$
$$\rho_\beta \to \rho_- = \tfrac{1}{2}(\rho - s), \quad \text{(II.10)}$$

involving two quantities which are invariant under a unitary transformation of the spin coordinates. These are the total charge density,

$$\rho = \rho_{\alpha,\alpha} + \rho_{\beta,\beta}, \quad \text{(II.11)}$$

and the magnetization, s, whose square is given by,

$$s^2 = (\rho_{\alpha,\alpha} - \rho_{\beta,\beta})^2 + 2(\rho_{\alpha,\beta}^2 + \rho_{\beta,\alpha}^2). \quad \text{(II.12)}$$

The collinear limit of s is just the spin-polarization,

$$s \to \rho_\alpha - \rho_\beta, \quad \text{(II.13)}$$

after an appropriate choice of phase. The factor of 1/2 has been introduced by us so that,

$$\rho_+ \to \rho_\alpha$$
$$\rho_- \to \rho_\beta, \quad \text{(II.14)}$$

in the same limit. After taking derivatives and the noncollinear limit, the xc-kernel becomes,

$$\begin{bmatrix} f_{xc}^{\alpha,\alpha;\alpha,\alpha} & f_{xc}^{\alpha,\alpha;\beta,\beta} & f_{xc}^{\alpha,\alpha;\alpha,\beta} & f_{xc}^{\alpha,\alpha;\beta,\alpha} \\ f_{xc}^{\beta,\beta;\alpha,\alpha} & f_{xc}^{\beta,\beta;\beta,\beta} & f_{xc}^{\beta,\beta;\alpha,\beta} & f_{xc}^{\beta,\beta;\beta,\alpha} \\ f_{xc}^{\alpha,\beta;\alpha,\alpha} & f_{xc}^{\alpha,\beta;\beta,\beta} & f_{xc}^{\alpha,\beta;\alpha,\beta} & f_{xc}^{\alpha,\beta;\beta,\alpha} \\ f_{xc}^{\beta,\alpha;\alpha,\alpha} & f_{xc}^{\beta,\alpha;\beta,\beta} & f_{xc}^{\beta,\alpha;\alpha,\beta} & f_{xc}^{\beta,\alpha;\beta,\alpha} \end{bmatrix} = \begin{bmatrix} f_{xc}^{\alpha,\alpha} & f_{xc}^{\alpha,\beta} & 0 & 0 \\ f_{xc}^{\beta,\alpha} & f_{xc}^{\beta,\beta} & 0 & 0 \\ 0 & 0 & \frac{v_{xc}^{\alpha}-v_{xc}^{\beta}}{\rho_\alpha-\rho_\beta} & 0 \\ 0 & 0 & 0 & \frac{v_{xc}^{\alpha}-v_{xc}^{\beta}}{\rho_\alpha-\rho_\beta} \end{bmatrix}. \quad \text{(II.15)}$$

This approach to SF-TDDFT has been applied to the dissociation of H_2[18] and to calculate the spectra of open-shell molecules.[53–55] Very recent work has used the Wang–Ziegler approach to treat the reaction path for the *cis–trans* photochemical isomerization of 4-styrylpyridine.[56,57] The Wang–Ziegler approach has also been proposed as the basis of a more general spin-coupled TDDFT.[58]

At first glance, eqn (II.15) is very pretty because it contains ordinary TDDFT for spin-preserving (SP) transitions. However we can be more demanding. For example, we can require that the three triplets which are generated from the singlet referenced two-orbital model shown in Fig. 4 be strictly degenerate. In the TDA, ordinary TDDFT gives the $M_S = 0$ triplet excitation energy,

$$\omega_T = \varepsilon_a - \varepsilon_i + (ia|f_{xc}^{\alpha,\alpha} - f_{xc}^{\alpha,\beta}|ia). \quad \text{(II.16)}$$

Also in the TDA, SF-TDDFT gives the $M_S = \pm 1$ triplet excitation energies,

$$\omega_T = \varepsilon_a - \varepsilon_i + \left(ia\left|\frac{v_{xc}^{\alpha} - v_{xc}^{\beta}}{\rho_\alpha - \rho_\beta}\right|ia\right). \quad \text{(II.17)}$$

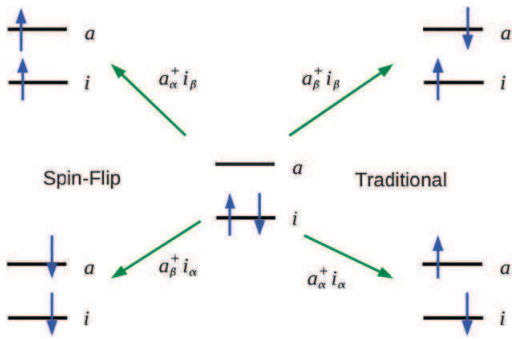

Fig. 4 Two-orbital model of TDDFT excitations with a closed-shell singlet reference configuration.

Since $\rho_\alpha = \rho_\beta$, the right-hand-side of eqn (II.17) can only be interpreted as a derivative. That is, we set $\rho_\alpha = \rho_\beta + \delta$ and take the limit that the function $\delta \to 0$. Then,

$$\frac{v_{xc}^{\alpha}(\mathbf{r}) - v_{xc}^{\beta}(\mathbf{r})}{\rho_\alpha(\mathbf{r}) - \rho_\beta(\mathbf{r})} = \lim_{\delta\to 0} \frac{v_{xc}^{\alpha}[\rho_\beta + \delta, \rho_\beta](\mathbf{r}) - v_{xc}^{\beta}[\rho_\beta + \delta, \rho_\beta](\mathbf{r})}{\delta(\mathbf{r})}$$
$$= \lim_{\delta\to 0} \frac{\int f_{xc}^{\alpha,\alpha}(\mathbf{r},\mathbf{r}')\delta(\mathbf{r}')d\mathbf{r}' - \int f_{xc}^{\beta,\alpha}(\mathbf{r},\mathbf{r}')\delta(\mathbf{r}')d\mathbf{r}'}{\delta(\mathbf{r})}, \quad \text{(II.18)}$$

which is rigorously only equal to $f_{xc}^{\alpha,\alpha} - f_{xc}^{\alpha,\beta}$ for the local density approximation (LDA), in which case eqn (II.16) and (II.17), reduce to the same thing. That, of course, is quite good (probably even adequate for most applications), but it would have been nice to have a theory which was completely general.

As emphasized in the introduction, the case that most interests us in practice is when we begin with a triplet reference configuration as in the two-orbital model of Fig. 2 and look at $\Delta M_S = -1$ transitions. This leads to a triplet–triplet SF-TDDFT TDA excitation energy which is equal to zero when orbital relaxation is neglected. The demonstration involves making use of the identity,

$$F_{p,q}^{\alpha} - F_{p,q}^{\beta} = \left(pq\left|\frac{v_{xc}^{\alpha} - v_{xc}^{\beta}}{\rho_\alpha - \rho_\beta}\right|aa\right) + \left(pq\left|\frac{v_{xc}^{\alpha} - v_{xc}^{\beta}}{\rho_\alpha - \rho_\beta}\right|ii\right). \quad \text{(II.19)}$$

However the usual SP-TDDFT excited singlet–triplet energy difference formula,

$$\omega_S - \omega_T = 2(ia|f_H + f_{xc}^{\alpha,\beta}|ia), \quad \text{(II.20)}$$

cannot be recovered in the SF-TDDFT formalism where instead is found,

$$\omega_S - \omega_T = 2\left(ii\left|\frac{v_{xc}^{\alpha} - v_{xc}^{\beta}}{\rho_\alpha - \rho_\beta}\right|aa\right). \quad \text{(II.21)}$$

The ground to triplet excitation energy formulae obtained from the two formalisms are equally different. Furthermore there is no analogue of Brillouin's theorem in the sense that the coupling between the ground configuration (lower left in Fig. 2) and the singly excited configurations (right hand side of Fig. 2) is nonzero in this formalism. Of course, a sort of Brillouin's theorem still holds by construction in the sense that there is no coupling in this formalism between the reference triplet (center in Fig. 2) and any of the excited states (left and right sides in Fig. 2).

While the above comments suggest that there are grave problems in harmonizing the formulae of the two different TDDFT formalisms, they do not suggest any fatal problems since different looking formulae can lead to nearly similar numerical results. It will, however, turn out that the SF-TDDFT triplet energy is lower than the corresponding SP-TDDFT triplet energy because orbital relaxation in the triplet is more easily described when beginning from a triplet reference than from a singlet reference. Thus the two formalisms are at least shifted with respect to one another.

Despite these unresolved problems, *we have chosen to use the Wang–Ziegler functional in the present paper for our noncollinear SF-TDDFT calculations*. This is because we believe pure density-functionals, rather than HF exchange, to be at the heart of DFT. It thus seems more attractive to us to use the LDA or a generalized gradient approximation (GGA) in conjunction with the Wang–Ziegler noncollinear spin-flip approach than not to use potentially different amounts of HF exchange in hybrid functionals for ground and excited states while completely ignoring the pure DFT part of the hybrid functional as implied by the pioneering SF-TDDFT approach of Krylov and coworkers.

III. Computational details

The benchmark geometries and electronic structure calculations used in the present work are taken from the literature. For the C_{2v} CC ring-opening pathway, we used the geometries and quantum Monte Carlo (QMC) potential energy curves given in Appendix C of ref. 21. The idea behind QMC is to use statistical techniques to go beyond typical high-quality *ab initio* calculations, such as complete active space self-consistent field (CASSCF) and configuration interaction (CI), through the use of more general types of wave functions. The QMC calculations of ref. 21 began with a conventional CASSCF calculation. This was then reoptimized by variational Monte Carlo in the presence of a Jastrow factor to include dynamical correlation. Finally diffusion Monte Carlo was used to further improve on the result of the variational Monte Carlo calculation. Suffice it to say that the result is an electronic structure calculation of very high quality (certainly better than the CASSCF starting point or multireference CI). Geometry optimizations are not presently possible with QMC, so the benchmark geometries are those obtained by C_{2v} structure optimization at fixed ring-opening angle using DFT with the B3LYP functional.[59] For asymmetric CO ring-opening, we used the geometries and QMC potential energy curves from Appendix C of ref. 7. The QMC calculations in this reference are similar to those of ref. 21, but are carried out along a typical pathway for CO ring-opening obtained by mixed TDDFT/classical surface hopping photodynamics calculations. They pass close to a CX which was characterized at the CASSCF level in ref. 7. While exact CXs with the ground state are impossible in conventional TDDFT,[41] it was shown in ref. 7 that the CX is described to a reasonably good approximation by TDDFT in the form of an interpenetrating double cone.

Calculations for the present work were performed with the Grenoble development version of deMon2k (density of Montreal 2000).[60] Where needed additional calculations were carried out with Gaussian 03[61] in order to fix orbital symmetry assignments since the particular version of deMon2k used here did not yet have automatic symmetry assignments. The deMon2k program makes use of two Gaussian-type basis sets. In addition to the usual orbital basis set, there is a second auxiliary charge-density fitting basis set. Its use permits the elimination of all four-center integrals. As with

other DFT programs, deMon2k uses a grid to evaluate xc-integrals. A description of the implementation of standard (spin-preserving) TDDFT in deMon2k has been published elsewhere.[62] The present work is the first reported use of our implementation of Wang–Ziegler SF-TDDFT in deMon2k. Results were compared against those obtained from the ADF (Amsterdam density-functional)[63] package and were found to be acceptably close.

The deMon2k calculations in the present work were carried out using the Vosko–Wilk–Nusair parameterization of the LDA.[64] Density-fitting was carried out *without* imposing the charge conservation constraint[62] using the GEN-A3* density-fitting basis. The orbital basis was the extensive 6-311++G**(2d,2p) basis set.[65,66] The SCF convergence was set at 10^{-7} and the FIXED FINE option was always used for the grid. Our SF-TDDFT calculations used the TDA and the reference state was always the lowest energy triplet. Full advantage was taken of deMon2k keywords allowing convergence of excited state configurations to explore alternative triplet reference configurations for SF-TDDFT.

IV. Results

We are interested in the ability of TDDFT to describe funnel regions. These are regions where potential energy surfaces (PESs) come close enough together that surface hopping becomes possible. Typical funnels are avoided crossings (AXs) and conical intersections (CXs).

Rather than being distinct phenomena, AXs and CXs are actually very closely related. The PESs of a molecule with f (15 in the case of oxirane) nuclear internal degrees of freedom, $\mathbf{R}$, is an f-dimensional hypersurface in an $(f + 1)$-dimensional hyperspace. The condition that the Ith and Jth PESs cross,

$$E_I(\mathbf{R}) = E_J(\mathbf{R}), \tag{IV.1}$$

reduces the dimensionality of the intersection to an $(f - 1)$-dimensional hyperline. If this were all that there were to it, then we could talk about "surfaces that cross without seeing each other." However quantum mechanics typically also requires zeroing out a configuration-interaction (CI) like coupling matrix element,

$$A_{I,J}(\mathbf{R}) = 0, \tag{IV.2}$$

denoted $\mathbf{A}$ here to indicate that it could be the linear response matrix in the TDA. (However we could equally well have called it $\boldsymbol{H}$ for the CI matrix in a CASSCF calculation.) This second condition reduces the dimensionality of the intersection to an $(f - 2)$-dimensional hyperpoint. CXs are impossible for diatomics for states belonging to the same irreducible representation of the molecular point group because $f = 1$ and $f - 2 = -1$ is impossible. So only AXs are seen for diatomics in this case. [Crossings may occur for states belonging to different irreducible representations because eqn (IV.2) is then a consequence of symmetry and so no longer useful as a condition defining the intersection space.] However, in general, there will be two coordinates in hyperspace along which the two intersecting PESs will separate. These two branching coordinates are normally defined by the derivative nonadiabatic coupling vector (DC),

$$h_q^{(I,J)} = \mathbf{X}_I^\dagger \frac{\partial \mathbf{H}}{\partial q} \mathbf{X}_J, \tag{IV.3}$$

and the unscaled gradient difference (UGD) vector,

$$g_q^{(I,J)} = \mathbf{X}_I^\dagger \frac{\partial \mathbf{H}}{\partial q} \mathbf{X}_I - \mathbf{X}_J^\dagger \frac{\partial \mathbf{H}}{\partial q} \mathbf{X}_J, \tag{IV.4}$$

and there is quite a literature on finding and characterizing them (see *e.g.*, ref. 67). Within the 3-dimensional space defined by the two branching coordinates plus the energy coordinate, a CX takes on the form of a double cone. Choosing a one-dimensional slice within the space of branching coordinates means that we will typically pass near but not through the CX and so see an AX.

In this section we report the results of our calculations to see to what extent SF-TDDFT calculations give a better than ordinary SP-TDDFT description of funnel regions in oxirane photochemistry in comparison with the results of previously reported-high benchmark calculations.[21] Results are divided into two parts. In the first part we look at C_{2v} ring opening which involves breaking the CC single bond. This is a one-dimensional slice and so any funnel region will appear as an AX. However it has two advantages: firstly that it represents our "normal" picture of how bonds break and secondly that we can analyze it in great detail. In the second part we look at the CX region for asymmetric CO ring opening along the typical photochemical pathway. Here we are restricted to using CASSCF branching coordinates because we are not yet able to find CXs within TDDFT. From this point of view, our conclusions cannot be conclusive as those of the recent study of Minezawa and Gordon,[13] but nevertheless we believe the present calculations to be indicative of some of the strengths and weaknesses of Ziegler-Wang SF-TDDFT for this type of application.

A C_{2v} Ring opening

The present SF-TDDFT work is perhaps best understood in the light of previous work which is now briefly reviewed. Aryl substitution of oxirane favors symmetric ring opening *via* CC bond cleavage. Cordova *et al.* investigated the ability of TDDFT to describe C_{2v} as well as conrotatory and disrotatory ring opening of oxirane, by comparing TDDFT results against results from high-quality quantum Monte Carlo (QMC) calculations.[21] The high symmetry C_{2v} ring-opening pathway allowed a particularly detailed analysis. Investigation of conrotatory and disrotatory ring opening was inspired by the Woodward–Hoffmann theory of electrocyclic ring-opening reactions. The three principal UV absorption peaks were assigned to Rydberg excitations from the oxygen nonbonding orbital, which are difficult to describe quantitatively because of the well-known problem of underestimation of the ionization threshold,[68] but which can nevertheless be described qualitatively correctly even with the simple local density approximation (LDA). The C_{2v} ring-opening pathway showed a cusp in the ground state potential energy surface when the occupied $6a_1(\sigma)$ and unoccupied $4b_2(\sigma^*)$ orbitals became quasidegenerate. This region also showed an "effective failure

of NVR," which is to say that the energy of the lowest unoccupied molecular orbital (LUMO) fell below that of the highest occupied molecular orbital (HOMO). A consequence of this effective failure are severe self-consistent field (SCF) convergence problems when using a program which tries to enforce the *Aufbau* principle. Triplet instabilities were found to be omnipresent for all the symmetric ring-opening pathways investigated. It was pointed out that the TDA is a practical necessity for avoiding triplet instabilities and singlet near instabilities. With the TDA, the excited-state potential energy surfaces were found to be energetically reasonable even during bond breaking. In principle, SF-TDDFT can improve upon the previous SP-TDDFT calculations in two ways: first by removing the cusp along the C_{2v} ring-opening pathway through an improved description of the AX, and second through the use of a triplet reference which bypasses the effective failure of NVR in the ground singlet state and so may lead to improved convergence.

The reference in our SF-TDDFT calculations is the lowest triplet. While the configuration of oxirane at the intial equilibrium geometry,[21]

$$\cdots[6a_1(\sigma)]^2[2b_1(n)]^2[7a_1(3s)]^0[4b_2(\sigma^*)]^0\cdots. \qquad \text{(IV.5)}$$

suggests that the reference is the $1^3B_1[2b_1(n) \rightarrow 7a_1(3s)]$ state, this is at most true below a ring-opening angle of about 75°. Beyond this angle the reference triplet is the $1^3B_2[6a_1(\sigma) \rightarrow 4b_2(\sigma^*)]$ state. This is true not only in the range 75–120° when the configuration is,

$$\cdots[2b_1(n)]^2[6a_1(\sigma)]^2[4b_2(\sigma^*)]^0[7a_1(3s)]^0\cdots, \qquad \text{(IV.6)}$$

but also beyond 120° when the σ and σ^* orbitals change order,

$$\cdots[2b_1(n)]^2[4b_2(\sigma^*)]^2[6a_1(\sigma)]^0[7a_1(3s)]^0\cdots, \qquad \text{(IV.7)}$$

Fig. 5 shows the frontier molecular orbitals in our SF-TDDFT calculations (which however make use of all, not just the of the frontier, molecular orbitals). Both the ground X^1A_1 and doubly excited D^1A_1 configurations are accessible by spin-flip from the R^3B_2 reference state. Taking the symmetric and antisymmetric combinations of the $6a_1(\sigma)$ and $4b_2(\sigma^*)$ SF configurations leads to B_2 states, the triplet of which is expected to be degenerate with the R^3B_2 reference state. Two states of mixed spin symmetry ($^MB_2$ and $^MA_1$) are also formed. These states are unphysical and yet are necessarily present in any SF-TDDFT calculation (including in the Krylov approach to SF-TDDFT). They are readily identifiable in our calculations and have been excluded from the following discussion.

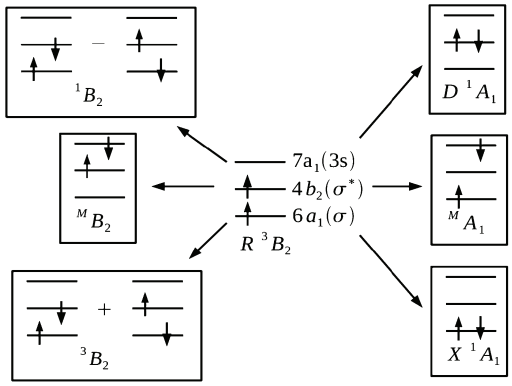

Fig. 5 Principal frontier molecular orbital spin-flip transitions involved in the C_{2v} ring-opening of oxirane beginning from the $R^3B_2[6a_1(\sigma) \rightarrow 4b_2(\sigma^*)]$ reference state.

Fig. 6 shows the results of the SF-TDDFT calculations. The four states predicted in our qualitative discussion are all present. The R^3B_2 SCF reference curve and the corresponding $^3B_2$ SF-TDDFT curve are not identical, but they are indistinguishable on the scale of the Figure. The Figure also shows a very important feature, namely the classic avoided crossing corresponding to the breaking of the CC σ bond. The traditional picture is that of H_2 described in the introduction where mixing of the σ^2 and $(\sigma^*)^2$ configurations is necessary for bond breaking. In order to confirm this two-orbital model, we isolated the part of the SF-TDDFT corresponding to the $4b_2(\sigma^*) \rightarrow 6a_1(\sigma)$ and $6a_1(\sigma) \rightarrow 4b_2(\sigma^*)$ SF transitions. Diagonalizing this 2 × 2 matrix gives the two-orbital model adiabatic curves in Fig. 6, which are seen to be in semiquantitative agreement with the results of the full SF-TDDFT calculation. The diagonal elements of the 2 × 2 matrix give the corresponding diabatic curves. These show how the σ^2 ground state configuration at small angles continues on at large angles to become an excited state and how the $(\sigma^*)^2$ excited state configuration at small angles continues on at large angles to become the ground state at large angles. Thus it would seem that SF-TDDFT can correctly describe avoided crossings associated with bond breaking.

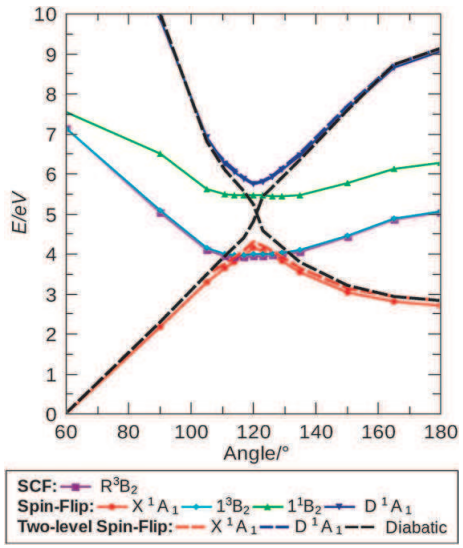

Fig. 6 C_{2v} potential energy curves: full calculation (solid lines), two-orbital model (dashed lines).

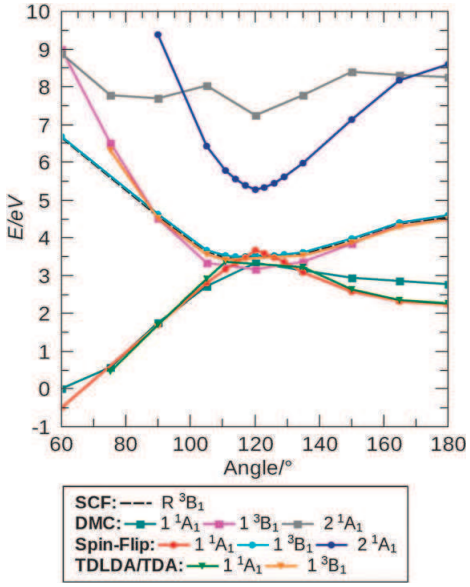

Fig. 7 Comparison between different methods for the X^1A_1, 1^3B_2, and D^1A_1 C_{2v} ring-opening potential energy curves: SF-TDDFT triplet SCF reference state (black dashed line), SF-TDDFT (circles), SP-TDDFT (squares), and DMC (triangles). All curves have been shifted to give the same ground state energy at a ring-opening angle of 80°.

Fig. 7 compares the present SF-TDDFT calculations with both ordinary SP-TDDFT calculations obtained with the LDA functional and the TDA (ref. 21) and with the QMC benchmark calculations. Let us begin first with the comparison with SP-TDDFT calculations. As explained in ref. 21, the bond-breaking region around 120° is an example of effective failure of NVR where the LUMO falls lower in energy than the HOMO. The result is that "normal" DFT programs which insist on filling the Kohn–Sham orbitals according to the *Aufbau* principle will inevitably fail to converge in this region. This is why there are neither SCF ground state nor SP-TDDFT results near 120° in the figure. Very significantly, few convergence difficulties are encountered for the triplet reference state. This would seem to be very good news for those who would like to carry out routine photodynamics calculations where SCF convergence failures can be highly inconvenient if not fatal to the calculations.

In the region where the SCF ground state does converge the *shape* of the ground X^1A_1 and excited 1^3B_2 curves are very similar for SF-TDDFT and SP-TDDFT calculations. Before shifting the SF-TDDFT curves are actually 0.41 eV in energy higher than the corresponding SP-TDDFT curves. Differences between SCF and TDDFT triplet excitation energies have been previously discussed by Casida *et al.*[44] who gave an analysis within a two-level model. The result is that the SF-TDDFT triplet reference is expected to be higher in energy than the SP-TDDFT triplet by the charge-transfer

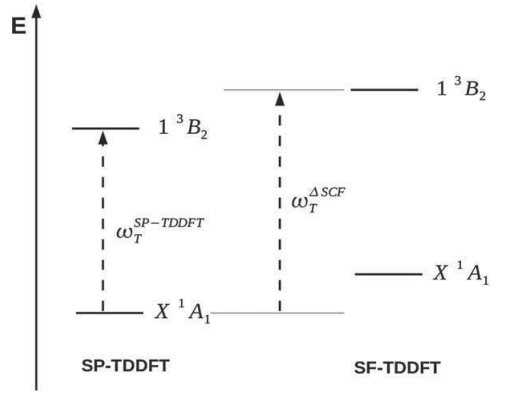

Fig. 8 Illustration of orbital relaxation effects in SF *versus* SP TDDFT.

correction (really a density-transfer correction or relaxation effect),

$$\omega_T^{\Delta SCF} - \omega_T^{SP\text{-}TDDFT} \approx \tfrac{1}{2}(\Delta\rho|f_H + f_{xc}^{\alpha,\alpha}|\Delta\rho) > 0. \quad (IV.8)$$

This is illustrated in Fig. 8. Simultaneously there is a problem describing the ground state with orbitals optimized for a triplet. The result is that the SF-TDDFT method overestimates the ground state energy. However energy differences do appear to be similar in SF-TDDFT and in SP-TDDFT when the same configurations are concerned, so that a rigid shift of energy levels is reasonable.

Having established the similarity and differences of the DFT approaches, let us now compare against the QMC benchmark calculations. Just as relaxation effects lead to the underestimation of the SP-TDDFT $1^3B_2[6a_1(\sigma) \rightarrow 4b_2(\sigma^*)]$ state with respect to the SF-TDDFT SCF reference state, so we can expect the SF-TDDFT $D^1A_1\{[6a_1(\sigma)]^2 \rightarrow [4b_2(\sigma^*)]^2\}$ to be underestimated with respect to an SCF calculation with the doubly-excited configuration. This may help to explain why the SF-TDDFT D^1A_1 is significantly below the corresponding QMC curve. Consequently we may also expect important differences between the SF-TDDFT and QMC description of the ground state curve in the region of the avoided crossing. Nevertheless, except for the point at 60°, the shape of the QMC and DFT ground state curves agree reasonably well below about 100°. Significant differences only really appear in Fig. 7 between the DFT and QMC ground state curves at higher angles. We must conclude that SF-TDDFT is not able to capture all of the correlation effects present in QMC at these angles. Note that the QMC D^1A_1 also seems to be mixing with one or more singly-excited states (see Table 2 of ref. 21), none of which are accessible to the SF-TDDFT formalism used here. The result is a QMC D^1A_1 curve which is rather flatter than its SF-TDDFT counterpart.

B Photochemical pathway

Alkyl substitution of oxirane and indeed oxirane itself does not undergo symmetric ring opening. Rather photochemical ring-opening of oxirane is believed to proceed *via* the three

step Gomer–Noyes mechanism shown in Fig. 1. In ref. 7, Tapavicza *et al.* carried out Tully-type TDDFT/classical trajectory surface-hopping photodynamics calculations using the TDA. This study confirmed and detailed the Gomer–Noyes mechanism. It was shown that the $^1(n,3p_z)$ Rydberg state is directly linked to a $^1(n,\sigma^*)$ valence CO antibonding state. Initial excitation leads within 100 femtoseconds or so to population of the $^1(n,3p_z)$ state and thereby to spontaneous ring-opening (step 1 in Fig. 1). Structure (II) of Fig. 1 is a CX with mixed zwitterionic and biradical character permitting electronic de-excitation directly to a vibrationally hot (4000 K) electronic ground state. At this point there is enough energy for several things to happen, one of which is hydrogen abstraction (III) followed by CC bond breaking. High-quality QMC calculations were carried out along a typical trajectory and used for comparison purposes. Once again an effective failure of NVR was encountered, but difficulties with SCF convergence problems are minimized in dynamics calculations by restarting the SCF for each new geometry from the converged result of the previous geometry, so that orbital-following rather than *Aufbau* filling is enforced.

In this subsection we compare the results of our SF-TDDFT calculations with results of other methods along this trajectory. The trajectory involves the following "events": Only the initial geometry has C_{2v} symmetry, so we fall back on a more chemical nomenclature for key molecular orbitals. The first excited singlet state, S_1, is initially assigned as $1^1B_1[b_1(n) \rightarrow a_1(3s)]$ and thereafter as simply $^1(n, 3s)$. This state remains of Rydberg character throughout the photoreaction. However the second excited singlet state, S_2, does not. Instead, S_2 is initially $2^1B_1[b_1(n) \rightarrow a_1(3p_z)]$, remains of $^1(n, 3p_z)$ Rydberg type for only a short time, soon falling in energy to become the new S_1 as it takes on valence-type CO antibonding character, $^1(n,\sigma^*_{CO})$. At that point $^1(n, 3s)$ is the new S_2. In fact, what happens is qualitatively very much in-line with the Woodward–Hoffmann orbital correlation scheme described in ref. 21 (Fig. 1 of that reference) for the C_{2v} ring-opening reaction but without the symmetry. The trajectory finally passes through (or near) a CX where surface hopping takes place. The nature of this CX has been discussed in ref. 7. Suffice it to say that it is probably best described by the resonance structure II shown in Fig. 1, which has both biradicaloid and zwitterionic character.

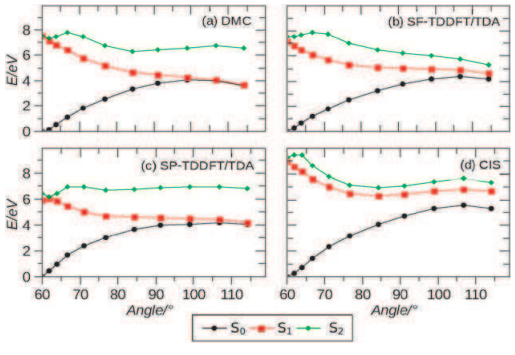

Fig. 9 Potential energy curves for asymmetric ring-opening in oxirane calculated with various methods.

Results are shown in Fig. 9 alongside those from the QMC and SP-TDDFT calculations of ref. 7. Configuration interaction singles (CIS) calculations obtained using GAUSSIAN[61] and the same basis set have also been included in the figure. It appears from this Figure that the S_1/S_0 CX is perhaps a bit better described by SP-TDDFT than by SF-TDDFT and, as expected, that both are significantly better than the CIS description of the same CX. Most dramatic however is the difference between the behavior of the SP-TDDFT S_2 state, which is in relatively good agreement with the QMC S_2 state and in qualitatively reasonable agreement with the CIS S_2 state, and the SF-TDDFT S_2 state which takes an energetic dive as the ring opens. This latter state is in fact highly spin-contaminated and hence unphysical.

It is clear from both the SP-TDDFT and SF-TDDFT calculations that the S_1 state is predominantly of $^1(n,\sigma^*_{CO})$ character. This confers a partial CO σ biradicaloid character by reducing the bond index to 1/2. The SF-TDDFT reference configuration is geometry dependent but for most geometries is,

$$\begin{aligned} &\text{spin}\,\alpha : \cdots n^1\sigma^1_{CO}(\sigma^*_{CO})^1\cdots \\ &\text{spin}\,\beta : \cdots \sigma^1_{CO}n^0(\sigma^*_{CO})^0\cdots. \end{aligned} \tag{IV.9}$$

Formation of the $\sigma^2_{CO} \rightarrow (\sigma^*_{CO})^2$ is thus impossible. Rechoosing the orbital occupations as,

$$\begin{aligned} &\text{spin}\,\alpha : \cdots n^1\sigma^1_{CO}(\sigma^*_{CO})^1\cdots \\ &\text{spin}\,\beta : \cdots n^1\sigma^0_{CO}(\sigma^*_{CO})^0\cdots, \end{aligned} \tag{IV.10}$$

makes the usual $\sigma^2_{CO}/(\sigma^*_{CO})^2$ description of a biradical possible but explicit calculations (not shown here) show S_0 and S_1 potential energy surfaces which are misshapen and much too high in energy, something we can only partly attribute to the use of orbitals optimized for a triplet excited state. As the electronic configuration around the CX likely has both some $^1(n,\sigma^*_{CO})$ and some $\sigma^2_{CO}/(\sigma^*_{CO})^2$, it is remarkable that SP-TDDFT and SF-TDDFT with reference configuration (IV.9) do as well as they do.

C Conical intersection

Let us now take a closer look at what is happening around the CX, first reviewing some of the conclusions of ref. 7. Earlier Levine *et al.* had noted that a true CX could not exist between S_0 and S_1 because condition (IV.2) is a consequence of the formalism and hence cannot serve as a criterion for fixing the dimensionality of the intersection space.[41] Tapavicza *et al.* verified this point but showed that an approximate CX did exist in adiabatic TDDFT for the asymmetric ring opening of oxirane, provided appropriate care was taken in treating convergence problems. These convergence problems result from an effective failure of NVR near the CX as shown schematically in Fig. 10. The representation can only be schematic because the orbitals mix and their energetic ordering varies with the mixing. However this representation, while simplified, is as close as possible to what emerged during

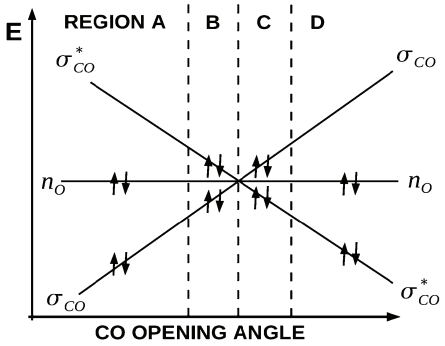

Fig. 10 Schematic Walsh diagram showing how the orbital fillings during asymmetric ring-opening in a normal TDDFT calculation (figure n_0 = text n). Regions B and C show effective violation of NVR.

lengthy discussions between one of us (MEC) and Enrico Tapavicza.[69] However Tapavicza *et al.* were able to maintain the lower energy solution with its "hole below the Fermi level" by a sort of "orbital following." The result is an approximate TDDFT CX in the form of interpenetrating double cones as shown in Fig. 11. The similarity between the behavior of the TDDFT and CASSCF PESs is perhaps even more clear in Fig. 12 where the $S_0 \rightarrow S_1$ excitation energy is shown for the CASSCF branching plane.

Given the results obtained in the case of the symmetric C_{2v} CC ring-opening reaction, we expected that SF-TDDFT would give a rather good description of the asymmetric CO ring-opening reaction by mixing configurations with doubly occupied σ_{CO} and doubly occupied σ^*_{CO} orbitals. Levine *et al.* also suggested that SF-TDDFT might be the solution to the CX problem in TDDFT.[41] Fig. 11 and 12 show that the situation is not so simple. These results do seem to confirm what is expected theoretically, namely that SF-TDDFT is able to produce a CX by coupling ground and excited states. However the SF-TDDFT S_0/S_1 intersection is located at a position between that found in CIS and that found with CASSCF (and approximately by SP-TDDFT).

It is worth taking a closer look. Fig. 11 shows that, while not identical, the SF-TDDFT ground state more closely resembles the CIS ground state than the CASSCF ground state. In particular both the SF-TDDFT and the CIS PESs have a minimum at (DC,UGD) = (0,2) while the CASSCF PES has its minimum at the origin. This indicates that it is highly unlikely that $\sigma^2_{CO}/(\sigma^*_{CO})^2$ configuration mixing is actually occurring near (DC,UGD) = (0,0). (As might be expected, straight DFT also gives a result similar to SF-TDDFT for the ground state.) Our explanation is shown schematically in Fig. 13 which shows how the reference triplet configuration evolves with ring-opening angle. Though the spin α and β orbitals have different energies in our spin-unrestricted calculation and significant orbital remixing occurs, this explanation could still be confirmed by explicit orbital visualization. Conclusions based upon Fig. 13 explain our results rather well, because there is no geometry where SF-TDDFT can simultaneously lead to both the $(\sigma_{CO})^2$ and $(\sigma^*_{CO})^2$ configurations.

We have carried out SF-TDDFT by enforcing an initial $\sigma^1_{CO}(\sigma^*_{CO})^1$ triplet state [eqn (IV.10)], with significant degradation of results compared to the CASSCF and SP-TDDFT curves. This is in line with our above mentionned observations for the asymmetric ring opening pathway when the reference configuration was rechosen as (IV.10).

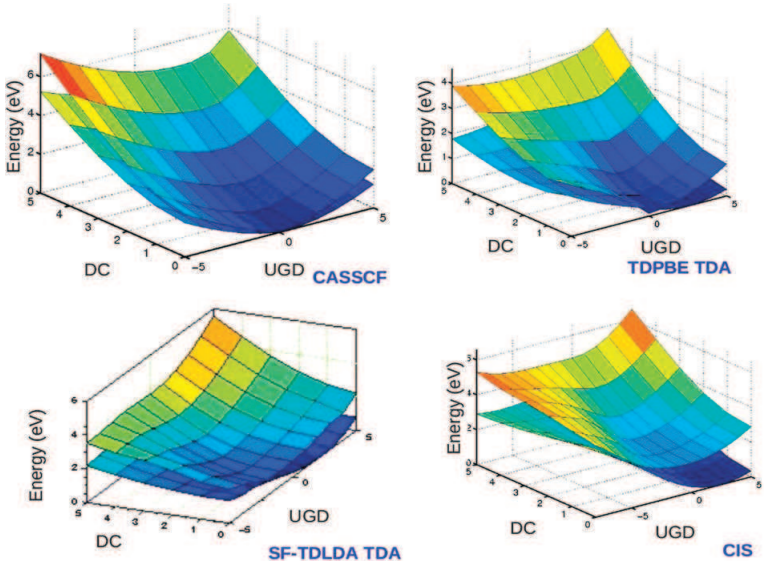

Fig. 11 Comparison of the S_0 and S_1 PESs calculated using different methods for the CASSCF branching coordinate space. All but the SF-TDDFT part of the Figure have been adapted from ref. 7. See also that reference for a detailed description of the branching coordinates.

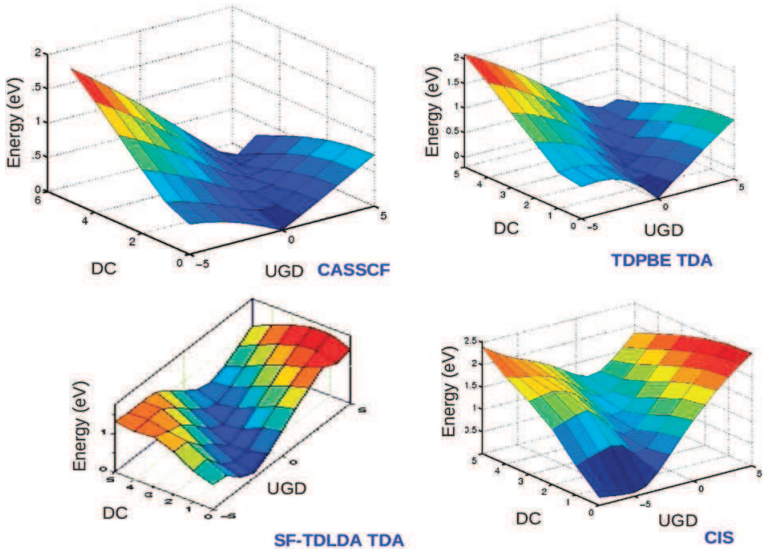

Fig. 12 Comparison of the $S_0 \rightarrow S_1$ excitation energy surfaces calculated using different methods for the CASSCF branching coordinate space. See ref. 7 for a detailed description of the branching coordinates.

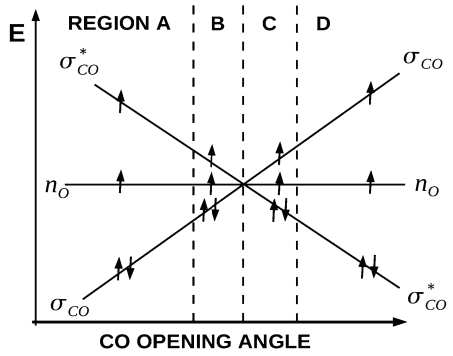

Fig. 13 Schematic Walsh diagram showing how the orbital fillings vary during asymmetric ring-opening in a SF-TDDFT calculation (figure n_0 = text n).

V. Conclusion

The present paper is a contribution to our understanding of how well TDDFT, and SF-TDDFT in particular, is able to describe critical funnels in photochemical reactions. We have chosen the small molecule oxirane for our study because of the availability of previously reported high-quality *ab initio* results[7,21] for comparison and have investigated the avoided crossing (AX) in the C_{2v} ring-opening pathway, the more physical CO ring-opening pathway, and the associated conical intersection (CX).

As pointed out in the introduction, the recent development of mixed TDDFT/classical trajectory SH photodynamics[7–12] is fueling investigations of the ability of TDDFT to describe critical funnel regions.[7,21,41,70–75] Such regions often correspond to the formation of diradicals through bond breaking. Traditional wisdom tells us that a correct description of such regions requires mixing of the ground-state configuration with doubly-excited configurations, which are not normally available to ordinary spin-preserving (SP) TDDFT. In particular, Levine *et al.* argued convincingly that CXs cannot exist between the ground and excited states in SP-TDDFT in the usual case where the TDDFT adiabatic approximation is employed.[41] This is counter to the idea that exact TDDFT should be able to describe this coupling[21] and that an approximate CX has been found in practice.[7] Nevertheless it is highly desirable to find a way to include double excitations so as to obtain a more rigorous description of funnel regions. One active area of research which may lead to a better understanding of the problem, if not a solution, is the explicit inclusion of 2- and higher-electron excitations through the frequency-dependence of the xc-kernel.[35–40] In the meantime, spin–flip (SF) TDDFT[14,15,18,19,47–49,53–58] offers an attractive alternative. Indeed this was also recognized by Levine *et al.*[7] The present work reports our implementation of Wang–Ziegler noncollinear SF-TDDFT in the program deMon2k and constitutes a test of the usefulness of SF-TDDFT for photochemical funnels.

We know of only two previous works on this subject. One is unpublished work by Lawson Daku, Linares, and Boillot who used Wang–Ziegler SF-TDDFT to investigate the *cis*/*trans* photoisomerization of 4-styrylpyridine.[56,57] The other is recent work by Minezawa and Gordon who characterized CXs in ethylene using the Krylov variant of SF-TDDFT.[13] While both of those applications appeared to be successful, they are both restricted to *cis*/*trans* isomerization around a double bond. Here we treat something very different, namely

photochemical ring-opening and are only able to report mixed success.

We first applied SF-TDDFT to study the AX along the C_{2v} ring-opening pathway. A few problems show up which are not present in the obligatory test of dissociation of H_2 (Fig. 3). One problem is the presence of unphysical states of mixed spin symmetry (Fig. 5). Fortunately these were readily identifiable and so could be appropriately ignored. A second problem arises in comparing the results of SP-TDDFT beginning from the ground-state singlet determinant reference and SF-TDDFT beginning from the lowest triplet determinant reference. The different choice of reference immediately implies the possible presence of an orbital relaxation energy correction and indeed the SF-TDDFT potential energy curves are shifted by about 0.4 eV from the corresponding SP-TDDFT curves. Nevertheless SF-TDDFT is to be quite successful in describing the interesting AX.

This is especially true when it is realized that the usual SP-TDDFT calculations run into serious convergence problems in the vicinity of the AX.[21] This is exactly a region of effective violation of noninteracting *v*-representability.[7] Minimizing the total energy with integer occupation number leads to a violation of the *Aufbau* principle with the LUMO below the HOMO or (to put it in more solid-state physics language) with a hole below the Fermi level. Most quantum chemistry programs seek to enforce the *Aufbau* principle even in this case with the result that convergence is not possible at this geometry. In contrast, no particular convergence problems were encountered using SF-TDDFT and the triplet reference.

The question arises as to what can be done in order to remove the unphysical mixed spin-symmetry states in the SF-TDDFT calculations. Vahtras and Rinkevicius have proposed what appears to be a very elegant formal solution.[58] They propose a reformulation of TDDFT which makes use from the very beginning of explicit spin-coupled excitation and de-excitation operators. This requires using the same orbitals for different spin (*i.e.*, a spin-restricted formalism) which is often viewed as at odds with the variational principle in density-functional theory, but this perhaps is a small price to pay. (Note however that our own experience in the present work is that spin-restricted calculations can be significantly more difficult to converge than spin-unrestricted calculations. This is one reason why all of our calculations have been done in the spin-unrestricted formalism.) More importantly putting the Vahtras–Rinkvicius scheme into practice still means finding explicit ways to include matrix elements involving 2-electron and higher excitations. We have already mentioned research aimed at the explicit inclusion of 2- and higher-electron excitations through the frequency-dependence of the xc-kernel.[35–40] Another approach which should be mentioned is to handle these states by a transformed reference *via* an intermediate configuration Kohn–Sham TDDFT procedure proposed by Seth and Ziegler with its very appropriate acronym "TRICKS-TDDFT".[54] The basic idea is to combine SF-TDDFT with different reference states using ideas from the Ziegler–Rauk–Baerends multiplet sum method to make first-order estimates of the pure spin-states corresponding to the mixed states.[77] Thus, in the case of the ${}^{M}(a_1 \rightarrow b_1)$ mixed state on the right hand side of Fig. 5 obtained from SF-TDDFT, we could calculate the energy for the corresponding ${}^{3}(a_1 \rightarrow b_1)$ triplet state from conventional SP-TDDFT and then use the multiplet sum formula

$$\omega_S^{\text{TRICKS-TDDFT}} = 2\omega_M^{\text{SF-TDDFT}} - \omega_T^{\text{SP-TDDFT}}, \quad \text{(V.1)}$$

to estimate the energy of the ${}^{1}(a_1 \rightarrow b_1)$ singlet state. Similar ideas have been used to advantage in the recent study of the reaction path for the *cis*/*trans* photochemical isomerization of 4-styrylpyridine.[56,57] The main drawback, and the reason that this approach was not considered here, is that finding corresponding spin α and β orbitals is not only not always easy but also not always possible in the spin-unrestricted (*i.e.*, different-orbitals-for-different-spins) approach. It turns out that this is especially true in the funnel regions which interest us most.

Perhaps the most interesting and important result in this paper came when we pursued the CO ring-opening path way and examined the physically-important CX. The situation is very different than the case of *cis*/*trans* photoisomerization. In that case, the HOMO and LUMO are typically the π and π^* orbitals associated with the double bond around which rotation is occurring. It is also true that the HOMO and LUMO involved in the C_{2v} ring-opening reaction are the σ and σ^* orbitals associated with breaking the CC bond. The oxygen lone pair (n) is tightly enough bound that it stays out of the way. However along the physical CO ring-opening reaction route, elementary chemical arguments indicate that the oxygen lone pair intercedes as HOMO between the relevant CO σ and σ^* orbitals. This means that taking the lowest triplet as reference does not necessarily lead to an optimal description of the biradical present at the CO ring-opening CX. In particular, attempts to include the doubly-excited $\sigma^2 \rightarrow (\sigma^*)^2$ configuration exclude the possibility of the ${}^{1}(n,\sigma^*)$ configuration whose importance is well-established, and did not prove useful. Nevertheless S_0/S_1 coupling exists in SF-TDDFT meaning that a CX is theoretically possible. Indeed such a feature is seen in our lowest energy triplet SF-TDDFT calculations roughly half-way between the location of the CASSCF CX and the CIS seam.

We conclude that, depending upon the molecule and the CX, the lowest triplet state may or may not be the optimal choice of reference for SF-TDDFT. However the asymmetric ring-opening reaction in oxirane should be taken as a warning that choosing a suitable triplet reference for SF-TDDFT may require a nontrivial use of chemical intuition. This is likely to be especially problematic for larger molecules and is unlikely to be practical for on-the-fly photodynamics calculations. Thus, for the moment, SF-TDDFT remains an *ad hoc* solution for particular problems rather than a universal panacea.

Acknowledgements

We thank Enrico Tapavicza, Ivano Tavernelli, and Claudia Filippi for helpful discussions and Todd Martinez, Irmgard Frank, and Tom Ziegler for their comments on a preprint. Latévi Max Lawson Daku is thanked for supplying comparison data from the ADF program so that we could double check the correctness of our implementation of the noncollinear spin-flip method in DEMON2K. Rosendo Valerio Montero is also thanked for sharing with us his experience with our

implementation of SF-TDDFT in deMon2k. C. M. W. would like to acknowledge a scholarship from the French Embassy in Kenya. M. H. R. would like to acknowledge an *Allocation de Recherche* from the French Ministry of Education. B. N. would like to acknowledge a scholarship from the *Fondation Nanoscience*. A.I. would like to acknowledge postdoctoral funding from the *Laboratoire d'Études Dynamiques et Structurales de la Séléctivité* (LEDSS) which has now become part of the *Département de Chimie Moléculaire* (DCM). Those of us at the *Université Joseph Fourier* would like to thank Pierre Vatton, Denis Charapoff, Régis Gras, Sébastien Morin, and Marie-Louise Dheu-Andries for technical support at the (DCM) and for technical support in the context of the *Centre d'Expérimentation du Calcul Intensif en Chimie* (CECIC) computers used for the calculations reported here. This work has been carried out in the context of the French Rhône-Alpes *Réseau thématique de recherche avancée* (*RTRA*): *Nanosciences aux limites de la nanoélectronique* and the Rhône-Alpes Associated Node of the European Theoretical Spectroscopy Facility (ETSF).

References

1 E. W.-G. Diau, C. Kotting and A. H. Zewail, *ChemPhysChem*, 2001, **2**, 273.
2 E. W.-G. Diau, C. Kotting and A. H. Zewail, *ChemPhysChem*, 2001, **2**, 294.
3 E. W.-G. Diau, C. Kötting, T. I. Sølling and A. H. Zewail, *ChemPhysChem*, 2002, **3**, 57.
4 T. I. Sølling, E. W.-G. Diau, C. Kötting, S. D. Feyter and A. H. Zewail, *ChemPhysChem*, 2002, **3**, 79.
5 J. C. Tully, *J. Chem. Phys.*, 1990, **93**, 1061.
6 J. C. Tully, in *Modern Methods for Multidimensional Dynamics Computations in Chemistry*, ed. D. L. Thompson, World Scientific Singapore, 1998, p. 34.
7 E. Tapavicza, I. Tavernelli, U. Rothlisberger, C. Filippi and M. E. Casida, *J. Chem. Phys.*, 2008, **129**, 124108.
8 N. L. Doltsinis and D. Marx, *J. Theor. Comput. Chem.*, 2002, **1**, 319.
9 E. Tapavicza, I. Tavernelli and U. Rothlisberger, *Phys. Rev. Lett.*, 2007, **98**, 023001.
10 U. Werner, R. Mitrić, T. Suzuki and V. Bonačić-Kouteck, *Chem. Phys.*, 2008, **349**, 319.
11 R. Mirić, U. Werner and V. Bonačić-Kouteck, *J. Chem. Phys.*, 2008, **129**, 164118.
12 C. F. Craig, W. R. Duncan and O. V. Prezhdo, *Phys. Rev. Lett.*, 2005, **95**, 163001.
13 N. Minezawa and M. S. Gordon, *J. Phys. Chem. A*, 2009, **113**, 12749.
14 Y. Shao, M. Head-Gordon and A. I. Krylov, *J. Chem. Phys.*, 2003, **118**, 4807.
15 L. V. Slipchenko and A. I. Krylov, *J. Chem. Phys.*, 2003, **118**, 6874.
16 A. D. Becke, *Phys. Rev. A: At., Mol., Opt. Phys.*, 1988, **38**, 3098.
17 C. Lee, W. Yang and R. G. Parr, *Phys. Rev. B: Condens. Matter*, 1988, **37**, 785.
18 F. Wang and T. Ziegler, *J. Chem. Phys.*, 2004, **121**, 12191.
19 F. Wang and T. Ziegler, *Int. J. Quantum Chem.*, 2006, **106**, 2545.
20 E. Hasegawa and M. Kamata, in *CRC Handbook of Organic Photoreactions and Photobiology*, ed. W. Horspool and F. Lenci, CRC Press, New York, 2nd edn, 2004, p. 53.
21 F. Cordova, L. J. Doriol, A. Ipatov, M. E. Casida, C. Filippi and A. Vela, *J. Chem. Phys.*, 2007, **127**, 164111.
22 J. Friedrichs and I. Frank, *Chem.–Eur. J.*, 2009, **15**, 10825.
23 P. Hohenberg and W. Kohn, *Phys. Rev.*, 1964, **136**, B864.
24 W. Kohn and L. J. Sham, *Phys. Rev.*, 1965, **140**, A1133.
25 E. Runge and E. K. U. Gross, *Phys. Rev. Lett.*, 1984, **52**, 997.
26 M. E. Casida, in *Recent Advances in Density Functional Methods*, ed. D. P. Chong, World Scientific, Singapore, 1995, p. 155.
27 J. Schirmer and A. Dreuw, *Phys. Rev. A: At., Mol., Opt. Phys.*, 2007, **75**, 022513.
28 N. T. Maitra, K. Burke and R. van Leeuwen, *Phys. Rev. A: At., Mol., Opt. Phys.*, 2008, **78**, 056501.
29 J. Schirmer and A. Dreuw, *Phys. Rev. A: At., Mol., Opt. Phys.*, 2008, **78**, 056502.
30 *Time-dependent Density Functional Theory*, ed. M. A. L. Marques, C. A. Ullrich, F. Nogueira, A. Rubio, K. Burke and E. K. U. Gross, Lecture Notes of Physics, Springer, Berlin, 2006.
31 M. A. L. Marques and A. Rubio, *Phys. Chem. Chem. Phys.*, 2009, **11**(22), 4421–4688; Themed Issue on time-dependent density-functional theory.
32 M. E. Casida, H. Chermette and D. Jacquemin, *J. Mol. Struct. (THEOCHEM)*, 2009, **914**; Special Issue on time-dependent density-functional theory.
33 M. E. Casida, in *Accurate Description of Low-Lying Molecular States and Potential Energy Surfaces*, ed. M. R. H. Hoffmann and K. G. Dyall, ACS Press, Washington, DC, 2002, p. 199.
34 M. E. Casida, *J. Mol. Struct. (THEOCHEM)*, 2009, **914**, 3.
35 M. E. Casida, *J. Chem. Phys.*, 2005, **122**, 054111.
36 R. J. Cave, F. Zhang, N. T. Maitra and K. Burke, *Chem. Phys. Lett.*, 2004, **389**, 39.
37 N. T. Maitra, F. Zhang, R. J. Cave and K. Burke, *J. Chem. Phys.*, 2004, **120**, 5932.
38 G. Mazur and R. W lodarczyk, *J. Comput. Chem.*, 2009, **30**, 811.
39 P. Romaniello, D. Sangalli, J. A. Berger, F. Sottile, L. G. Molinari, L. Reining and G. Onida, *J. Chem. Phys.*, 2009, **130**, 044108.
40 O. V. Gritsenko and E. J. Baerends, *Phys. Chem. Chem. Phys.*, 2009, **11**, 4640.
41 B. G. Levine, C. Ko, J. Quenneville and T. J. Martinez, *Mol. Phys.*, 2006, **104**, 1039.
42 S. Hirata and M. Head-Gordon, *Chem. Phys. Lett.*, 1999, **314**, 291.
43 M. E. Casida, A. Ipatov and F. Cordova, in *Time-Dependent Density Functional Theory*, ed. M. Marques, C. Ulrich, F. Nogueira, A. Rubio and E. Gross, Springer, Berlin, 2006.
44 M. E. Casida, F. Gutierrez, J. Guan, F. Gadea, D. Salahub and J. Daudey, *J. Chem. Phys.*, 2000, **113**, 7062.
45 C. Jamorski, M. E. Casida and D. R. Salahub, *J. Chem. Phys.*, 1996, **104**, 5134.
46 M. Grüning, A. Marini and X. Gonze, *Nano Lett.*, 2009, **9**, 2820.
47 R. Kishi, M. Nakano, S. Ohta, A. Takebe, M. Nate, H. Takahashi, T. Kubo, K. Kamada, K. Ohta, B. Champagne and E. Botek, *J. Chem. Theory Comput.*, 2007, **3**, 1699.
48 A. Thomas, K. Srinivas, C. Prabhakara, K. Bhanuprakasha and V. J. Rao, *Chem. Phys. Lett.*, 2008, **454**, 36.
49 A. D. L. Lande, H. Gérard and O. Parisel, *Int. J. Quantum Chem.*, 2008, **108**, 1898.
50 J. Gao, W. Zou, W. Liu, Y. Xiao, D. Peng, B. Song and C. Liu, *J. Chem. Phys.*, 2005, **123**, 054102.
51 H. Eshrig and V. D. P. Servedio, *J. Comput. Chem.*, 1999, **20**, 23.
52 C. van Wüllen, *J. Comput. Chem.*, 2002, **23**, 779.
53 F. Wang and T. Ziegler, *J. Chem. Phys.*, 2005, **122**, 074109.
54 M. Seth and T. Ziegler, *J. Chem. Phys.*, 2005, **123**, 144105.
55 J. Guan, F. Wang, T. Ziegler and H. Cox, *J. Chem. Phys.*, 2006, **125**, 044314.
56 L. M. Lawson Daku, J. Linares and M.-L. Boillot, *Phys. Chem. Chem. Phys.*, 2010, **12**, 6107.
57 L. M. Lawson Daku, personal communication.
58 O. Vahtras and Z. Rinkevicius, *J. Chem. Phys.*, 2007, **126**, 114101.
59 Becke3LYP Method References and General Citation Guidelines, in *Gaussian NEWS*, 1994, vol. 5, p. 2.
60 deMon2k@Grenoble, the Grenoble development version of deMon2k, Andreas M. Köster, Patrizia Calaminici, Mark E. Casida, Roberto Flores-Morino, Gerald Geudtner, Annick Goursot, Thomas Heine, Andrei Ipatov, Florian Janetzko, Sergei Patchkovskii, J. Ulisis Reveles, Dennis R. Salahub and Alberto Vela, *The International deMon Developers Community*, Cinvestav-IPN, Mexico, 2006.
61 M. J. Frisch, G. W. Trucks, H. B. Schlegel, G. E. Scuseria, M. A. Robb, J. R. Cheeseman, J. A. Montgomery, Jr., T. Vreven, K. N. Kudin, J. C. Burant, J. M. Millam, S. S. Iyengar, J. Tomasi, V. Barone, B. Mennucci, M. Cossi, G. Scalmani, N. Rega, G. A. Petersson, H. Nakatsuji, M. Hada, M. Ehara, K. Toyota, R. Fukuda, J. Hasegawa, M. Ishida, T. Nakajima, Y. Honda, O. Kitao, H. Nakai, M. Klene,

X. Li, J. E. Knox, H. P. Hratchian, J. B. Cross, V. Bakken, C. Adamo, J. Jaramillo, R. Gomperts, R. E. Stratmann, O. Yazyev, A. J. Austin, R. Cammi, C. Pomelli, J. Ochterski, P. Y. Ayala, K. Morokuma, G. A. Voth, P. Salvador, J. J. Dannenberg, V. G. Zakrzewski, S. Dapprich, A. D. Daniels, M. C. Strain, O. Farkas, D. K. Malick, A. D. Rabuck, K. Raghavachari, J. B. Foresman, J. V. Ortiz, Q. Cui, A. G. Baboul, S. Clifford, J. Cioslowski, B. B. Stefanov, G. Liu, A. Liashenko, P. Piskorz, I. Komaromi, R. L. Martin, D. J. Fox, T. Keith, M. A. Al-Laham, C. Y. Peng, A. Nanayakkara, M. Challacombe, P. M. W. Gill, B. G. Johnson, W. Chen, M. W. Wong, C. Gonzalez and J. A. Pople, *GAUSSIAN 03 (Revision B.05)*, Gaussian, Inc., Wallingford, CT, 2004.

62 A. Ipatov, A. Fouqueau, C. P. del Valle, F. Cordova, M. E. Casida, A. M. Köster, A. Vela and C. J. Jamorski, *J. Mol. Struct. (THEOCHEM)*, 2006, **762**, 179.

63 G. te Velde, F. M. Bickelhaupt, E. J. Baerends, C. Fonseca, C. Guerra, S. J. A. van Gisbergen, J. G. Snijders and T. Ziegler, *J. Comput. Chem.*, 2001, **22**, 931.

64 S. Vosko, L. Wilk and M. Nusair, *Can. J. Phys.*, 1980, **58**, 1200.

65 R. Krishnan, J. S. Binkley, R. Seeger and J. A. Pople, *J. Chem. Phys.*, 1980, **72**, 650.

66 T. Clark, J. Chandrasekhar and P. v. R. Schleyer, *J. Comput. Chem.*, 1983, **4**, 294.

67 *Modern Methods and Algorithms of Quantum Chemistry*, eds. W. Domcke, D. R. Yarkony and H. Koeppel, vol. 15 of *Advanced Series in Physical Chemistry*, World Scientific, 2004.

68 M. E. Casida, C. Jamorski, K. C. Casida and D. R. Salahub, *J. Chem. Phys.*, 1998, **108**, 4439.

69 E. Tapavicza, personal communication.

70 V. Chernyak and S. Mukamel, *J. Chem. Phys.*, 2000, **112**, 3572.

71 R. Baer, *Chem. Phys. Lett.*, 2002, **364**, 75.

72 C. Hu, H. Hirai and O. Sugino, *J. Chem. Phys.*, 2007, **127**, 064103.

73 C. Hu, H. Hirai and O. Sugino, *J. Chem. Phys.*, 2008, **128**, 154111.

74 I. Tavernelli, E. Tapavicza and U. Rothlisberger, *J. Chem. Phys.*, 2009, **130**, 124107.

75 I. Tavernelli, E. Tapavicza and U. Rothlisberger, *J. Mol. Struct. (THEOCHEM)*, 2009, **914**, 22.

76 T. Ziegler, A. Rauk and E. J. Baerends, *Theor. Chim. Acta*, 1977, **43**, 261.

77 E. Gomer and J. W. A. Noyes, *J. Am. Chem. Soc.*, 1950, **72**, 101.

APPENDIX B

CURRICULUM VITAE

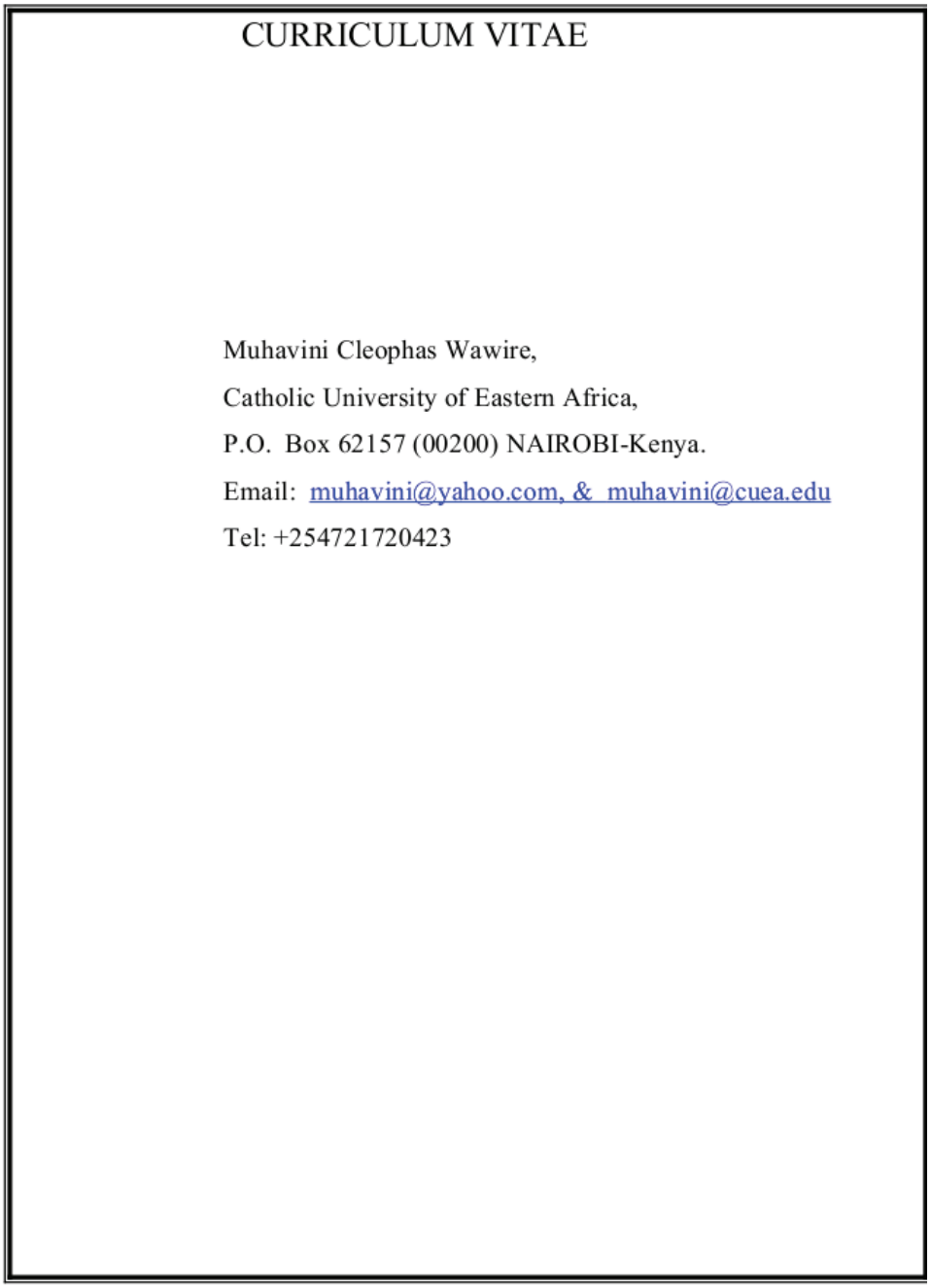
CURRICULUM VITAE

Muhavini Cleophas Wawire,
Catholic University of Eastern Africa,
P.O. Box 62157 (00200) NAIROBI-Kenya.
Email: muhavini@yahoo.com, & muhavini@cuea.edu
Tel: +254721720423

Figure B.1: Muhavini's CV as per June 2012

Muhavini Cleophas Wawire

Contact Information	Lecturer The Catholic University of Eastern Africa-CUEA Natural Sciences Department-Chemistry Section	*P.O. Box:* 62157 - code 00200, Nairobi Kenya *Mobile:* +254-721-720423 *E-mail:* muhavini@cuea.edu, muhavini@yahoo.com

Biodata

Sex: *Male*
Languages: *Swahili, English, Luhya, French, Lingala and Kinyarwanda/Kirundi*
Citizenship: Kenyan
Marital Status: Married
Next of Kin: Lydia Kendi (Wife)-c/o Muhavini C. Wawire, Catholic University of Eastern Africa, P.O Box 62157-00200, Nairobi-Kenya.

Educational Background

Ph.D., **Joseph Fourier University-Grenoble 1**, Département de Chimie Moléculaire, DCM

Computational Chemistry, June 2012

- Thesis Topic: *Theoretical Investigation of Ruthenium Photosensitizers*
- Supervisor: Professor Mark E. Casida

M.Sc., **Kenyatta University**, Chemistry Departement

Modeling Chemistry, May 2002

- Thesis Topic: *Lead and Cadmium in Fresh Tobacco and its Products and the Potentiometric Study of their Complexes with Nicotinic Acid*
- Supervisors: Dr. Jane I. Murungi and Dr. Charles O. Onindo

B.Ed., **Kenyatta University**, Education, Science, Mathematics & Computer Science

Education and Science-Chemistry, Mathematics and Computing, October 1995

High School, Chavakali High School (KCSE), 1989

Primary School, Buhayi Primary school (KCPE), 1986

Other Courses

[1] **Alliance Française de Paris (Nairobi)**, Diplome de Langue, 1994

[2] **Nairobi Technical Training Institute**, Practical skills in Modern Chemical Technology-Production of various chemical products useful to man-World Bank Project Focusing on Poverty Alleviation in Kenya)-2000

[3] **ENS-Lyon**, RFCT/ATOSIM graduate intensive courses in Theoretical & Computational Chemistry in Lyon (France): (Quantum Chemistry, Density-Functional Theory (DFT), Statistical Thermodynamics, Monte Carlo Methods, Advanced Molecular Dynamics-CPMD—Hands on sessions-2008

[4] **APEX-Nairobi**, Environmental Impact and Audit Assessment training-2011

Employment History

Assistant Lecturer **August 2004 to Present**

The Catholic University of Eastern Africa

Lecturer **March 2001 to August 2004**

Kigali Institute of Education, P.O. Box 5039, Kigali-Rwanda

Lecturer **Januay 1998 to February 2001**

Nairobi Technical Training Institute, P.O. Box 30039, Nairobi-Kenya

Teacher **June 1995 to November 1996**

Nembu High School, P.O. Box 21153, Nairobi-Kenya

Temporary Appointment Teacher **1992**

Chebuyusi Secondary School, P.O. Box 286, Kakamega-Kenya

Workshops, Seminars and Conferences attended

- Practical Exercises in Biology and Chemistry For Science Laboratory Training in TTIs and ITs (Workshop Sponsored by GTZ), Nairobi, Kenya, November, 1999
- Practical Skills in Modern Chemical Technology workshop (Easy ways of producing various chemical products useful to man) - World Bank Project, Nairobi, Kenya, August, 2000
- Role of Science in Poverty Alleviation in Rwanda, Butare, Rwanda, February, 2002
- Bioactive and other constituents of two Hugonia plants and some wild Mushrooms, CUEA, Nairobi, Kenya, November, 2006
- Bioactive and other constituents of two Hugonia plants and some wild Mushrooms, CUEA, Nairobi, Kenya, November, 2006
- Module writing workshop, Resurrection Garden, Nairobi, Kenya, November, 2006
- Analysis in Thin Film Technology, CUEA, Nairobi, Kenya, March, 2007
- Improving farm yield and income through aquaculture-agriculture in the lake Victoria basin, CUEA, Nairobi, Kenya, November, 2007
- Mushroom Growing Skills Workshop, KARI, Kakamega, Kenya, February, 2007
- Mushroom Production Strategic Plan, Lugari, Kenya, February, 2007
- CHE-Research Dissemination Workshop, Mombasa, Kenya, August, 2008
- Molecular Optical Switches in Grenoble & Nairobi, Grenoble, France, November 2008

- Workshop on Nanosciences and Nanotechnology: From Smart Materials to Devices at the Hôtel de la Poste à Autrans, A meeting between the Université Joseph Fourier and the University of Texas at Austin. Grenoble, France, October 2009
- Workshop on Needs Assessment Training, at Kolping Organization of Kenya-Nairobi, May 2010
- Workshop on Implementers Training for ISO 9001: 2008 Standard, at Kolping Organization of Kenya-Nairobi, September 2010

Oral Presentations

- C. Muhavini Wawire, "Ab initio study of Nanoscale Ruthenium Complexes as candidates for incorporation into solar cells and photocatalysts by use of computational tools and skills", Presentation to Faculty of Science, CUEA, Nairobi, Kenya, 27^{th} October 2011.
- C. Muhavini Wawire, "Computational, Modeling Chemistry & Software Development" Presentation during the French Alumni Launch at IFRA, Nairobi Kenya , 21^{st} June 2010.
- S. Terah and C. Muhavini Wawire, "Demystification of Software Development and Scripting in Sciences", presentation during the Faculty of Science Interdisciplinary Session at CUEA, Nairobi, Kenya, 26^{th} March 2010.
- C. Muhavini Wawire, "Trends in the Teaching of Science, Maths and Technology", presentation during the Faculty of Science Interdisciplinary Session at CUEA, Nairobi, Kenya, 26^{th} March 2010.
- C. Muhavini Wawire, "Modeling of Nanoscale Ruthenium Complexes for Photochemical Molecular Devices (Photocatalysts, Solar Cells)", Theoretical Chemistry Laboratory Group-LCT- Grenoble, France, 4^{th} December 2009.
- C. Muhavini Wawire, "Typesetting Technology and Computational Science", Interdisciplinary Workshop, CUEA, Nairobi, Kenya, 27^{th} March, 2009.
- G. A. Mwayuli & C. Muhavini Wawire, "Education and demand driven courses in Africa: Is Science still relevant?" Interdisciplinary Workshop, CUEA, Nairobi, Kenya, 26^{th} March, 2009.
- C. Muhavini Wawire, "Computational Chemistry/Science and Pedagogical Implications", Moi University, Eldoret, Kenya, 4^{th} September 2009.
- C. Muhavini Wawire, "Computational Chemistry Science", Science Club, Catholic University of East Africa, Nairobi, Kenya, 12^{th} March 2008.

Posters

Bhaarathi Natarajan, M. Huix-Rotllant, A. Ipatov, C. M. Wawire, T. Deutsch, and M. E. Casida, "Behaviour of Conical Intersections within Noncollinear Spin-Flip Time-Dependent Density-Functional Theory: Oxirane as Test Case", 13^{th} International Conference on the Applications of Density Functional Theory in Chemistry and Physics, DFT09, 31^{st} August to 4 th September 2009, Lyon, France.

Membership to International Bodies

- Member of the Computational Chemistry List (CCL).

Research Projects

- Lead and cadmium in fresh tobacco and its products and the potentiometric study of their complexes with nicotinic acid (2001).

- Commission of Higher Education (CHE)-Research Project on Mushroom Farming in Lugari District, Kenya (November 2006-2009).
- Production of herbal soaps and detergents using local plant oil blends: a poverty alleviation option for rural communities of the ASALS of Kenya (2005).
- PhD Research Project- Investigation of Nanoscale Ruthenium Photosensitizers)—2008-2012

Student Supervision and Mentorship

Dorothy Moga: *Analysis of Chang'aa for its compliance with the KEBS-set standards.* 2012
Pablo Baudin: *Étude Théorique des Spectres UV-Visible et des PDOS de complexes du Ruthénium par les méthodes DFT et TDDFT.* 2011
Sauli Jacinta: *A correlational study of Mathematics and Chemistry on students performance in 2006 KCSE. A case study of Masinga Division-Machakos District.* 2009
Grace Momanyi: *Investigation of the quality of the locally made soaps in relation to specifications set by the Kenya Bureau of Standards-KEBS.* 2006

Publications

- Sarah Wambui Kimani, Elias Kiarie Kagira, Kendi Lydia and Cleophas Muhavini Wawire, "Shoppers Perception of Retail Service Quality: Supermarkets versus Small Convenience Shops (Dukas) in Kenya" *Journal of Management and Strategy, Vol. 3, No. 1;* February 2012.
- C . Muhavini Wawire, 2011. Subject Methods Chemistry-MODULE : Self-Study Materials for the Bachelor of Education Degree. CUEA PRESS (Nairobi-Kenya)
- Miquel Huix-Rotllant, Bhaarathi Natarajan, Andrei lpatov, C. Muhavini Wawire, Thierry Deutsch, and Mark E. Casida, "Assessment of Noncollinear Spin-Flip Tamm-Dancoff Approximation Time-Dependent Density-Functional Theory for the Photochemical Ring-Opening of Oxirane", *Phys. Chem. Chem. Phys. 12, I2811-12825* (2010).
- C. Muhavini Wawire, 2002. Atomic Structure and States of Matter (module).

Submitted Journal Publications

"Density-Functional Study of Lumininescence in Polypyridine Ruthenium Complexes", C. Muhavini Wawire, Damien Jouvenot, Frédérique Loiseau, Pablo Baudin, Sébastien Liatard, Lydia Njenga , Geoffrey N. Kamau and Mark E. Casida

Books in Preparation

- Digitizing the University Core Processes in African Universities. The Technological Approach.
- Uses of Software Packages in Computational Chemistry. Sustainable Science Learning & Teaching in Africa: Highlighting African Realities.

- Demystification of Multi-media for enhanced e-Learning in the Sub-Sahara Region.

Awards

- Commission of Higher Education (CHE)-Research Project on Mushroom farming in Lugari District , Kenya (November 2006-2009).
- CUEA-Research project on production of herbal soaps and detergents using local plant oil blends: a poverty alleviation option for rural communities of the Asals of Kenya (2006).
- French Government PhD-Scholarship (August 2008)- July 2012.
- Joseph Fourier University-Doctoral School Award to attend specialized course in Computational Science at Lyon (Ecole Normale Superieure de Lyon - ENSL) in France-October 2008

Other Professional and Community Activities- (Other Responsibilities

- Participation in the translation of Science books and Journals from English to French and vice versa for the Distance Training Programme (DTP) of Kigali Institute of Education-Rwanda.
- Participation in committees in the university such as students/staff committee (faculty of science), and also a faculty publications representative.
- Active participation in the establishment of partnerships between the Catholic University of Eastern Africa and Community Organizations in Lugari District, Western Province- Kenya.
- Co-authorship of Modules used in the Mushroom Farming Project Lugari District- Kenya.
- Setting up of a Computational Chemistry Center in CUEA- The first ever in Kenya, Eastern Africa and Africa excluding South Africa.
- Working on a joint venture to set up a Computational Chemistry Center for Eastern and Central Africa at MMUST and CUEA.

Personal Interest

- Music (guitar making and playing, Musical Keyboard playing and Music composition.
- Linguistics (Kiswahili, English, French, Lingala, Kinyarwanda/Kirundi and Luhya.
- Open source software and other Internet resources for doing, teaching and learning Science.
- Skills in identification, installation, customization and use of e-learning engines.
- Programming, scripting and application of these skills to software development.
- Gathering and implementing ideas and skills to do with website design/development, hosting and use.

Referees

Prof. Mark E. Casida
Laboratoire de Chimie Théorique
Département de Chimie Moléculaire (DCM, UMR 5250)
Institut de Chimie Moléculaire de Grenoble (ICMG, FR260)
Université Joseph Fourier (Grenoble I)
F-38041 Grenoble, FRANCE

Dr. Nicholas W. Twoli
Kenyatta University
Comm. Tech. Department
P.O. Box 43844
Nairobi Kenya

Prof. Genevieve Mwayuli
The Catholic University of Eastern Africa
Natural Sciences Department
P.O. Box 62157-(00200)
Nairobi-Kenya

APPENDIX C

COMPUTATIONAL CHEMISTRY IN KENYA

Computational Chemistry in Kenya is still in its infancy. There have been efforts to start this important area of research but the progress is quite unsatisfactory. The very first person to do some calculations using GAUSSIAN 03 was Dr. Kibe of Kenyatta university. His thesis was on "**Study of the Mechanism of Acid Catalyzed Esterification**." This was carried out in South Africa at Kwazulu Natal University in 2005. Ever since he came back, there is not much in terms of infrastructural growth to enable the growth of computational Chemistry. The study itself involved some expensive residential sessions in S. Africa. It was also mounted on Microsoft windows platform. This made it very difficult to continue with this area after completion.

Moi University has a fairly advanced kind of cluster which is coming up. They have received donations from Japan and S. Africa and right now the attention is on ensuring that the system is up and running. Unlike Kenyatta University, the situation in Moi is slightly better because there are many people involved and it is a system as opposed to a **one-man** show in Kenyatta university. Moi system is also superior because they use linux operating system which enables calculations through **secure shell-ssh** and **sftp** approaches.

The unfortunate part of the Moi situation is that the only people who carry out calculations are physicists. It is only recently that some efforts were made to incorporate a chemistry student. Right now there are all sorts of activities to ensure that the servers in Moi and their partner institutions are up and efficiently running because the university is to host the 2^{nd} African School on 'Electronic Structure Methods and Applications' (ASESMA 2012). This school seeks to fulfil a number of things such as:

1. encourage growth of computational calculations,

2. start and enhance collaborations between physicists and chemists,

3. formulate follow-up activities to ensure that computational science growth is sustained,

4. explore possibilities of exposing the young participants to more of these computations in other parts of the world.

There have been other efforts by the HP-Initiative to start what is called '*East African Computational Chemistry Infrastructure Project*'. It was to be set up at the Masinde Muliro University of Science and Technology (MMUST) in Western Kenya. Since I was a key member of the team I am aware that the necessary forms of sponsorship came in terms of servers and computers in 2011 early but up to now there is nothing to show for it. Possible reasons are many but my own take is that poor leadership and bad local politics could be behind this delay. The aim of this project was to set up a grid in conjunction with Binghamton University. The collaboration was meant to create a link in which MMUST students could do some calculations using the high quality chemistry resources at Binghamton University, and which are not possible here due to their high cost. Personnel and students from MMUST and its partners such as The Catholic University of Eastern-CUEA were to connect to the servers in Binghamton University in the US, learn and then apply the acquired skills to the study of ways to mitigate environmental toxins and the development of natural anti-malarial products. This is yet to take off as earlier mentioned and one thing that I saw there was the lack of linux skills.

Finally there is a fairly functional system at The Catholic University of Eastern Africa-CUEA. From many points within the CUEA firewall, I am able to connect to the Supercomputers in France and submit my jobs to the queue system awaiting the calculations. My office has computers that operate on linux-(**ubuntu-distro**). Through the commandline, I connect to a local server and then enter the cluster with many machines. I also use secure file transfer protocol (sftp) to submit and recover output files for analysis. Following the success of our connections and working, quite a number of universities are keen to learn and replicate this mode of learning. At CUEA itself, quite a number of departments are now on ubuntu. Some computers are fully linux and others dual boot. The computer department is also adjusting to linux.

From the experience on the ground, there are some efforts to move forward in this field. We need just to define where to start. The acknowledgement that linux can make a difference is one of the ways and I am happy that this is now happening.

INDEX